MECHANICAL CONTROL OF REGENERATION IN THE INNER EAR

A Dissertation

presented to the faculty of the Neuroscience Graduate Program

at the University of Virginia

In partial fulfillment

of the requirements for the degree of

Doctor of Philosophy in Neuroscience

by

Mark A. Rudolf

May, 2020

SIGNATURE PAGE

ABSTRACT

Hundreds of millions of people around the world suffer from disabling hearing loss or have vestibular deficits. A major and irreversible cause of these impairments is the loss of sensory hair cells in the neuroepithelium of the inner ear, which can occur due to loud sounds, ototoxic compounds, infections, and aging. Birds, fish, and amphibians mount a regenerative response to such damage whereby neighboring supporting cells divide and differentiate into replacement hair cells, ultimately leading to recovery of hearing and balance function. In humans and other mammals, these repair processes occur to a limited extent during development, but in adults supporting cells remain largely quiescent. I hypothesized that the regenerative replacement of hair cells in the mammalian inner ear was limited by the development of reinforced apical junctions in mammalian supporting cells, which does not occur in the supporting cells of nonmammals.

The first chapter of this dissertation introduces the inner ear, the public health impact of sensory hair cell losses, and the field of hair cell regeneration. It also briefly introduces the findings that led to for the original research herein.

The second chapter is a comprehensive literature review focusing on cell junctions and mechanical aspects of regeneration in the inner ear. A primary focus is observations that supporting cells in mammals develop uniquely reinforced, E-cadherin-rich apical junctions during postnatal maturation. These junctions are bracketed by thick circumferential bands of filamentous actin that are exceptionally thick and stable. The growth of these F-actin bands correlates to postnatal declines in the rates of spreading and proliferation of supporting cells. In mammals, these reinforced junctions are found both in pillar and Deiters cells within the cochlea, as well as in supporting cells throughout vestibular organs such as the utricle. Supporting cells of birds, fish, and amphibians hardly express E-cadherin and possess thin bands of filamentous actin. Major open questions include the following: (1) Does the reinforcement of junctions in mammalian supporting cells stiffen the epithelium relative to those in nonmammals? (2) Does reversing this junctional reinforcement overcome proliferative quiescence in the mature mammalian utricle? And

finally, (3) What signaling pathways in mammalian supporting cells act downstream of junctional reinforcement to maintain their quiescence? These questions are explored in the subsequent chapters.

In the third chapter, I test the hypothesis that the postnatal reinforcement of junctions in mammalian supporting cells mechanically stabilizes the epithelium. For this, I performed mechanical measurements of the utricular epithelia of mice and chickens at various ages. Using a customized micropipette aspiration technique that allows for the visualization of epithelial deformations due to a controlled suction force, I found that the sensory epithelium of the mouse stiffens during postnatal maturation. Pharmacologic disruption of filamentous F-actin made the utricular epithelia of the mice less stiff. In contrast, there was no difference in stiffness between utricles of hatchling chicks and older pullets. I also analyze supporting cell shape as an indirect measure of intraepithelial tension. Supporting cells in the mouse had round apical domains, while supporting cells in the chicken utricle developed progressively more elongated shapes throughout embryonic development, suggesting that they are readily deformable in response to intraepithelial tension. Taken together, the results indicate that the postnatal reinforcement of supporting cell junctions in the mammalian utricle causes an increase in stiffness that restricts responses to cell loss.

The fourth chapter describes the effects of reversing junctional reinforcement in the mouse utricle. An incidental discovery revealed that a combination of growth factors and pharmacologic agents reversed junctional reinforcement in supporting cells of cultured mouse utricles. Detailed time course experiments revealed that the cocktail first thinned the F-actin bands in supporting cells throughout the utricle. Then, levels of E-cadherin declined in supporting cells within the striolar region, located centrally within the utricle. After these changes, the rate of proliferation sharply increased in striolar supporting cells. Epidermal growth factor and a small molecule inhibitor of glycogen synthase kinase 3 were the two components of the cocktail that mediated these effects. This represents the first evidence that the reversal of junctional reinforcement

correlates with cell cycle re-entry and proliferation in the long-quiescent supporting cells in a mature mammalian utricle.

It remained unclear what signaling pathways operate downstream of junctional reinforcement to maintain mammalian supporting cells in a state of persistent quiescence. One intriguing candidate was the Hippo pathway and its effector Yes-associated protein (YAP), which respond to changes in mechanical tension at cell junctions and partner with TEAD transcription factors to control epithelial proliferation. In the fifth chapter, I tested the hypothesis that HC loss would activate YAP in the ears of nonmammals, but would not in the ears of mammals which harbor reinforced apical junctions. I found that YAP accumulated in nuclei of supporting cells in the chicken utricle after hair cell loss and mediated regenerative proliferation. In mouse utricles, the YAP remained cytoplasmic after hair cell loss, and little proliferation occurred. I sought to bypass this inhibition using a genetically engineered mouse model that allowed for the expression of an activated variant of YAP. This activated YAP-TEAD transcriptional activity and drove proliferation and mitotic hair cell production in utricles of living mice. Further experiments indicated suggested that inhibitory phosphorylation limited the proliferative effect of YAP in the mouse utricle. Conditional deletion of the Large tumor suppressor (LATS) kinases abolished inhibitory phosphorylation of YAP and led to proliferation of striolar supporting cells, even in adults.

To conclude, I formulate a working model to explain why supporting cells in nonmammals mount a robust proliferative response to hair cell loss, whereas those in mammals remain in a state of proliferative quiescence: Hair cell loss the ears of birds elicits a change in local intraepithelial tension that rapidly propagate through the pliable epithelium and results in physical expansion of neighboring supporting cells. This mechanical signal bypasses or inactivates the Hippo pathway in the supporting cells, leading to the nuclear accumulation of YAP and TEAD-dependent regenerative proliferation. In mammals, thickened circumferential bands of filamentous actin produce a rigid epithelium that impedes the transmission of intraepithelial tension and slows the shape changes that arise upon hair cell loss. The absence of substantial

changes in tension and high levels of E-cadherin allow LATS kinases to remain activated, which phosphorylate and inhibit YAP to maintain supporting cells in a state of persistent quiescence. I describe outstanding questions and additional experiments to further interrogate this model. Overall, the work presented here suggests that genetic or pharmacologic targeting of the E-cadherin/LATS/YAP/TEAD axis could represent a therapeutic target for acquired hearing loss and balance disorders by promoting regenerative proliferation in sensory epithelia of the inner ear.

TABLE OF CONTENTS

LIST OF IMPORTANT ABBREVIATIONS

Abbreviation	Meaning
HC	Hair cell
SC	Supporting cell
IHC	Inner hair cell
F-actin	Filamentous actin
OHC	Outer hair cell
YAP	Yes-associated protein
LATS	Large tumor suppressor
TEAD	TEA/ATTS domain (transcription factor)
N:C ratio	Nuclear:Cytoplasmic ratio

ACKNOWLEDGEMENTS

The PhD has been without a doubt the greatest challenge of my life so far. Perhaps the most challenging aspect has been to reckon with the gradual pace of discovery, especially when so many exciting and important questions are at our fingertips. Biomedical research requires patience and diligence, as well as considerable financial resources. It is an enormous privilege to be a scientist—few people in the world have the opportunity to do research, and I feel incredible gratitude, and responsibility to be in this position.

To Jeff: I still remember approaching you after a medical school lecture. I was already fascinated with hair cells, but now can comfortably say that vestibular supporting cells are my favorite cell type. Thank you for taking on another student at this stage in your career, for sending me to the Marine Biological Lab at Woods Hole twice, for experimental help (usually with microscopy), for opening the door to every possible opportunity for me, for setting a high bar (especially with respect to scientific rigor and writing), for reviewing hundreds of drafts until we got it right, and for sharing your enthusiasm for science. It is incredible to have had the opportunity to be a trainee of a scientist who has had such a large impact on the biology of the inner ear.

To Jung-Bum, thank you for being there as a co-mentor who I could always talk to. In sports, people often talk about a “player’s coach”, and you are definitely a “trainee’s PI”. It has been such a blessing to have a bigger lab family and being around great science. To Xiaowei, I am thankful that you have been a part of the Inner Ear Supergroup at UVA during my time in the lab. I also thank my committee members Bettina Winckler, Adrian Halme, Sarah Kucenas, and Ray Keller for their guidance and encouragement. I have had the opportunity to work with collaborators at the NIDCD, and thank Alexander Cartagena-Rivera, Alejandro Anaya, Richard Chadwick, and Matthew Kelley for welcoming me to their labs.

I want to thank the staff of Medical Research Building 4, especially Simenesh and Amber, without whom none of the work in this dissertation would be possible. Nobody has given me more day-to-day help in the lab than each of you.

To my colleagues: I am so grateful to have had such wonderful people to work alongside for my entire PhD. I'd like to thank Robin Singleton for her help in the laboratory and for organizing lab bake-offs; Lorela Ciraku, who is a great friend and budding scientist; and Anna Andreeva, who helped me on a daily basis when I was a new graduate student, laid the foundation for an important project, and produces the most beautiful images. I want to especially thank Mikolaj Kozlowski, who supercharged our output and was always ready to talk regeneration with me. I don't think it's an exaggeration to say that our collaboration and discoveries helped to turn a conceptual corner in this field. To Sihan Li, Beth Wagner, Andre Landin-Malt, and Ting Du: Thank you for your advice, encouragement, and kindness. To my undergraduate students Priyal Ghandi, Christina Kim, Bailey Moskowitz, Anthony DeNovio, and Tony Koshar: Thank you for your energy and help during this process.

To my friends: You have made the past few years unforgettable. We have grown so incredibly close during this time. I am excited for the contributions you have made and have yet to make to our understanding of cell biology.

Grace, thank you for being in my life and helping me through the homestretch of this PhD.

I thank my family, Rainer, Kristine, Rob, and Julia, for their love and support. You are always looking out for what's best for me. And of course, Alice—this is just the start!

This work was supported by

NIDCD/NIH R01 DC000200 to JTC

NIDCD/NIH F30 DC016806 to MAR, a Double Hoo Award to MAR and CEK, and

NIDCD/NIH ZIA DC000059 to MWK.

CHAPTER 1
Hair Cell Regeneration: Background and Motivation for this Thesis

Sensory epithelia within the inner ear contain hair cells and supporting cells

The inner ear is a set of sensory structures encased within the temporal bone of vertebrates that enables our senses of hearing and balance. In humans and other mammals, the inner ear harbors the sound-detecting cochlea, and five vestibular organs which detect gravity and accelerations of the head: The saccule and utricle sense vertical and horizontal linear accelerations, respectively, and three orthogonal semicircular canal cristae sense angular acceleration. Each organ contains an epithelium comprised of sensory hair cells (HCs) that are each surrounded by non-sensory supporting cells (SCs). Acoustic vibrations and accelerations of the head can deflect the hair bundle, an organelle protruding from each HC's apical surface (Figure 1-1), opening mechanically-gated channels that allow ions to enter and depolarize the HC. The resulting electrical signal is propagated via the vestibulocochlear nerve to the central nervous system, conveying sensory information to the brain.

Hair cell losses are a major and irreversible cause of hearing loss and balance dysfunction

Hearing loss is a highly prevalent public health issue. An estimated 466 million people—over 5% of the world's population—have disabling hearing loss, as defined by a threshold shift of ≥40 dB in the better hearing ear in adults, and a ≥30 dB shift in children (World Health Organization, 2020). Hearing loss can be classified as conductive or sensorineural (**Error! Reference source not found.**-2). Conductive hearing loss arises from problems with the conduction of sound from the external environment through the external and middle ear. Common causes include obstruction of the ear canal, rupture of the tympanic membrane, and otitis media (J. B. Nadol, 1993). Conductive hearing losses are often treatable.

Sensorineural hearing loss (SNHL) stems from dysfunction of the cochlea, acoustic nerve, or brainstem. The loss of cochlear HCs is a major and irreversible cause of SNHL, because they are few in number (~16,000 HCs per cochlea) and are not replaced in mammals. This means that

hearing function relies on the same complement of HCs from mid-gestation to the end of life (Lim and Brichta, 2016). HCs are lost due to loud sound, ototoxic drugs (including commonly used aminoglycoside antibiotics, platinum-based chemotherapeutics, and diuretics), infections, trauma, and aging (J. B. Nadol, 1993). Acquired HC losses account for the lion's share of age-related increases in the prevalence of hearing loss (Bredberg, 1968; Davis, 1989) (Figure 1-3).

Unfortunately, treatment options for sensorineural hearing loss are limited. Aside from prevention, the main intervention is the use of hearing aids, which merely amplify sound. Cochlear implants, which bypass the inner ear entirely, can also restore some sense of hearing in the profoundly deaf, but they are invasive, expensive, and limited to the most severe cases. With 1.1 billion teenagers and young adults at risk for hearing loss through recreational noise (World Health Organization, 2020), the unmet clinical need will likely grow.

Vestibular dysfunction is also a significant public health issue. Vestibular HCs are sensitive to many of the same insults as those in the cochlea, and HC counts decrease linearly with age (Rauch et al., 2001). Over one third of adults experience vestibular dysfunction, which is associated with a 12-fold increased risk of falls (Agrawal et al., 2009). Currently, there are limited treatment options available for patients with vestibular dysfunction, and vestibular implants are not currently available. It was discovered in 1993 that mature vestibular organs in humans and other mammals have some capacity to generate replacement HCs, but the extent of this response is limited and does not appear to result in sustained functional recovery (Forge et al., 1993; Sayyid et al., 2019; Warchol et al., 1993).

Supporting cells are the source of replacement hair cells

Studies of sharks, skates, frogs, and birds revealed that these nonmammalian vertebrates maintain a lifelong capacity to add (Corwin, 1985, 1983, 1981) and regenerate (Corwin and Cotanche, 1988) HCs. This enabling them to recover hearing and vestibular function within weeks after being subjected to deafening noise or challenged with aminoglycosides (Carey et al., 1996;

Woolley et al., 2001). This is accomplished by two major mechanisms: SCs can either divide and generate progeny that can differentiate into HCs, or convert into HCs without an intervening cell division (Baird et al., 1996; Corwin and Cotanche, 1988) (Figure 1-4). These processes have been shown to spontaneously occur in mice at early developmental stages, however the capacity for HC replacement declines sharply in the first postnatal week (Burns et al., 2012a; Cox et al., 2014). This raises a fundamental question: Why can nonmammals efficiently regenerate HCs, but humans and other mammals cannot? This is the question at the basis of my dissertation.

Studying regeneration of vestibular organs enables a comparative approach

Nonmammalian vertebrates have served as a powerful model organism to study the regenerative replacement of sensory HCs. They have shown us that regeneration is possible, that SCs serve as resident stem cells, and provided insight as to the molecular mechanisms that govern the regenerative response. In this thesis, I compare the utricles of chickens and mice of various ages. This comparative approach allowed me to use both “age” and “species” as independent variables in my experiments. This extra dimension has yielded valuable insight.

Why study the utricle? First, it should be noted that the mammalian cochlea is highly distinct and difficult to study. It contains exactly one row of inner HCs, three rows of outer HCs, and a diverse milieu of SC subtypes, each with a unique morphology. No spontaneous regeneration occurs in the adult mammalian cochlea, and there are likely to be multiple layers of additional regulatory control compared to the vestibular system (Jen et al., 2019). The mature cochlea rapidly deteriorates in culture, making experimental manipulations difficult. Lastly, there is no analogous structure in the ears of nonmammals.

In contrast, the mammalian vestibular system is highly similar to that which developed 450 million years ago in bony fish. Vestibular SCs of mammals largely resemble those of nonmammals, appearing relatively undifferentiated. Vestibular SCs in adult mammals retain a limited capacity to divide and differentiate into replacement HCs, placing the development of a regenerative therapy within closer reach. The utricle in particular is a convenient vestibular organ

to study. It is relatively large, planar, and relatively easy to access. Even utricles from adults can be maintained in culture for extended periods without degenerating. It is also the best-studied vestibular organ, bringing a wealth of knowledge and tools to bear.

Shape change controls proliferation of SCs

It has long been recognized that HC loss results in the concomitant expansion of SC apical domains (Cotanche, 1987; Forge, 1985). Soon after HC regeneration was discovered in the chicken cochlea, these shape changes were proposed to trigger SC proliferation in nonmammals (Corwin et al., 1991).

Subsequent studies of isolated epithelial sheets from the utricle advanced the notion that shape changes control SC proliferation. When epithelial sheets from the embryonic mouse utricle were placed in culture, normally columnar SCs rapidly changed shape, adopting a more squamous morphology as they spread out. After changing shape, the SCs proliferated. However, in identically prepared explants from utricles of mice that were six days old, these shape changes were slower to occur. Only SCs near the edge of the explant changed shape and proliferated (Figure 1-5) (Davies et al., 2007). In explants from fifteen-day-old mice, there was almost no shape change or proliferation. Thus, in SCs of the mammalian utricle, the capacity for shape change and proliferation decline with age.

Remarkably, these age-related declines in the ability of SCs to change shape and proliferate in culture did not occur in epithelia isolated from chicken utricles (Figure 1-6). Thus, postembronic changes that occurred in the mouse utricle prevented SCs from readily spreading and changing shape, but those changes did not occur in the utricles of chickens.

Maturational reinforcement of intercellular junctions coincides with age-related declines in the plasticity of mammalian SCs

Vestibular SCs in mammals and nonmammals have a similar morphology, but the composition of their adherens junctions differs substantially (Figure 1-7). The adherens junctions of mammalian SCs contain high levels of E-cadherin, a tumor suppressor that inactivates multiple

signaling pathways important for cell proliferation (Pećina-Slaus, 2003). Their junctions also are associated with thick circumferential F-actin bands that extend across 89% of the SC on average (Burns et al., 2008; Collado et al., 2011b). The growth of these thick F-actin bands junctions closely correlates with the aforementioned declines in the capacity to change shape ($R = -0.989$) and proliferate ($R = -0.975$) in culture. In contrast, SCs of chickens, fish, and amphibians express E-cadherin at low levels, and their circumferential F-actin bands remain thin throughout life (Burns et al., 2013). These observations raised the hypothesis that the reinforced junctions limit regenerative responses in mammalian SCs.

Time-lapse recordings of HC loss in GFP::actin-expressing mice provided a clue that the reinforced apical junctions may restrict the mechanical signals arising from cell loss. In the newborn mouse utricle, HC loss evoked dynamic shape changes in SCs several cell diameters away. The SCs adjacent to the wound assembled a multicellular F-actin purse string that constricted to reseal the epithelial barrier (Burns and Corwin, 2014). Similar events were described in the utricles of chickens (Bird et al., 2010). In utricles from adult mice, however, responses to HC loss were far less dynamic. Only the SCs immediately adjacent to the lost HC responded, slowly extending lamellipodial projections to reseal the epithelial barrier (Burns and Corwin, 2014). Thus, the reinforced junctions appeared to restrict shape changes and the transmission of tension throughout the epithelium—mechanical signals that arise from cell loss and govern epithelial repair (Guillot and Lecuit, 2013). This hypothesis is explored in Chapter 3.

The question remained as to whether dismantling the reinforced junctions would allow mature mammalian SCs to proliferate. Unfortunately, a previous experiment involving conditional deletion of E-cadherin in SCs of the mouse utricle was inconclusive, as depletion of E-cadherin from intercellular junctions was slow, and accompanied by the upregulation of N-cadherin in an apparent compensatory response (M.S. Collado and J.T. Corwin, unpublished results; see Chapter 6 for discussion). Luckily, an incidental observation provided an opportunity to test

whether depletion of E-cadherin and thinning the F-actin bands would release mature mammalian SCs from proliferative quiescence. This is described in Chapter 4.

YAP integrates mechanical signals and stimulates proliferation

What is the molecular mechanism by which reinforced intercellular junctions that develop in mammalian SCs restricts their proliferative responses? In recent years, the Hippo pathway and its effector, Yes-associated protein, (YAP) have been identified as a major mechano-sensitive signaling pathway (Dupont, 2016). Mechanical signals, including the stretching of cells, induce YAP to accumulate in nuclei, where it associates with TEAD transcription factors to promote proliferation. When cells are at high density, YAP is phosphorylated by LATS1/2 kinases and sequestered in the cytoplasm (Figure 1-8).

I conducted a study to test the hypothesis that differences in the activation of YAP may account for the distinct regenerative capacities of SCs in mammals and nonmammals. The results are reported here in Chapter 5.

FIGURES AND FIGURE LEGENDS

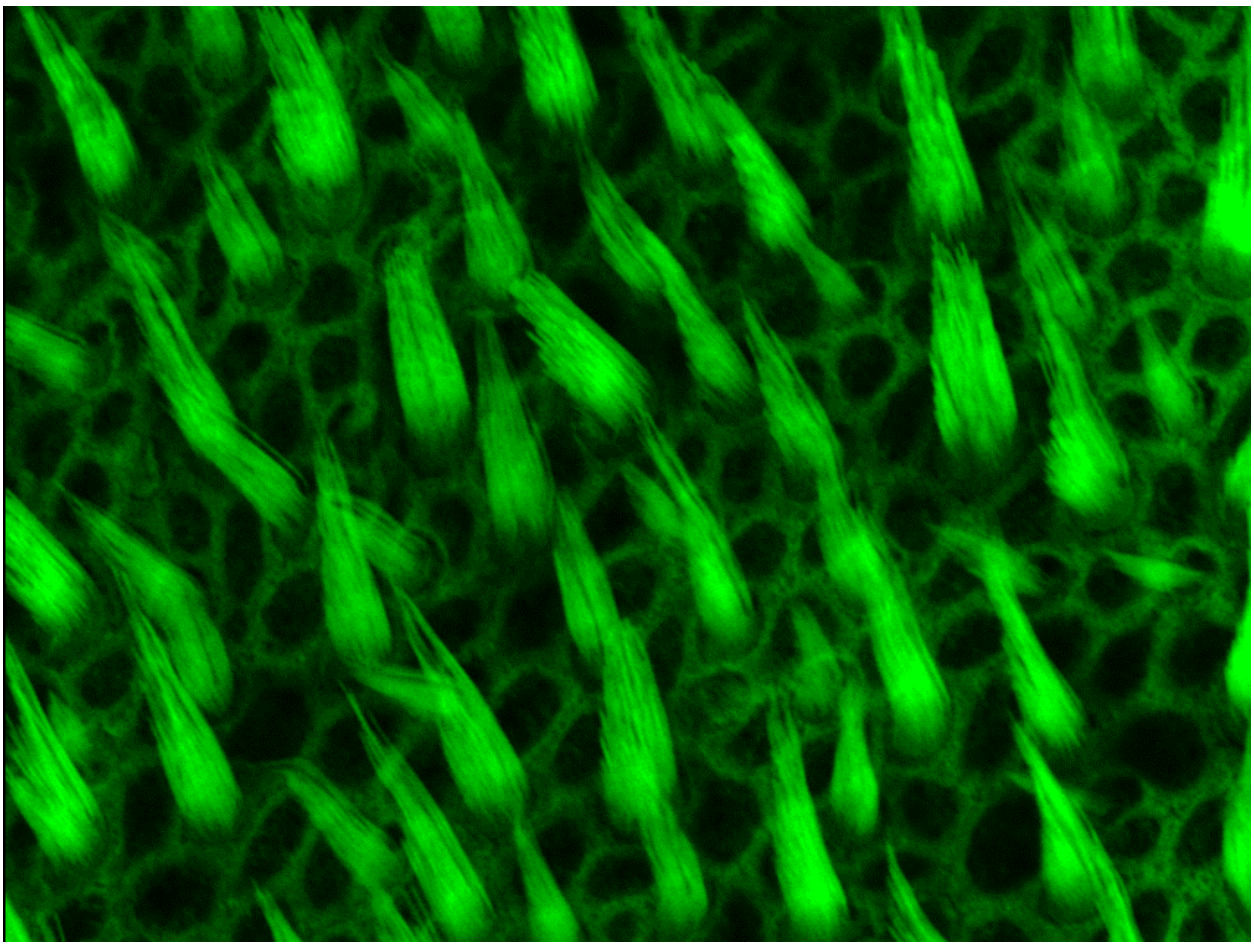

Figure 1-1. Confocal micrograph a mouse utricle stained with fluorophore-conjugated phalloidin to label filamentous actin. Hair bundles protrude from the apical surfaces of sensory hair cells (HCs), each of which is surrounded by non-sensory supporting cells (SCs).

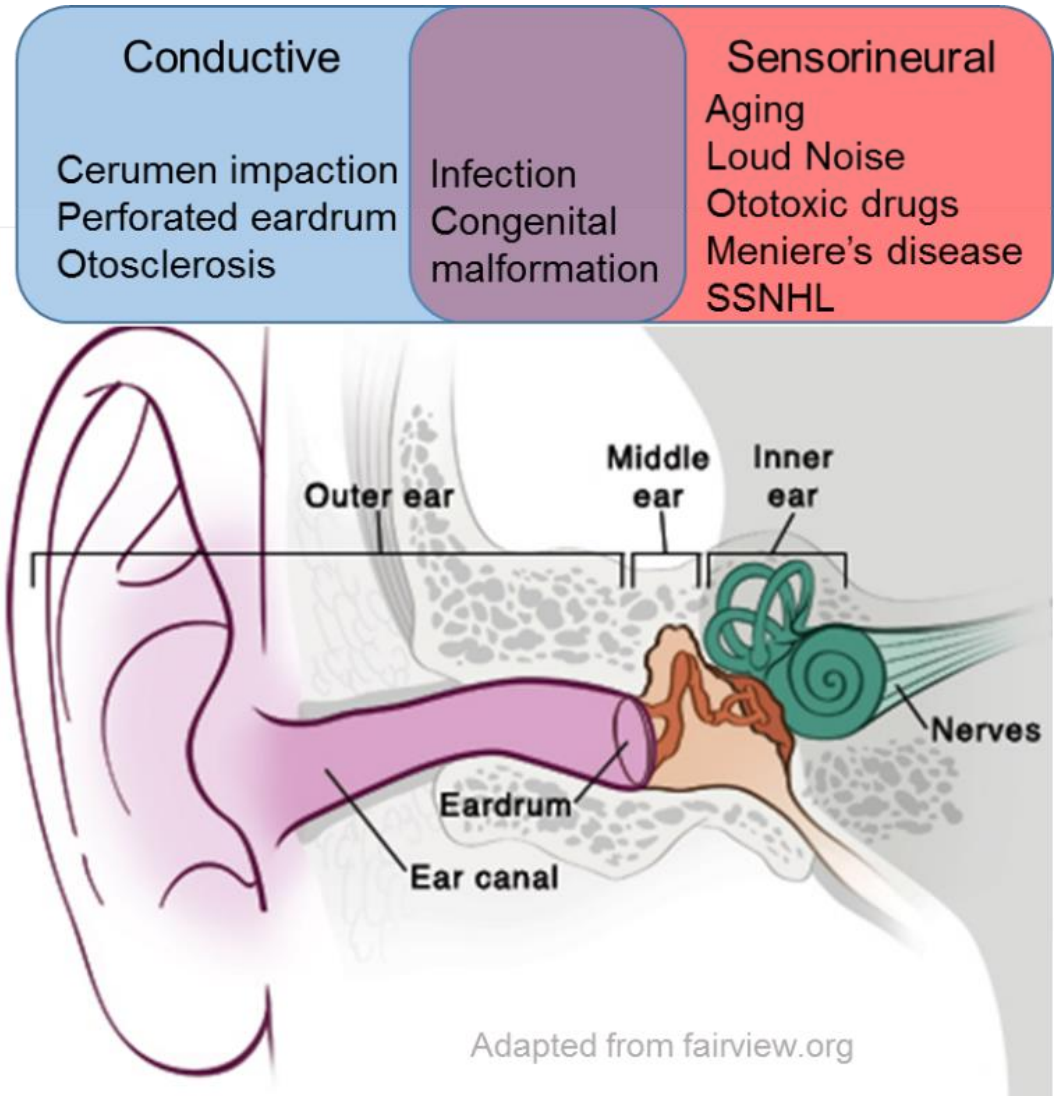

Figure 1-2. Conductive hearing loss is caused by disruption of the sound conduction pathway through the outer and middle ears. Sensorineural hearing loss arises due to pathology affecting the inner ear or nerves. SSNHL = sudden sensorineural hearing loss.

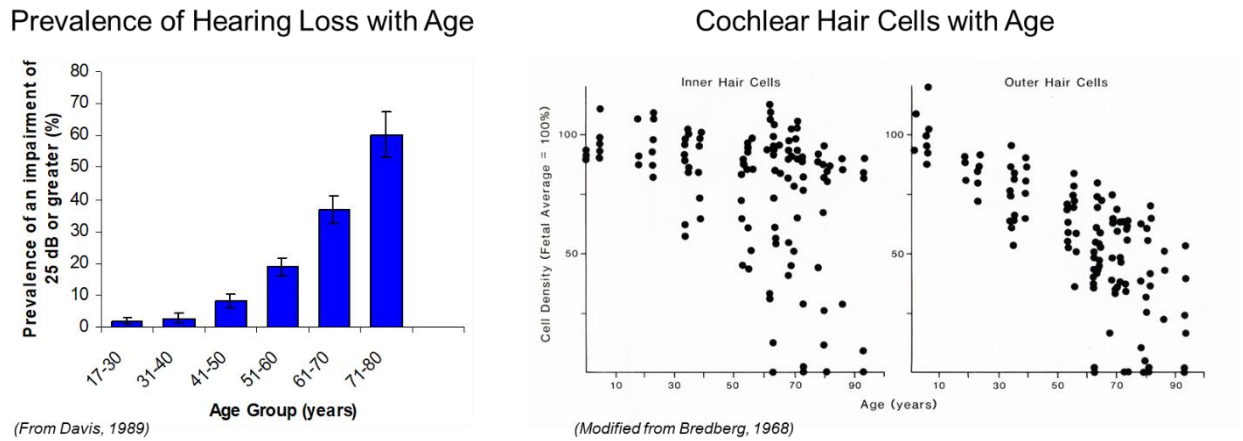

Figure 1-3. Age-related hearing loss correlates with a decline in cochlear hair cell counts. Adapted from Davis 1989 and Bredberg 1968.

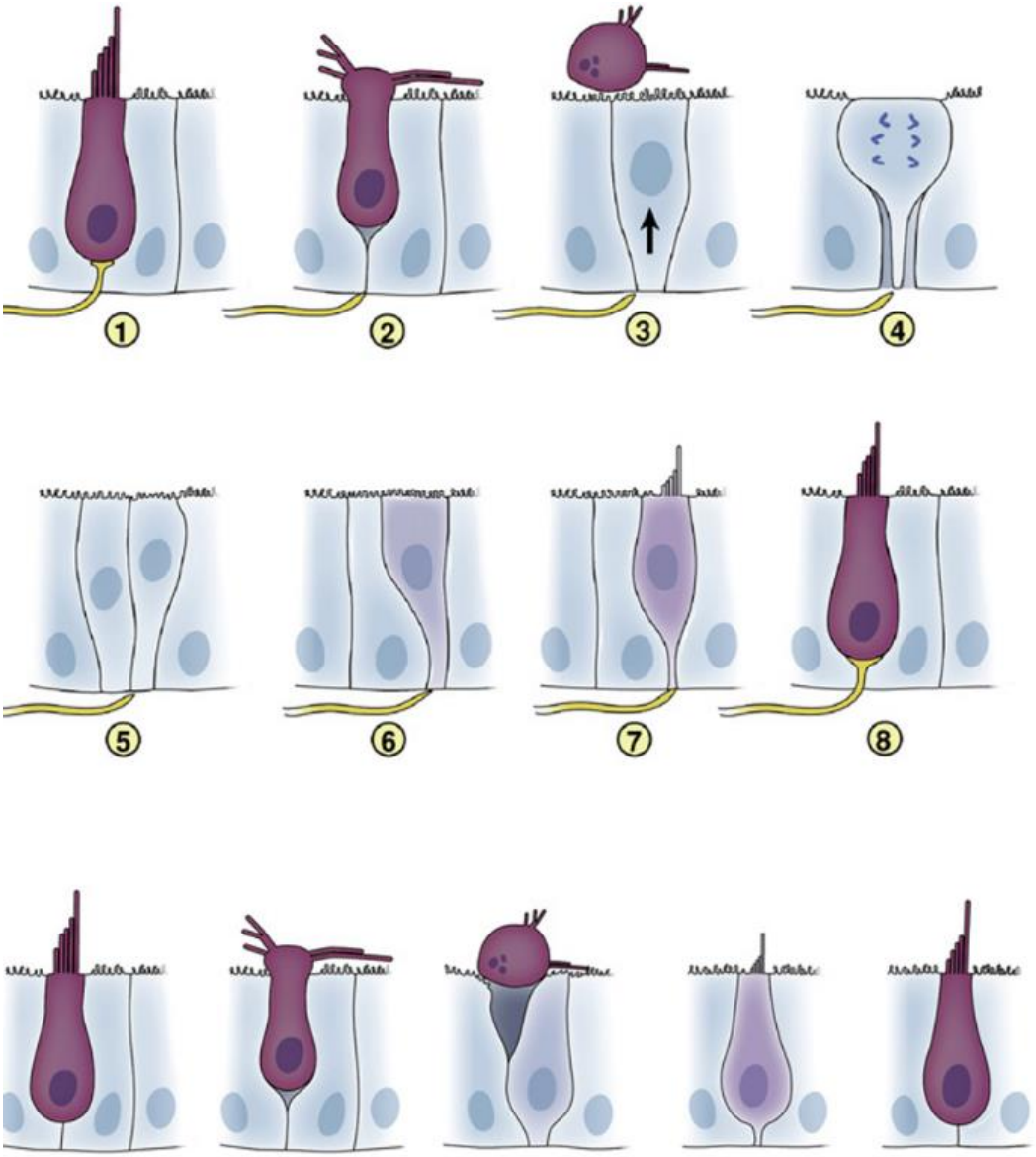

Figure 1-4. Hair cells (magenta) are regenerated by supporting cells (blue). In one mechanism, supporting cells divide and generate progeny that differentiate into replacement hair cells (top two rows). In another mechanism, supporting cells can convert directly into hair cells without an intervening cell division, a process sometimes referred to as “direct transdifferentiation” (bottom row). Adapted from Burns and Corwin 2013.

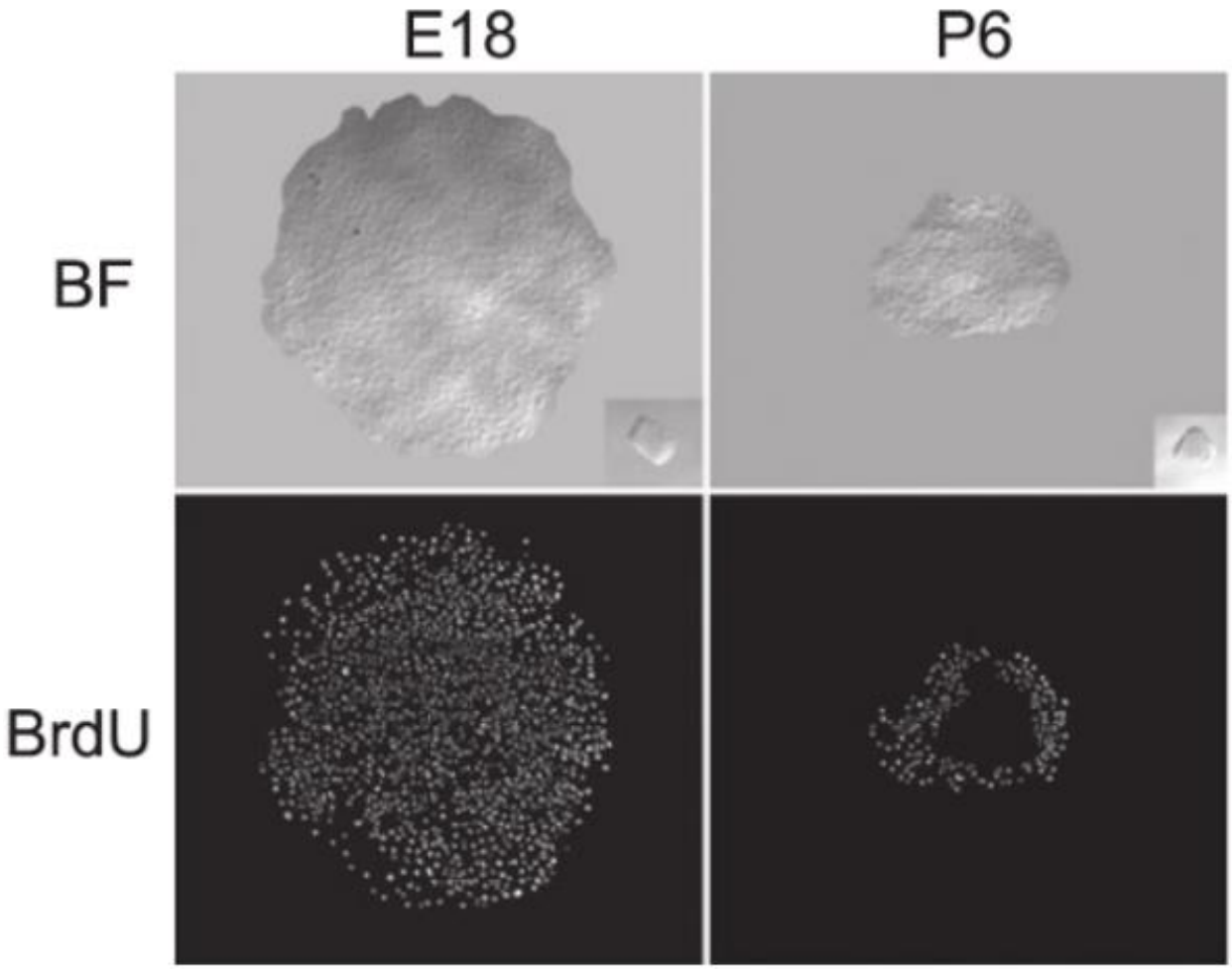

Figure 1-5. In isolated sheets of utricular epithelia from mice, SC shape changes precede and correlate with proliferation. The capacity for shape change and proliferation each decline with age. Insets depict the initial size of the explant at the start of culture, and the images depict the explants after 72 h in culture. and proliferation (BrdU) images depict Isolated sheets SCs in utricles from embryonic mice readily change shape and proliferate. E18, embryonic day 18. P6, postnatal day 6. BF, brightfield. BrdU is a marker of S-phase entry. Adapted from Davies et al. 2007.

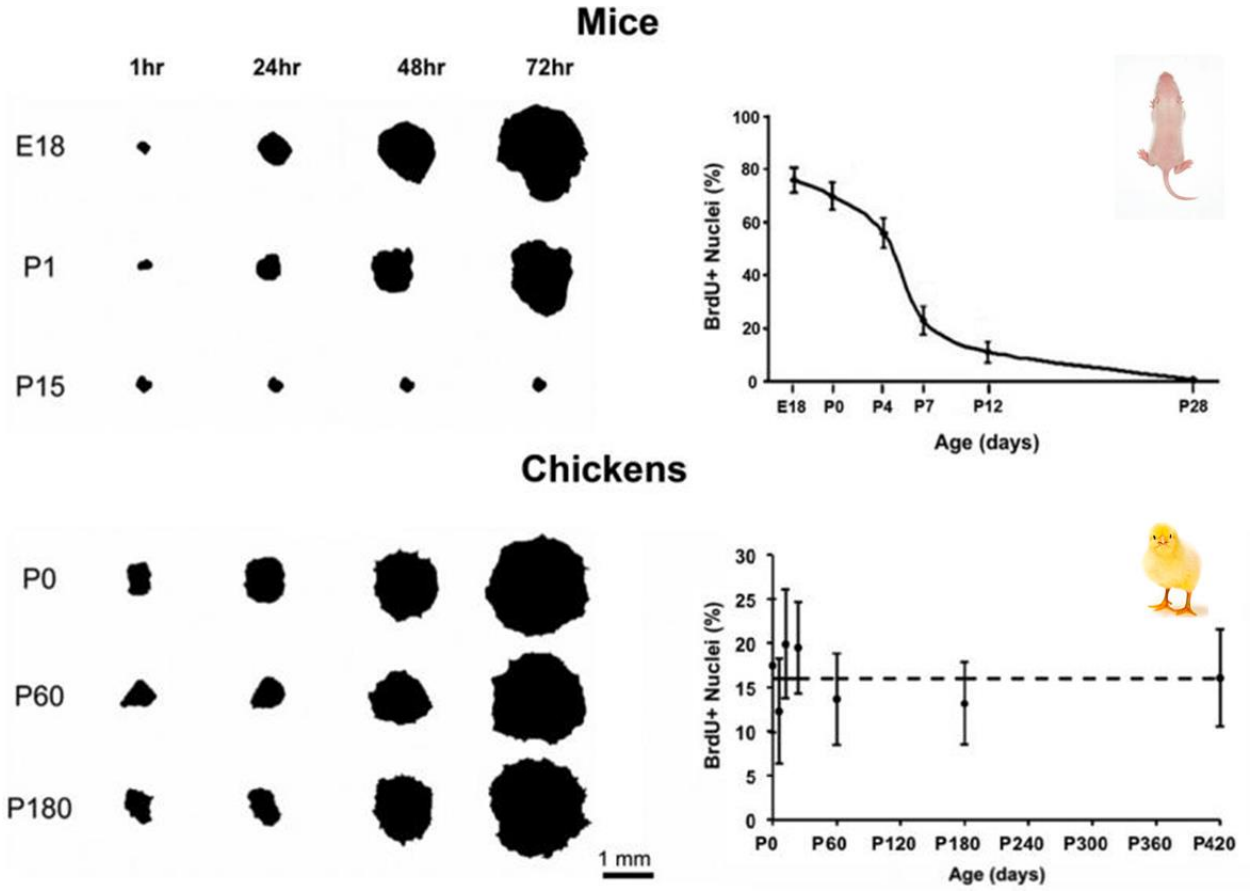

Figure 1-6. Explanted utricular epithelia from mice exhibit age-related declines in spreading and proliferation. In contrast, explanted utricular epithelia from the chickens rapidly spread and proliferate regardless of age. Adapted from Burns and Corwin 2013.

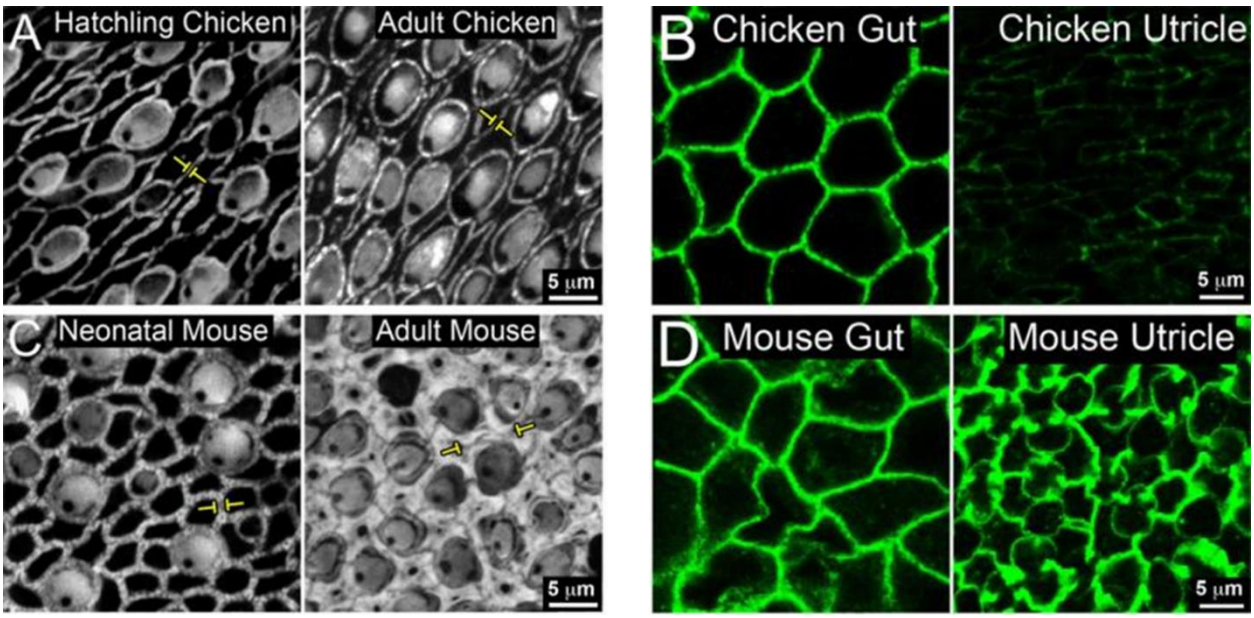

Figure 1-7. SCs in the mouse utricle develop E-cadherin-rich apical junctions that are bracketed by thick circumferential F-actin bands. SCs in the chicken utricle hardly express E-cadherin and retain thin F-actin bands throughout life. Gut was used as a positive control for E-cadherin immunostaining. Adapted from Burns and Corwin 2013.

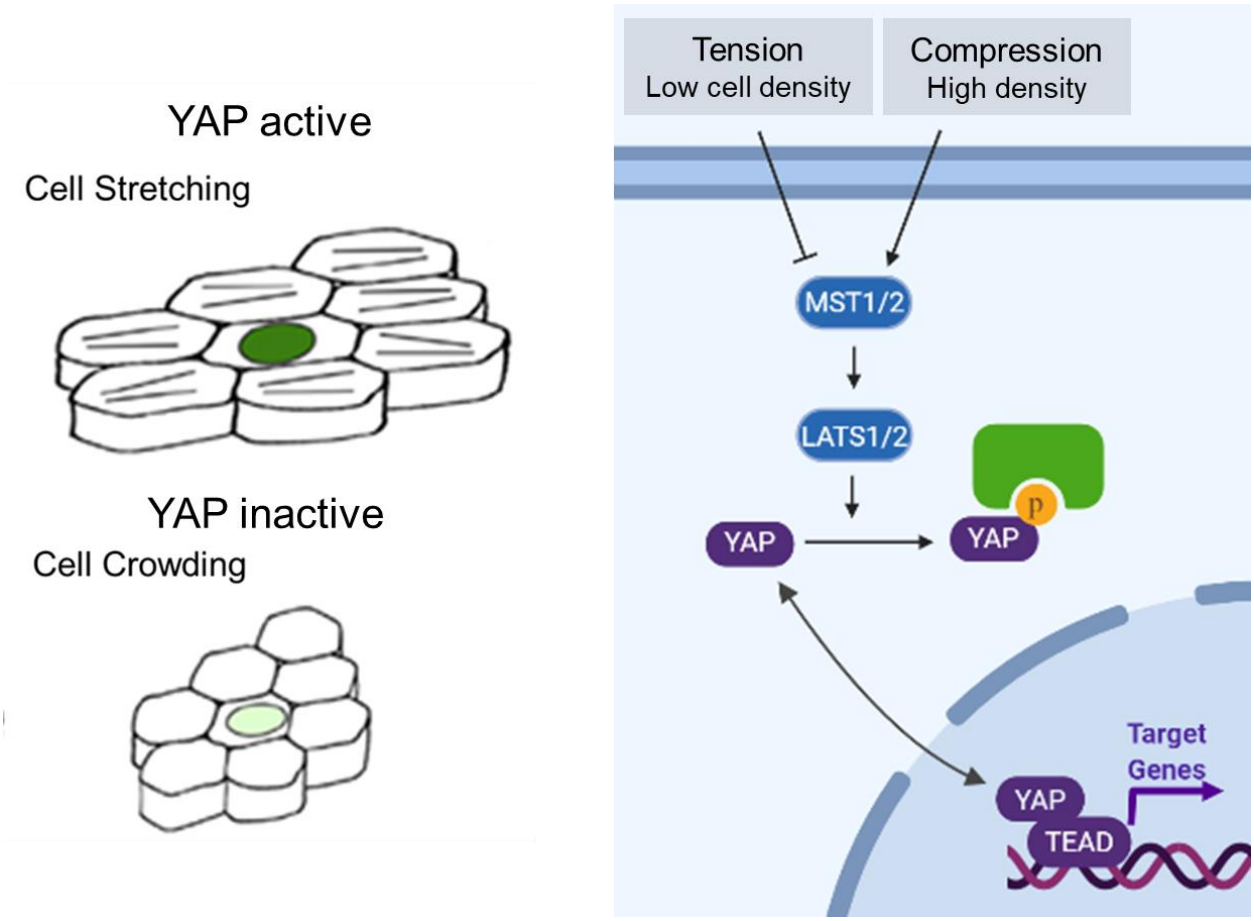

Figure 1-8. Mechanical signals such as cellular stretching induce nuclear accumulation of YAP, which partners with TEAD transcription factors to promote proliferation. In the setting of high cell density or other inactivating signals, the Hippo kinase cascade phosphorylates YAP, leading to its cytoplasmic sequestration. Adapted from Dupont 2016.

CHAPTER 2

CELL JUNCTIONS AND THE MECHANICS OF HAIR CELL REGENERATION

INTRODUCTION

Whereas SCs in birds, fish, and amphibians all appear to be relatively undifferentiated, those in mammals adopt characteristics of more highly differentiated cells. Notably, mammalian SCs develop reinforced junctions, including E-cadherin-rich adhesions that are bracketed by thick circumferential F-actin bands. These reinforced junctions have garnered attention for several reasons. First, their development tightly correlates with age-related declines in SC plasticity (Burns et al., 2008; Collado et al., 2011b). Second, SCs in birds, fish, and amphibians express little E-cadherin and retain thin circumferential F-actin bands throughout life (Burns et al., 2008, 2013). Finally, mechanosensitive signaling mechanisms such as the canonical Wnt and Hippo pathways have been shown to guide the proliferation and differentiation of SCs (Shi et al., 2014; Gnedeva et al., 2017). Are these reinforced junctions merely hallmarks of an advanced state of differentiation, or do they directly impede regenerative processes? This chapter reviews cell junctions and mechanical signaling in the inner ear with known or hypothesized roles in regeneration.

CELLS SENSE AND GENERATE FORCES

The ability of cells to sense and generate forces is essential for development, physiological function, and regeneration (Guillot and Lecuit, 2013). The mechanical stimuli that cells encounter include shear forces from fluid flow and cell migration, hydrostatic pressure, tension and compression from surroundings, and the stiffness of underlying connective tissue. These mechanical signals are transduced into biochemical signaling cascades by junctions at cell-cell and cell-matrix interfaces. Cadherin-based cell-cell junctions are especially important in epithelia, coupling individual cells into a mechanical syncytium such that mechanical stimuli propagate throughout the tissue and coordinate cellular responses (Harris et al., 2014). Junctions are linked to cytoskeletal filaments which dictate cell structure and movement. Cells remodel the

composition of their junctions and cytoskeleton in response to applied force and produce forces of their own through actomyosin contractility, cytoskeletal polymerization, and regulation of osmotic properties.

THE MATCHING OF CELL LOSS AND PRODUCTION IN HAIR CELL EPITHELIA

Spatial constraints limit proliferation in epithelia. The importance of such mechanical control is evident in HC epithelia, where cell density inversely correlates with proliferation during periods of growth, turnover, and regeneration.

Vestibular HC epithelia in sharks, rays, toads, and chickens undergo turnover, whereby spontaneously degenerating HCs are mitotically replaced such that the spatial density of HCs remains constant throughout life (Kil et al., 1997; Goodyear et al., 1999). In other epithelia, this precise matching of cell loss and proliferation is mechanically regulated along two major paradigms. In the first, ongoing cell growth and proliferation compresses neighbors, leading to their apoptosis or extrusion (Matamoro-Vidal and Levayer, 2019). In the alternative “demand-driven” system, cell loss triggers proliferation by affecting the shape and tension of remaining cells (Mesa et al., 2018).

HC epithelia operate according to the “demand-driven” model. SCs in the chicken basilar papilla remain quiescent unless HCs are lost. Treatments with caspase inhibitors that blocked ongoing HC loss associated with turnover in cultured chicken utricles also suppressed SC proliferation (Matsui et al., 2002). The proliferative response to HC loss is spatially restricted to the site of damage. This was observed in the first account of mitotic HC regeneration after acoustic overstimulation in the chicken (Corwin and Cotanche, 1988), and later demonstrated in laser microbeam experiments where the region of HC ablation could be more precisely controlled. Interestingly, the vast majority of proliferating SCs were located within 100 µm from the lesion site (Warchol and Corwin, 1996), which is about how far mechanical perturbations propagate throughout epithelial monolayers after cell loss (Karsch et al., 2017).

Although these experiments indicated that HC loss precedes SC proliferation, they did not disentangle the mechanical consequences of HC loss from its biochemical factors. Since then, studies have found that shape changes have a potent mitogenic effect on SCs, with those that spread out being more likely to proliferate than those that retain their usual columnar morphology (Meyers and Corwin, 2007; Warchol, 2002). Studies of other epithelia have shown that a combination of mechanical parameters (e.g. cortical tension) and geometric properties predict cell cycle progression better than geometric properties alone, but to date only the latter has been formally evaluated in HC epithelia (usually planar area).

A recently proposed model described how spatial constraints could control proliferation in the developing mouse utricle. It specified that elastic forces from the surrounding non-sensory tissue resist the macula's continued expansion (Figure 2-1). This, in turn, would cause an increase in cell density, leading to inactivation of YAP-TEAD signaling and cell cycle exit (Gnedeva et al., 2017). This mechanical model compared favorably to a diffusible morphogen model, better recapitulating the spatial distribution of cell cycle exit (Gnedeva et al., 2017). Using "bubble cultures" in which the external mechanical constraints could be experimentally reduced, utricles grew to supraphysiological sizes, leading to a reduction in cell density and YAP-TEAD-dependent SC proliferation. It remains to be tested whether a similar paradigm governs the cessation of SC proliferation in the context of regeneration.

SCs in nonmammals can execute four different behaviors during regeneration (Figure 2-2). They can phenotypically convert into a HC without an intervening mitosis, a process often termed "direct transdifferentiation". SCs can also divide to produce two HCs (symmetric, differentiating division), two SCs (symmetric, amplifying division), or one HC and one SC (asymmetric division). Each asymmetric division adds one HC without changing the number of SCs, but the other processes either deplete or add to the SC population. Recent evidence suggests that these different modes of regeneration may be balanced such that the density of SCs remains constant. For example, in the streptomycin-damaged chicken utricle, ~3/4 of

regenerated striolar HCs arose from via asymmetric divisions, with the remaining 1/4 inferred to arise via direct transdifferentiation (Scheibinger et al., 2018). Remarkably, the SC density remained constant, with transdifferentiation events appearing to be matched by an equal number of amplifying divisions that replenished the SC population (Scheibinger et al., 2018). In the zebrafish lateral line, almost all regenerated HCs are produced through symmetric divisions. After neomycin-mediated HC ablation, the number of differentiating and amplifying divisions were matched such that SC density remained roughly constant (Romero-Carvajal et al., 2015). These data suggest that the different modes of regeneration are governed in part by mechanical cues related to the local density of SCs.

While changes in cell density do not represent a purely mechanical signal, they inherently involve changes in cell shape and can include changes in actomyosin contractility and adhesion. Mechanical signals are by no means the only factors that promote SC proliferation, as diffusible factors and juxtacrine signals such as Notch-Delta signaling have documented roles. However, the tendency of SC proliferation to occur within and near the site of damage in cells that experience shape change is consistent with a substantial role of cell geometry and mechanical tension in promoting proliferation in concert with those diffusible ligands and juxtacrine signals.

CELLULAR JUNCTIONS IN HAIR CELL EPITHELIA

Tight Junctions

Tight junctions are the apical-most intercellular junctions in vertebrate epithelia and regulate the paracellular diffusion of ions and small molecules while restricting passage of large molecules (Figure 2-3). This barrier function is especially critical in the inner ear, where it partitions the potassium-rich interstitial fluid at the apical side of the sensory epithelium, known as endolymph, from the sodium-rich perilymph at the basolateral side. As HCs are highly vulnerable to local changes in their microenvironment, deficiency of tight junction components frequently compromises barrier function and leads to HC loss and cochlear degeneration. This presents a

challenge for studying their potential role in regeneration, which could be circumvented by studying vestibular organs, where HCs often survive such manipulation.

Whether tight junctions regulate regenerative processes in HC epithelia remains unexplored, but numerous tight junction components such as claudin 18, JAM-A, occludin, and ZO-2 are expressed in the HC epithelia and have been shown to control proliferation in other epithelia, often by sequestering signaling molecules such as ZONAB and YAP at cell junctions (Díaz-Coránguez et al., 2019; Kitajiri et al., 2004).

Adherens Junctions

Adherens junctions couple epithelial cells into a cohesive mechanical syncytium and are the primary interface through which they sense the mechanical forces arising from cell loss. The cadherin-based intercellular adhesions interface with the F-actin cytoskeleton via catenin linkers, which serve as structural and signaling molecules (Figure 2-4). Actomyosin contractility at adherens junctions generates tension that drives cellular shape change during wound closure. The maturational reinforcement of adherens junctions in mammalian SCs has been deeply implicated in their age-related loss of plasticity.

Cadherins

Classical cadherins are the major adhesion proteins at adherens junctions and require Ca^{2+} ion for binding in trans. Of the more than 350 members of the cadherin superfamily, the best-studied are Epithelial (E-) cadherin and Neural (N-) cadherin. E-cadherin is a tumor suppressor that restricts proliferation through a variety of mechanisms, including by activating p27kip1, limiting signaling by receptor tyrosine kinases such as EGFR, inhibiting canonical Wnt signaling, and suppressing YAP-TEAD transcriptional activity (Mendonsa et al., 2018). The downregulation of E-cadherin is a hallmark of epithelial-mesenchymal transition and is often accompanied by the upregulation of N-cadherin.

The expression of E-cadherin increases 6-fold between P1 and adulthood in the mouse utricle, where it is enriched at SC-SC junctions (Figure 2-5) (Collado et al., 2011b), and increases

56% between P0 and P7 in the organ of Corti, where it is expressed in lateral domain including pillar cells, Deiters cells, and to a lesser extent outer hair cells (OHCs) (Luo et al., 2018). SCs in birds, fish, and express little E-cadherin (Figure 2-6) (Warchol, 2007; Burns et al., 2013). Thus, E-cadherin expression correlates not only with age-dependent declines in the plasticity of mammalian SCs, but also with the differences in regenerative capacity between mammals and other vertebrates.

The factors driving E-cadherin expression in mature mammalian SCs are not well understood, and are likely related to broader mechanisms of SC maturation. GSK3β-mediated suppression of canonical Wnt signaling is likely involved in enhancing E-cadherin transcription, as inhibiting GSK3β or expressing stabilized β-catenin depleted E-cadherin and evoked SC proliferation in the developing utricle and cochlea (Lu and Corwin, 2008; Shi et al., 2014). GSK3β may also repress Snail and Slug, transcription factors known to repress E-cadherin transcription (Collado et al., 2011b). Differences in Wnt-responsiveness may prevent this downregulation from occurring in certain subpopulations of mature SCs, as GSK3 inhibition depleted E-cadherin from mature striolar SCs, but not those in the extrastriola (Kozlowski et al., 2020).

E-cadherin has been implicated in preventing the phenotypic conversion of SCs into HCs. Notch inhibition led to internalization of E-cadherin in striolar SCs and Deiters cells of neonatal mice as they began to convert into HCs (Collado et al., 2011b; Luo et al., 2018). However, the SCs from older mice failed to internalize E-cadherin and convert into HCs. The downregulation of E-cadherin was not associated with changes in E-cadherin transcription but did require protein synthesis (Collado et al., 2011b). It remains unclear whether the accumulation of E-cadherin limits conversion, or whether age-related changes in Notch responsiveness prevent SCs from enacting a gene expression program that leads to the internalization of E-cadherin.

Direct manipulations of E-cadherin in the inner ear are needed to establish whether causally limits SC proliferation and direct transdifferentiation, but have proven challenging; upon conditional knockout of E-cadherin in mature, Plp1+ SCs, depletion of E-cadherin from junctions

occurred slowly and was accompanied by an increase in N-cadherin expression (M. S. Collado and J. T. Corwin, unpublished results). It was shown that E-cadherin transfection in an SC-derived cell line increased the number of intercellular junctions, reduced proliferation, and inhibited expression of certain HC-specific genes including Myo7a (Hackett et al., 2002), but these promising results require follow-up.

N-cadherin is expressed throughout the utricular macula and in medial region of the organ of Corti, including inner hair cells and phalangeal cells. It is also expressed in HC epithelia of nonmammalian vertebrates. Microbeads coated with an N-cadherin function-blocking antibody bound to the edges of epithelial sheets of the chicken utricle and attenuated SC proliferation (Warchol, 2002), leading to the hypothesis that the loss of N-cadherin adhesions upon HC loss represents a mitogenic injury signal. However, it is unclear whether proliferation was reduced by N-cadherin-specific contact inhibition, or the mechanical effects of limiting SC spreading.

Little is known about the expression and function of other cadherins in the inner ear, though R-cadherin has been localized to the utricular macula of neonatal mice (Burns et al., 2015).

Catenins

Catenins are intracellular components of adherens junctions that connect the cytoplasmic tail of cadherins to the F-actin cytoskeleton. They also signal in the canonical Wnt and YAP/TAZ-TEAD pathways (Nelson and Nusse, 2004; Schlegelmilch et al., 2011).

p120-catenin stabilizes cadherin/catenin complexes. Deletion of p120-catenin depleted levels of E- and N-cadherin in the developing cochlea, resulting in convergent extension defects (Chacon-Heszele et al., 2012), but its role regulating SC plasticity has not been directly tested. p120-catenin is upregulated during maturation of the organ of Corti, where it colocalizes with E-cadherin contribute to the age-related decline in E-cadherin internalization and SC-to-HC conversion upon treatment with Notch inhibitors (Figure 2-7) (Luo et al., 2018).

β-catenin binds the cytoplasmic tail of cadherins and links them to the actin cytoskeleton via α-catenin. In addition to this structural role, β-catenin serves as the transcriptional co-activator

in canonical Wnt signaling. It is thought that these different functions are antagonistic, competing for the same pool of β-catenin (Nelson and Nusse, 2004). This is an attractive hypothesis, but surprisingly, the expression of β-catenin at cell membranes in the utricle is not reported to increase with age, despite the maturational increase in E-cadherin expression in mammalian SCs (Collado et al., 2011b).

The structural role of β-catenin was shown to be required for establishment of the mediolateral boundary in the developing organ of Corti, independent of its function in Wnt signaling (Jansson et al., 2019). Through its Wnt signaling function, β-catenin is required both for SC proliferation as well as HC differentiation, as it directly binds the enhancer of *Atoh1*, the master regulator of HC differentiation (Jacques et al., 2012; Shi et al., 2014).

Expression of a gain-of-function variant of β-catenin potentiated regenerative proliferation and mitotic HC replacement in Lgr5+ SCs of the neonatal mouse utricle and cochlea after diphtheria-toxin mediated HC ablation (T. Wang et al., 2015; Atkinson et al., 2018). In those studies, β-catenin activation had no mitogenic effect in the absence of damage (T. Wang et al. 2015; Atkinson et al. 2018). This corresponds to functional evidence that HC loss activates canonical Wnt signaling, leading to the upregulation of the canonical Wnt target gene Lgr5 in striolar SCs of the neonatal mouse utricle (T. Wang et al. 2015), and Wnt-induced proliferation in the zebrafish lateral line (Romero-Carvajal et al., 2015). However, the evidence that β-catenin accumulates in nuclei of SCs after damage is rather limited. Some nuclear β-catenin was observed in forskolin-treated sheets of utricular epithelium from the rat (Kim et al., 2004) and in SCs of the delaminated chicken utricle (Warchol, 2002).

The proliferative response to β-catenin stabilization declines with age in the mouse cochlear and utricular epithelium (Lu and Corwin, 2008; Samarajeewa et al., 2018), despite evidence that TCF/Lef reporters can still be activated and continued expression of Wnt pathway components (Geng et al., 2016). This has been attributed to age-dependent changes in chromatin accessibility or cross-talk with other signaling pathways, but another possibility is that the age-

dependent increase in E-cadherin could sequester β-catenin at SC apical junctions. Consistent with that possibility, extended culture of adult mouse utricles in EGF and a GSK3 inhibitor led to depletion of E-cadherin in striolar SCs, which was accompanied by a reduction in apical β-catenin expression and proliferation of those SCs (Kozlowski et al., 2020).

α-catenin links cadherin adhesions to the F-actin cytoskeleton while also acting as a tumor suppressor, inhibiting YAP/TAZ signaling (Schlegelmilch et al., 2011). Like p120-catenin, α-catenin colocalizes with E-cadherin in HC epithelia, where its expression is enriched at SC-SC contacts and increases during postnatal maturation (Gnedeva et al., 2017; Leonova and Raphael, 1997). Whether α-catenin regulates proliferation in the inner ear remains unknown. Upon conditional deletion of αE-catenin in Plp1+ SCs in the murine utricle, depletion of the protein from cell junctions was slow and accompanied by the upregulation of αN-catenin (M. S. Collado and J. T. Corwin, unpublished results). Dual knockout of αE-catenin and αN-catenin may be required to circumvent this apparent compensatory upregulation.

Immunoglobulin Superfamily Cell Adhesion Molecules

Cell adhesion molecules of the immunoglobulin (Ig) superfamily form homophilic, calcium-independent interactions. Neural cell adhesion molecule (NCAM) and L1 are expressed in the developing mouse cochlea (Whitlon and Rutishauser, 1990; Whitlon et al., 1999). These molecules likely regulate axon guidance, but have been shown to regulate proliferation of other cell types (Brand et al., 2013).

Nectins are calcium-independent adhesion molecules at adherens junctions that connect to the F-actin cytoskeleton via afadins. OHCs express Nectin-1 and Deiters cells express Nectin-3, and the heterophilic interaction of these molecules facilitates the checkerboard-like cellular patterning of the reticular lamina (Togashi et al., 2011). There is some evidence implicating nectins in the control of cell proliferation (Takai et al., 2008), but this has not been investigated in the inner ear.

Desmosomes

Desmosomes are button-like intercellular contacts associated with intermediate filaments. They consist of desmogleins and desmocollins, which are transmembrane adhesive proteins whose cytoplasmic tails bind plakoglobin. Plakoglobin, in turn, binds desmoplakins, which link to intermediate filaments.

Desmosomes are prominent at SC-SC junctions in the organ of Corti, but absent from contacts between OHCs and Deiters cells (Gulley and Reese, 1976). They have also been visualized on Type II HCs of the vestibular epithelium (Meiteles and Raphael, 1994). However, desmosomal contacts have received little attention in the inner ear following these initial electron microscopy studies. In the years since, studies of epidermis have revealed roles of desmosomal proteins in proliferation and differentiation (Johnson et al., 2014). For example, Desmoglein 1 promotes differentiation of keratinocytes by suppressing EGFR signaling (Getsios et al., 2009), and Desmoglein 3 is reported to regulate E-cadherin remodeling and YAP localization in response to mechanical loading (Uttagomol et al., 2019).

Focal Adhesions and Hemidesmosomes

Focal adhesions are integrin-based contacts to the extracellular matrix (ECM) that link to the F-actin cytoskeleton. Integrins are comprised of an α and β subunit, and their affinity for different substrates depends on which subunits are expressed, the presence of divalent cations, and modifying adapter molecules. Hemidesmosomes are integrin-based adhesions to the ECM that link to intermediate filaments. Little is known about the presence and role of these structures in HC epithelia, though a limited number of studies have shown that manipulation of integrin signaling can control SC spreading and proliferation on 2D culture. Transmission electron micrographs of the SC-ECM boundary of the mouse utricle revealed the age-dependent maturation of electron-dense regions suggestive of hemidesmosomal plaques (Figure 2-) (Davies et al., 2007). Age-dependent changes in integrin composition correlate with a postnatal decline in spreading of epithelial sheets from the mouse utricle. The spreading and proliferation of SCs in the sheets was limited by a function-blocking antibody to integrin α6 (Davies et al., 2007). It will

be necessary to investigate the role of integrin signaling *in vivo* or in organotypic culture, where SCs remain in contact with their native ECM.

Focal adhesion kinase (FAK) and Src are tyrosine kinases that localize to focal adhesions and are activated upon adhesion. In delaminated epithelial sheets from the chicken utricle, the extent of SC spreading and proliferation correlated with the concentration of fibronectin, and FAK localized to focal contacts along with phosphotyrosine immunoreactivity (Warchol, 2002). Concordant with these observations, a fibronectin-FAK-Src axis activates YAP in other epithelial cells in 2D culture (Kim and Gumbiner, 2015), however it remains untested whether FAK or Src are required for SC proliferation.

Integrin signaling is influenced by the biochemical and mechanical characteristics of the basal lamina, and studies of delaminated utricular sensory epithelia have shown that SC spreading and proliferation varies depending on substrate composition and stiffness (Collado et al., 2011a; Davies et al., 2007). Specific components of the basement membranes have been identified (Davies et al., 2007; Ishiyama et al., 2009), but it is not known whether these components change throughout development, nor have their mechanical properties been investigated.

Gap Junctions

Gap junctions are prevalent in SCs in all vertebrates, forming plaques that can exceed 10 μm^2 that facilitate rapid intercellular communication (Jagger and Forge, 2015). HCs and SCs are not connected via gap junctions.

Gap junctions are essential for the regulation of certain developmental and repair processes in HC epithelia (Jagger and Forge, 2015). Mutations in *GJB2*, which encodes connexin 26, are the most common cause of non-syndromic deafness, and conditional deletion of *Gjb2* in newborn mice affected development of phalangeal processes in Deiters cells and reduced microtubule formation in pillar cells (Chen et al., 2018). Connexin 30 is not essential for cochlear development, but facilitates the coordination of SCs in response to HC loss. Rather than multiple

SCs collaborating to reseal the epithelial barrier, only one SC immediately adjacent to the lost HC expands to occupy the wound (Forge et al., 2013). A similar finding was shown in the chicken cochlea, where pharmacologic blockade of gap junction intercellular communication prevented the apical extrusion of HCs after gentamicin treatment, allowing degenerating HC corpses to remain in the epithelium (Figure 2-9) (Jagger et al., 2014). It remains unknown how gap junctions lead to the coordination of SC responses to HC loss, and whether blocking their communication impairs SC proliferation in nonmammals.

Structure and Regulation of the circumferential F-actin Bands in Supporting Cells

Maturational Growth of Circumferential F-actin Bands in Mammalian Supporting Cells

All epithelial cells possess circumferential bands of F-actin that bracket their apical junctions. As mammalian SCs mature, their circumferential F-actin bands become exceptionally thick and stable (Burns et al., 2008; Burns and Corwin, 2014). The widths of the F-actin bands across SC-SC junctions increase five-fold postnatally in the mouse utricle, ultimately extending across 89% of the SC on average (Figure 2-10). The growth of the F-actin bands strongly correlates to age-related declines in spreading ($R = -0.989$) and proliferation ($R = -0.975$) of SCs in explanted sheets of delaminated utricular epithelia. In contrast, nonmammalian SCs retain thin F-actin bands and readily spread and proliferate throughout life. These findings led to the hypothesis that the reinforced F-actin bands may limit the regenerative responses of mature, mammalian SCs.

This hypothesis remains to be directly tested, because there has not yet been a way to perform a direct experimental manipulation of the F-actin bands. One potential avenue to do so would be to identify actin crosslinkers within the bands and test whether their conditional deletion in mature mammalian SCs would restore some proliferative capacity. Another approach would be

to identify and perturb the mechanisms required for growth of the bands, though these remain unknown.

Recently, it was shown that EGF and a GSK3 inhibitor each thin the F-actin bands in cultured utricles from mature mice (Kozlowski et al., 2020), presenting an indirect but nonetheless informative opportunity to study the influence of the bands on SC proliferation without the need for harsh treatments with actin-depolymerizing agents (Figure 2-11). Treatment with both agents in combination thinned the F-actin bands in SCs throughout the macula to levels normally present in newborn mice. This led to a depletion in E-cadherin in striolar SCs, followed by a resurgence of proliferation exclusively in that region. Thus, while thinning the F-actin bands is not sufficient to release extrastriolar SCs from their state of persistent quiescence, the results did not refute the hypothesis that the thick F-actin bands restrict proliferation in mature mammalian SCs. It remains unknown which intracellular signaling pathways downstream of EGFR and GSK3 inhibition mediated dismantling of the F-actin bands.

Though the dimensions of the F-actin bands in mammalian SCs have been extensively measured, their ultrastructure has not been characterized. Whether the F-actin is present as bundles or branched filaments influences whether nonmuscle myosin II can efficiently generate tension on the network (Ennomani et al., 2016). In typical epithelial cells, the apical domain size is regulated by continuous actomyosin contractility along the zonula adherens. The robust and mechanically stable F-actin network at the apical junctions of mature mammalian SCs may obviate the need for this ATP expenditure by passively stabilizing the reticular lamina. At the same time, limiting the influence of actomyosin contractility could limit the activation of intracellular signaling pathways that usually respond to changes in epithelial tension, such as YAP-TEAD (Pan et al., 2016).

Sarcomeric Actomyosin Network at Cochlear Apical Junctions

The circumferential actomyosin network in the organ of Corti of neonatal rodents is stereotypical of other simple epithelia. The circumferential F-actin bands associate with regularly

spaced (~400-600 nm), bipolar filaments of nonmuscle myosin II that interlace with the actin crosslinker α-actinin1, reminiscent of a sarcomeric network (Figure 2-12) (Ebrahim et al., 2013). Consistent with the idea that actomyosin contractility exerts tension at these apical junctions, treatments with blebbistatin, an inhibitor of myosin II contractility, caused a reversible expansion of the apical surfaces of HCs and SCs in the neonatal organ of Corti (Ebrahim et al., 2013; Cohen et al., 2019). Whether such expansion would occur in the mature organ of Corti, which has a stiffer reticular lamina and thicker circumferential F-actin bands in SCs that surround HCs (Szarama et al., 2012; Burns et al., 2013), has not been directly tested (Figure 2-13). However, experimental induction of HC loss has been shown to cause significant contraction of the reticular lamina in E18 mice, but not in adults (Anttonen et al., 2017).

Rho GTPases in the organ of Corti

Rho GTPases regulate cytoskeletal dynamics at cell junctions and assume a variety of functions depending on the local availability of scaffold proteins, effector molecules, guanine nucleotide exchange factors (GEFs), GTPase activating proteins (GAPs), and guanine nucleotide dissociation inhibitors (GDIs) (Arnold et al., 2017). RhoA, Rac1, and Cdc42 are three well-studied members of this family of 20 proteins.

Active RhoA interacts with formin to promote F-actin bundling and Rho-associated coil-coil kinase (ROCK), which phosphorylates myosin regulatory light chain to promote actomyosin contractility (Arnold et al., 2017). Deletion of RhoA in cochlear SCs did not affect junctional maturation in SCs (Anttonen et al., 2017), but RhoA has been implicated in wound closure. Closure of excision lesions in mouse utricles was accelerated by treatments with lysophosphatidic acid, which activates RhoA through GPCR signaling. Conversely, pharmacological inhibition of ROCK prevented wound closure (Meyers and Corwin, 2007).

The role of Rac1 in mature HC epithelia has not been investigated. Co-deletion of Rac1 and Rac3 in the otocyst disrupted E-cadherin and ZO-1 expression, severely impairing morphogenesis (Grimsley-Myers et al., 2012).

Cdc42 regulates the development of F-actin bands and adherens junctions in Deiters and pillar cells of the cochlea, and is downregulated in the organ of Corti by P20 (Anttonen et al., 2012). The structural defects that result from Cdc42 deletion in neonatal stages eventually lead to collapse of the basal organ of Corti in adult mice (Anttonen et al., 2012). Cdc42 is required in Deiters cells for proper wound closure and barrier integrity after OHC loss (Anttonen et al., 2014).

MECHANICS OF HAIR CELL LOSS

In most HC epithelia, HCs have convex, flask-like shapes and are assumed to be more rigid than SCs, which surround HCs and conform to their shape. One exception is the mammalian organ of Corti, in which SCs surround HCs but adopt highly specialized morphologies themselves. SCs span from the basement membrane to the reticular lamina, but HCs do not maintain contact to the basement membrane. Thus, HC losses generate mechanical tension at the level of adherens junctions, but would not perturb SC-ECM contacts, at least initially.

Remodeling of Supporting Cell Junctions During Repair

As HCs degenerate, neighboring SCs remodel their apical F-actin cytoskeleton and form new junctions such that barrier function is maintained (Leonova and Raphael, 1997). To accomplish this, tight junctions between the degenerating HC and neighboring SCs remain intact temporarily as SCs extend underneath the degenerating HC's cuticular plate to form a new junction, often referred to as a "scar" (Leonova and Raphael, 1997). Multiple SCs participate in the wound closure, coordinating to extrude the dying HC or sever its soma from the cuticular plate. Typically, the three adjacent SCs surrounding the dying HC participate in wound closure. However, transmission electron micrographs from the mouse cochlea have indicated that basolateral processes of more distant Deiters cells or Hensen's cells contribute to the scar in some cases, suggesting that the damage signal emanating from the lost HC propagates beyond its immediately adjacent SCs (Anttonen et al., 2017). It is unclear how such processes are guided

to the wound site or whether this phenomenon occurs in other HC epithelia, but it could be unique to the mammalian cochlea where there is substantial space between basolateral cell membranes.

The nature and speed of wound closure is dictated by the wound curvature and organization of F-actin at SC apical junctions. Since HCs are round, SCs at the wound margin have negative (i.e. concave) curvature. This curvature promotes the formation of actomyosin cables that close in a “purse-string” mechanism in other epithelia, as opposed to lamellipodial protrusions which tend to form at wound edges of positive curvature (Ravasio et al., 2015). Consistent with this, a supracellular F-actin cable forms after large excision lesions in mouse utricles (Meyers and Corwin, 2007). Time lapse microscopy showed that the wounds became more circular as they progressed, were halted by ROCK inhibition, and accelerated by treatment with lysophosphatidic acid (LPA), indicating that actomyosin contractility was required for wound closure (Meyers and Corwin, 2007).

Subsequent studies revealed that similar processes govern wound closure after aminoglycoside-mediated HC losses. In utricles of chickens and newborn mice, SCs formed a supracellular F-actin cable which constricts beneath the HC cuticular plate. This occurred rapidly in chicken utricles, which required only 3-6 minutes to close the wound (Bird et al., 2010). Wound closure was slower in the newborn mouse utricle, occurring within one hour of HC death, and in adult mice this process required up to 4 h (Burns and Corwin, 2014). Wound closure was reported to qualitatively differ in adult mouse utricles. The thick F-actin bands remained in place, and F-actin purse strings did not form. Rather, F-actin formed lamellipodial structures that resealed the wound (Burns and Corwin, 2014). Though it remains to be shown, these differences in the speed and mechanism of wound closure may be accounted for by the reinforcement of circumferential F-actin bands in mammalian SCs. Not only do the bands appear to make mammalian SCs more resistant to deformation, but branching and crosslinking within the thick F-actin bands would reduce the efficiency of F-actin contractility (Ennomani et al., 2016).

These differences in wound closure are likely to have consequences for the activation of regenerative processes in SCs. The rapid wound closure by SCs in chickens and newborn mice deforms SCs several cell diameters away from the wound, which is sufficient to activate YAP and β-catenin signaling in other epithelia (Benham-Pyle et al., 2015). In mature mammalian utricles, only the SCs immediately adjacent to the lost HC respond.

Elimination of Dying Hair Cells

After SCs reform intercellular junctions beneath the cuticular plate of a dying HC, the degenerating HC corpse is eliminated via phagocytosis. Along with professional phagocytes (Kaur et al., 2015), SCs can also phagocytose HCs (Anttonen et al., 2014). SCs in adult mice develop a phagosome that can persist for at least 15 hours (Monzack et al., 2015). In the mouse utricle, phagosomes are concentrated in the peristriolar region and are occasionally associated along with F-actin “spikes” that contain cross-linker espin (Bucks et al., 2017). SCs of the chicken utricle have been observed to collaborate to create a phagosome that engulfs the soma of degenerating HCs (Bird et al., 2010).

Besides phagocytosis within the epithelium, dead and dying HCs can also be apically extruded from the epithelium, with the predominant mechanism varying by species and tissue (Francis and Cunningham, 2017). Extrusion does not result in the separation of the hair bundle from the HC soma and appears to be the more common elimination mechanism in HC epithelia of nonmammalian vertebrates (Mangiardi et al., 2004). In mammals, extrusion has been documented in the vestibular but not auditory epithelia (Li et al., 1995). Extrusion may produce larger, more rapid deformations in SCs than phagocytic clearance, and thus constitute a more potent signal for regenerative processes.

INTRACELLULAR SIGNALING ASSOCIATED WITH MECHANICAL SIGNALS

Cell loss elicits tension changes that widely propagate throughout epithelia (Karsch et al., 2017). These forces are transduced into biochemical signaling cascades that can facilitate

regenerative responses. Some prominent mechanosensitive pathways are summarized here with known or potential roles in HC regeneration.

YAP/TAZ and the Hippo Pathway

YAP and its paralog TAZ are transcriptional co-activators that integrate mechanical and biochemical signals to control cell behavior (Figure 2-14) (Totaro et al., 2018). In the evolutionarily conserved Hippo pathway, MST1/2 kinases (Hippo in *Drosophila*) phosphorylate LATS1/2 (Warts in *Drosophila*), which in turn phosphorylate YAP/TAZ to induce their cytoplasmic sequestration and degradation. Absent this inhibitory phosphorylation, YAP/TAZ accumulate in nuclei and partner with transcription factors such as TEADs to mediate changes in gene expression that can control proliferation and stemness.

SC proliferation is associated with changes in intraepithelial tension, cell density, substrate stiffness, and cadherin adhesion. All of these stimuli affect YAP/TAZ activity in other epithelia, but only recently has the role of YAP in SC proliferation been directly explored.

Damage activates YAP-TEAD signaling in SCs. Mechanical lesions in neonatal mouse utricles caused YAP to enter SC nuclei and mediate TEAD-dependent proliferation (Gnedeva et al., 2017). The extent of nuclear accumulation correlated to the degree of cellular shape change, indicative of mechanical control. However, HC loss was not sufficient to induce detectable nuclear accumulation of YAP in SCs of the murine utricle, even in neonates. In contrast, HC loss in the chicken utricle induced nuclear translocation of YAP in SCs, and pharmacologic inhibition of YAP-TEAD signaling attenuated regenerative proliferation (Rudolf et al., 2020). Thus, the damage-evoked activation of YAP occurs more readily in nonmammalian SCs than those in mammals and may contribute to species differences in regenerative proliferation. Surprisingly, bulk RNA-sequencing studies of the regenerating chicken utricle, zebrafish lateral line, and neonatal mouse utricle have not provided strong evidence for damage-evoked increases in YAP-TEAD transcriptional activity. Thus, it will be important to test the effects of genetic inactivation of YAP in these models to confirm its role in regenerative proliferation.

It is not yet clear what limits the activation of YAP in mammalian SCs compared to those of nonmammals, but LATS1/2 kinases have been shown to play a major inhibitory role. YAP variants that evade inhibitory phosphorylation entered SC nuclei and spurred TEAD-dependent proliferation, but ectopic wild type YAP was phosphorylated and sequestered in the cytoplasm. Conditional deletion of LATS1/2 reduced inhibitory phosphorylation of YAP at Ser127 and evoked proliferation in SCs of the mouse utricle, even in adults (Rudolf et al., 2020). Furthermore, a novel pharmacologic inhibitor of LATS1/2 kinase activity induced YAP-dependent proliferation in the murine utricle and made mature SCs transcriptionally resemble those of embryonic mice (Kastan et al., 2020). Thus, constitutive activity of LATS1/2 kinases is required to inhibit YAP-TEAD signaling and maintain quiescence in mature vestibular SCs. LATS1/2 inhibition did not induce proliferation of cochlear SCs, for reasons that are yet unclear

The upstream signals that control LATS1/2 activity in SCs are beginning to be understood. Pharmacologic inhibition of MST1/2 kinase activity induced nuclear translocation of YAP in SCs of the chicken utricle (Rudolf et al., 2020). However, the same inhibitor failed to induce nuclear translocation of YAP in SCs of the mouse utricle (Kastan et al., 2020; Rudolf et al., 2020), suggesting that LATS1/2 are regulated by a distinct mechanism in mammalian SCs.

Interestingly, E-cadherin controls the LATS-YAP-TEAD axis in other epithelial cell lines independent of MST1/2 (Kim et al., 2011). E-cadherin's role in limiting the activity of YAP in SCs remains to be directly shown, but there are hints of an association between E-cadherin and YAP. Pharmacologic treatments that deplete E-cadherin in striolar SCs of the mouse utricle led to a decrease in YAP in the apical domains of those cells (Figure 2-15) (Kozlowski et al., 2020), and overexpression of YAP-S127A in the mouse utricle led to upregulation of E-cadherin in SCs in apparent negative feedback (Rudolf et al., 2020). Other documented regulators of YAP/TAZ activity in HC epithelia include LPA signaling and the junction-associated protein Angiomotin-like 2a (Agarwala et al., 2015; Wang et al., 2018; Xia et al., 2020).

Factors downstream of YAP/TAZ inhibitory phosphorylation also may contribute to the age-dependent decline in plasticity of mammalian SCs. TEAD2 expression declines during postnatal maturation of the utricle, paralleling the downregulation of SoxC transcription factors for which it is a direct target (Gnedeva and Hudspeth, 2015). This may explain observations that mature murine SCs require larger shape changes than those of neonatal mice or chickens before their likelihood of entering S-phase increases (Collado et al., 2011a).

YAP/TAZ also regulate differentiation in epithelial cells. Across various epithelia, YAP/TAZ activity is high in cells that contact the basal lamina, and low in cells that lose contact with the basal lamina and differentiate (Elbediwy et al., 2016). HCs lose contact with the basal lamina as they differentiate, but it remains untested whether downregulation of YAP/TAZ is required for SCs to assume a HC fate.

Canonical Wnt Signaling

Wnts are a family of secreted ligands that bind Frizzled and LRP5/6 receptors. Canonical Wnt signaling allows β-catenin to accumulate in nuclei, where it serves as a transcriptional coactivator by modulating gene expression with TCF/Lef transcription factors (Nelson and Nusse, 2004). In the absence of canonical Wnt signaling, the cytoplasmic pool of β-catenin is degraded by a mechanism that involves casein kinase I phosphorylation of Ser45 and then GSK3β phosphorylation of multiple serine and threonine residues. Analyses of TCF/Lef and Lgr5 reporter mice have suggested that canonical Wnt signaling is active in the embryonic cochlear duct (Chai et al., 2011; Jacques et al., 2012) and in striolar SCs of the developing utricle (T. Wang et al. 2015), but this activity declines postnatally for reasons that are yet unclear.

Adhesion and canonical Wnt signaling may be antagonistic, competing for β-catenin in the cell (Nelson and Nusse, 2004). Multiple studies have identified that inhibition of GSK3β or expression of β-catenin variants can enhance SC proliferation and mitotic HC production, but few have examined the interplay between canonical Wnt signaling and cadherin junctions in SCs. GSK3β inhibition and expression of activated β-catenin each reduced E-cadherin levels and

enhanced proliferation in HC epithelia (Lu and Corwin, 2008; Shi et al., 2014). Depletion of E-cadherin from SC-SC junctions is associated with a reduction in membranous β-catenin (Figure 2-15) (Kozlowski et al., 2020). A simple, but yet untested, hypothesis is that increased levels of E-cadherin in mature mammalian SCs sequester β-catenin and limit canonical Wnt signaling.

Mechanical tension also induces β-catenin transcriptional activity. Strain applied to the E-cadherin-based adhesions of MDCK monolayers causes β-catenin to accumulate in nuclei and mediate S-phase entry with TCF/Lef (Benham-Pyle et al., 2015). Such tension-mediated regulation of β-catenin remains unexplored in the inner ear.

MRTF and SRF

Like YAP/TAZ and β-catenin, the transcriptional coactivators MRTF-A/B translocate into nuclei upon mechanical and biochemical stimuli, where they partner with SRF to mediate changes in gene expression. The balance of monomeric (G-) actin and F-actin is an important regulator of MRTF-SRF function; MRTF binds actin monomers, and the polymerization of actin filaments frees MRTF to translocate into the nucleus. Significant changes to the G-actin:F-actin ratio occur upon HC differentiation (Zhu et al., 2019), but the role of MRTF-SRF in the inner ear remains unexplored.

Calcium ion signaling

Connexins and Gap Junction Intercellular Communication

In the neonatal mouse cochlea, mechanical damage and laser ablation were shown to induce actively propagated waves of intercellular Ca^{2+} (Gale et al., 2004). Connexins 26 and 30 were essential for this intercellular Ca^{2+} signaling, with pharmacologic experiments revealing that gap junctions were required for the initial propagation of the waves, and hemichannels were required for further propagation (Anselmi et al., 2008). Waves were associated with the activation of ERK1/2 in Deiters cells (Lahne and Gale, 2008), but whether they are present in other HC epithelia, occur upon HC loss, or contribute to epithelial repair remains unclear. In *drosophila* epidermis, Ca^{2+} waves coordinate the formation of a supracellular actomyosin cable at wound

edges (Hunter et al., 2015). Such a mechanism warrants investigation, as gap junction intercellular communication is required for SC coordination during HC elimination.

Stretch-activated Ion Channels

PIEZO1/2 are Ca^{2+}-permeable ion channels that are sensitive to mechanical stretch and can influence proliferation and cell fate decisions. In MDCK monolayers, PIEZO1 mediates both compression-induced apoptosis and stretch-induced proliferation (Gudipaty et al., 2017). PIEZO2 has been localized to the apical domain of OHCs and vestibular HCs near SC junctions and is required for reverse polarity currents that occur upon tip link disruption, deletion of mechanotransduction channel components, or mechanical damage to the epithelium (Wu et al., 2017). Whether PIEZO1/2 are expressed in SCs at low levels and mediate regenerative responses remains unexplored.

The LINC Complex

The Linker of Nucleoskeleton and Cytoskeleton (LINC) complex connects the F-actin, intermediate filament, and microtubule cytoskeletons of the cytoplasm to the nuclear lamina (Méjat and Misteli, 2010). LINC complexes are comprised of SUN proteins which span the inner nuclear membrane and Nesprins which span the outer nuclear membrane. High actomyosin contractility transmitted through the LINC complex has been shown to open nuclear pores and facilitate the nuclear entry of YAP (Elosegui-Artola et al., 2017). Such a mechanism could underlie the nuclear accumulation of YAP in SCs that undergo large shape changes, which exhibit large nuclei (Rudolf et al., 2020), but so far the role of the LINC complex remains unexplored in HC epithelia.

MECHANICAL CONSIDERATIONS FOR THE PLANAR POLARIZATION OF REGENERATED HAIR CELLS

The establishment of the HC-SC mosaic and planar polarization of hair bundles occurs during embryogenesis, when the epithelium is relatively compliant and cell morphology is highly sensitive to changes in actomyosin contractility (Ebrahim et al., 2013; Cohen et al., 2019). The

ability of cells to exchange neighbors and tune their actomyosin contractility is crucial for proper patterning and polarization in HC epithelia (Andreeva et al., 2014; Cohen et al., 2019).

Evidence from the chicken basilar papilla showed that the orientation of bundles atop regenerated HCs was variable at first, but became more uniform throughout subsequent days (Cotanche and Corwin, 1991). Whether bundles of regenerated HCs in the mammalian utricle achieve proper planar polarity remains unknown, but it is plausible that the reinforced junctions and cytoskeletal components of mature mammalian SCs could restrict the processes that enable polarization during development.

SUMMARY

A Hypothetical Model for Mechanical Control of Hair Cell Replacement

Current evidence suggests that YAP-TEAD transcriptional activity is high during embryonic development of HC epithelia, facilitating robust progenitor cell proliferation that leads to organ growth (Gnedeva et al., 2017). Eventually, mechanical constraints imposed by the surrounding tissue or the bony labyrinth restrict growth, so further proliferation leads to an increase in cell density (Gnedeva et al., 2017). In other epithelia, such crowding leads to reduced cell-matrix adhesion, increased cell-cell adhesion, and reduced cortical tension (Miroshnikova et al., 2018), all of which serve to reduce YAP-TEAD transcriptional activity. These factors collaborate with changes to gene expression to arrest proliferation in progenitor cells (Warchol, 2002; Gnedeva et al., 2017). Such developmental regulation is likely to occur in HC epithelia of mammals and nonmammals alike.

In nonmammals and juvenile mammals, HC elimination involves rapid shape changes in SCs, which coordinate to form an F-actin purse string that undergoes ROCK-dependent constriction and reseals the epithelial barrier (Meyers and Corwin, 2007; Bird et al., 2010). Waves of Ca^{2+} signaling may facilitate the formation of a coordinated supracellular F-actin purse-string (Hunter et al., 2015). These changes in cell shape and contractility increase the likelihood of SC proliferation (Meyers and Corwin, 2007; Collado et al., 2011a), possibly by promoting the nuclear

accumulation of YAP and β-catenin, which stimulate TEAD- and TCF/Lef-dependent transcription, respectively (Benham-Pyle et al., 2015).

SCs which undergo either direct transdifferentiation or symmetric differentiating division leave a SC-sized vacancy on the basal lamina, that in theory would increase the cell-ECM contact area of remaining SCs—a known stimulus of YAP-TEAD transcriptional activity in other cell types (Dupont et al., 2011). The signaling evoked by this increased footprint would in theory be a convenient mechanism to trigger the amplifying divisions which occur in nonmammals to replenish the SC population (Romero-Carvajal et al., 2015; Scheibinger et al., 2018).

Such damage-evoked responses appear to be impeded in SCs of mature mammals, whose junctions are reinforced by thick circumferential F-actin bands (Burns et al., 2008; Burns and Corwin, 2014) and high levels of E-cadherin and p120-catenin (Collado et al., 2011b; Luo et al., 2018). These reinforced junctions could form a mechanical block by restricting the rate and extent of SC shape changes after HC loss (Burns and Corwin, 2014; Anttonen et al., 2017), in addition to a biochemical block by restricting signaling from growth factor receptors, activating inhibitory LATS1/2 kinases, and sequestering β-catenin (Nelson and Nusse, 2004; Perrais et al., 2007; Kim et al., 2011).

Outstanding Questions and Opportunities

A few important open questions related to the role of cell junctions and epithelial mechanics in the regenerative replacement of HCs are as follows:

1. What developmental processes lead to the development of E-cadherin-rich junctions and thick F-actin bands in mammalian SCs, but not those of fish, amphibians, or birds? Can these maturational processes be recapitulated in organoids or other *in vitro* systems to enable high-throughput studies?
2. Does experimental deletion of E-cadherin activate YAP-TEAD signaling and canonical Wnt signaling and evoke proliferation of mature mammalian SCs? Do the thick F-actin bands stabilize E-cadherin at SC-SC junctions?

3. What upstream signaling processes lead to activation of LATS1/2 kinases in mammalian SCs? After YAP and TEAD mediate cell cycle re-entry, are progeny able to differentiate as HCs? Does HC loss evoke YAP-TEAD transcriptional activity in SCs of nonmammals?
4. How significant is integrin signaling at the basal lamina to the regenerative proliferation of SCs? Does the molecular composition or mechanical properties of the basal lamina change with age? Does loss of contact with the basement membrane guide HC differentiation?
5. How are the regenerative responses that occur in nonmammalian HC epithelia terminated? What is the role of mechanics in this process?
6. Do damage-evoked Ca^{2+} waves appear following HC loss or in vestibular epithelia? Does this signaling enable formation of intercellular F-actin “purse-strings” or cue other regenerative processes?

Techniques for Measurement and Manipulation of Mechanical Properties

The application of new techniques to measure and manipulate the mechanical properties of HC epithelia will accelerate our understanding of development and regeneration. Atomic force microscopy and micropipette aspiration have already been used to characterize mechanical properties of HCs and HC epithelia, and recent technological advancements have enabled high-resolution, non-contact measurement of epithelial and bundle mechanics (Spector et al., 1996; Cartagena-Rivera et al., 2019). Brillouin microscopy enables the optical interrogation of mechanical properties of biological specimens (Prevedel et al., 2019). Traction force microscopy is used to characterize the forces that cells exert on their substrate (Colin-York et al., 2017). Genetically encoded FRET sensors can measure tension at the molecular level (Cost et al., 2019). Epithelial tension can also be indirectly inferred from time lapse imaging (Cohen et al., 2019), analysis of cell shape (Francou et al., 2017), and measuring junctional recoil velocity following laser ablation (Behrndt et al., 2012).

Three-dimensional bubble cultures can be used to tune the external mechanical environment (Gnedeva et al., 2018). Optical tweezers enable the mechanical manipulation of individual

molecules (Bartsch et al., 2019), and multiple techniques have been developed to apply strain on epithelial monolayers (Harris et al., 2014; Benham-Pyle et al., 2015).

Conclusions

The central goal of HC regeneration research is to identify and circumvent factors that limit the regenerative proliferation and differentiation of mammalian SCs. The downregulation of embryonic gene expression patterns for growth and development and changes in chromatin accessibility are likely to heavily influence the lack of a robust regenerative response in mature mammalian SCs (Gnedeva and Hudspeth, 2015; Jen et al., 2019). In addition to those downstream factors, the development of reinforced junctions and cytoskeletal features in mammalian SCs represents a very promising area for further discovery. Direct experimental manipulations of these junctional and cytoskeletal components are needed to determine whether the strong correlations between junctional reinforcement, stiffening of SCs, and decreased SC plasticity are indicative of a causal relationship.

Figures and Figure Legends

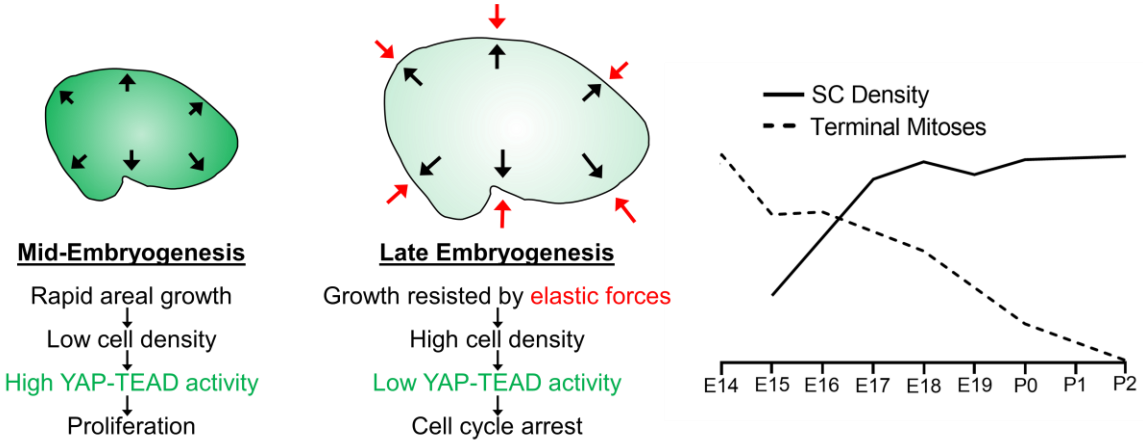

Figure 2-1. Schematic depicting the hypothesized relationship between utricular growth, cell density, YAP-TEAD transcriptional activity, and proliferation during development. The graph depicts the inverse relationship between supporting cell density and terminal mitoses in the developing mouse utricle.

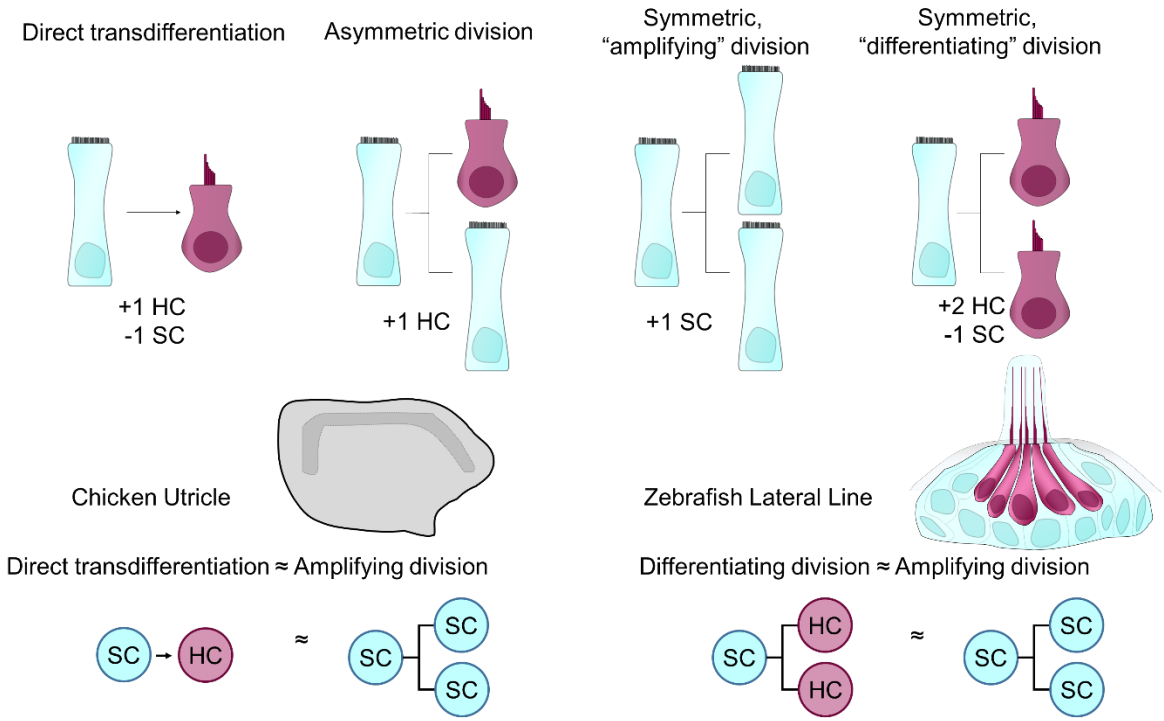

Figure 2-2. Supporting cells have been observed to undergo four behaviors during regeneration in nonmmals: Direct transdifferentiation, asymmetric divisions, or symmetric divisions that produce either two supporting cells or two hair cells. In the regenerating chicken utricle and zebrafish lateral line, certain modes of regeneration occur in approximately equal proportions such that the density of supporting cells remains roughly constant (Scheibinger et al. 2018, Romero-Carvajal et al. 2015).

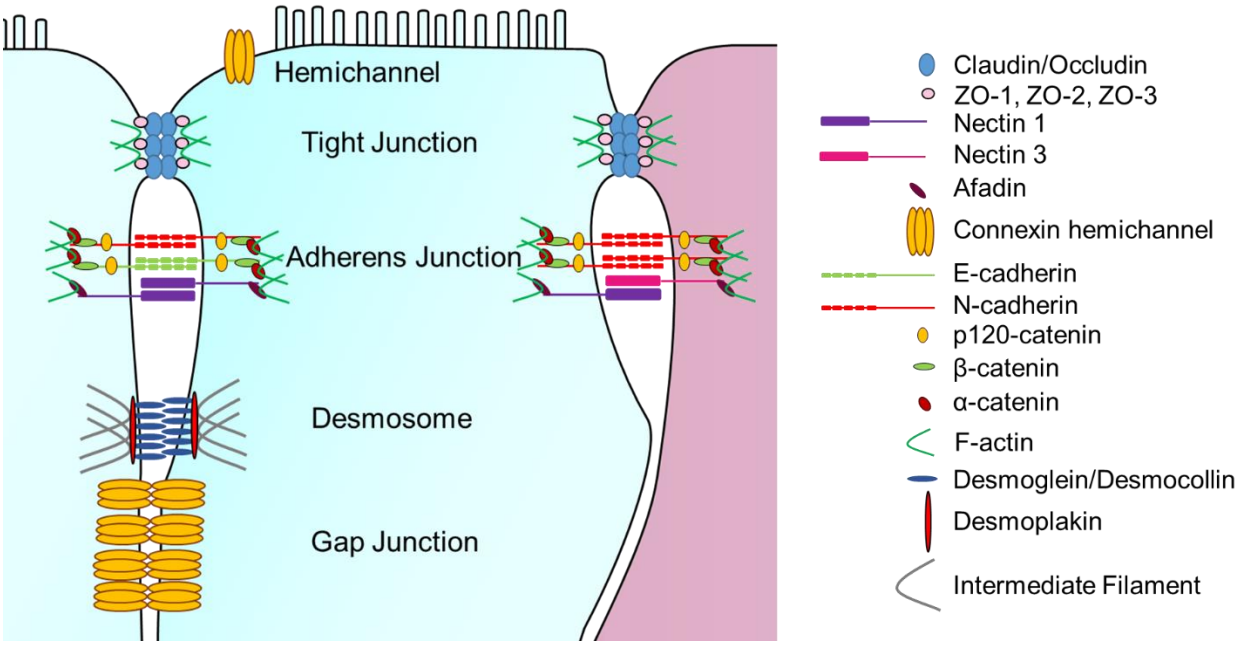

Figure 2-3. Cell-cell junctions in HC epithelia. SC depicted in blue, and HC depicted in purple.

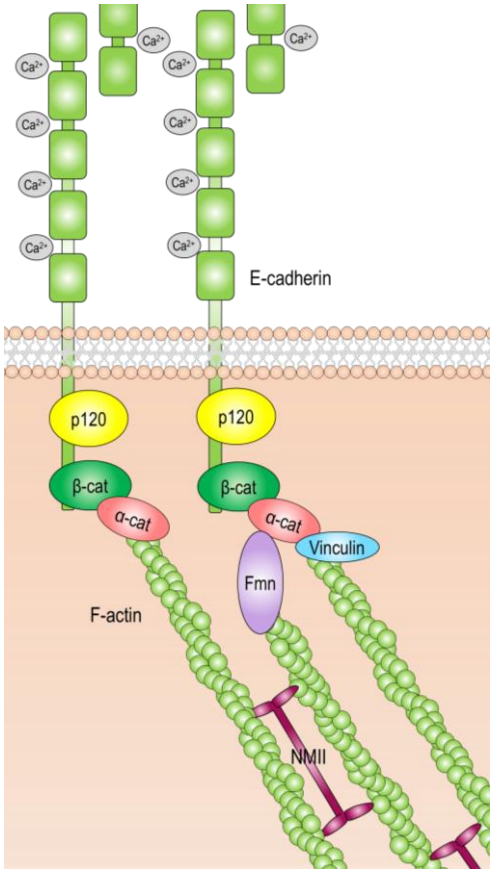

Figure 2-4. Schematic of cadherin-catenin complex at the adherens junction.

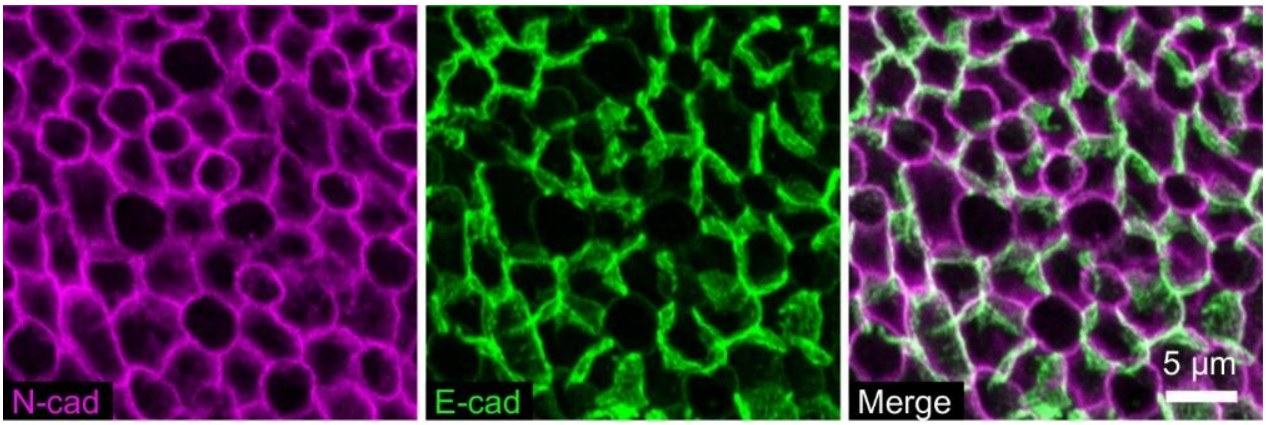

Figure 2-5. In the adult mouse utricle, N-cadherin is present at HC-SC and SC-SC junctions. E-cadherin is enriched at SC-SC junctions. Adapted from Kozlowski et al. 2020.

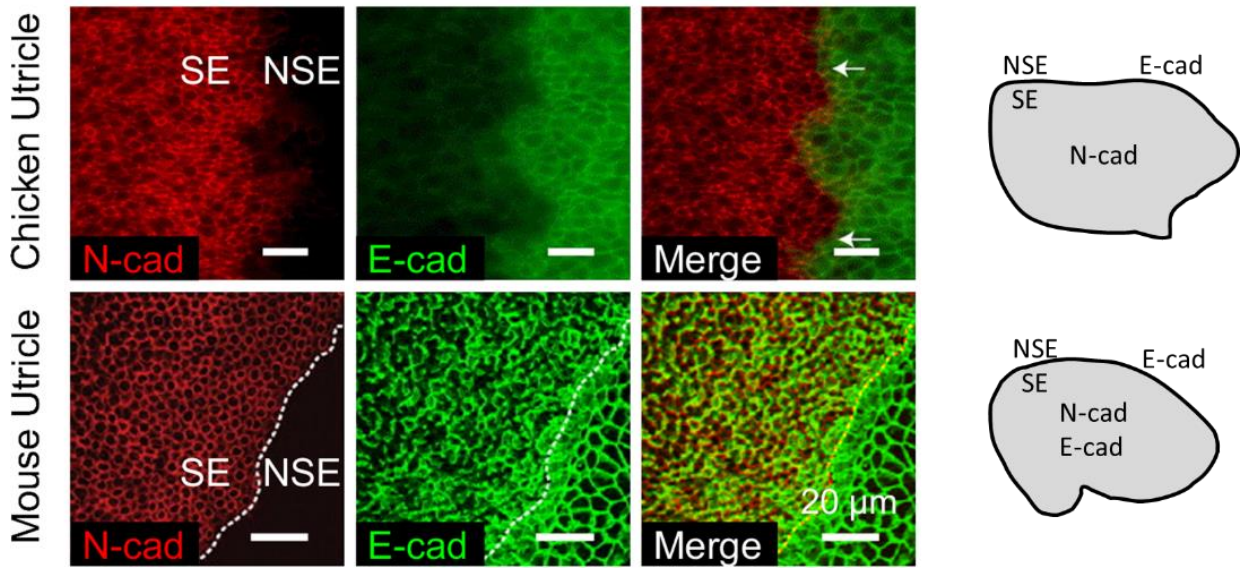

Figure 2-6. Regional and species differences in cadherin expression. In chicken utricles, N-cadherin is expressed within the sensory epithelium (SE) and E-cadherin is expressed in the surrounding nonsensory epithelium (NSE). In mouse utricles, N-cadherin is also expressed in the SE, but E-cadherin is expressed both in the SE and NSE. Chicken images adapted from Warchol 2007. Mouse images adapted from Collado et al. 2011b.

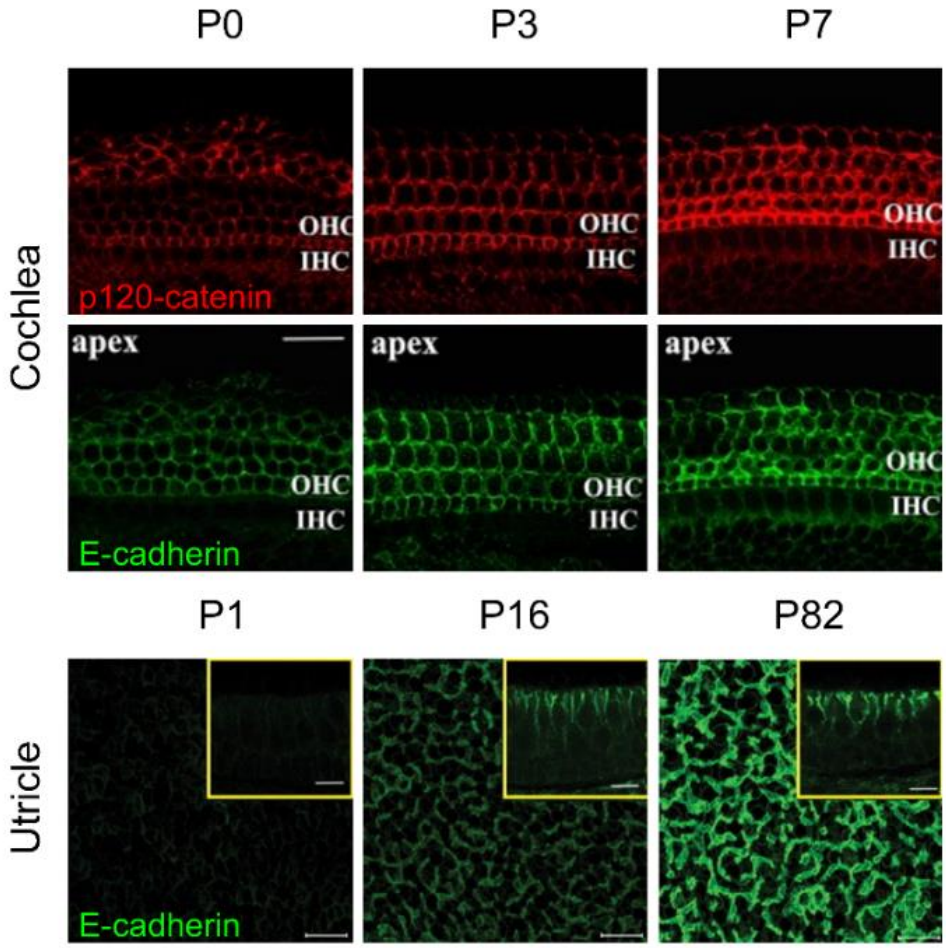

Figure 2-7. Levels of p120-catenin and E-cadherin increase during postnatal maturation. Cochlear images adapted from Luo et al. 2018 with scale bar denoting 20 µm. Utricle images adapted from Collado et al. 2011b with scale bars denoting 10 µm.

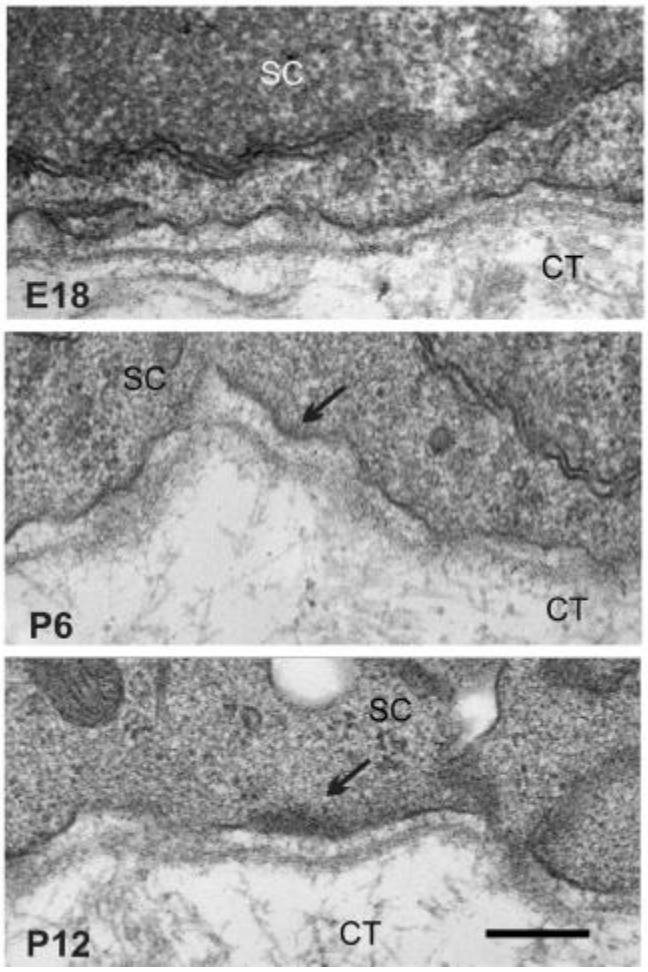

Figure 2-8 Transmission electron micrographs of the supporting cell-basal lamina interface from utricles of mice at different ages. Arrows depict progressive maturation of hemidesmosome-like plaques. SC, supporting cell. CT, connective tissue. Scale bar denotes 250 nm. Adapted from Davies et al. 2007.

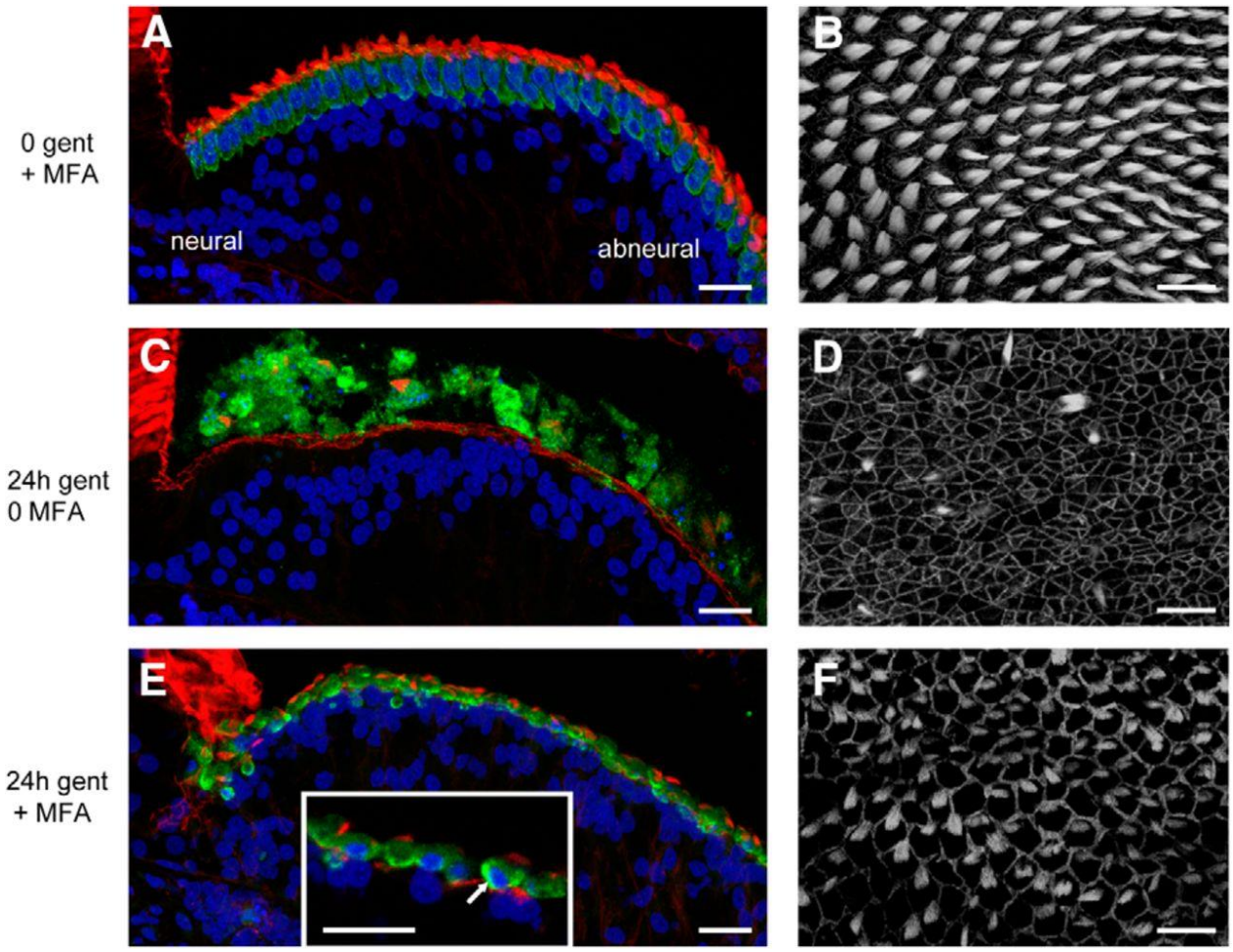

Figure 2-9. Pharmacologic inhibition of gap junctions prevents the extrusion of hair cells from the gentamicin-damaged chicken cochlea. MFA, meclofenamic acid. Scale bars denote 20 µm. Adapted from Jagger et al. 2014.

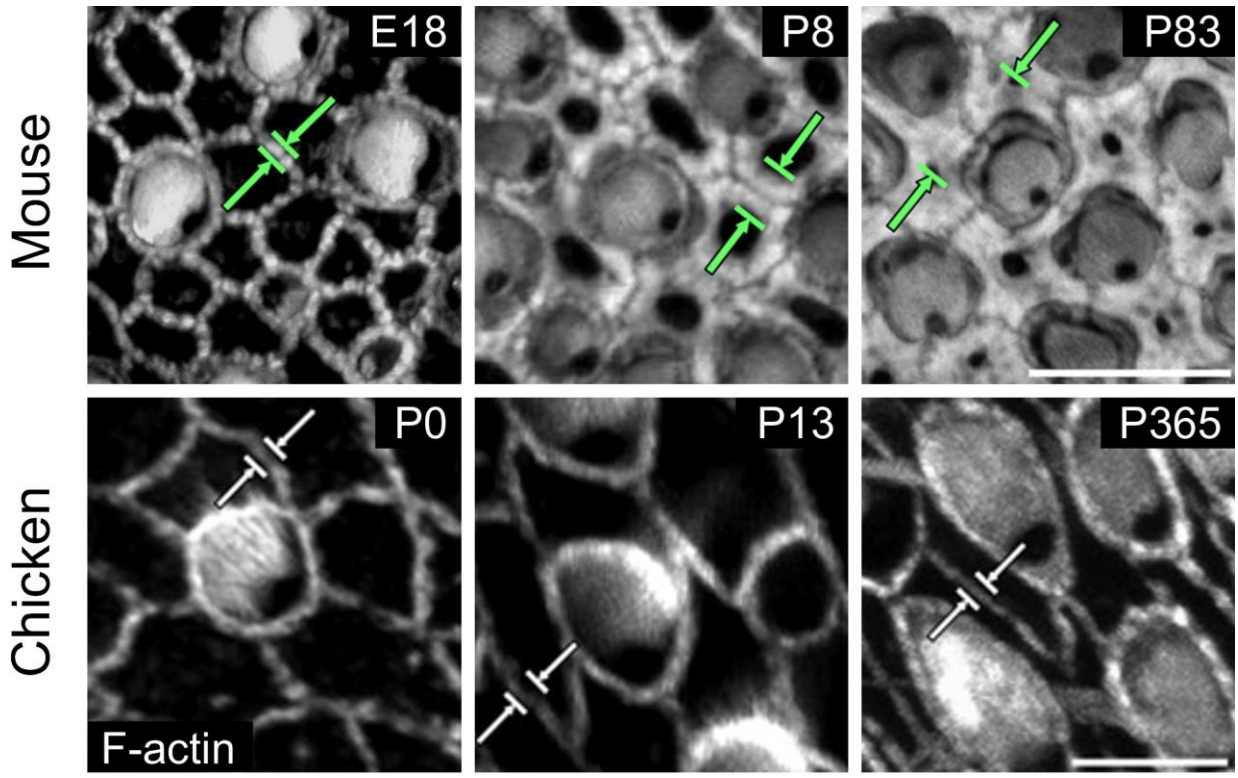

Figure 2-4. F-actin bands in vestibular SCs of the mammalian utricle thicken postnatally. F-actin bands in chickens remain thin throughout life. Scale bars denote 10 µm for mouse images and 5 µm for chick images. Adapted from Burns et al. 2008.

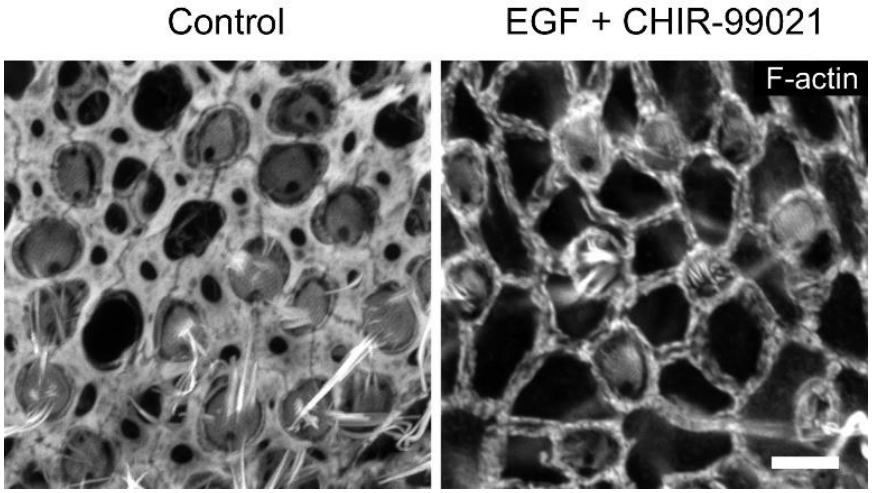

Figure 2-11. EGF and the GSK3 inhibitor CHIR-99021 each thin the F-actin bands of SCs in cultured mouse utricles. Scale bar denotes 5 μm. Adapted from Kozlowski et al. 2020.

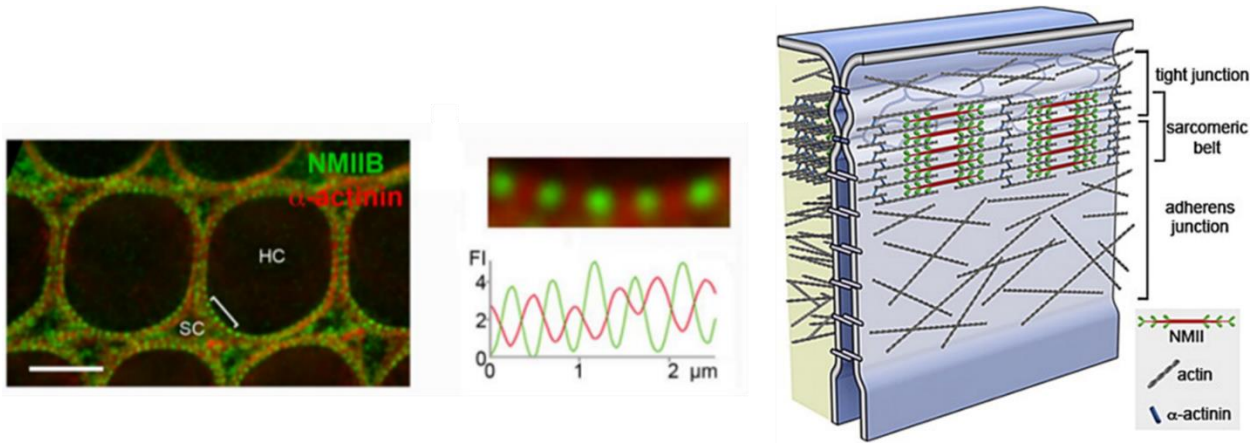

Figure 2-12. Sarcomeric network at HC-SC apical junctions in the P2 rat organ of Corti. Scale bar represents 3 µm. The middle panel depicts an enlarged view of the bracketed region along with relative fluorescence intensity traces of nonmuscle myosin IIB (green) and α-actinin 1 (red). Adapted from Ebrahim et al. 2013.

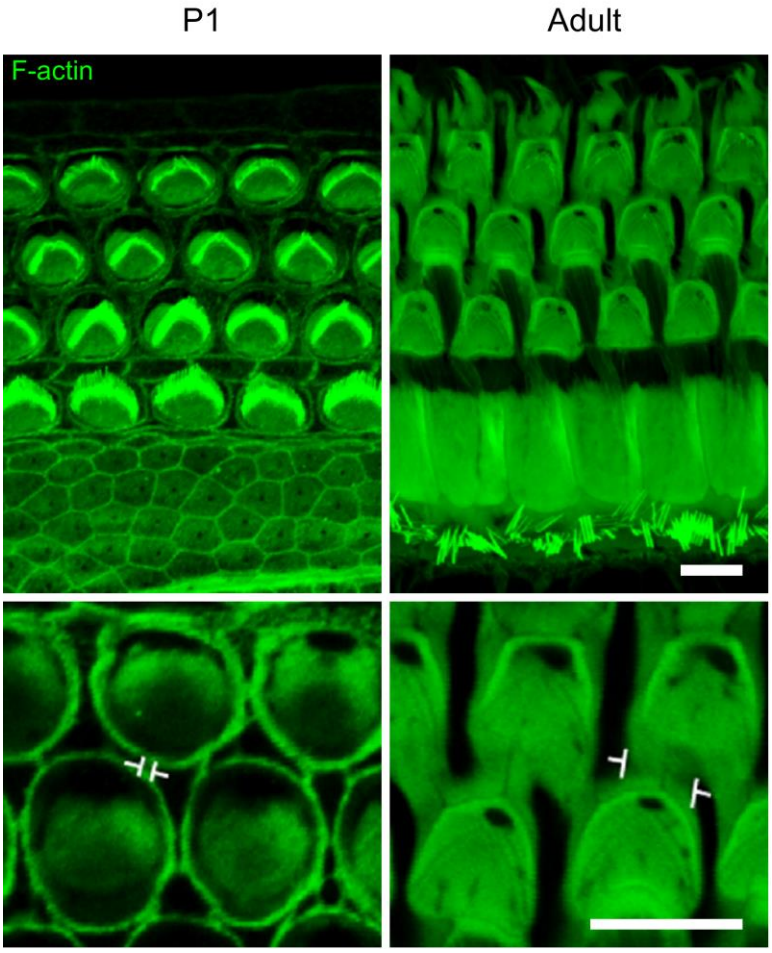

Figure 2-13. F-actin labeling at the apical surface of the neonatal and adult mouse cochlea. Brackets in the lower panel depict the age-related thickening of F-actin bands at DC-DC junctions. Scale bar depicts 5 µm. Adapted from Burns et al. 2013.

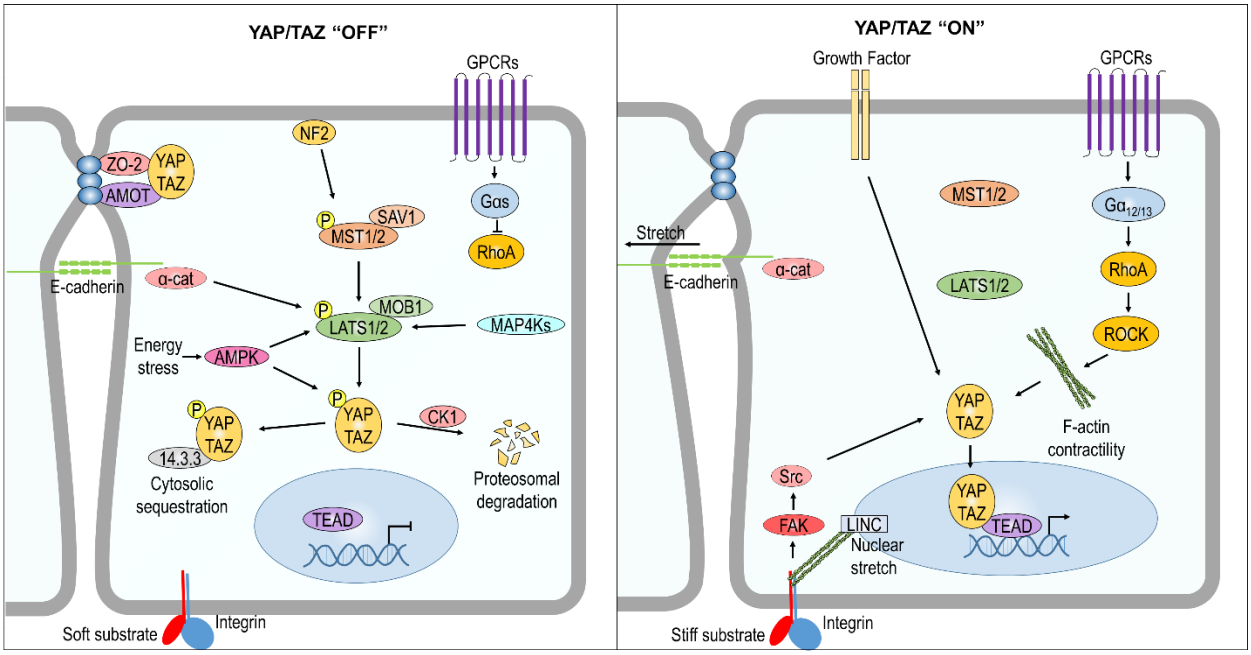

Figure 2-14. Overview of YAP/TAZ regulation.

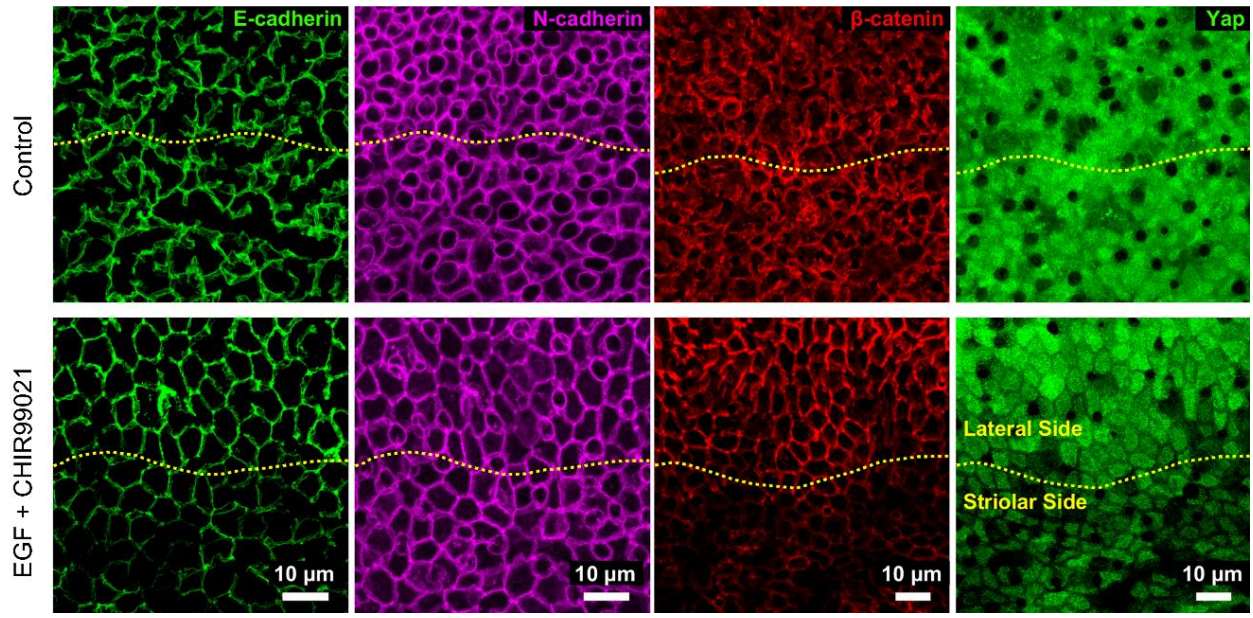

Figure 2-15. Culture with EGF and a GSK3 inhibitor depletes E-cadherin, but not N-cadherin, from striolar SC junctions of adult mouse utricles. Levels of the transcriptional co-activators β-catenin and YAP are reduced in the apical domains of those striolar SCs. Adapted from Kozlowski et al. 2020.

CHAPTER 3

The Thick Circumferential F-actin Bands that Develop in Mammalian Supporting Cells Impose a Biomechanical Brake Upon Epithelial Repair

ABSTRACT

Hair cell losses cause permanent hearing and balance deficits in humans and other mammals, but nonmammals recover sensory function after supporting cells divide and replace hair cells. The proliferative capacity of mammalian supporting cells declines as develop thick circumferential F-actin bands at their adherens junctions. We hypothesized that these reinforced junctions limit the regenerative response by impeding the changes in cell shape and tension that coordinate repair. We applied a customized micropipette aspiration technique to measure stiffness of the hair cell epithelium's apical surface. The surface of the mature mouse utricle was more resistant to deformation than the surfaces of utricles from chickens and newborn mice. Depolymerization of the F-actin bands reduced the stiffness of mature mouse utricles. Supporting cells in the chicken utricle are subject to constant anisotropic tension, orienting their cell divisions and harboring elongated apical domains that expand upon inhibition of nonmuscle myosin II. In contrast, supporting cells in the mouse utricle maintained round apical domains that were unaffected by changes in actomyosin contractility. Thus, the highly regenerative supporting cells of birds display mechanical behavior consistent with that of typical epithelia, where cell loss produces generates increases in intraepithelial tension that coordinate repair. In contrast, the thick F-actin bands that develop in mammalian supporting cells physically restrict shape changes and appear to impede the efficiency of actomyosin contractility, processes known to activate mitogenic signaling pathways.

INTRODUCTION

A major and permanent cause of the hearing loss that affects more than 400 million people worldwide and vestibular dysfunction that affects over a third of adults is the loss of sensory hair cells (HCs) of the inner ear (Agrawal et al., 2009; World Health Organization, 2020). HCs are vulnerable to loud sound, ototoxic drugs, and aging, but are not effectively replaced in humans and other mammals (J. B. Nadol, 1993). In nonmammalian vertebrates, such insults evoke a regenerative response whereby neighboring supporting cells (SCs) divide and differentiate into replacement HCs, or convert directly into HCs. The factors that account for these species-specific differences in regenerative capacity remain unclear.

An emerging paradigm in epithelial repair is that mechanical signals arising from cell loss induce a proliferative response (Mesa et al., 2018). The forces produced by cell loss propagate through cell-cell junctions, directing direct shape changes and increasing cortical tension in nearby cells, which activate mechanosensitive signaling molecules such as YAP (Benham-Pyle et al., 2015). With this in mind, we examined the major differences that exist between the cell-cell junctions in vestibular SCs of mammals and nonmammals.

In the mouse utricle, SCs develop E-cadherin-rich junctions that are bracketed by exceptionally thick circumferential F-actin bands (Burns et al., 2008; Collado et al., 2011b). The growth of the F-actin bands strongly correlates to declines in the ability to change shape ($R = -0.989$) and proliferate ($R = -0.975$) in culture (Burns et al., 2008). In contrast, SCs in birds, fish, and amphibians express little E-cadherin, retain thin junctional F-actin bands, and readily change shape and proliferate throughout life (Burns et al., 2013). It was also shown that HC loss led to nuclear accumulation YAP in SCs of the chicken utricle, but did not in mice (Rudolf et al., 2020). We hypothesized that the thin F-actin bands in nonmammalian SCs permit them to readily change shape and proliferate, while the thick F-actin bands in mammalian SCs limit such deformations.

To test that, we measured stiffness of the apical surfaces of utricles from mice and chickens of various ages using a custom modification of micropipette aspiration, a simple method

to apply a standardized negative pressure to the surface of a biological specimen and visualize its ensuing deformations (Hochmuth, 2000). We also examined the capability of actomyosin contractility to affect the shape of SC apical domains.

We find that the thick F-actin bands physically stabilize the apical domains of mammalian SCs, limiting their deformations to applied force and appearing to diminish the influence of actomyosin contractility on the apical domain morphology. In stark contrast, SCs in chickens behaved as though coupled in a mechanical syncytium, exhibiting collective alignment and elongation and orienting their divisions with respect to anisotropic tension. Their apical domain sizes were actively regulated by tonic actomyosin contractility. The data suggest that the stiff F-actin bands of mature mammalian SCs constitute a biomechanical “brake” that impedes the mechanical signals that arise from HC loss and would otherwise activate regenerative programs such as YAP-TEAD signaling.

MATERIALS AND METHODS

Animals and dissection of vestibular organs

All animals were handled in accordance with protocols approved by the Animal Care and Use Committee at the University of Virginia (protocol #1835 07 18). Utricles from embryonic day 16 (E16), postnatal day zero (P0), or adult (>6 week old) mice of either sex were used with staging of embryos according to The Atlas of Mouse Development (Kaufman, 1992). Swiss Webster mice were obtained from Charles River Laboratories. Transgenic mice that express a γ-actin and green fluorescent protein (GFP) fusion protein were generated in the laboratory of Dr. Andrew Matus (Fischer et al., 1998). Fertilized White Leghorn (W-36) eggs were obtained from Hy-Line and incubated at 37°C in a humidified chamber with rocking until E18, after which eggs were incubated without rocking. Embryos were staged according to morphometric features (Hamburger and Hamilton, 1951). Animals of either sex were used for all experiments.

For tissue harvest, labyrinths were dissected from temporal bones in ice-cold, HEPES-buffered DMEM/F-12 (Thermo Fisher Scientific), vestibular organs were isolated, and the roof and the otoconia were mechanically removed.

Organ culture

Utricles dissected from mice and chickens under aseptic conditions were transferred to glass-bottom dishes (Mat-Tek) coated with Cell-Tak (1 µL air-dried onto the glass; BD Biosciences #354240) and adhered with the nerve side down. Utricles were cultured in DMEM/F-12 + HEPES with 1% fetal bovine serum (FBS; Invitrogen) and 10 µg/ml Ciprofloxacin (Bayer) at 37°C and 5% CO_2. In some experiments, cytochalasin D (Sigma-Aldrich), blebbistatin (Calbiochem), or streptomycin sulfate (Sigma) were added to the culture medium at the concentrations and durations indicated below.

Micropipette aspiration

To measure the mechanical stability of sensory epithelia from chickens and mice of various ages, we adapted micropipette aspiration to quantify tissue-level resistance to deformation in utricular sensory epithelia. This technique enables direct observation of deformation lengths produced by a calibrated suction pressure, and can be applied in length scales from single cells (Hochmuth, 2000) to whole embryos (Porazinski et al., 2015). Micropipettes were fabricated from borosilicate glass tubes on a Sutter Instruments puller, scored with a tile and broken to clean edge of 22.5 µm in diameter (which spans ~5 HCs). The tip of the micropipette was dipped in Sigmacote before use (Sigma SL2) to minimize adhesion to debris.

On the day of tissue harvest, utricles for micropipette aspiration measurement were cultured atop 0.08 µm Nucleopore membranes (Whatman) at the meniscus of the culture medium. On the following day, utricles were transferred to a glass-bottom POCR chamber (Zeiss) containing DMEM/F12 + HEPES supplemented with 5% FBS, and the utricle was adhered to the Cell-Tak-coated glass with the nerve side down. Under an upright microscope with a heated stage set to 37°C, the utricle was partially lifted from the glass using fine forceps, with one edge

remaining adhered to the glass. Two micropipettes were used, each connected with plastic tubing to an open-barreled syringe filled with water (the “water reservoir”) to serve as a manometer. The first “stabilizing” pipette of 50-100 µm internal diameter was maneuvered with a micromanipulator to contact the nerve side of the utricle in order to stabilize it such that the utricle’s planar apical surface was parallel to the optical axis (Figure 1A). The second, “aspiration” micropipette of 22.5 µm internal diameter was used for micropipette aspiration measurements of the apical surface. The apical surface of the utricle and tip of the micropipette were visualized with differential interference contrast microscopy with a 60x, 0.9 NA water immersion objective.

To perform a measurement, the water reservoir was positioned such that its meniscus was at the same height as the utricle, such that no suction pressure would be present upon contact. Then, a micromanipulator was used to bring the aspiration pipette into light contact with the sensory epithelium’s apical surface. Then the water reservoir was lowered to apply a ramped negative pressure, creating a deformation that could be visualized with differential interference contrast video microscopy (Figure 3-1B-D; Movie 3-1). Specifically, the water reservoir was lowered at a rate of 3 cm/s for 10 s (equivalent to a negative pressure ramp of 3 cm H_2O/s or ~300 Pa/s), and then held with the meniscus 30 cm below the height of the utricle (equivalent to a negative pressure of 30 cm H2O or ~3 kPa) for an additional 10 s. As the utricle’s apical surfaced deformed during that process, images of the deformation were acquired at 1 s increments using a SPOT Idea CMOS camera. After the 20 s acquisition, the final deformation length was measured in a blinded fashion using FIJI software. Each utricle was measured at least three times, and the individual measurements from each utricle were averaged together to generate a single value for each utricle, which was considered a single independent observation for statistical analysis.

Immunohistochemistry

Utricles were fixed in 4% paraformaldehyde for one hour at room temperature or Shandon Glyo-Fixx overnight at 4°C. After washing in PBS with 0.1% Triton X-100 (PBST), utricles were blocked in 10% normal goat serum (Vector) in PBST for 2 hours at room temperature. Primary

antibodies were incubated with 2% normal goat serum at 4°C overnight. After washing in PBST, secondary antibodies were added in 2% normal goat serum and incubated for 2 hours at room temperature. Where indicated below, AlexaFluor-conjugated phalloidin (1:100) and Hoechst 33452 (1:500) were incubated along with secondary antibodies to detect actin and nuclei. After washing in PBST, samples were mounted in Prolong Diamond and imaged using a Zeiss 880 confocal microscope or a Zeiss Axiovert 200M widefield microscope. Primary antibodies used included: Rabbit anti-Calretinin (Millipore Sigma AB5054, 1:200), mouse anti-N-cadherin (BD Biosciences 610920, 1:200), rabbit anti-ZO-1 (Thermo Fisher Scientific 40-2200, 1:200), rabbit anti-Chick Occludin (generous gift from Shoichiru Tsukita, 1:200), mouse anti-Spectrin (Millipore MAB1622, 1:200), rabbit anti-phospho-Histone H3 (Ser10) (Millipore 06-570, 1:400), and rabbit anti-Cingulin (Zymed 36-4401, 1:200).

Cell shape measurements

SC apical junctions were visualized by immunostaining for ZO-1 or N-cadherin in mouse utricles and immunostaining for cingulin, occludin, or N-cadherin in chicken utricles. For cell shape measurements, five images were acquired per utricle with 30 contiguous SCs quantified in each region, all of which were pooled and considered an independent observation. Mouse utricles were imaged in five standardized locations (lateral extrastriolar, anterior, medial, posterior, and central (striolar) regions). All images of the chicken utricle were acquired in the large, medial extrastriolar region.

All image analysis was done using FIJI. First, SC apical domains were hand-traced from high-magnification images of the utricular apical surface, with 30 contiguous cells analyzed per image. The apical domain area of each SC was measured. Then, each SC apical domain was fit to an ellipse using the software's built-in function, which provided the length of each apical domain's major axis, minor axis, and angular orientation. Elongation was calculated from the ratio of the major and minor axis of each apical domain. The intercellular alignment for a given image

was calculated using Eq. 1., where *n* is the number of apical domains analyzed in the image (30), θ_{med} is the median ellipse orientation for a given image, and θ_i is the orientation of ellipse *i*.

$$Intercellular\ alignment = \frac{1}{n}\sum_{i=1}^{n} |\theta_{med} - \theta_i| \quad \text{Eq. 1}$$

Using this definition, perfectly aligned cells have a value of 0° deviation from the median angle, and randomly aligned cells have a value of 45° deviation from the median angle.

Measurement of cell division orientation

To measure cell division orientation in the developing chicken utricle, utricles were harvested at E14 and immunostained for phospho-histone H3 (PH3) to label dividing cells and spectrin to label cuticular plates and HCs. Using an Axiovert 200M inverted microscope, cells in metaphase and anaphase were identified. Images of the mitotic figure and nearby cuticular plates were acquired for each dividing cell. The division orientation of a cell in metaphase was determined by drawing a line that spanned the metaphase plate, measuring its angle in FIJI, and adding 90° to account for the fact that metaphase cells divide perpendicular to the orientation of their metaphase plate. The division orientation of a cell in anaphase was determined by drawing a line from one pole to the other and measuring its angle in FIJI. The local axis of HC polarity was determined by averaging the polarity of the six closest HCs to each mitotic figure; to do that, a line was drawn that bisected the HC's cuticular plate and terminated at the fonticulus as visualized by immunostaining for spectrin; the angle of the line was measured in FIJI. The difference between each cell division orientation and the axis of local HC polarity was recorded as "degrees deviation from local HC polarity." Using this definition, the cell division orientation can range from 0° (parallel to the local axis of HC polarity) to 90° (perpendicular to the local axis of HC polarity).

To measure cell division orientation in the regenerating chicken utricle, utricles from P2 chickens were harvested and cultured 24 h in medium containing 1 mM streptomycin sulfate to ablate HCs. Utricles were then transferred to a dish containing standard culture medium and incubated an additional 48 h prior to fixation. Utricles were immunostained with cingulin to label

cell junctions, and Hoechst 33342 was used to label nuclei. The orientations of dividing cells in metaphase or anaphase were measured as described above. Because HCs were ablated, the orientation of cell divisions was measured with respect to the long axis of neighboring SCs, which runs parallel to the axis of HC polarity in undamaged utricles (data not shown). To do this, the apical domains of the six closest SCs were outlined using cingulin immunoreactivity and fit to an ellipse using FIJI. Then, the orientations of the major axes of the ellipses were averaged together. The difference between the division orientation and axis of local SC elongation was recorded as "degrees deviation from local SC elongation." Using this definition, the cell division orientation can range from 0° (parallel to the local axis of SC elongation) to 90° (perpendicular to the local axis of SC elongation).

Time-lapse imaging

Chicken utricles were harvested and cultured as described above. Prior to imaging, utricles were incubated in medium containing 100 nM SiR-actin (Cytoskeleton CY-SC006) for 6 h to label F-actin and then transferred to DMEM/F-12 + HEPES containing 3 µM FM1-43FX (ThermoFisher F35355) for 3 min to label HCs. For imaging, utricles were transferred to a Zeiss POCR chamber with a 42 mm coverglass that contained DMEM/F-12 + HEPES supplemented with 10% FBS. A wax barrier bisected the chamber for the simultaneous imaging of two samples. Utricles were immobilized HC-side down with a miniature "harp" (gold wire threaded with fine nylon) as previously described (Bird et al., 2010). Then, the imaging chamber was placed on a 37°C heated stage insert supplemented with 5% CO_2. Just prior to image acquisition, blebbistatin was spiked into one side of the bisected chamber at a final concentration of 50 µM, and DMSO was added to the second side as a vehicle control. The time-lapse was acquired on a Zeiss 880 confocal microscope, with z-stacks obtained at 10 min intervals for a duration of 10 h.

Statistics

GraphPad Prism 8 software was used for statistical tests. For pairwise comparisons, unpaired Student's t-tests were used. ANOVA was used to analyze comparisons between three

or more groups, and Tukey's test was applied where indicated in the figure legend. The Kolmogorov-Smirnov (KS) test was used to test whether cell division orientations were randomly oriented, with a uniform distribution as the null hypothesis. Bar graphs display mean ± 95% confidence interval, with dots denoting independent biological replicates. Test statistics, sample sizes, degrees of freedom, and p-values are reported on the graphs or in the figure legends. For all tests, a p-value less than 0.05 was considered statistically significant.

RESULTS

Utricular sensory epithelia of mature mice were more resistant to deformation than those of developing mice and chickens

To test whether the surface of the mouse becomes more resistant to deformation with age, we applied our customized micropipette aspiration technique to utricles from E16, P0, or adult mice. The deformation lengths of E16 and P0 mouse utricles were comparable at 10.1 ± 0.7 µm and 9.5 ± 1 µm, respectively (mean ± standard deviation), but utricles from adults deformed less than half as much (4.4 ± 1.6 µm; $p < 0.0001$, $F_{(2, 13)} = 38.16$, ANOVA, n = 4-7 utricles per condition, Figure 3-1E). To determine whether resistance to deformation would increase with age in a nonmammalian vertebrate, we applied the same technique to utricles of P3 and P36-40 chickens. There was no significant difference between their mean deformation lengths (12.2 ± 0.6 µm vs 11.6 ±1.6 µm, $p = 0.36$, $t_{(17)} = 0.93$, unpaired t-test, n = 6-13 utricles per condition, Figure 3-1E). Furthermore, the deformation lengths of P36-40 chicken utricles were 2.6-fold greater than those of adult mice ($p < 0.0001$, $t_{(15)} = 7.7$, unpaired t-test, n = 4-13 utricles per condition, Figure 3-1E). The data indicate that postembryonic changes in the mouse utricle cause its apical surface to become more resistant to deformation than the apical surface of the chicken utricle, where such postembryonic changes do not occur.

F-actin depolymerization reduced the stiffness of mature mouse utricles

The increasing resistance to deformation of the murine utricle's apical surface correlated with the development of thick, junction-associated F-actin bands in SCs (Burns et al., 2008).

Micropipette aspiration of P0 and adult γ-actin—GFP mice revealed that F-actin at the reticular lamina is deformed, and thus could contribute to the stiffness measurements (Movie 3-2). To test whether F-actin affects the stiffness of the apical surface, we cultured utricles from adult mice in the presence of the F-actin depolymerizing agent cytochalasin D for 24 h. As previously shown (Burns and Corwin, 2014), cytochalasin D treatment disrupts the F-actin bands compared to DMSO-treated controls (Figure 3-2A, B). Micropipette aspiration revealed that cytochalasin D treatment resulted in a nearly 40% increase in deformation length over controls (7.3 ± 0.7 vs 5.3 ± 1.2 µm, $p = 0.002$, $t_{(12)} = 3.941$, unpaired t-test, n = 7 utricles per condition, Figure 3-2C-E). The results show that the thick F-actin bands which develop in mammalian SCs significantly limit the deformation of the utricle's apical surface in response to an applied force. This mechanical stability would prevent the forces arising from HC loss from eliciting rapid shape changes that are associated with nuclear accumulation of YAP and proliferation in SCs (Rudolf et al., 2020).

Progressive SC elongation in the chicken utricle revealed the emergence of anisotropic tissue tension

We observed that the apical domains of SCs in the mouse utricle resemble regular polygons, whereas those of chicken SCs are elongated and aligned along the axis of HC polarity (Figure 3-3A, B). To quantify the degree of elongation and alignment, we traced the apical domains of SCs from confocal images of the apical junctions, and fit each outline to an ellipse with determined length, width, and orientation (Figure 3-3C-H). The length:width ratio provided a measure of elongation. The degree of alignment was determined by identifying the median orientation in each image and calculating the average deviation from that, such that perfectly aligned cells have an average deviation of 0°, and randomly oriented cells have an average deviation of 45° (Figure 3-3I).

In the mouse utricle, SCs maintained regular shapes from E16 through adulthood (Figure 3-4A-C), though the area of the apical domains increased by ~80% ($p = 0.0008$, $F_{(2, 8)} = 20.0$, ANOVA, n = 3-4 utricles per condition, Figure 3-4H). The length:width ratios of the cells marginally

increased by ~8% ($p = 0.044$, $F_{(2, 8)} = 4.7$, ANOVA, n = 3-4 utricles per condition), indicating a very slight elongation, and SCs did not become aligned with age ($p = 0.18$, $F_{(2, 8)} = 2.1$, ANOVA, n = 3-4 utricles per condition).

The apical domains of chicken SCs increased ~50% in area from E7 to P0 ($p = 0.001$, $F_{(3,16)} = 9.05$, ANOVA, n = 3-7 utricles per condition). But unlike the regular shapes of murine SCs, SCs in the chicken utricle became progressively elongated and aligned during embryonic development (Figure 3-4D-H). By P0, the average chicken SC had a length:width ratio of 4.2 ± 0.7, more than twice that of E7 SCs ($p = 0.001$, $F_{(3,16)} = 25.5$, ANOVA, n = 3-7 utricles per condition). The average deviation from the local median angle shrank from 23° ± 4° to only 7° ± 1° ($p < 0.0001$, $F_{(3, 18)} = 39.9$, ANOVA, n = 3-7 utricles per condition). The measurements indicate that SCs in the mouse utricle maintain standard hexagonal close-packing, whereas the progressive elongation and alignment of SCs in the chicken utricle suggests that they are deformed by anisotropic tension.

During development and regeneration, SC divisions in the chicken utricle are oriented and occur perpendicular to the axis of HC polarity

In epithelial monolayers that experience anisotropic stress, cell divisions are oriented such that they occur along the long axis of the cell, resulting in dissipation of stress (Wyatt et al., 2015). To test whether the elongated and aligned SCs in the chicken utricle undergo oriented cell divisions, we harvested utricles at E14 and immunostained them with an antibody for phospho-Histone 3 (PH3), which identifies cells that are in the M-phase of the cell cycle. The orientations of mitotic figures in metaphase or anaphase were analyzed with respect to the local axis of HC polarity, as determined by spectrin immunostaining. Surprisingly, metaphase plates were usually parallel with axis of HC polarity, such that an ensuing cell division would be expected to occur perpendicular to that axis (Figure 3-5A, B). In anaphase cells, divisions also tended to occur perpendicular to the axis of HC polarity (Figure 3-5 C, D). Quantification of 119 mitotic figures showed that the distribution was heavily skewed with divisions occurring perpendicular to the axis

of HC polarity. The measured distribution of cell division orientations was very unlikely to be random ($p = 1.512e^{-10}$, D = 0.313, KS test, n = 119 cells, Figure 3-5J).

To test whether regenerative cell divisions were oriented in the chicken utricle, we cultured utricles from P2 in the presence of 1 mM streptomycin for 24 h to ablate HCs, and fixed after a total of 72 h to assess the orientation of dividing cells. Similar to the E14 utricle, mitotic figures in metaphase and anaphase tended to be aligned such that the cell division would occur perpendicular to the axis of SC elongation (Figure 3-5F-I). Quantification of 141 mitotic figures produced a distribution that was heavily skewed perpendicular to the axis of SC elongation, and a KS test revealed that the distribution was very unlikely to match that of randomly oriented divisions ($p = 2.368e^{-8}$, D = 0.254, KS test, n = 141 cells, Figure 3-5J). The results suggest that cell divisions in the developing and regenerating chicken utricle tend to be oriented along the short axis of the cell—appearing to contribute to, rather than dissipate, anisotropic stress.

Murine SCs maintain their shape independent of non-muscle myosin II contractility, but chicken SCs require actomyosin contractility to maintain their anisotropic shapes

The apical domains of epithelial cells are shaped by the contractility of non-muscle myosin II on the junction-associated F-actin belt (Ebrahim et al., 2013). We tested whether interfering with this contractility would affect the shapes of SCs in utricles from P0 mice and P0 chickens. Utricles were cultured for 5 h in either DMSO or blebbistatin, an inhibitor of non-muscle myosin II contractility. Most cultures were either fixed and processed for immunohistochemistry at that point, and some blebbistatin-treated cultures were rinsed and fixed after a total of 16 h.

There were no significant differences in the area, elongation, or alignment of SCs in the P0 mouse utricle upon blebbistatin treatment (area: $p = 0.24$, $t_{(6)} = 1.30$; length:width ratio: $p = 0.51$, $t_{(6)} = 0.70$; alignment: $p = 0.88$, $t_{(6)} = 0.15$, unpaired t-test, n=4 utricles per condition, Figure 3-6A, B, F). In contrast, blebbistatin treatment of chicken utricles resulted in a 20% increase SC area and a 20% decrease in length:width ratio (area: $p = 0.027$, $t_{(8)} = 2.7$; length:width ratio: $p = 0.0485$, $t_{(8)} = 2.3$; alignment: $p = 0.11$, $t_{(8)} = 1.8$, unpaired t-test, n = 5 utricles per condition, Figure

3-6C-F). The effects of blebbistatin on the chicken utricle were reversible upon washout (area: $p = 0.0062$, $t_{(8)} = 3.7$; length:width ratio: $p = 0.027$, $t_{(8)} = 2.3$; alignment: $p = 0.042$, $t_{(8)} = 2.7$, unpaired t-test, n = 5 utricles per condition). Thus, the size and shape of the SC apical domain appeared to be maintained independent of non-muscle myosin II contractility in the mouse utricle. In sharp contrast, SCs in the chicken utricle required tonic actomyosin contractility to maintain their compact, elongated, and aligned shapes.

To further examine the importance of non-muscle myosin II contractility for maintaining SC shapes in the P0 chicken utricle, we monitored the effects of blebbistatin treatment using time lapse microscopy. F-actin was visualized with SiR-actin, a cell permeable dye that labeled F-actin at cell junctions and in hair bundles. At the start of the acquisition, DMSO was spiked into the medium of one half of a bisected imaging chamber, and blebbistatin was spiked into the other half at a final concentration of 50 μM. The shapes of SCs in the DMSO-treated utricles did not change throughout the 9 h time lapse (Movie 3-3). In the blebbistatin-treated utricles, however, apical surfaces of SCs began to enlarge starting at ~3 h and continuing through 9 h. The shape changes did not occur stochastically in individual SCs, but rather groups of SCs changed shape in concert.

Dramatic changes to epithelial morphology occurred when P0 chicken utricles were cultured in blebbistatin for longer durations. After 24 h in culture, DMSO-treated controls maintained their typical planar apical surface, but those cultured in blebbistatin had a “ruffled” appearance (Figure 3-6G-I). The “ruffles” had a regular spacing of ~25 μm and ran parallel to the local axis of HC polarity. The results show that upon inhibition of non-muscle myosin II contractility, SC relaxation is anisotropic, with short axes of the SCs expanding to a greater degree than the long axis of the cell. As the sensory epithelium was constrained within the original macular borders, these anisotropic expansions led to buckling out of the original tissue plane.

DISCUSSION

Vestibular SCs in mammals and nonmammals share most characteristics, but have very different capacities for regeneration. The development of E-cadherin-rich junctions with thick

circumferential F-actin bands in mammalian SCs has been hypothesized to function as a “brake” on the regenerative processes that occur readily in nonmammalian SCs. Here, we present the first direct evidence that the thick F-actin bands function biomechanically to restrict the collective mechanical behavior that normally governs epithelial repair. This stands in stark contrast to the chicken utricle, were such collective behavior is evident in SCs.

Epithelial cell loss produces different types of mechanical signals. One is the physical deformation of neighboring cells. Another is an increase in cortical tension due to increased actomyosin contractility (Karsch et al., 2017). The likelihood of an epithelial cell to progress through the cell cycle is predicted well by the combination of these geometric and mechanical properties (Uroz et al., 2018). The data indicate that the F-actin bands in mammalian SCs can restrict both. First, micropipette aspiration measurements revealed that the apical surface of the mouse utricle resists deformation in an age- and F-actin-dependent manner (Figure 3-1, 2), explaining why SC shape changes in response to HC loss are less dynamic in mature mouse utricles than in utricles from newborn mice (Burns and Corwin, 2014). Second, the activity of nonmuscle myosin II does not influence the SC shape in the murine utricle (Figure 3-6), suggesting impairment in the ability to modulate cortical tension upon cell loss. The efficiency of actomyosin contractility depends on the ultrastructural features of the F-actin network and its degree of crosslinking (Ennomani et al., 2016). Further studies are required to investigate those parameters in the F-actin bands of SCs in the mammalian utricle.

Although it is logical that inhibition of nonmuscle myosin II contractility has different effects on SCs in the chicken utricle than those in the mouse utricle, we observed that even SCs in newborn mice are be insensitive to the inhibition of actomyosin contractility. In comparison, blebbistatin treatments have been shown to induce expansion of SC apical domains in the cochlear explants from embryonic and early neonatal mice (Cohen et al., 2019; Ebrahim et al., 2013). This apparent discrepancy can be explained by accounting for the variation in F-actin band thickness that is apparent between utricular and cochlear SCs in newborn mice. It was reported

that SCs in the P0 mouse utricle have circumferential F-actin bands ~30% thicker than those of Deiters cells in the P1 mouse cochlea, and they are twice as thick as the bands in SCs in the chicken utricle (Burns et al., 2008, 2013). The thinner F-actin bands in the developing cochlear SCs may facilitate the convergent extension, intercalation, and precise patterning that occur during development. As the circumferential F-actin bands between Deiters cells and pillar cells also thicken with age (Burns et al., 2013), we predict that those cochlear SCs too would eventually lose their sensitivity to blebbistatin treatment. Consistent with the notion that cochlear SCs too become mechanically stable with age, the thick F-actin bands appear to serve as a scaffold that preserves positions of surviving cells after HC loss in the mature organ of Corti (Anttonen et al., 2017).

The findings here indicate that the thick circumferential F-actin bands confer two potential evolutionary advantages to mammals. First, the thick F-actin bands allow the apical surface of the mammalian HC epithelium to become stiffer than those in nonmammals. The fidelity of HC mechanoelectrical transduction is enhanced by the high rigidity of the reticular lamina (Tomo et al., 2007). Second, the thick F-actin bands impart mechanical stability via a passive mechanism that does not rely on constitutive activity of nonmuscle myosin II. By avoiding the need to expend ATP to maintain the shapes of their apical membrane, mammalian SCs may have a lower metabolic requirement than those of nonmammals. Whether such metabolic differences exist between mammalian and nonmammalian SCs remains unexplored.

The mechanical signals that arise from cell loss eventually must influence intracellular signaling pathways in order to evoke proliferation. One such candidate is the Hippo pathway and its effector YAP. It has recently been shown that YAP enters SC nuclei and evokes regenerative proliferation after HC losses in the chicken utricle, but in the mouse utricle YAP remains cytoplasmic after HC loss (Borse et al., 2020; Rudolf et al., 2020). Further, shape changes correlate with the nuclear accumulation of YAP in SCs (Rudolf et al., 2020). The relationship between actomyosin contractility and YAP activation remains to be directly established in HC

epithelia, although this has been shown in other epithelia (Furukawa et al., 2017; Pan et al., 2016; Rauskolb et al., 2014).

Our results suggest that dismantling the thick circumferential F-actin bands would amplify regenerative responses in mammalian SCs. It was recently shown that treatments with EGF and a GSK3β inhibition thin the F-actin bands throughout the macula of cultured utricles from adult mice (Kozlowski et al., 2020). The treatment eventually led to the depletion of E-cadherin from the junctions between striolar SCs, and a resurgence in striolar proliferation. These results indicated that thinning the F-actin bands is not sufficient to release extrastriolar SCs from proliferative quiescence. However, that study did not explore whether the treatment increased the responsiveness of SCs to nonmuscle myosin II contractility.

SC shape changes have been firmly established to control proliferation of SCs (Collado et al., 2011a; Gnedeva et al., 2017; Meyers and Corwin, 2007; Warchol, 2002), whereas the influence of contractility in HC epithelia has been relatively less explored (Meyers and Corwin, 2007; Xia et al., 2020). We argue that it is important to consider this latter parameter in addition to shape change. For example, in the utricles of chickens and newborn mice, many SCs expand a small amount to accommodate vacancies left by lost HCs. In contrast, only SCs adjacent to the lost HC change shape (Burns and Corwin, 2014). Thus, SCs in mature mice have to undergo larger shape changes after HC loss. Why, then, are they less likely to proliferate? Clearly, the cortical tension and rate of shape change must be considered, and not merely shape change alone. The relative influence of these parameters could be explored using a computational model.

The progressive elongation and alignment of SCs in the embryonic chicken utricle is a hallmark of the accumulation of anisotropic stress. Typically, cells orient their divisions such that they occur along the cell's long axis (Hertwig, 1884), which serves to dissipate this stress (Campinho et al., 2013; Wyatt et al., 2015). We find that SC divisions in the developing and regenerating chicken utricle indeed are oriented (Figure 3-5). But in apparent contradiction to "Hertwig's rule", they occur along the short axis of the SC, such that they would appear to promote

the accumulation of anisotropic stress. It will be necessary to conduct time lapse experiments to confirm this unexpected finding. One clue as to a potential purpose for this behavior is that SC elongation occurs along the local axis of HC polarity in this planar polarized epithelium, and that HCs themselves are elongated. Thus, one intriguing possibility is that the unusual orientation of these SC divisions promotes the accumulation of anisotropic stress, thereby aiding the polarization of HCs.

In summary, the work here sharpens our understanding of how junctional reinforcement mechanistically act as a “brake” that limits regenerative processes specifically in mammalian SCs. The thick circumferential F-actin bands act as a “biomechanical brake” that limits SC deformations and actomyosin-generated tension. The E-cadherin adhesions may act as a “biochemical brake” that sequesters mitogenic signaling molecules at adherens junctions (Kozlowski et al., 2020). Both of these mechanisms may impinge on the activation of YAP (Rudolf et al., 2020). These mechanisms explain, in part, why mammalian SCs largely remain in a state of proliferative quiescence after HC loss, whereas those in nonmammals readily replace HCs and enable recovery of hearing and balance function.

FIGURES AND FIGURE LEGENDS

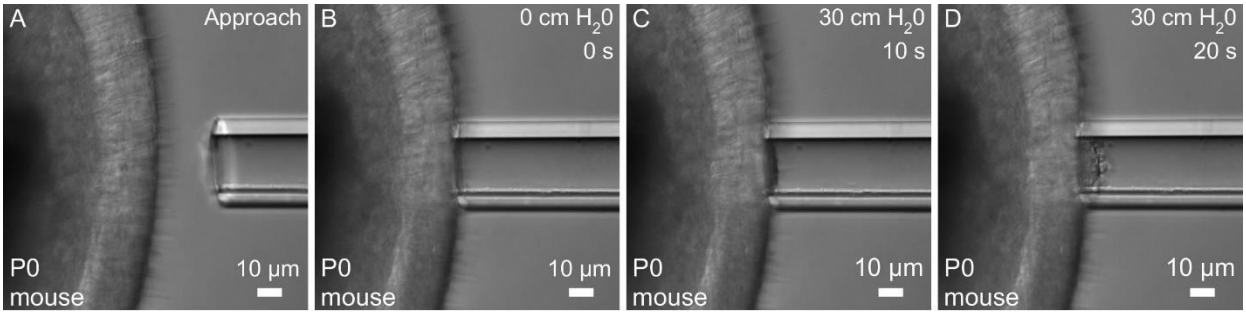

Stills from Movie 3-1. Micropipette aspiration of the apical surface of a utricle from a P0 mouse.

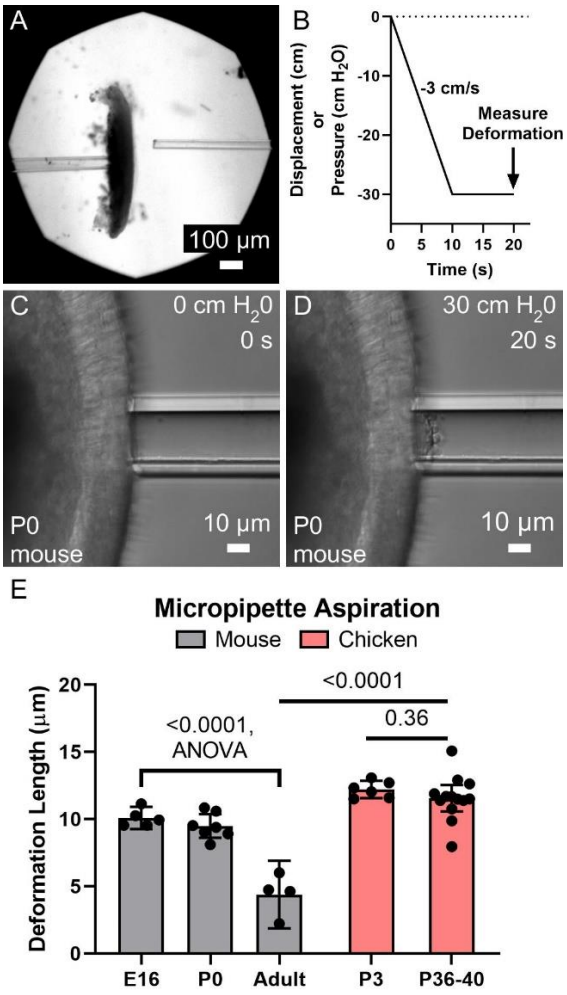

Figure 3-1. Micropipette aspiration measurements reveal that the apical surface of utricles from mature mice are significantly more resistant to deformation than those of newborn mice and chickens. **(A)** Low magnification image of a mouse utricle prior to micropipette aspiration. A stabilizing pipette ~50-100 µm in diameter (left) was used to apply light suction on the "nerve side" to maintain the utricle in place. Another pipette 22.5 µm (~5 cell apices) in diameter (right) was used to apply a defined negative pressure to the apical surface of the utricle. **(B)** The negative pressure was ramped from 0 cm H2O to -30 cm H2O over a span of 10 s, and then maintained at -30 cm H2O for an additional 10 s. The deformation length of the apical surface was after the full 20 s "pull" was recorded. **(C, D)** High magnification images of the apical surface of a P0 mouse utricle during application of negative pressure. **(E)** Plot of mean deformation length of utricles from mice and chickens of various ages. Error bars denote 95% confidence interval. Dots represent an average of at least three measurements from a single utricle. P-values are listed for relevant statistical comparisons. The mean deformation length of the mouse utricle significantly differed with age ($p < 0.0001$, $F_{(2, 13)} = 38.16$, ANOVA, n = 4-7 utricles per condition). The mean deformation lengths did not significantly differ between P3 and P36-40 chicken utricles ($p = 0.36$, $t_{(17)} = 0.93$, unpaired t-test, n = 6-13 utricles per condition). The mean deformation length was significantly lower in adult mouse utricles than P36-40 chicken utricles ($p < 0.0001$, $t_{(15)} = 7.7$, unpaired t-test, n = 4-13 utricles per condition).

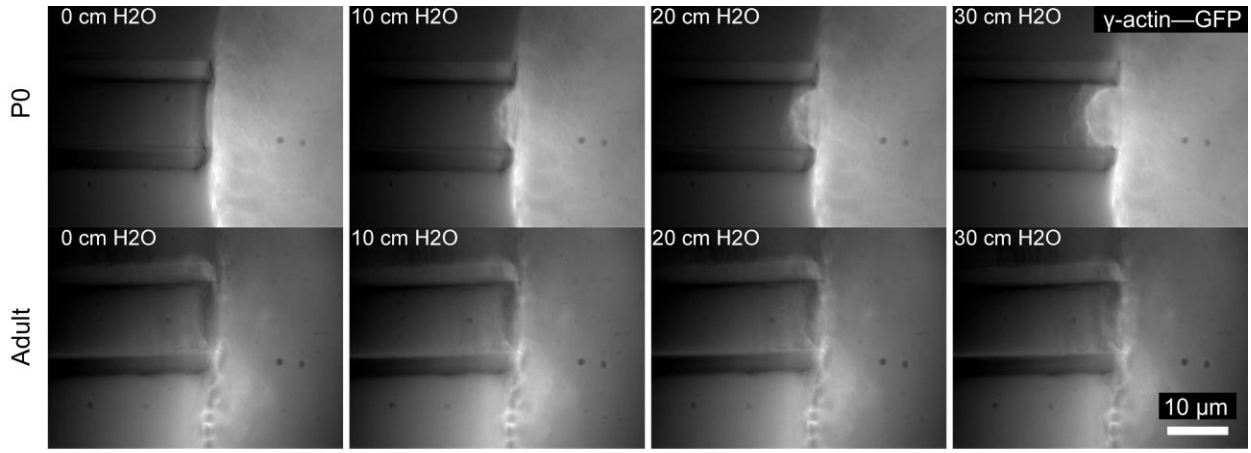

Stills from Movie 3-2. Micropipette aspiration of P0 and adult γ-actin—GFP mice revealed that F-actin at the reticular lamina is deformed, and thus could contribute to the stiffness measurements.

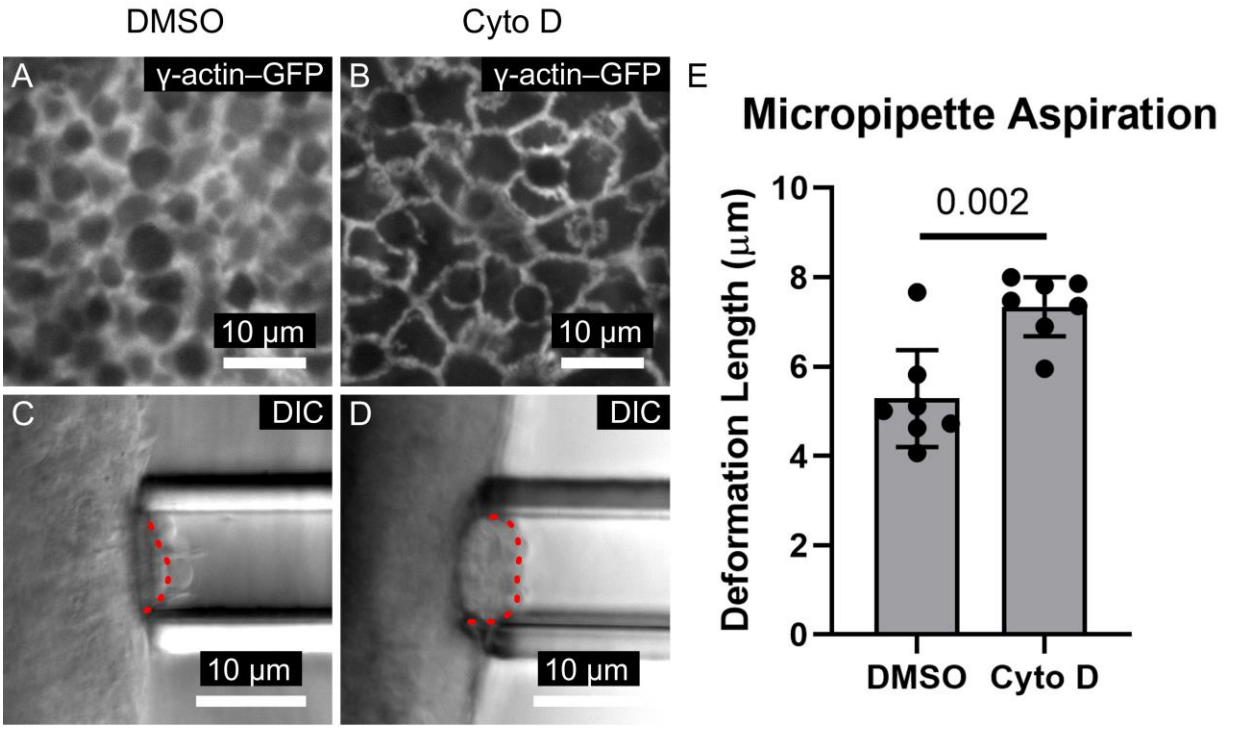

Figure 3-2. F-actin depolymerization thins the circumferential F-actin bands in SCs of adult mouse utricles and reduces stiffness of the apical surface. **(A, B)** Fluorescent images of utricles from adult γ-actin—GFP mice that were cultured for 24 h in DMSO or 100 nM cytochalasin D (Cyto D), an F-actin depolymerizing agent. **(C, D)** Representative micropipette aspiration images of utricles from adult Swiss Webster mice that were cultured in DMSO or 100 nM Cyto D for 24 h. Red dashed lines denote the deformations. **(E)** Blinded quantification revealed that the mean deformation length of utricles cultured in Cyto D was significantly greater than that of DMSO-treated controls ($p = 0.002$, $t_{(12)} = 3.941$, unpaired t-test, $n = 7$ utricles per condition). Data are shown as mean ± 95% confidence interval. Dots represent an average of at least three measurements from a single utricle.

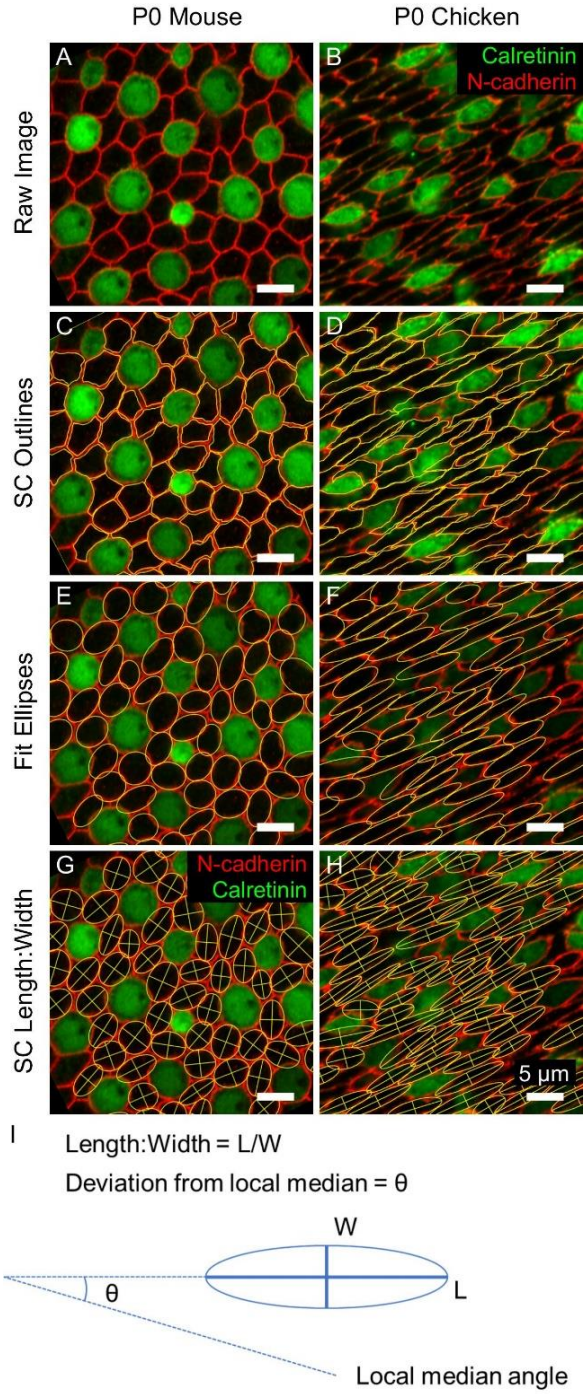

Figure 3-3. Elongation and alignment analysis of SCs in utricles from mice and chickens. **(A, B)** Utricles were immunostained for N-cadherin to denote apical junctions and the HC marker Calretinin to distinguish HCs from SCs and imaged on a confocal microscope. **(C, D)** The apical domains of at least 30 contiguous SCs were outlined. **(E, F)** Each SC outline was fit to an ellipse. **(G, H)** The length, width, and angle of each ellipse was recorded. **(I)** The length:width ratio (L/W) provided a measure of SC elongation. To quantify local alignment, the local median angle was calculated for each image. The deviation θ of each ellipse from the local median angle was averaged to provide a measure of local alignment, ranging from 0 degrees deviation (perfect alignment) to 45 degrees deviation (random alignment).

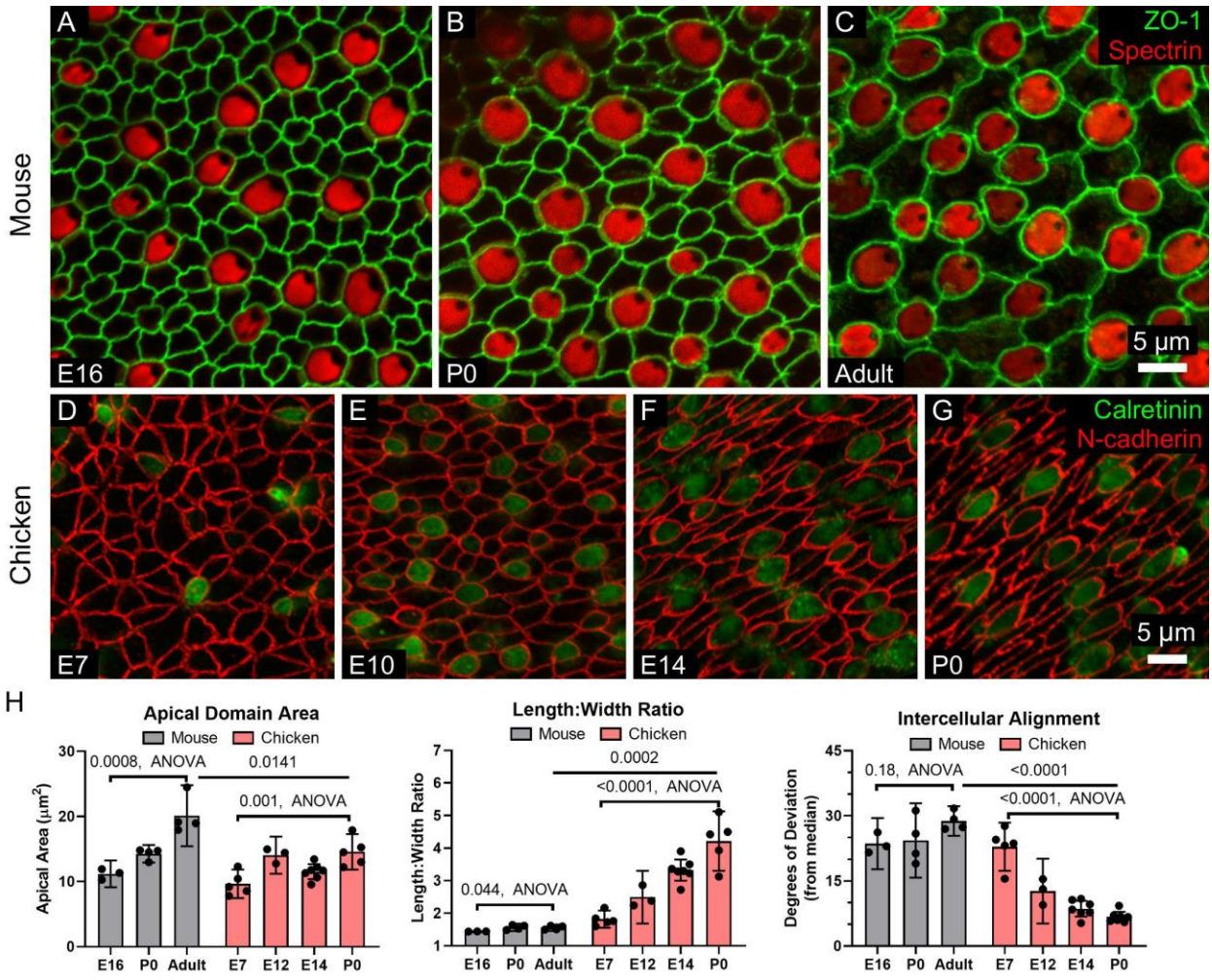

Figure 3-4. SCs in mouse utricles do not undergo dramatic shape changes during development and postnatal maturation, whereas those in chickens become more elongated and locally aligned during development. **(A-C)** Confocal images of utricles from mice of various ages. Images are from the striolar region. **(D-G)** Confocal images of utricles from chickens of various ages. **(H)** Quantification reveals that SC apical domains become significantly larger over time (Mouse: $p = 0.0008$, $F_{(2, 8)} = 20.0$, ANOVA, n = 3-4 utricles per condition; Chicken: $p = 0.001$, $F_{(3,16)} = 9.05$, ANOVA, n = 3-7 utricles per condition). The mean SC area was significantly greater in adult mice than P0 chickens ($p = 0.0141$, $t_{(7)} = 3.2$, unpaired t-test, n = 4-5 utricles per condition). Both murine and chicken SCs became significantly more elongated with age (Mouse: $p = 0.044$, $F_{(2, 8)} = 4.7$, ANOVA, n = 3-4 utricles per condition; Chicken: $p = 0.001$, $F_{(3,16)} = 25.5$, ANOVA, n = 3-7 utricles per condition), though elongation was significantly greater in P0 chicken SCs compared to SCs in adult mice ($p = 0.0002$, $t_{(7)} = 7.1$, unpaired t-test, n = 4-5 utricles per condition). Alignment did not significantly change in murine SCs with age ($p = 0.18$, $F_{(2, 8)} = 2.1$, ANOVA, n = 3-4 utricles per conditions), but significantly increased with age in chicken SCs ($p < 0.0001$, $F_{(3, 18)} = 39.9$, ANOVA, n = 3-7 utricles per condition). SCs of the P0 chicken utricle were significantly more aligned than those of adult mouse utricles ($p < 0.0001$, $t(9) = 21.9$, unpaired t-test, n = 4-7 utricles per condition).

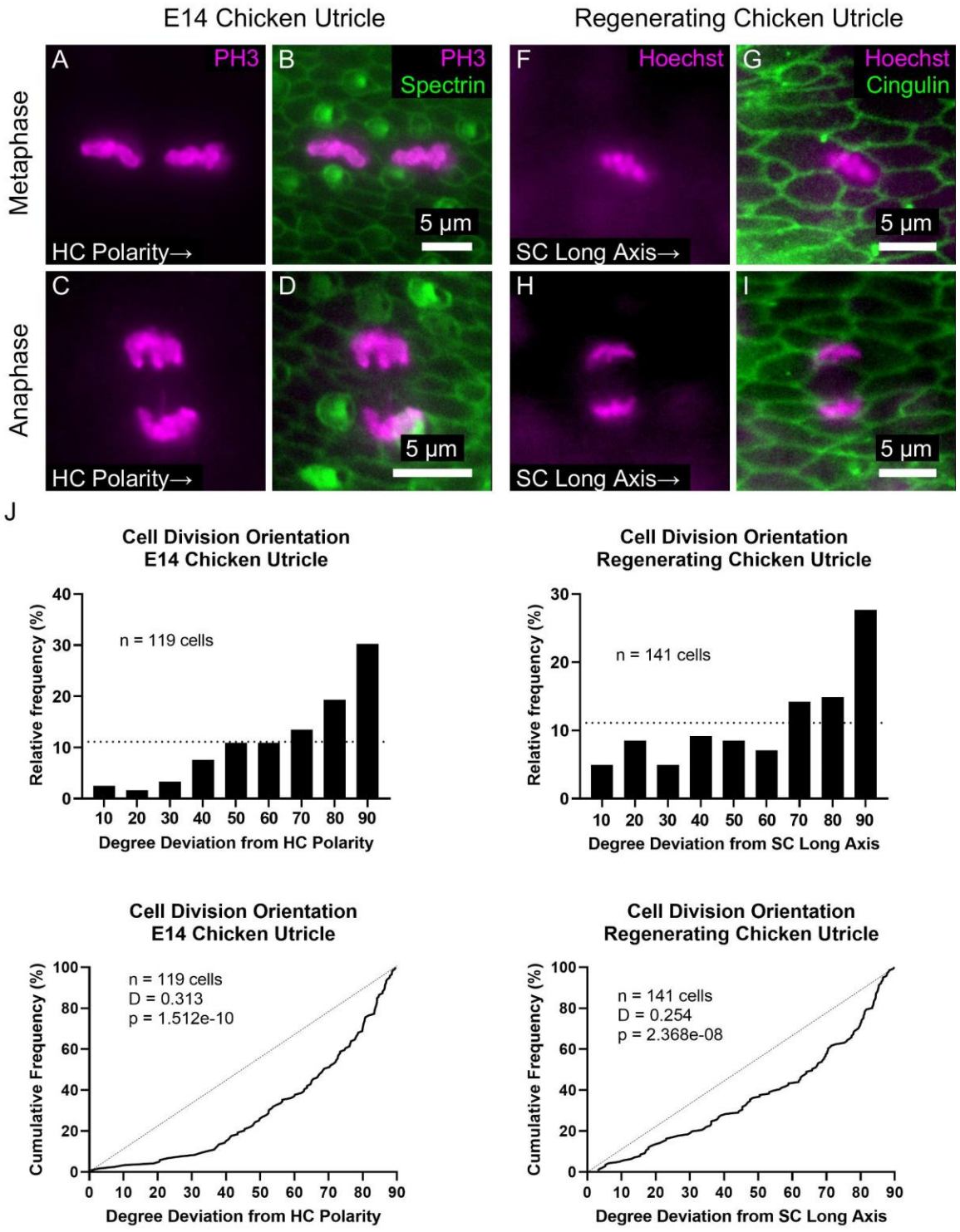

Figure 3-5. Cell divisions are oriented in the developing and regenerating chicken utricle, occurring perpendicular to the axes of HC polarity/SC elongation. **(A-D)** The orientation of PH3-labeled mitotic figures in metaphase (A, B) and anaphase (C, D) were measured with respect to the local axis of HC polarity, as visualized by spectrin immunostaining. **(E-H)** To determine whether regenerative cell divisions were oriented, utricles from P2 chickens were cultured for 24 h to ablate HCs and fixed after a total of 72 h. Images of cells

in metaphase (E, F) and anaphase (G, H) were acquired with Hoechst labeling of cell nuclei, and the orientation of mitotic figures was measured with respect to the local axis of SC elongation, as visualized by cingulin immunostaining. **(G)** *Top:* Histograms of cell division orientation during development and regeneration. The bins have a width of 10 degrees and the x-axis labels denote the upper boundary of each bin. The dashed lines denote a uniform distribution (i.e. randomly oriented divisions). *Bottom:* Cumulative distribution functions of cell division orientation during development and regeneration. Dashed lines denote randomly oriented cell divisions. KS tests revealed that the measured cell division orientations were significantly non-random during development ($p = 1.512e-10$, $D = 0.313$, $n = 119$ cells) and regeneration ($p = 2.368e-8$, $D=0.254$, $n = 141$ cells).

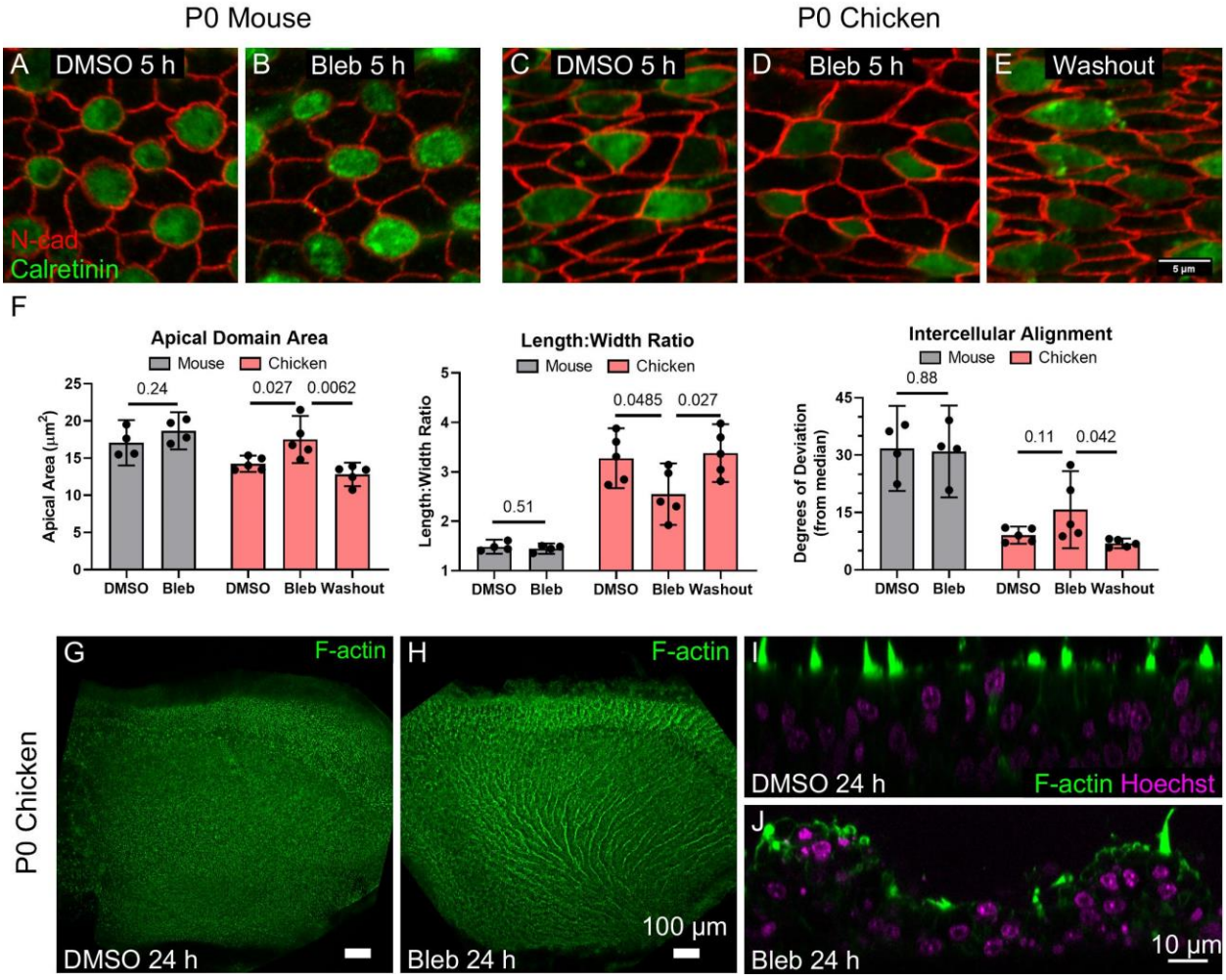

Figure 3-6. Inhibition of nonmuscle myosin II activity had no effect in the mouse utricle, but disrupted SC shape in utricles of chickens. **(A-E)** Utricles from P0 mice and P0 chickens were cultured for 5 h in the presence of 50 µM blebbistatin or DMSO vehicle control before fixation. Some blebbistatin-treated utricles of P0 chickens were rinsed and fixed after a total of 16 h (Washout, E). **(F)** Quantification revealed that in SCs of mouse utricles, there were no statistically significant differences in apical domain area ($p = 0.24$, $t_{(6)} = 1.30$, unpaired t-test, n=4 utricles per condition), length:width ratio ($p = 0.51$, $t_{(6)} = 0.70$, unpaired t-test, n=4 utricles per condition), or intercellular alignment ($p = 0.88$, $t_{(6)} = 0.15$, unpaired t-test, n=4 utricles per condition) between DMSO-treated and blebbistatin-treated utricles. In contrast, blebbistatin treatment significantly affected SC area ($p = 0.027$, $t_{(8)} = 2.7$, n = 5 utricles per condition) and length:width ratio ($p = 0.0485$, $t_{(8)} = 2.3$, n = 5 utricles per condition) in chicken utricles, with alignment not reaching statistical significance ($p = 0.11$, $t_{(8)} = 1.8$, n = 5 utricles per condition). Upon washout of blebbistatin, changes to SC area ($p = 0.0062$, $t_{(8)} = 3.7$, n = 5 utricles per condition), elongation ($p = 0.027$, $t_{(8)} = 2.3$, n = 5 utricles per condition), and intercellular alignment ($p = 0.042$, $t_{(8)} = 2.7$, n = 5 utricles per condition) were reversible. **(G, H)** After 24 h in culture, chicken utricles treated with DMSO (G) appeared normal, but treatment with 50 µm blebbistatin (H) led to buckling of the epithelial surface. **(I, J)** Z-projections depicting buckling of the epithelium after blebbistatin treatment.

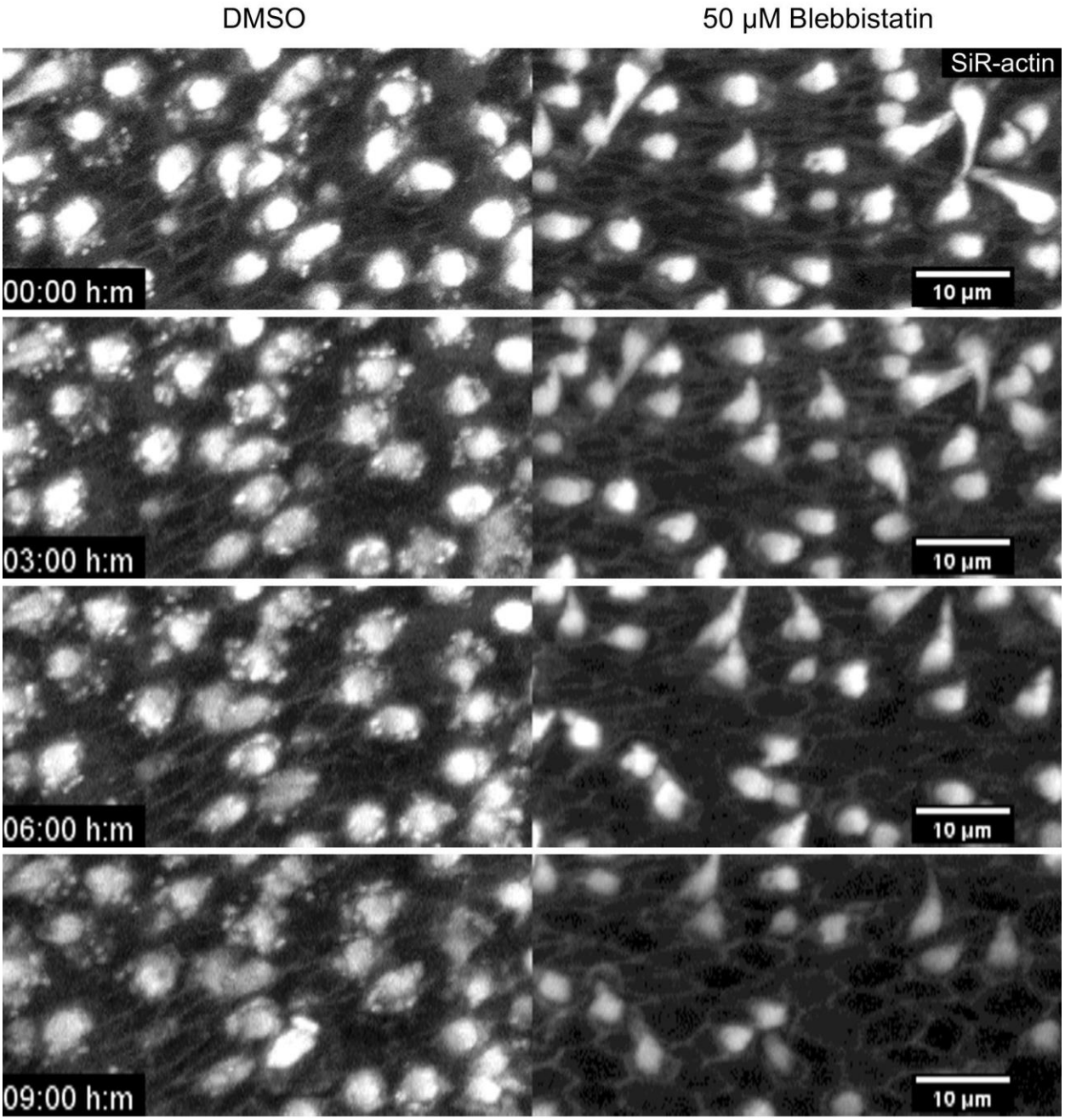

Stills from Movie 3-3. Inhibition of nonmuscle myosin II causes shape changes in SCs of the posthatch chicken utricle. P0 chicken utricles were harvested and incubated with the vital dye SiR-actin at 100 nM for 6 h, which labeled F-actin in hair bundles and cell junctions. Utricles were incubated with 3 µM FM1-43 for 3 min to label HCs prior to placement in a two-sided chamber for live imaging on a Zeiss 880 confocal microscope. One utricle was incubated in DMSO-containing medium as a negative control, and another utricle was incubated in medium containing 50 µM blebbistatin. Utricles were maintained in a humidified chamber at 37°C, and z-stacks were acquired every 10 min. Images are displayed as a maximum intensity projection with gamma level 0.5 to enhance visualization of the cell junctions. Only the SiR-actin channel is displayed here.

SUPPLEMENTAL DISCUSSION

An emerging paradigm in epithelial repair specifies that mechanical signals coordinate a focal, proliferative response to cell loss. This appendix briefly summarizes key principles related to epithelial mechanics, mechanical signals that arise from cell loss, and the ensuing intracellular pathways activated by those signals.

Cell loss produces mechanical signals that govern epithelial repair

The size of an isolated cell depends on the balance of two factors: (1) intracellular pressure, which acts to increase cell size, and (2) cortical tension, which acts to decrease cell size. Cortical tension arises from stretching of the lipid bilayer and tension generated by actomyosin contractility at the cell cortex.

In a crowded epithelium, cells also experience external compressive forces which can be viewed as an external pressure. Thus, the size of an epithelial cell is dictated by the balance of its intracellular pressure with its cortical tension and external pressure (Figure 3-S1).

Epithelial cells do not behave as passive materials in the face of mechanical perturbation. Rather, they actively adjust their cortical tension in response to changes in external forces (Noll et al., 2017). These adjustments to cortical tension often act as a homeostatic mechanism to minimize cellular deformation (Kasza and Zallen, 2011; Pan et al., 2016). The “mechanical feedback” model specifies that cells experiencing an increase in external compressive forces (e.g. via proliferation of neighboring cells) reduce their cortical tension, and cells experiencing a reduction in external compressive forces (e.g. due to nearby cell loss) adaptively increase their cortical tension (Figure 3-S1) (Pan et al., 2016).

Cell losses in epithelia initiate a process by which the surrounding cells coordinate to remove the dying cell and establish new intercellular junctions. In MDCK cell monolayers, the apoptotic cell initiates this process by exerting tension on its neighbors via contraction of its apical actomyosin cable. Then, surrounding cells form a multicellular F-actin purse string that contracts to extrude the dying cell (Kuipers et al., 2014). This wound closure increases cortical

tension and induces shape changes in nearby cells, both of which are detectable several cell diameters away (Karsch et al., 2017). This mechanism of F-actin purse string closure occurs after HC loss in the utricles of chickens and newborn mice (Bird et al., 2010; Burns and Corwin, 2014).

These mechanical signals that arise from cell loss (i.e. changes in shape and cortical tension) are associated with proliferation. In MDCK monolayers, the combination of cortical tension and cell area strongly predicts whether a cell will progress through G1-phase of the cell cycle (Uroz et al., 2018).

Mechanistically, these mechanical signals activate YAP signaling. The nuclear level of YAP positively correlates with phosphorylated myosin regulatory light chain at the apical junction, a readout of cortical tension (Perez Gonzalez et al., 2018). Physically stretching epithelial monolayers stimulates nuclear translocation of YAP (Benham-Pyle et al., 2015).

The exact mechanism of YAP activation is not well understood. Rauskolb *et al*. demonstrated that in the *Drosophila* wing, tension promoted Jub-dependent recruitment of Warts (LATS1/2 in mammals) to adherens junctions, thereby dis-inhibiting Yorkie (YAP/TAZ in mammals) (Rauskolb et al., 2014).

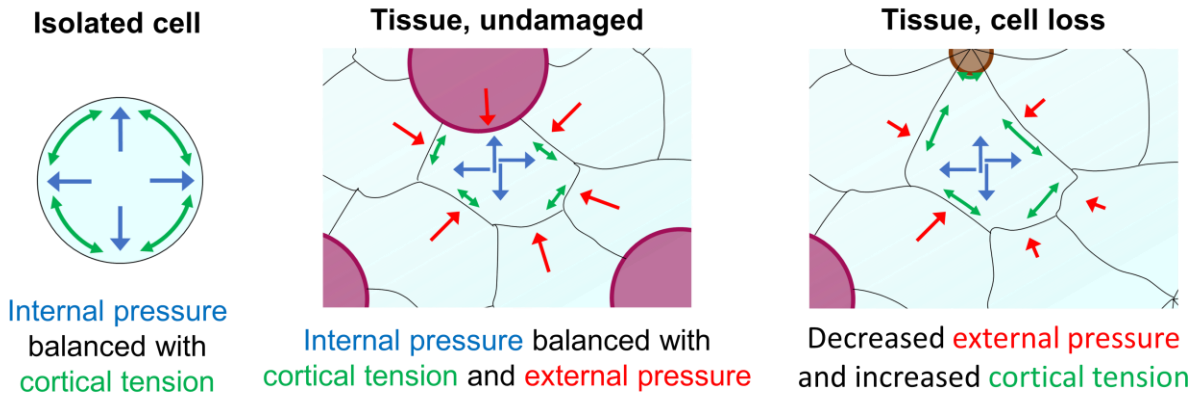

Figure 3-S1. Schematic of force balance in an isolated cell (left), an undamaged hair cell epithelium (middle), and a damaged hair cell epithelium (right). Upon loss of a hair cell (magenta), the supporting cells (blue) change shape and likely increase cortical tension as part of a homeostatic response to limit cellular deformation. Shape changes and increases in cortical tension are mechanical signals that arise from cell loss, and each activates mitogenic signaling as a process of epithelial repair.

CHAPTER 4
EGF and a GSK3 Inhibitor Deplete Junctional E-cadherin and Stimulate Proliferation in the Mature Mammalian Ear[1]

ABSTRACT

Sensory hair cell losses underlie the vast majority of permanent hearing and balance deficits in humans, but many nonmammalian vertebrates can fully recover from hearing impairments and balance dysfunctions because supporting cells (SCs) in their ears retain lifelong regenerative capacities that depend on proliferation and differentiation as replacement hair cells. Most SCs in vertebrate ears stop dividing during embryogenesis; and soon after birth, vestibular SCs in mammals transition to lasting quiescence as they develop massively thickened circumferential F-actin bands at their E-cadherin-rich adherens junctions. Here, we report that treatment with EGF and a GSK3 inhibitor thinned the circumferential F-actin bands throughout the sensory epithelium of cultured utricles that were isolated from adult mice of either sex. That treatment also caused decreases in E-cadherin, β-catenin, and YAP in the striola, and stimulated robust proliferation of mature, normally quiescent striolar SCs. The findings suggest that E-cadherin-rich junctions, which are not present in the SCs of the fish, amphibians, and birds which readily regenerate hair cells, are responsible in part for the mammalian ear's vulnerability to permanent balance and hearing deficits.

[1] This is a reproduction of Kozlowski, Rudolf, and Corwin 2020. It has been modified to fit the terminology and style of this thesis.

SIGNIFICANCE STATEMENT

Millions of people are affected by hearing and balance deficits that arise when loud sounds, ototoxic drugs, infections, and aging cause hair cell losses. Such deficits are permanent for humans and other mammals, but nonmammals can recover hearing and balance after supporting cells regenerate replacement hair cells. Mammalian supporting cells lose the capacity to proliferate around the time they develop unique, exceptionally reinforced, E-cadherin-rich intercellular junctions. Here, we report the discovery of a pharmacological treatment that thins F-actin bands, depletes E-cadherin, and stimulates proliferation in long-quiescent supporting cells within a balance epithelium from adult mice. The findings suggest that high E-cadherin in those supporting cell junctions may be responsible, in part, for the permanence of hair cell loss in mammals.

INTRODUCTION

Over 400 million people live with disabling and permanent hearing deficits that commonly arise when sensory hair cells (HCs) are lost through exposure to loud sounds and ototoxic drugs, infections, or as the consequence of aging (Nadol, 1993; World Health Organization, 2020). Millions more are afflicted with balance disorders caused by HC losses in the vestibular epithelia (Agrawal et al., 2009). Severe HC losses produce hearing and balance deficits in mammals and nonmammals alike, but nonmammals recover from deafening and imbalance within weeks via regeneration that depends on epithelial supporting cells (SCs) whose progeny differentiate as replacement HCs, as well as SCs that can directly convert into HCs without an intervening cell division (Corwin and Cotanche, 1988; Ryals and Rubel, 1988; Jones and Corwin, 1996; Golub et al., 2012; Scheibinger et al., 2018). Regenerative proliferation is limited in mammals because their SCs become quiescent as they mature (Hume et al., 2003; Davies et al., 2007; Gu et al., 2007; Oshima et al., 2007; Lu and Corwin, 2008; Burns et al., 2012b). Just what maturational changes restrict proliferation of mammalian SCs has remained unanswered.

Early in development, SCs in the inner ears of mammals resemble their nonmammalian counterparts which readily proliferate and replace HCs after damage. However, as mammals mature, their vestibular SCs and the pillar and Deiters cells within the organ of Corti develop intercellular junctions with specializations that are not found in most nonmammalian SCs. At about the time when those specializations arise, mammalian SCs become proliferatively quiescent. The "parking brake hypothesis" (Burns and Corwin, 2013) suggests that proliferation is limited not only by downregulation of developmental growth pathways, which occurs in both mammals and nonmammals, but also by the unique features of mammalian SCs that emerge with their maturation. One candidate for such an inhibitory feature is the massive maturational reinforcement of circumferential F-actin bands at the adherens junctions of mammalian vestibular SCs (Burns et al., 2013). Another candidate is the E-cadherin that accumulates at the junctions between the maturing vestibular SCs. Less pronounced F-actin reinforcement and E-cadherin expression occur in pillar cells and Deiters cells of the maturing organ of Corti. Both aspects of junctional reinforcement strongly correlate with declines in the capacity for mammalian vestibular SCs to proliferate in response to exogenous mitogens or damage to the epithelium (Burns et al., 2008; Collado et al., 2011b). Neither occurs in SCs of fish, amphibians, or birds that readily replace HCs (Burns et al., 2013).

Here, we report that short-term culture with a cocktail of seven factors (7F) (McLean et al., 2017) stimulated robust proliferation of SCs in utricles from neonatal mice, but failed to stimulate proliferation in utricles from mice older than one week, even after HC loss. When utricles from such mice were cultured for longer durations, 7F progressively thinned the F-actin bands in SCs throughout the macula and reduced E-cadherin in striolar SCs. These changes preceded a sharp increase in S-phase entry in the striola. Other experiments showed that two components of 7F—EGF and the GSK3 inhibitor CHIR-99021—are responsible for these effects. When combined, EGF and CHIR-99021 thinned F-actin bands throughout the sensory epithelium, reduced levels

of E-cadherin, apical β-catenin, and apical YAP just in the striolar SCs, and led to mitosis in the striola even in utricles from adults. The findings are consistent with the parking brake hypothesis, and suggest a model in which the maturational reinforcement of E-cadherin-rich SC junctions leads to the sequestration of β-catenin and YAP and the maintenance of SC quiescence, which contributes to the permanence of hearing and balance deficits in mammals.

MATERIALS AND METHODS

Utricle dissection and organotypic culture

All animals were handled in accordance with protocols approved by the Animal Care and Use Committee at the University of Virginia. Swiss-Webster mice of either sex were obtained from Charles Rivers Laboratories. Three-day-old and younger mice were killed on ice, and mice older than 3 d were killed with carbon dioxide. After decapitation, each head was skinned and disinfected in ice-cold 70% ethanol for 15 min. Heads were next moved to ice-cold DMEM/F12 with HEPES (Invitrogen) where utricles were isolated from temporal bones and the roof, otoconia, otolithic membrane, and nerve were mechanically removed. The dissected organs contained the entire sensory epithelium, a small portion of the surrounding nonsensory epithelium, and the underlying stromal tissue. Utricles were next adhered to glass-bottom dishes (Mat-Tek) that were coated with Cell-Tak (Corning), as described previously (Meyers and Corwin, 2007), and cultured in medium. Media were changed every 24 h. To ablate HCs, 2 mM neomycin sulfate (Sigma Millipore) was added to the culture media for 24 h and then washed out with 3 rinses of media. To trace the incidence of S-phase entry, utricles were cultured with 5-ethynyl-2′-deoxyuridine (Cayman Chemical) at a concentration of 2.5 μg/ml. To interfere with the polymerization of microtubules, utricles were cultured with nocodazole (Sigma Millipore) at a concentration of 50 ng/ml.

Preparation of culture media

All media were serum-free and composed of DMEM/F12/HEPES medium (Invitrogen) supplemented with N2 and B27 nutrients (Invitrogen), Glutamax (Invitrogen), and ciprofloxacin

(10 µg/ml; Bayer). For preparation of EC and 7F media, we additionally used EGF (50 ng/ml; Invitrogen), bFGF (50 ng/ml; Stemfactor), IGF-1 (50 ng/ml; Invitrogen), CHIR-99021 (3 µM; LC Laboratories), valproic acid (1 mM; Millipore), phospho-vitamin C (100 µg/ml; Sigma Millipore), and the inhibitor 616452 (2 µM; Calbiochem).

Immunohistochemistry

Utricles were fixed in 4% PFA (Electron Microscopy Sciences) for 1 h at room temperature or in Glyofixx (Thermo Fisher Scientific) overnight at 4°C. Fixed utricles were then washed with PBS/0.02% Triton X-100 (PBST) solution and blocked at room temperature for 1 h in PBST containing either 10% normal goat serum (Vector Laboratories) or 3% normal donkey serum (Jackson ImmunoResearch Laboratories). Samples were next incubated overnight at 4°C with appropriate primary antibodies, washed with PBST, and incubated with AlexaFluor-conjugated secondary antibodies (Invitrogen; 1:500) at room temperature for 2 h. Then samples were washed with PBST and mounted on glass coverslips in ProLong Diamond Antifade Mountant. Images were acquired on a Zeiss 880LSM Airyscan confocal microscope.

Antibody characterization, EdU imaging, and F-actin labeling

To label SCs, we used rabbit anti-Sox2 (Cell Signaling Technology; 1:200; 23064S) and mouse IgG1 anti-Sox2 (Thermo Fisher Scientific; 1:100; MA1-014). To label HCs, we used mouse IgG1 anti-spectrin (Millipore; 1:50; MAB1622) and mouse IgG1 anti-Myo7a (Developmental Studies Hybridoma Bank; 1:50; 138-1). To image striolar HCs, we used goat anti-oncomodulin (Santa Cruz Biotechnology; 1:100; sc-7446) and rabbit anti-oncomodulin (Swant; 1:1000; OMG4). To image junctional proteins, we used rabbit anti-ZO-1 (Invitrogen; 1:200; 40-2200), mouse IgG1 anti-N-cadherin (BD Transduction Laboratories, 1:100; 610920), and mouse IgG2a anti-E-cadherin (BD Transduction Laboratories, 1:200; 610181), which recognizes the cytoplasmic domain of E-cadherin. We also used mouse IgG1 anti-β-catenin (BD Transduction Laboratories, 1:400; 610153) and mouse IgG2a anti-YAP (Santa Cruz Biotechnology, 1:50; sc-101199). To image cells in late G2 and mitosis phases, we used mouse IgG1 anti-pH3 (Cell Signaling

Technology, 1:200; 9706S). EdU-positive cells were imaged using the Click-iT EdU AlexaFluor-488 and -647 Imaging Kits (Thermo Fisher Scientific). To label F-actin, utricles were incubated with phalloidin conjugated to AlexaFluor-488 nm (Invitrogen; 1:200; A12379).

Calculation of Hair Cell Density

To measure and calculate mean HC density, utricles were fixed and immunostained with antibodies against spectrin, which is expressed in cuticular plates of HCs. Then, confocal image stacks were acquired at 20× magnification to visualize the entire macula. Counts of spectrin-positive cells from five 100 × 100 μm regions located in the anterolateral, anteromedial, central, posterolateral, and posteromedial regions of the utricle were tabulated. The mean densities of HCs were calculated by dividing the counts by the areas sampled.

Measurements of apical junction regions

To measure widths of AJRs, high-magnification images were taken from lateral, striolar, and medial regions of each mouse utricle using an Axiovert 200M microscope (Carl Zeiss). Regions within each utricle were distinguished with the use of antibody against oncomodulin, which labels striolar HCs. Widths of AJRs were determined from the phalloidin label intensity along a perpendicular line across the homotypic SC-SC adherens junction. The measurement line spanned circumferential F-actin bands in the two cells that shared each junction as previously described (Burns et al., 2008). Heterotypic SC-HC junctions were not measured. To avoid measurement bias, a custom R script was used to identify the start and end of each AJR. We measured widths of 35–40 AJRs in each region (105–120 AJRs per utricle) and calculated the mean widths for each region and whole macula.

Code accessibility

R script for measurement of AJRs is available at Github (https://github.com/utricle/AJR-Width-Quantification).

Measurement of E-cadherin, N-cadherin, β-catenin, and YAP immunostaining intensities

To measure peak intensities of E-cadherin, N-cadherin, and β-catenin immunostaining, high-magnification images centered on the line of polarity reversal were taken with an LSM 880 confocal microscope (Carl Zeiss) to simultaneously capture portions of the lateral and striolar regions. We drew lines across 40 junctions of striolar SCs and 40 junctions of lateral SCs. To measure peak intensities of YAP immunostaining, we placed 1.5-μm-diameter ROIs within 40 striolar SCs and within 40 lateral SCs. Those measurements were used to calculate average intensities of immunostaining for E-cadherin, N-cadherin, β-catenin, and YAP in striolar SCs and lateral extrastriolar SCs. Next, we normalized the immunoreactivity of each protein in the apical domain of striolar SCs to that of lateral extrastriolar SCs in the same utricle, producing a striolar/lateral intensity ratio (S/L ratio) to facilitate comparisons.

Quantification of macular area

For quantification of macular area, images of cultured utricles were acquired with an LSM 880 confocal microscope (Carl Zeiss) at 20× magnification, and Sox2 staining was used to delineate the border of the sensory epithelium. The area inside each outlined region was calculated using ImageJ.

Experimental design and statistical analysis

The experimental design is illustrated in the figures and described in figure legends. Images were carefully selected to show the average effect obtained for each experimental condition. All descriptive statistics are presented as mean ± SD. For statistical comparisons, Microsoft Excel was used to conduct two-sample, two-tailed t tests, and GraphPad Prism 8 software was used to conduct ANOVA and post hoc pairwise comparisons. Each utricle was considered an independent observation for statistical analysis. Animals of either sex were used. P-values < 0.05 were considered statistically significant. No methods were used for sample size determination.

RESULTS

A mixture of seven factors stimulates robust S-phase entry in utricles from newborn mice, but responses wane postnatally

McLean et al. induced significant proliferation in 3D cultures of cells that were dissociated from the neonatal mouse cochlea and cultured in a medium supplemented with seven factors (EGF, bFGF, IGF-1, phosphorylated vitamin C, and small molecules that inhibit GSK3, HDAC, and TGFβRI) (McLean et al., 2017) (Figure 4-1a). To test whether that medium, which we call ”7F”, would overcome the age-related decline in the capacity for mammalian SCs to enter the cell cycle (Hume et al., 2003; Davies et al., 2007; Gu et al., 2007; Oshima et al., 2007; Lu and Corwin, 2008; Burns et al., 2012a), we dissected utricles from mice of different ages (P0, P2, P4, P6, P8, P16, and 6 weeks) and cultured them in either 7F or control medium and EdU for 72 hours (Figure 4-1b, c). SCs were identified by labeling with an antibody to Sox2.

The P0 utricles that were cultured in 7F contained 8.6-fold more EdU+/Sox2+ cells than utricles cultured in the control medium (1107 ± 279 vs 128 ± 39, respectively, mean ± SD; $p = 0.00008$, two-tailed t test, $n = 7$ or 8), showing that 7F's stimulatory effects extend even to SCs in undamaged vestibular epithelia. As mice grew older, the incidence of EdU+/Sox2+ cells declined quite sharply. The 7F culture protocol yielded 581 ± 111 EdU+/Sox2+ cells in utricles harvested on P2, and 136 ± 34 and 11 ± 4 EdU+/Sox2+ cells in utricles harvested from P4 and P8 mice, respectively (Figure 4-1d, e). While the 7F mixture evoked robust cell cycle entry of SCs in utricles of newborn mice, the 72 h exposure to activators of the EGF, bFGF, IGF-1, and Wnt pathways combined with inhibitors of HDAC and the TGFβ pathway failed to evoke substantial proliferation in utricles from older neonates, highlighting the dominant nature of quiescence that occurs with the postnatal maturation of mammalian SCs (Figure 4-1e).

Hair cell loss does not restore proliferation in older utricles

To test whether HC loss would increase SC responses in older ears, we dissected utricles from P0, P2, P4, P6, P8, P16, and 6-week-old mice and cultured them for 24 h in control medium with or without 2 mM neomycin. After 3 rinses in control medium, all utricles were cultured for 3

more days in 7F and EdU (Figure 4-2a). In the neomycin-treated utricles from P8 and younger mice, counts of spectrin-labeled cuticular plates showed a 50%–65% decrease in the average spatial density of HCs compared with the age-matched utricles cultured without neomycin, and HC density decreased 32% and 19% in the neomycin-treated utricles from P16 and 6-week-old mice, respectively (Figure 4-2b, c). As expected, the loss of HCs significantly increased the numbers of EdU+/Sox2+ cells in the utricles from P0 and P2 mice (P0 neo: 907 ± 167 vs P0 control: 690 ± 144; p = 0.01481, two-tailed t test, n = 8; P2 neo: 519 ± 89 vs P2 control: 271 ± 50, p = 0.00773, two-tailed t test, n = 7). However, the loss of HCs did not significantly increase the incidence of EdU+/Sox2+ cells in the utricles from P4 and older mice (P4 control 145 ± 67 vs P4 neo 203 ± 86, p = 0.18728, n = 7; P6 control 20 ± 8 vs P6 neo 5 ± 2, p = 0.01257, n = 6; P8 control 5 ± 4 vs P8 neo 9 ± 4, p = 0.13777, n = 6; P16 control 1 ± 1 vs P16 neo 1 ± 1, p = 0.71659, n = 6; Adult control 1 ± 1 vs Adult neo 1 ± 1, p = 0.87938, n = 6, two-tailed t tests) (Figure 4-2d). Indeed, after 3 d in 7F and EdU, EdU+/Sox2+ cells were rarely observed in either the treated or control utricles from P6, P8, P16, and 6-week-old mice (Figure 4-2e). The fact that HC loss failed to restore the capacity for SCs to enter the cell cycle after a 3 d exposure to 7F suggests that the damage-evoked responses, which potentiate proliferation of P0 SCs, cannot surmount the age-related changes that prevent quiescent SCs from transitioning into a proliferative state.

7F thins F-actin bands in utricles from P8 mice

The preceding results were consistent with the hypothesis that maturational changes somehow limit the proliferative capacity of mammalian SCs. One of the most prominent known maturational changes is the exceptional postnatal thickening of the circumferential bands of F-actin that bracket the SC-SC junctions in mammalian vestibular organs and in the Deiters and pillar cells in the organ of Corti (Meyers and Corwin, 2007; Burns et al., 2008, 2013). In contrast to mammalian ears, the circumferential F-actin bands in nonmammalian SCs, which readily replace HCs, remain thin throughout life (Burns et al., 2013). In a pilot study, we incidentally observed that culture in 7F appeared to result in thinning of the F-actin bands. To explore that

possibility, we conducted an expanded investigation to test the hypothesis that culture in 7F reduces the thickness of the F-actin bands in mammalian vestibular SCs over time.

Since SCs in the utricles of P8 mice have thickened F-actin bands (Burns et al., 2008) and rarely entered the cell cycle during a 72 hour culture with 7F (Figure 4-1), groups of P8 utricles were cultured in either 7F or control medium and fixed after 1, 2, 3, 4, or 5 d. For comparison, we fixed utricles from P8 mice at the time of dissection. After staining with AlexaFluor phalloidin and antibodies against oncomodulin, a calcium-binding protein expressed in striolar HCs, we acquired images from standardized regions in the lateral, striolar, and medial sections of each utricle and measured the widths of AJRs, which span the F-actin bands in a pair of adjacent SCs and the intercellular junction those cells share (Burns et al., 2008).

In P8 utricles that were fixed immediately after dissection (time = 0 d), the AJRs averaged 2.26 ± 0.12 μm (Figure 4-3a). During the first 3 d of culture in 7F, we observed progressive thinning of the SC's F-actin bands (0.40 μm/d), resulting in a halving of the AJR width. At that point, AJR widths averaged 1.09 ± 0.07 μm, similar to the average width of AJRs for SCs in P0 utricles in vivo (1.12 μm) (Burns et al., 2008) (Figure 4-3b). After that, the thinning effects of 7F slowed (0.04 μm/d) and widths stabilized at ~1.0 μm. Regional analysis showed that AJRs of striolar SCs were slightly thinner at the start of culture (0 DIV) and thinned more quickly than those of the lateral and medial extrastriolar SCs (Figure 4-3c). The width of AJRs in utricles cultured in control medium for 3 d decreased by 17% (0.12 μm/d to an average width of 1.87 ± 0.21 μm). The results showed that one or more of the constituents of 7F led to partial dismantling of the robust F-actin bands that are found in the SCs of mammalian ears, which thicken as the proliferative capacity of those SCs declines.

Culture in 7F reduces E-cadherin in striolar SC junctions

The SCs in vestibular and auditory epithelia of most nonmammalian ears express E-cadherin at very low levels or levels below normal detectability (Warchol, 2007; Burns et al., 2013). In contrast, the junctions between SCs in mammalian vestibular epithelia and those between inner

and outer pillar SCs and the three rows of Deiters cells in the organ of Corti express considerable E-cadherin at levels that increase postnatally (Hackett et al., 2002; Collado et al., 2011b; Burns et al., 2013). In mouse utricles, junctional E-cadherin in SCs increases >2.5-fold between P1 and P16 and >6-fold between P1 and P82, extending down the basolateral membranes (Collado et al., 2011b). Since 7F thinned the circumferential F-actin bands at the SC-SC junctions in cultured utricles, we asked whether it also would reduce the levels of E-cadherin.

To address that question, we cultured P8 utricles in either 7F or control medium, fixed them after 1, 3, or 5 d, and immunostained them with antibodies against E-cadherin, oncomodulin, and N-cadherin. N-cadherin is expressed in all HC-SC and SC-SC junctions and delineated the sensory epithelium. We observed no noticeable changes in the intensity of junctional E-cadherin immunostaining in the utricles that were cultured up to 5 d in control medium, but the level of E-cadherin immunostaining in utricles cultured in 7F decreased progressively in the striola while appearing to remain unchanged in the extrastriolar region (Figure 4-4a). To quantify this, we acquired stacks of high magnification, confocal images centered on the line of polarity reversal which runs between the striolar and lateral regions of the macula and calculated striola/lateral (S/L) ratios of E-cadherin and N-cadherin intensity (Figure 4-4b) (see Methods). For the utricles cultured in control medium, S/L ratios for E-cadherin ranged between 0.95 and 0.98, independent of culture duration. In the utricles cultured in 7F, E-cadherin decreased in the striolar SCs and S/L ratios for E-cadherin declined progressively. After 3 d in 7F, the E-cadherin S/L ratio was significantly lower (0.59 ± 0.09 vs 0.95 ± 0.06 in the controls; $p = 0.00050$, two-tailed t test, $n = 4$) and decreased to 0.44 ± 0.06 after 5 d in 7F (0.98 in controls; $p = 0.00001$, two-tailed t test, $n = 4$) (Figure 4-4d). There were no noticeable changes in the intensity of N-cadherin immunostaining (Figure 4-4c) and the S/L ratios for N-cadherin did not differ significantly among the utricles cultured in 7F or control medium for 1, 3, or 5 d (1 DIV: $p = 0.48887$, two-tailed t test, $n = 4$; 3 DIV: $p = 0.39816$, two-tailed t test, $n = 4$; 5 DIV: $p = 0.42423$, two-tailed t test, $n = 4$) (Figure 4-4e).

Thus, 7F appeared to selectively reduce junctional E-cadherin in striolar SCs, whereas levels of N-cadherin remained unchanged.

After their F-actin bands thin and E-cadherin decreases, striolar SCs enter S-phase

In light of the preceding results, we decided to extend the culturing of utricles to determine whether a longer exposure to 7F would increase S-phase entry. In these experiments, we cultured P8 utricles in 7F or control medium for various durations and added EdU for the final 24 h, which allowed us to assess the kinetics of S-phase entry over the third, fourth, fifth, sixth, and seventh day of culture (Figure 4-5a).

The number of EdU+/Sox2+ cells never exceeded 3 in any of the P8 utricles cultured in control medium, independent of the duration. The numbers of Sox2+ cells that labeled with EdU also remained relatively low on the third and fourth days of culture in 7F, consistent with our earlier results (3 d: 10 ± 8, 4 d: 12 ± 7; Figure 4-1e). On the fifth day of culture, the number of EdU+/Sox2+ cells increased ~5-fold (55 ± 34) and rose further on the sixth and seventh day (83 ± 19 and 77 ± 48, respectively). Virtually all of the Sox2+ cells that had incorporated EdU on the fifth, sixth, and seventh day of culture in 7F were in the striola, which the oncomodulin labeling of HCs delineated (Figure 4-5c, d). SCs that transitioned from quiescence to S-phase on the fifth day and later in 7F were restricted to the striola, where the levels of E-cadherin began to decline after 3 d.

When delaminated utricular epithelia from rodents are maintained in direct contact with rigid substrates in prolonged culture, that can result in tissue spreading and increased S-phase entry (Gu et al., 2007). To control for that, we measured the areas of the sensory epithelium in P8 utricles that were cultured in 7F or control medium for 3, 4, 5, 6, and 7 d. The mean area measurements were slightly, but not significantly, greater for utricles that were cultured in 7F compared with controls (3 DIV: $p = 0.35597$, two-tailed t test, $n = 6$; 4 DIV: $p = 0.07991$, two-tailed t test, $n = 6$; 5 DIV: $p = 0.18047$, two-tailed t test, $n = 6$; 6 DIV: $p = 0.45152$, two-tailed t test, $n = 6$; 7 DIV 7 DIV: $p = 0.77690$, two-tailed t test, $n = 6$), but areas did not increase with time in culture,

consistent with the expected absence of spreading in the semi-intact utricle cultures used here (Figure 4-5b).

EGF and the GSK3 inhibitor CHIR-99021 thin F-actin bands, decrease E-cadherin, and induce striolar SCs to enter S-phase

To determine which factors in 7F were responsible for thinning the F-actin bands and inducing the striolar SCs to transition from quiescence to the cell cycle, we cultured P8 utricles in seven different media. Each was supplemented with just one of the factors from the 7F mixture: EGF, bFGF, IGF-1, CHIR-99021, valproic acid, phosphorylated vitamin C, or 616452 (E/F/I/C/V/P/6). After 3 d, we fixed each sample, labeled F-actin with AlexaFluor phalloidin, and measured the widths of AJRs in the lateral, striolar, and medial regions as in earlier experiments.

Only the medium that contained EGF (E) and the medium that contained CHIR-99021 (C) resulted in significant thinning of the AJRs between SCs in the P8 utricles (E: $p < 0.0001$, ANOVA and then post hoc t test, $n = 4$; C: $p < 0.0001$, ANOVA and then post hoc t test, $n = 4$) (Figure 4-6a). The average width of AJRs decreased by 40% (to 1.36 ± 0.19 μm) in the EGF medium and 34% (to 1.50 ± 0.18 μm) in the CHIR-99021 medium. The widths of AJRs in other media decreased modestly and similarly to the AJRs in utricles cultured in control medium. We then cultured P8 utricles in medium that contained both EGF and CHIR-99021 (EC medium). After 3 d, the average width of AJRs decreased by 50%, reaching 1.14 ± 0.09 μm ($p < 0.0001$, ANOVA and then post hoc t test, $n = 4$), which was significantly lower than AJR widths in utricles cultured in E or C alone ($p = 0.00215$ and $p = 0.00001$, respectively, two-tailed t test, $n = 4$) (Figure 4-6a, b). Earlier, we found that treatment with complete 7F decreased the average width of AJRs by 52% (to 1.09 ± 0.07 μm). The similarity suggests that EGF and CHIR-99021 are largely responsible for 7F's thinning of the F-actin bands.

Next, we tested whether culture in EC medium would reduce E-cadherin in the striolar SC junctions. For this, P8 utricles were cultured in EC medium for 5 d, then fixed and immunostained with antibodies against E-cadherin, N-cadherin, and oncomodulin. In those utricles, the S/L ratio

for E-cadherin was significantly reduced to 0.55 ± 0.04 ($p < 0.00001$, two-tailed t test, $n = 4$), showing an effect restricted to the striolar SCs (Figure 4-6c, d), and similar to P8 utricles cultured in 7F (Figure 4-4c). Thus, EC medium is sufficient to induce a decrease in E-cadherin at the junctions of striolar SCs.

Since the treatment with EC medium thinned the F-actin bands and decreased the average intensity of E-cadherin immunostaining in the junctions of striolar SCs, we asked whether it would induce quiescent SCs to enter S-phase. We tested that by culturing P8 utricles in EC medium for 7 d and adding EdU 48 h before fixing and immunostaining with antibodies against Sox2 and oncomodulin. Counts of EdU+/Sox2+ cells in the utricles treated with EC medium showed levels of S-phase entry significantly greater than in control cultures and indistinguishable from those in utricles cultured in 7F (98 ± 83 vs 103 ± 70, respectively; 7F: $p = 0.00529$, two-tailed t test, $n = 8$; EC: $p = 0.00108$, two-tailed t test, $n = 8$). Just as in the 7F-treated utricles, the EdU+/Sox2+ cells in the EC-cultured utricles were distributed throughout the striola, with a sharp boundary between the zones of EdU+ striolar SCs and EdU− SCs in the surrounding extrastriolar sensory epithelium (Figure 4-6e, f).

Treatment with EC medium reduces β-catenin and YAP in apical domains of striolar SCs

Since the treatment with EGF and CHIR-99021 induced S-phase entry exclusively in the SCs in which junctional E-cadherin had decreased, we decided to investigate the levels of β-catenin and YAP, junction-associated transcriptional coactivators with proliferative effects. β-catenin can directly bind to E-cadherin (Nelson and Nusse, 2004), and homophilic interactions between the extracellular domains of E-cadherin at cell junctions are reportedly required for the cytoplasmic sequestration of YAP (Kim et al., 2011; Benham-Pyle et al., 2015). We suspected that the decreases in F-actin and E-cadherin might lead to changes in the amount of β-catenin or YAP bound at the junctions between striolar SCs, and that such changes could underlie the increase in S-phase entry. To test the first of those hypotheses, we dissected P8 utricles, cultured them in

either EC or control medium for 7 d, fixed, and immunostained them with antibodies against β-catenin, YAP, and oncomodulin.

In the striola of the utricles cultured in EC medium, we observed decreased intensities of β-catenin and YAP immunostaining relative to the extrastriolar regions of those utricles and all regions of utricles cultured in control medium (Figure 4-7a, b). For quantitative comparisons, we captured high-resolution images centered on the line of polarity reversal and calculated S/L ratios for β-catenin and YAP intensity (see Materials and Methods). In the utricles cultured in control medium, S/L ratios were 0.91 ± 0.05 for β-catenin and 0.88 ± 0.03 for YAP. In the utricles cultured in EC medium, the S/L ratio for β-catenin decreased to 0.32 ± 0.08 ($p = 0.00001$, two-tailed t test, $n = 4$) and the S/L ratio for YAP decreased to 0.55 ± 0.07 ($p = 0.00010$, two-tailed t test, $n = 4$) (Figure 4-7d). The striolar-specific decreases in E-cadherin, β-catenin, and YAP are consistent with the hypothesis that those transcriptional coactivators participate in the transition of maturing SCs to cells that enter S-phase.

To investigate whether the maturing striolar SCs that entered S-phase would progress to mitosis, we cultured P8 utricles in either EC medium or control medium for 7 d. For the last day of culture, we added EdU to label cells that entered S-phase and nocodazole to arrest cells in mitosis. Then we immunostained for the mitosis marker phosphorylated histone-3 (PH3).

We observed robust S-phase entry in striolar SCs of the P8 utricles cultured in EC medium (154 ± 54 EdU+/Sox2+ cells), 15 ± 5 cells of which were EdU+/Sox2+/PH3+, demonstrating that maturing SCs in P8 utricles are able to progress to mitosis (Figure 4-7e, f). As in earlier experiments, EdU+/Sox2+ cells were rarely found in the P8 utricles cultured in control medium, and none was positive for PH3.

EC medium reverses junctional maturation and promotes proliferation of striolar SCs in utricles from adult mice

Since the combination of EGF and CHIR-99021 thinned the F-actin bands throughout P8 utricles and led to reductions in E-cadherin, β-catenin, and YAP, inducing SCs in the striola to

enter S-phase and progress in the cell cycle, we sought to determine whether EC medium would cause the long-quiescent SCs in adult utricles to enter S-phase. Earlier studies showed that the junctional F-actin bands in adult utricles are so thick that they occupy 89% of cell area at the level of the intercellular junction in the average SC (Burns et al., 2008). The junctions of adult SCs in both the utricle and the cochlea also contain correspondingly high levels of E-cadherin (Burns et al., 2008, 2013; Collado et al., 2011b). Therefore, we extended the duration of the culture period from 3 d (Figure 4-1) to 11 d to allow more time for the effects of EC medium to manifest in adult SCs.

As in the utricles from younger mice, culture of adult utricles in EC medium resulted in significantly thinner AJRs than culture in control medium (1.29 ± 0.03 vs 3.06 ± 1.08 μm; $p < 0.00001$, two-tailed t test, n = 4) (Figure 4-8a, b). Likewise, measurements of the intensities of E-cadherin, N-cadherin, β-catenin, and YAP immunostaining in adult utricles cultured in EC medium revealed significantly lower S/L ratios for E-cadherin ($p = 0.00552$, two-tailed t test, n = 4), β-catenin ($p = 0.00029$, two-tailed t test, n = 4), and YAP ($p = 0.00279$, two-tailed t test, n = 4), but not N-cadherin ($p = 0.55563$, two-tailed t test, n = 4), when comparisons were made to adult utricles cultured in control medium (Figure 4-9a-c).

Finally, to determine whether it would be possible to stimulate fully mature SCs to proliferate, we cultured utricles from adult mice in EC medium and added EdU for the final 48 h before fixation. The adult utricles cultured in EC medium contained on average 104 ± 40 EdU+/Sox2+ cells, 50-fold more than the utricles cultured in control medium (2 ± 2 EdU+/Sox2+; $p = 0.00002$, two-tailed t test, n = 7) (Figure 4-9d, e), and nearly all of the EdU+/Sox2+ cells were in the striola (Figure 4-9d). In a modification of the experiment, we added EdU and nocodazole 24 h before fixation to test whether fully mature and normally quiescent striolar SCs were blocked from cell cycle progression. On average, 3 ± 2 PH3+/EdU+/Sox2+ cells were observed in the utricles treated with EC medium (Figure 4-8c) and none were found in the utricles cultured in control medium.

Together, the findings indicate that stimulation with EGF and an inhibitor of GSK3 promotes proliferation of mature SCs in the striola of adult mice, which correlates in timing and location with thinning of the uniquely massive F-actin bands and decreases in the levels of E-cadherin, β-catenin, and YAP at the apical domains and cell junctions.

DISCUSSION

Vertebrate SCs share most characteristics, but vestibular SCs in mammals are distinct from those in nonmammals in that their intercellular junctions develop high levels of E-cadherin and unique, stable, and exceptionally thick circumferential F-actin bands, which grow to occupy 89% of the adult SC's area at the junction level (Meyers and Corwin, 2007; Burns et al., 2008; Collado et al., 2011; Burns and Corwin, 2014). Neither occurs in the SCs of fish, amphibians, and birds that readily regenerate HCs and recover sensory function (Burns et al., 2013). Those discoveries led to the hypothesis that mammalian SC junctions play a role in limiting proliferation. Our findings here have shown that exposure to EGF and CHIR-99021 caused SC junctions in utricles from mature mice to revert to thin circumferential F-actin bands like those found in the SCs of nonmammals and embryonic mammals, with thinning occurring throughout the sensory epithelium. When treatment duration was extended, junctional E-cadherin decreased significantly, but only in SCs within the striola. That, in turn, was followed by a dramatic restoration of the capacity for the adult striolar SCs to proliferate, consistent with expectations based on the hypothesis.

Prior experiments showed that F-actin near the junction is sensitive to latrunculin A, resistant to cytochalasin D, and relatively mobile, whereas F-actin in a zone further from the junction is resistant to latrunculin A, sensitive to cytochalasin D, and relatively immobile (Burns and Corwin, 2014). It appears that EGF and CHIR-99021 act on the latter zone, causing AJR widths to thin until they stabilize at ~1.0 μm. While thinning of the circumferential bands may play a role in returning mammalian SCs to a proliferative state, it was not sufficient to release them from quiescence. Thinning occurred throughout the utricular SC population, but proliferation

occurred only in striolar SCs where junctional E-cadherin decreased. Since downregulation of E-cadherin occurred just before the SCs' transition from quiescence to proliferation, it appears likely that the high levels of junctional E-cadherin are responsible for the quiescence of mature mammalian SCs. In cancer, downregulation of E-cadherin is strongly correlated with invasiveness, progression to malignancy, and poorer prognosis, hence its designation as a tumor suppressor gene (Pećina-Šlaus, 2003).

In an earlier attempt to investigate the role of E-cadherin in mammalian SCs, we generated conditional genetic KOs and found that many weeks were required before E-cadherin depletion became evident at utricular SC junctions (M. S. Collado and J.T.Corwin, unpublished results). In sharp contrast to that, the treatment with 7F led to a significant decrease in the expression of junctional E-cadherin in just 3 d (Figure 4-4), raising the possibility that its thinning of the circumferential F-actin bands accelerated the rate of E-cadherin depletion. Indeed, F-actin has been shown to stabilize E-cadherin clusters in cultured epithelial cells (Hong et al., 2013).

Our findings are consistent with the possibility that the release of apically localized β-catenin and YAP promotes cell cycle entry downstream of junctional E-cadherin depletion. E-cadherin adhesions are known to bind β-catenin directly and contribute to the cytoplasmic sequestration of YAP, limiting the ability for those transcriptional coactivators to induce proliferation in cultured cell lines (Heuberger and Birchmeier, 2010; Kim et al., 2011; Benham-Pyle et al., 2015). In utricles from neonatal mice, the canonical Wnt and YAP-TEAD pathways have been shown to mediate SC proliferation (T. Wang et al., 2015; Gnedeva et al., 2017). Our results in the striola build on that and suggest that E-cadherin mediated inhibition of the Wnt and YAP-TEAD pathways plays an important role in keeping mature vestibular SCs of mammals in a quiescent state.

Ligands such as EGF, TGF-α, and neuregulins have been shown to promote proliferation of SCs in cultured mammalian balance epithelia (Lambert, 1994; Yamashita and Oesterle, 1995; Zheng et al., 1997; Kuntz and Oesterle, 1998; Montcouquiol and Corwin, 2001). EGFR signaling

also stimulates regenerative proliferation of SCs in the cochlear epithelia of birds and has stimulatory effects on a subset of SCs after dissociation from the cochlea of neonatal mammals (White et al., 2012). Indeed, evidence in that study indicates that EGFR signaling can lift the p27kip1 inhibition of proliferation in the dissociated SCs, and suggests that a PI3K-dependent pathway appears to play a role in the p27kip1-independent proliferation of that subset of dissociated SCs from the neonatal mouse cochlea. The mitogenic effect of GSK3 inhibitors in neonatal HC epithelia is also well documented (Lu and Corwin, 2008; Roccio et al., 2015; Samarajeewa et al., 2018; You et al., 2018). Our results suggest that the stimulatory effects of these agents are closely linked with their capacity to remodel junctions once SCs have matured. However, questions remain about how EGF and the GSK3 inhibitor brought about the depletion of E-cadherin in the striolar SCs. Since the level of junctional N-cadherin remained unchanged, we can conclude that the mechanism of depletion is selective for E-cadherin, and does not act as a "cadherin switch" where downregulation of E-cadherin is accompanied by upregulation of N-cadherin as in epithelial-mesenchymal transition (Figs. 4, 8) Inhibition of GSK3β has been shown to increase transcription of Snail, which deacetylates the Cdh1 promoter, so the CHIR-99021-mediated depletion of E-cadherin could come about through a decrease in its transcription (Batlle et al., 2000; Bachelder et al., 2005; Lu and Corwin, 2008; Collado et al., 2011b; Kim et al., 2012; Liu et al., 2014). Indeed, EGFR activation inhibits GSK3 activity and leads to epithelial-mesenchymal transition. EGF also has been shown to induce E-cadherin internalization via caveolin-mediated endocytosis (Lu et al., 2003), micropinocytosis (Bryant et al., 2007), and following Hakai-mediated ubiquination via Src (Shen et al., 2008). EGF also can also induce proteolytic cleavage of E-cadherin by matrix metalloproteases (Cowden Dahl et al., 2008; Zheng et al., 2009; Chavez et al., 2012; Navarini et al., 2017). Additional studies will be required to determine which of those potential mechanisms may be responsible for the depletion of E-cadherin that occurs in striolar SCs exposed to EGF and CHIR-99021.

The distinct effects we observed in striolar and extrastriolar SCs indicate that yet-to-be-identified properties of extrastriolar SCs prevent them from downregulating E-cadherin and proliferating in response to EGF signaling and GSK3 inhibition. Since incidental HC loss occurs in both striolar and extrastriolar regions, striolar-specific losses do not appear likely to account for the region-specific effects observed. Previous studies have reported the following differences between striolar and extrastriolar SCs: Striolar SCs express the stem cell marker Lgr5 at embryonic stages, are more likely to proliferate after diphtheria-toxin-mediated HC ablation at P1, and are more likely to convert into HCs upon Notch inhibition before P12 than extrastriolar SCs (Collado et al., 2011b; T. Wang et al., 2015). In contrast, the limited nonproliferative HC replacement that occurs in adult mouse utricles after diphtheria-toxin-mediated HC ablation primarily occurs in the extrastriolar region, via direct phenotypic conversion (Golub et al., 2012). The identification of differences between striolar and extrastriolar SCs appears likely to reveal important clues about barriers that limit HC replacement in mammals. Recent research has shown that the developmental specification of striolar and extrastriolar regions is controlled by regional differences in retinoic acid metabolism, with higher retinoic acid levels in the extrastriolar epithelium (Ono et al., 2020). This raises the possibility that retinoic acid signaling, which is known to have diverse effects, including the promotion of cell cycle exit and differentiation in neural progenitors (Janesick et al., 2015), may lead to gene expression changes that limit the plasticity of extrastriolar SCs.

Proliferation in the adult mammalian utricle is extremely limited during homeostasis (Bucks et al., 2017) even after extensive HC loss (Warchol et al., 1993; Golub et al., 2012; Taylor et al., 2018). Replacement HCs can arise as SCs convert or directly transdifferentiate into HCs without an intervening cell division. That process appears to restore a significant, but limited fraction of the HCs and depletes the SC population (Golub et al., 2012; Taylor et al., 2018). In nonmammalian vertebrates, SC proliferation is often the primary contributor to the regenerative replacement of lost HCs (Corwin and Cotanche, 1988; Ryals and Rubel, 1988; Stone and Rubel,

1999; Wibowo et al., 2011; Mackenzie and Raible, 2012) and also serves to replenish SC numbers following direct transdifferentiation (Scheibinger et al., 2018). Adult murine SCs will enter the cell cycle after dramatic shape changes (Meyers and Corwin, 2007), after delaminaton when cultured on rigid substrates (Collado et al., 2011b), when transduced with oncogenes (Loponen et al., 2011; Burns et al., 2012c), or when dissociated from the epithelium Here we report that adult mammalian SCs in undamaged vestibular epithelia proliferate robustly after a relatively simple 11-d-long pharmacological treatment, which led to proliferation of 104 ± 40 SCs during the final 48 h of the treatment (Figure 4-9d, e). The results illustrate the potential for pharmacological approaches to promote repair in the mammalian ear.

In conclusion, findings outlined above support the hypothesis that the reinforcement of intercellular junctions, which takes place in mammalian ears but not in fish, amphibians, or birds, plays an important role in preventing mammalian SCs from proliferating. Our findings demonstrate, for the first time, that the partial dismantling of those junctions precedes and correlates with a resurgence of proliferation in the long-quiescent SCs of mature mammalian ears. While strengthening support for the hypothesis, these findings do not establish causality, since the reversion to less specialized junctional characteristics and the transition from quiescence to proliferation could occur independently in response to a common upstream control. Nonetheless, our results suggest that high expression of E-cadherin regulates signaling that maintains SCs in a quiescent state that appears to be responsible, in part, for the mammalian ear's vulnerability to permanent balance and hearing deficits.

FIGURES AND FIGURE LEGENDS

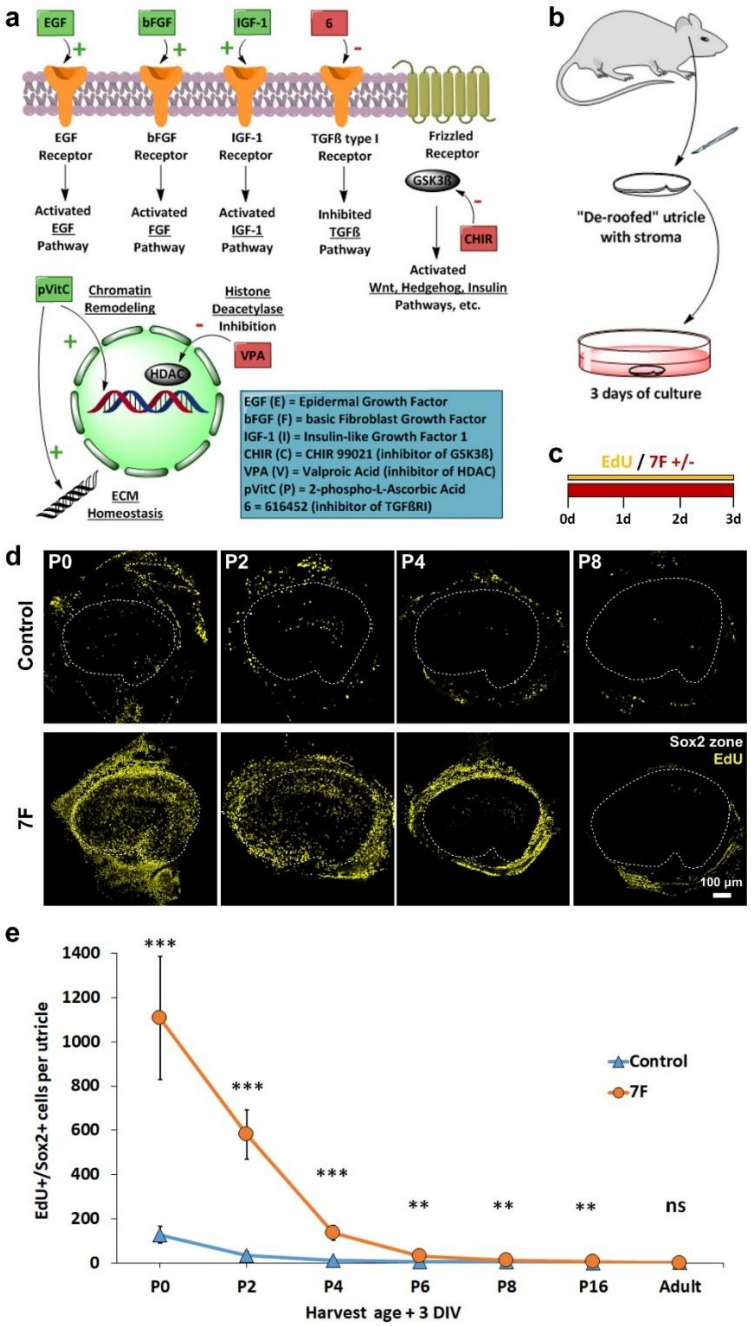

Figure 4-1. Three days in 7F medium induced robust S-phase entry in organ cultures of undamaged utricles from newborn (P0) mice, but not in utricles from 8-d-old (P8) mice. ***a***, Signaling pathways affected by the 7F medium. ***b***, Utricles were dissected from mice of different ages and cultured after removal of the roof and otolithic membrane. ***c***, Utricles were cultured for 3 d in the presence of EdU in medium with or without 7F. ***d***, Low-magnification images of robust S-phase entry in utricles from the youngest neonates, a response to the 7F medium that declined sharply in utricles from older mice. ***e***, Quantification of $EdU^+/Sox2^+$ SCs in mouse utricles cultured 3 d in control medium (blue) and 7F medium (orange) (n = 7 for P0, P2, P4, and n = 6 for P6, P8, P16, Adult for Control and 7F). Data are mean ± SD. ns, Not significant ($p \geq 0.05$). **$p < 0.01$, ***$p < 0.001$. ECM, extracellular matrix; DIV, days *in vitro*.

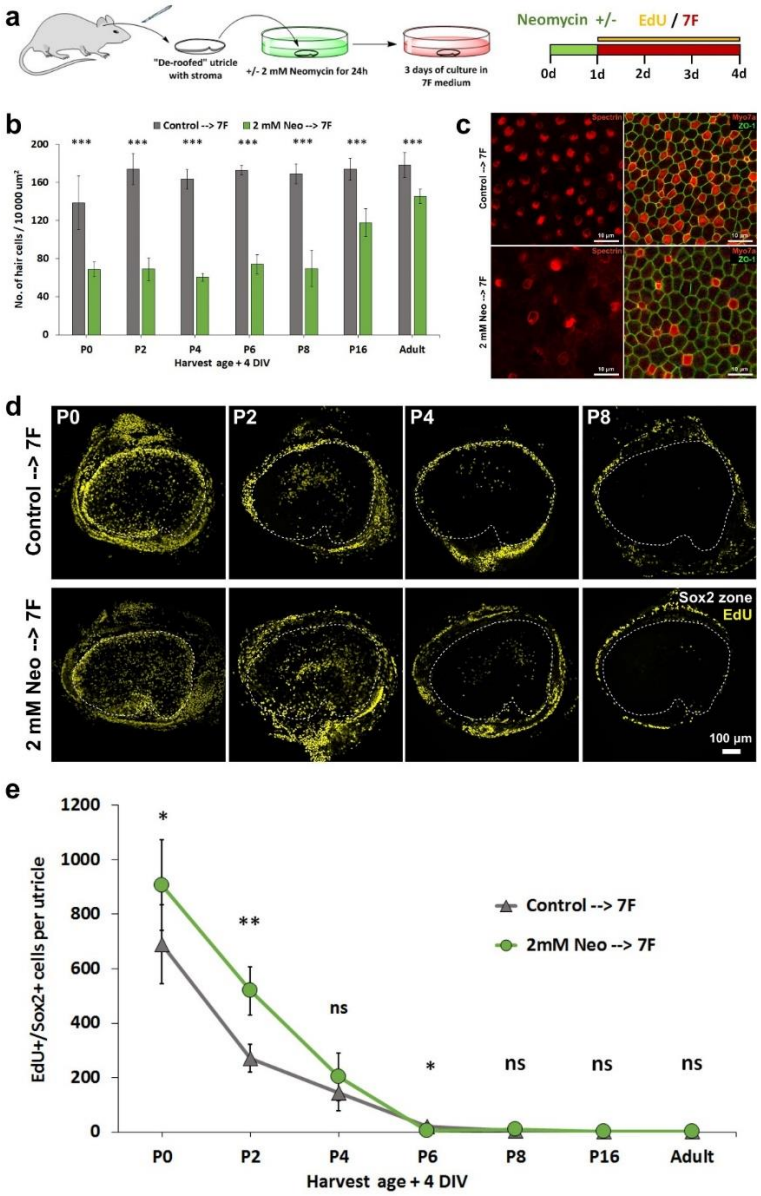

Figure 4-2. HC loss increased the amount of S-phase entry in utricles from the youngest neonates but did not extend the age of responsiveness beyond P8. ***a***, Utricles were cultured in control medium or that medium plus 2 mM neomycin for 24 h. Then, they were all cultured for 3 d in 7F medium with EdU. ***b***, Quantification of HC density in utricles cultured under the two conditions (n = 8 for P0, n = 7 for P2 and P4, and n = 6 for P6, P8, P16, Adult for Control and 7F). ***c***, Representative high-magnification images of P2 mouse utricles exposed to the 24 h pretreatment with 2 mM neomycin or control medium followed by 72 h in 7F medium and EdU. HCs were labeled with antibodies against myosin VIIA and spectrin. ***d***, Low-magnification images show that experimental induction of HC loss potentiated S-phase entry in utricles from P0 and P2 mice cultured in 7F medium but had no such effect in utricles from mice older than 1 week. **e**, Quantification of $EdU^+/Sox2^+$ SCs in neomycin-treated and control utricles cultured 4 d (n = 8 for P0, n = 7 for P2 and P4, and n = 6 for P6, P8, P16, Adult for Control and 7F). The difference in P6 utricles was statistically significant, but with the $EdU^+/Sox2^+$ cells in control cultures exceeding the number of such cells in neomycin-treated cultures (control: 20 ± 8 vs neo: 5 ± 2, p = 0.01257, n = 6). Data are mean ± SD. ns, Not significant ($p \geq 0.05$). *$p < 0.05$, **$p < 0.01$, ***$p < 0.001$. DIV, days *in vitro*.

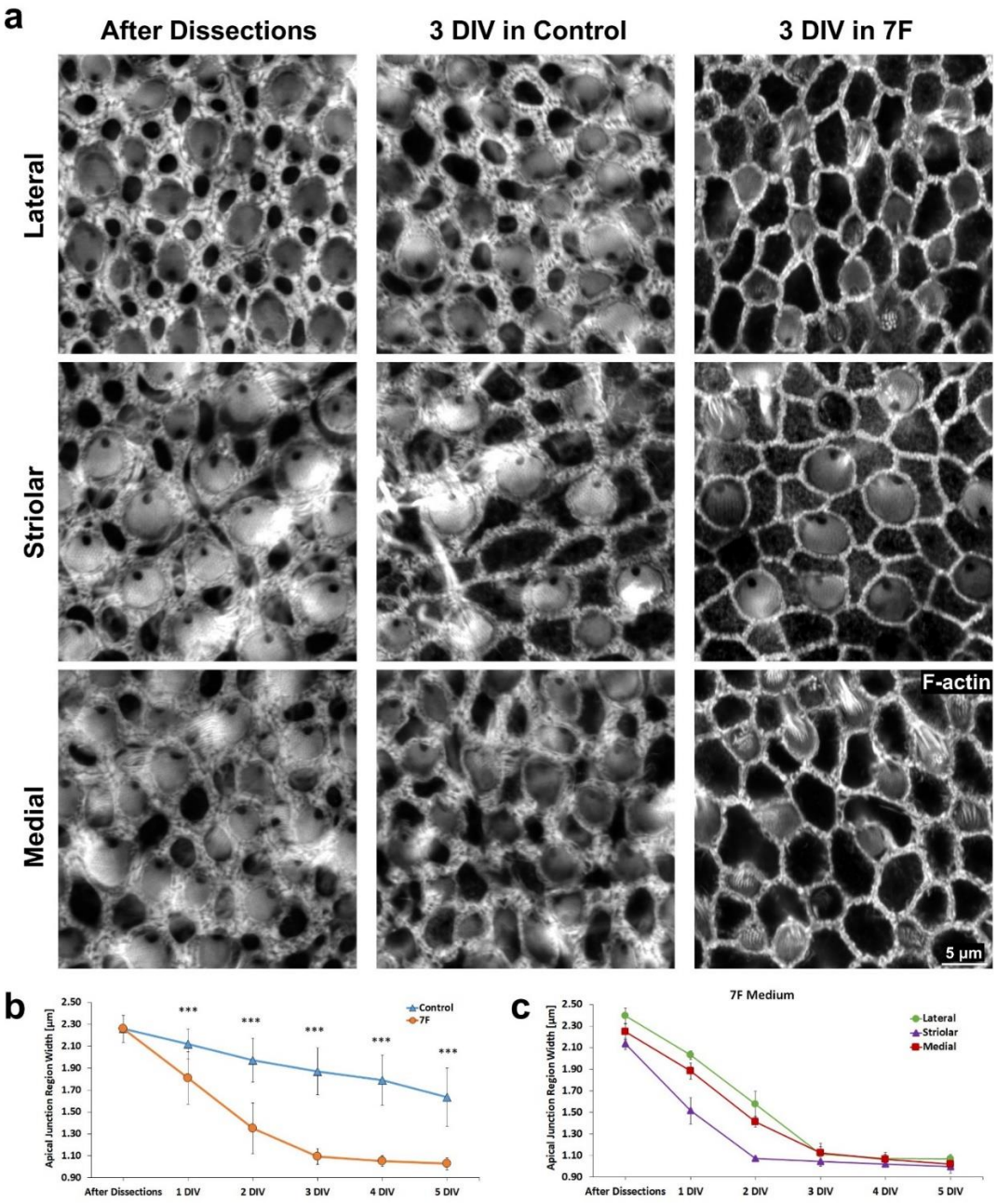

Figure 4-3. Culture in 7F medium dismantled the thick circumferential F-actin bands that bracket SC junctions throughout all regions of the P8 mouse utricle. The thick F-actin bands are a unique feature of mature SCs in the vestibular and cochlear epithelia of mammals. The thickening occurs early in postnatal maturation and is highly correlated with the age-related decline in the capacity for SCs to reenter the cell cycle. ***a***, Representative high-magnification images show visibly thinner F-actin bands in the lateral extrastriolar, striolar, and medial extrastriolar regions of P8 mouse utricles that were cultured in 7F medium. ***b***, The width of AJRs progressively decreased in the control medium, but more quickly and substantially decreased during the first 3 d in the 7F medium, plateauing at ~1 µm (n = 4 at each investigated time point for Control and 7F). ***c***, AJR widths decreased faster in the striola than in the lateral and medial extrastriolar regions of the sensory epithelium (n = 4 at each investigated time point). Data are mean ± SD. ns, Not significant ($p \geq 0.05$). ***$p < 0.001$. DIV, days *in vitro*.

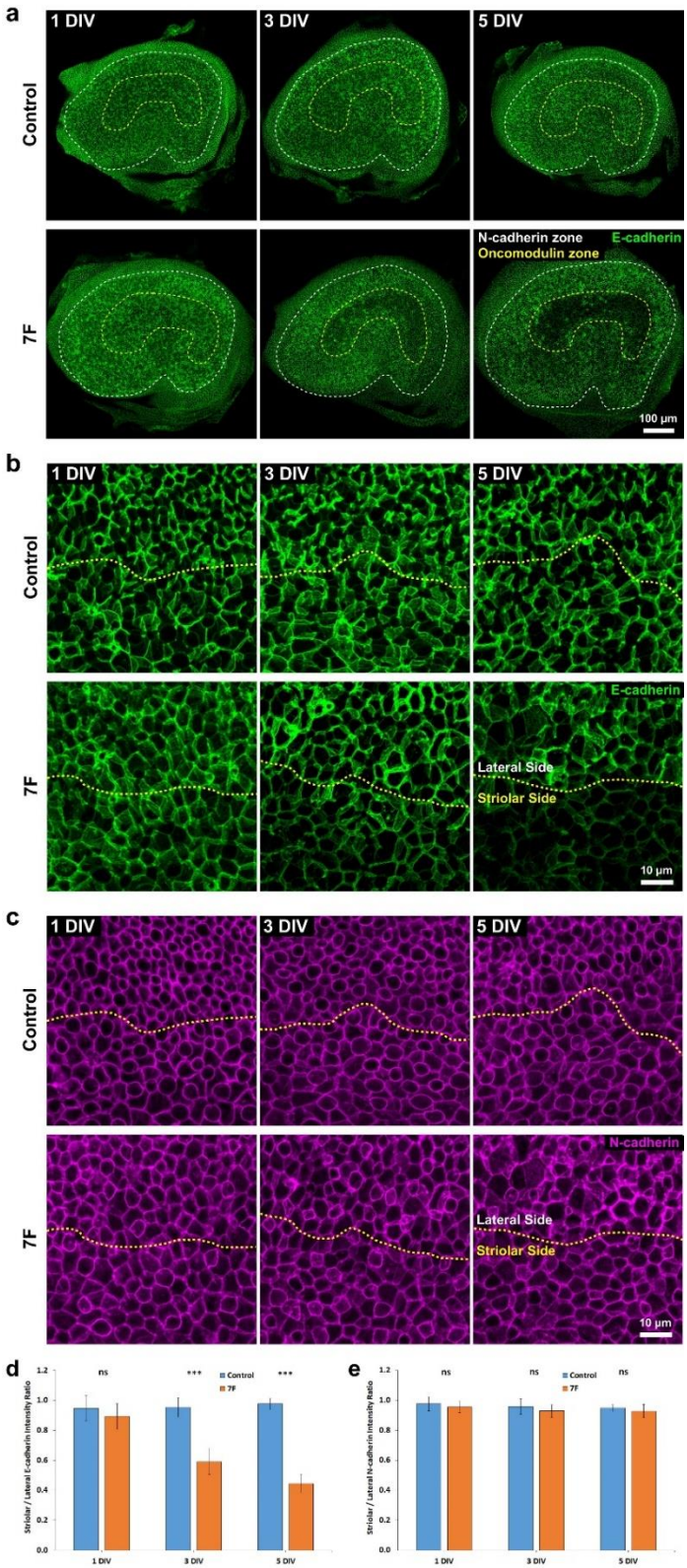

Figure 4-4. Prolonged culture of utricles from P8 mice in 7F medium led to decreased levels of E-cadherin, but not N-cadherin, at the junctions between SCs in the striola. ***a***, E-cadherin immunoreactivity decreased in the striola of P8 mouse utricles cultured in 7F medium, but not in those cultured in control medium. ***b***, High-resolution images

centered on the line of polarity reversal (yellow dashes) depicting the decrease in E-cadherin at cell junctions. ***c***, High-resolution images of N-cadherin immunostaining centered on the line of polarity reversal (yellow dashes). Levels of N-cadherin remained unchanged during culture in 7F and control medium. ***d***, The S/L ratio of E-cadherin stayed at the same level in P8 mouse utricles cultured in control medium (n = 4 at each investigated time point for Control and 7F) but progressively decreased in P8 mouse utricles cultured in 7F medium. ***e***, N-cadherin S/L ratios remained unchanged in both experimental conditions (n = 4 at each investigated time point for Control and 7F). Data are mean ± SD. ns, Not significant ($p \geq 0.05$). ***$p < 0.001$. DIV, days *in vitro*.

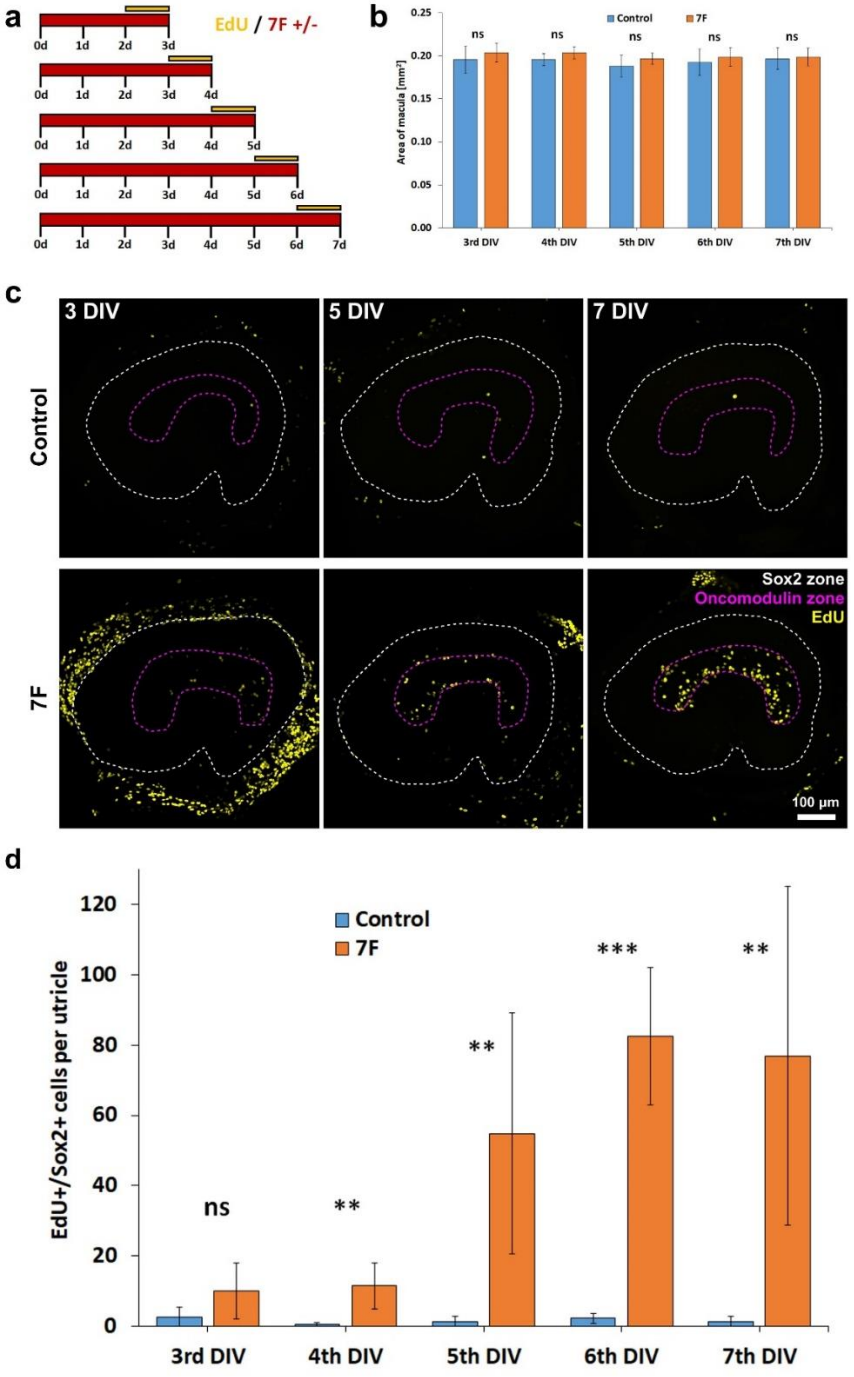

Figure 4-5. After E-cadherin decreased in the striola of the P8 utricles, many of the normally quiescent SCs in that region reentered the cell cycle and labeled with EdU. ***a***, To determine when quiescent SCs began to reenter the cell cycle, utricles from P8 mice were cultured for 3, 4, 5, 6, or 7 d, with EdU added for the final 24 h. ***b***, The sensory epithelia of P8 mouse utricles that were cultured in 7F medium did not significantly expand relative to those cultured in control medium (n = 6 at each investigated time point for Control and 7F). ***c***, Low-magnification images illustrate the S-phase entry of striolar SCs in P8 mouse utricles cultured in the 7F medium. ***d***, Quantification showed that the most notable increase in the incidence of S-phase entry in the striolar SCs occurred between the fourth and fifth days of culture (n = 6 at each investigated time point for Control and 7F). Data are mean ± SD. ns, Not significant ($p \geq 0.05$). **$p < 0.01$, ***$p < 0.001$. DIV, days *in vitro*.

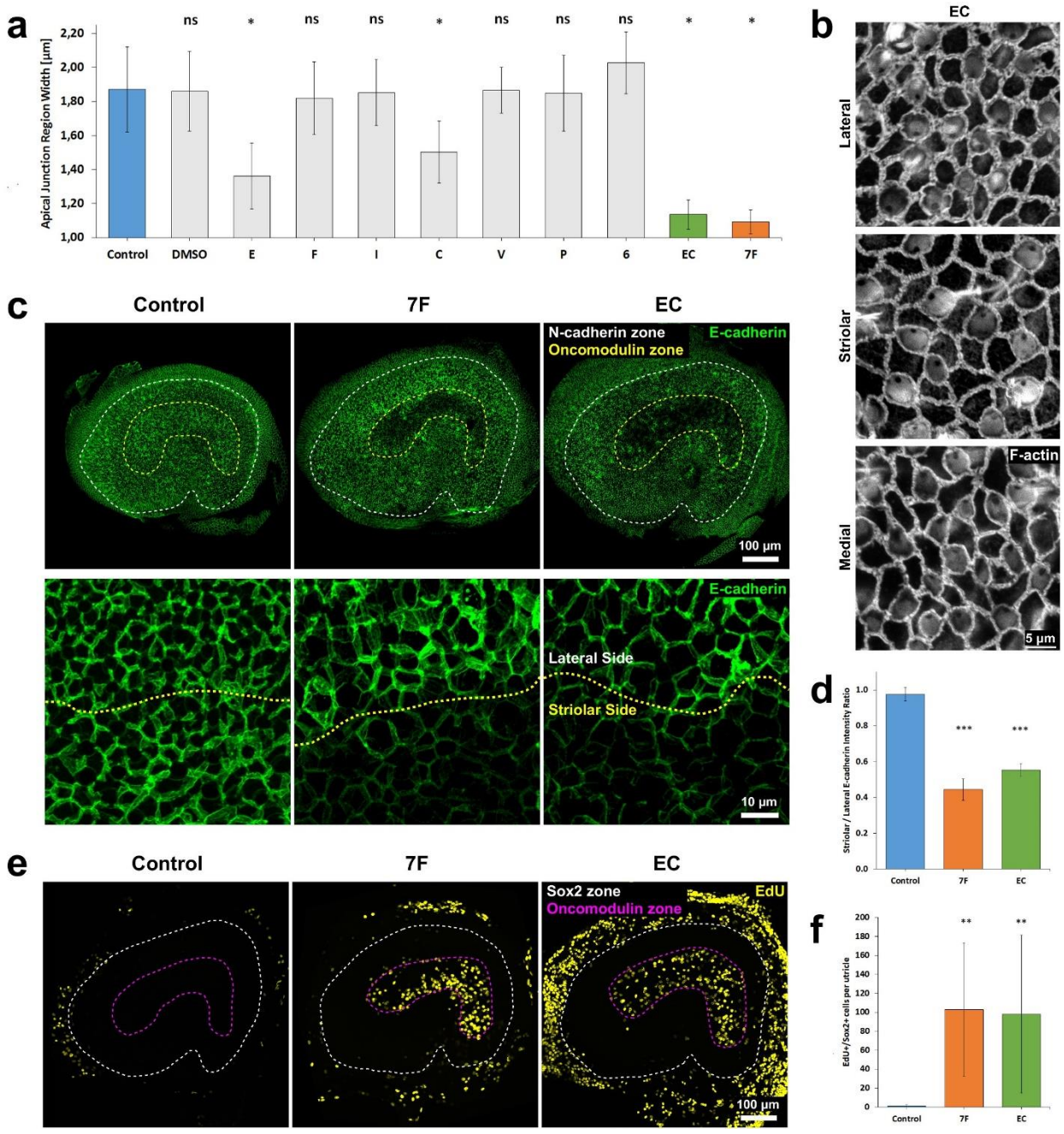

Figure 4-6. EGF and the GSK3β inhibitor CHIR-99021 are the factors in 7F medium that reverse junctional maturation and induce S-phase entry in striolar SCs. ***a***, Of seven factors (E, F, I, C, V, P, 6), only EGF (E) and CHIR-99021 (C) significantly decreased the average width of AJRs when individually tested. The effect of E and C resulted in thinning of the AJRs that was comparable with that of 7F medium (n = 4 for each experimental condition). Data are mean ± SD. ns, Not significant ($p \geq 0.05$). *$p < 0.0001$ (ANOVA and then *post hoc t* test comparing each experimental condition with the control group). ***b***, High-magnification images of thinned F-actin bands in P8 mouse utricles cultured in EC medium for 3 d. ***c***, Low- and high-magnification images illustrating that levels of E-cadherin immunostaining decreased in striolar SCs of P8 mouse utricles cultured in EC medium for 5 d. ***d***, Culture in 7F and EC medium each significantly decreased the E-cadherin S/L ratio compared with control medium (n = 4 for Control, 7F,

and EC). Data are mean ± SD. ns, Not significant ($p \geq 0.05$). ***$p < 0.001$ (statistical comparisons are *t* tests relative to control group). ***e***, Treatment with EC medium was sufficient to induce S-phase entry of striolar SCs in P8 mouse utricles. ***f***, Quantification of $EdU^+/Sox2^+$ cells revealed that culture in EC medium induced a level of S-phase entry in SCs comparable with culture in 7F medium ($n = 8$ for Control, 7F, and EC). Data are mean ± SD. ns, Not significant ($p \geq 0.05$). **$p < 0.01$ (statistical comparisons are *t* tests relative to control group).

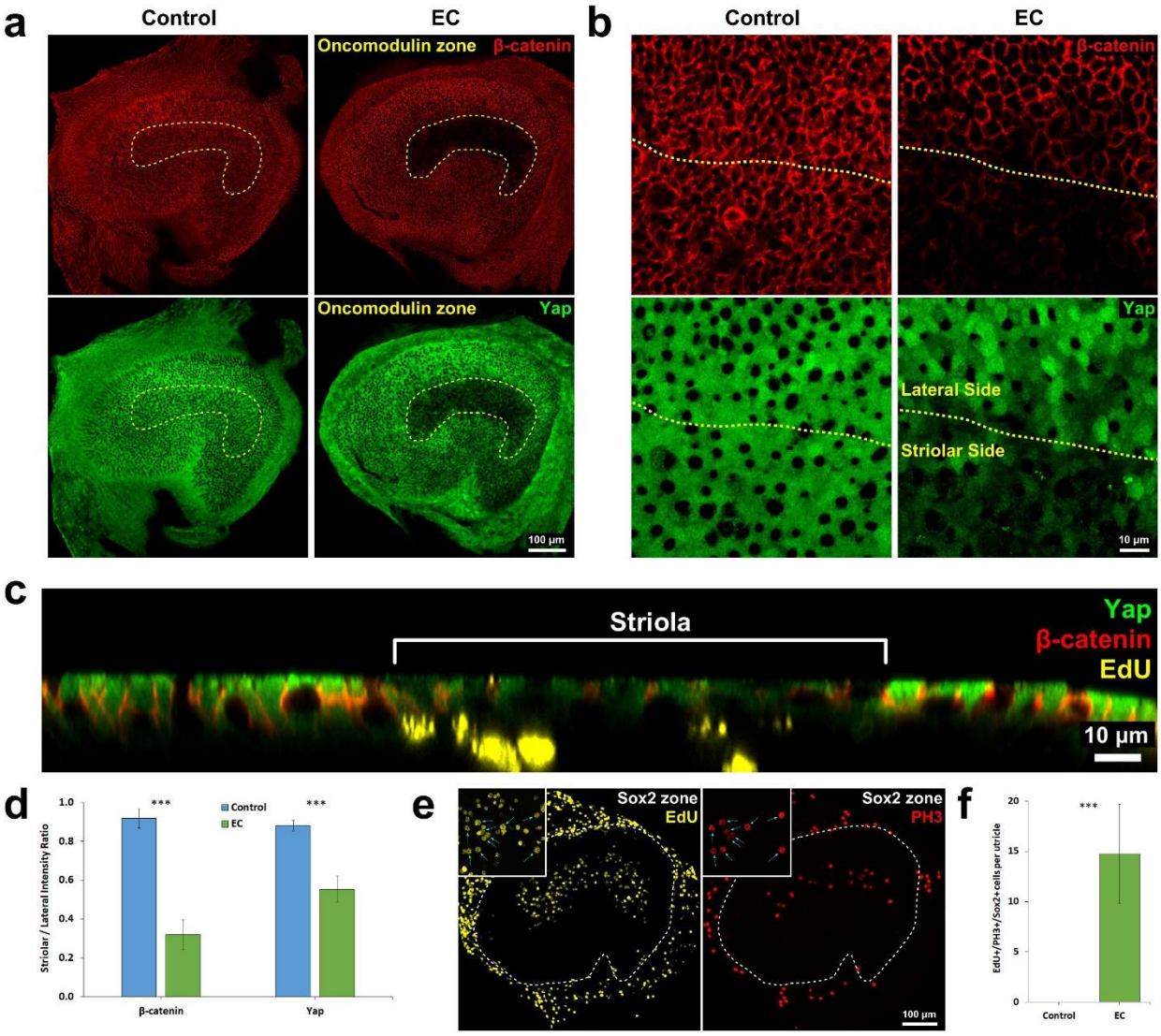

Figure 4-7. The levels of β-catenin and YAP decreased in the striola of P8 utricles upon treatment with EGF and the GSK3 inhibitor CHIR-99021. ***a***, Low-magnification images illustrating that the intensities of β-catenin and YAP immunostaining decreased in the striola of P8 mouse utricles cultured in EC medium, which did not occur in control medium. ***b***, High-magnification images centered on the line of the polarity reversal (yellow dashes) depicting the decrease in β-catenin and YAP immunostaining at the cellular level. ***c***, Orthogonal view of P8 mouse utricle cultured in EC that illustrates decrease in β-catenin and YAP immunostaining intensities in the striola and presence of EdU^+ striolar SCs. ***d***, β-catenin and YAP S/L ratios decreased in P8 mouse utricles cultured in EC medium compared with utricles cultured in control medium (n = 4 for Control and EC). ***e***, Low-magnification images of P8 mouse utricles cultured in EC medium for 7 d with EdU and nocodazole added for the final 24 h of culture. Insets, Cells that progressed from S-phase to mitosis ($EdU^+/PH3^+$ cells). ***f***, $EdU^+/Sox2^+/PH3^+$ cells were present only in utricles cultured in EC medium (n = 4 for Control and EC). Data are mean ± SD. ns, Not significant ($p \geq 0.05$). ***$p < 0.001$.

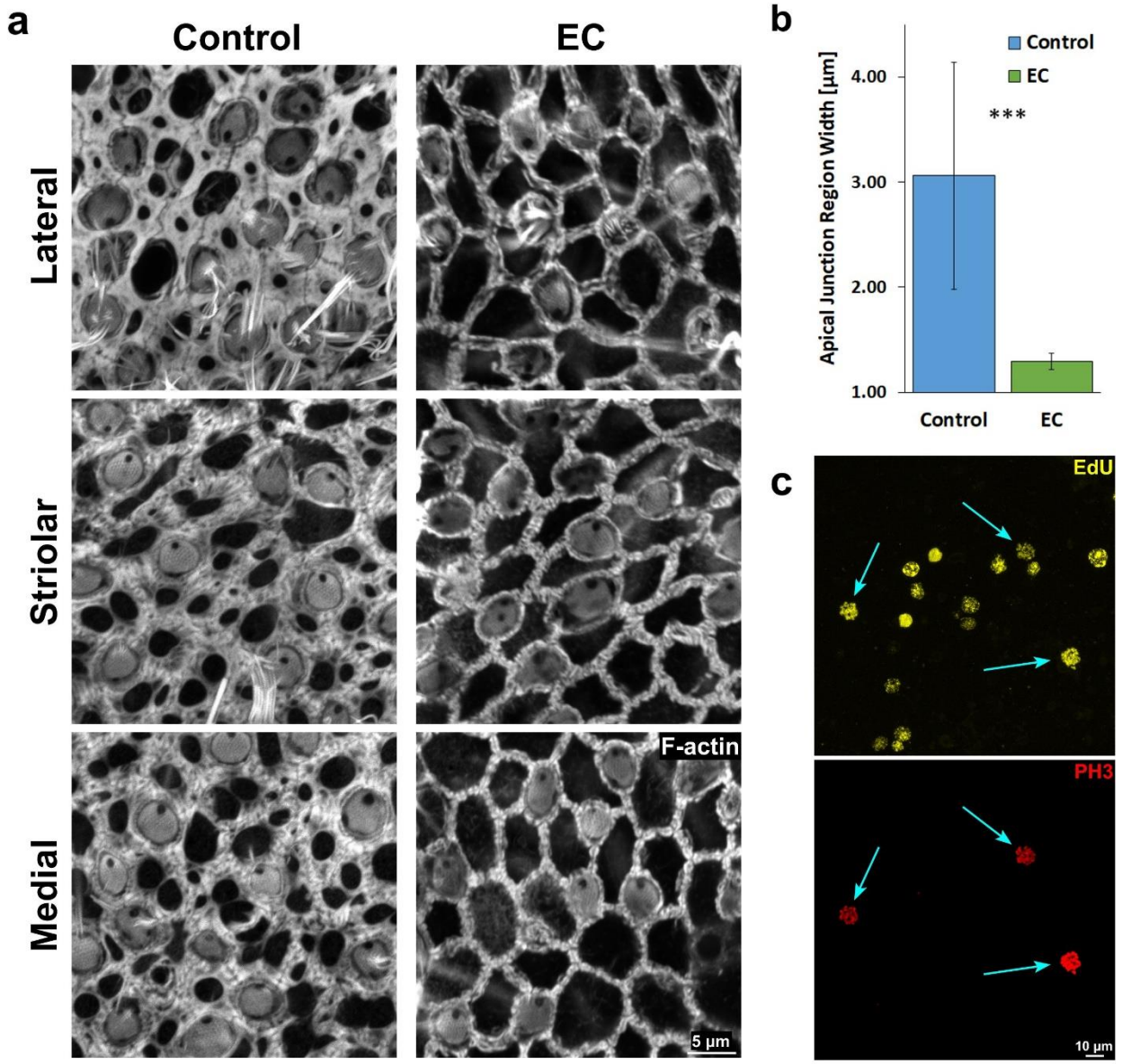

Figure 4-8. EGF and the GSK3 inhibitor CHIR-99021 thin F-actin bands and promote cell cycle progression in utricles from adult mice. ***a***, Representative high-magnification images show visibly thinner F-actin bands throughout the striolar and extrastriolar regions in adult mouse utricles that were cultured in EC medium for 11 d. ***b***, The width of AJRs significantly decreased in adult utricles cultured in the EC medium compared with control medium (n = 4 for Control and 7F). ***c***, High-resolution images depicting striolar SCs that progressed from S-phase to mitosis in adult mouse utricles cultured in EC medium. Data are mean ± SD. ***p < 0.001.

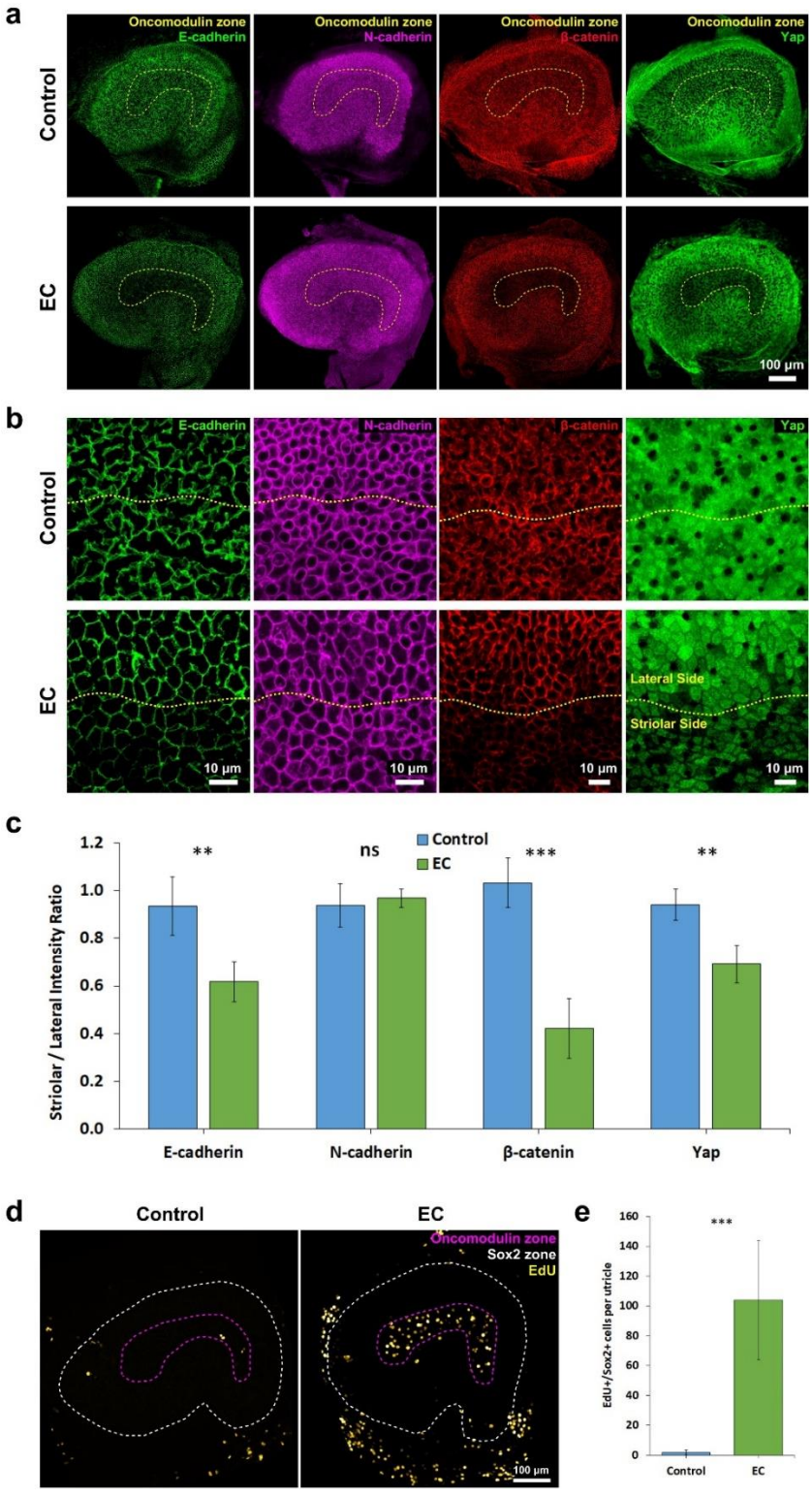

Figure 4-9. EGF and the GSK3β inhibitor CHIR-99021 reverse the reinforcement of SC-SC junctions and promote proliferation of striolar SCs in utricles from adult mice. ***a***, Low-magnification images illustrate that culture in EC medium for 11 d decreases the intensities of E-cadherin, β-catenin, and YAP immunostaining, but not N-cadherin immunostaining, in the striola of adult mouse utricles. Such decreases did not occur in the control medium. ***b***, High-

magnification images centered on the line of the polarity reversal (yellow dashes) depicting E-cadherin, N-cadherin β-catenin, and YAP immunostaining at the cellular level. ***c***, The S/L ratios of E-cadherin, β-catenin, and YAP significantly decreased in adult mouse utricles cultured in EC medium compared with utricles cultured in control medium (n = 4 for Control and EC). The S/L ratio of N-cadherin did not differ significantly. ***d***, Quantification of $EdU^+/Sox2^+$ cells revealed that culture in EC medium induced a 50-fold increase in the number of SCs that entered S-phase compared with the number of such SCs found in utricles cultured in control medium (n = 7 for Control and EC). ***e***, As in P8 utricles, culture of adult mouse utricles in EC medium induced S-phase entry in striolar SCs. Data are mean ± SD. ns, Not significant ($p \geq 0.05$). **$p < 0.01$, ***$p < 0.001$.

CHAPTER 5

YAP mediates hair cell regeneration in balance organs of chickens, but LATS kinases suppress its activity in mice.[2]

ABSTRACT

Loss of sensory hair cells causes permanent hearing and balance deficits in humans and other mammals, but for nonmammals such deficits are temporary. Nonmammals recover hearing and balance sensitivity after supporting cells proliferate and differentiate into replacement hair cells. Evidence of mechanical differences between those sensory epithelia and their supporting cells prompted us to investigate whether the capacity to activate YAP, an effector in the mechanosensitive Hippo pathway, correlates with regenerative capacity in acceleration-sensing utricles of chickens and mice of both sexes. After hair cell ablation, YAP accumulated in supporting cell nuclei in chicken utricles and promoted regenerative proliferation, but YAP remained cytoplasmic and little proliferation occurred in mouse utricles. YAP localization in supporting cells was also more sensitive to shape change and inhibition of MST1/2 in chicken utricles than in mouse utricles. Genetic manipulations showed that *in vivo* expression of the YAP-S127A variant caused robust proliferation of neonatal mouse supporting cells, which produced progeny that expressed hair cell markers, but proliferative responses declined postnatally. Expression of YAP-5SA, which more effectively evades inhibitory phosphorylation, resulted in TEAD-dependent proliferation of striolar supporting cells even in adult utricles. Conditional deletion of LATS1/2 kinases abolished the inhibitory phosphorylation of endogenous YAP and led to striolar proliferation in adult mouse utricles. The findings suggest that damage overcomes inhibitory Hippo signaling and facilitates regenerative proliferation in nonmammalian utricles, while constitutive LATS1/2 kinase activity suppresses YAP-TEAD signaling in mammalian utricles and contributes to maintaining the proliferative quiescence that appears to underlie the permanence of sensory deficits.

[2] This chapter is a reproduction of Rudolf et al. 2020. It has been re-formatted to match the terminology and style within this thesis.

SIGNIFICANCE STATEMENT

Loud sounds, ototoxic drugs, infections, and aging kill sensory hair cells in the ear, causing irreversible hearing loss and balance deficits for millions. In nonmammals, damage evokes shape changes in supporting cells, which can divide and regenerate hair cells. Such shape changes are limited in mammalian ears, where supporting cells develop E-cadherin-rich apical junctions reinforced by robust F-actin bands, and the cells fail to divide. Here, we find that damage readily activates YAP in supporting cells within balance epithelia of chickens, but not mice. Deleting LATS kinases or expressing YAP variants that evade LATS-mediated inhibitory phosphorylation induces proliferation in supporting cells of adult mice. YAP signaling eventually may be harnessed to overcome proliferative quiescence that limits regeneration in mammalian ears.

INTRODUCTION

Hearing loss affects 400 million people worldwide, and balance disorders afflict millions more (Agrawal et al., 2009; World Health Organization, 2020). The loss of sensory hair cells (HCs) in the inner ear is a major and permanent cause of these impairments, because lost HCs are not effectively replaced in humans and other mammals (J. B. Nadol, 1993; Forge et al., 1993; Warchol et al., 1993; Golub et al., 2012; Mizutari et al., 2013). In contrast, birds, fish, and amphibians efficiently replace HCs after damage and recover sensory function (Corwin and Cotanche, 1988; Ryals and Rubel, 1988; Jones and Corwin, 1996; Smolders, 1999; Harris et al., 2003; Smith et al., 2006; Lush and Piotrowski, 2014). In those nonmammals, neighboring supporting cells (SCs) generate progeny that replace HCs and in some cases convert directly into HCs (Balak et al., 1990; Adler and Raphael, 1996; Baird et al., 1996). Yet the capacity for mammalian SCs to divide and replace HCs declines sharply after birth, for reasons that are yet unclear (Burns et al., 2012a; Cox et al., 2014). Efforts to enhance the regenerative response of mammalian SCs have included treatments with growth factors, inhibition of Notch signaling, and stimulation of canonical Wnt signaling (Gu et al., 2007; T. Wang et al., 2015; You et al., 2018). These manipulations show promise in neonatal mice, but their efficacy diminishes as mammals mature and SCs transition to

a more persistent state of quiescence (Atkinson et al., 2018; Collado et al., 2011b; Gu et al., 2007; Maass et al., 2015; Samarajeewa et al., 2018). There remains a need to understand the mechanisms that maintain mammalian SCs in this quiescent state.

A possible explanation arose from studies of the utricle, a type of balance organ. In cultured sheets of utricular epithelia, SCs from immature mice rapidly spread and proliferate, but the ability to spread and proliferate declines abruptly with age (Davies et al., 2007; Meyers and Corwin, 2007; Lu and Corwin, 2008). At the same time, mammalian SCs develop reinforced apical junctions with high levels of E-cadherin and exceptionally thick circumferential F-actin bands (Burns et al., 2008, 2013; Collado et al., 2011b; Luo et al., 2018). In contrast, SCs from chickens express little E-cadherin, have thin F-actin bands at their apical junctions, and freely spread and proliferate throughout life (Burns et al., 2008, 2013). The implications led us to investigate the Hippo pathway and its effector, Yes-associated protein (YAP), which integrate mechanical and biochemical input to control proliferation (Irvine and Shraiman, 2017; Totaro et al., 2018).

In the canonical Hippo pathway, the kinase cascade of MST1/2 and LATS1/2 phosphorylates YAP, leading to its cytoplasmic sequestration and degradation (Dong et al., 2007; Zhao et al., 2007, 2010). In the absence of such inhibitory signaling, YAP can accumulate in nuclei where it promotes proliferation with TEAD transcription factors (Vassilev et al., 2001; Zhao et al., 2007). YAP-TEAD transcriptional activity declines in response to increases in cell density during utricular development, contributing to the initial arrest of growth (Gnedeva et al., 2017), but the role of MST1/2 and LATS1/2 in the inner ear has not yet been studied. We hypothesized that damage would readily reactivate YAP-TEAD signaling within SCs in the regenerative ears of nonmammals, but would not in the ears of mammals.

Here, we report that in the chicken utricle, MST1/2-dependent Hippo signaling sequestered YAP in the cytoplasm of SCs, and that HC loss caused YAP to accumulate in nuclei and promote regenerative proliferation. In SCs of the murine utricle, YAP remained cytoplasmic after HC loss. Their proliferative quiescence was overcome by expression of phosphorylation-

insensitive variants of YAP or conditional deletion of LATS1/2, even in utricles from adult mice. The findings provide a novel mechanistic basis to account for differences in the regenerative replacement of HCs between mammals and nonmammals, and demonstrate for the first time that YAP-TEAD signaling can be harnessed to promote the proliferation of SCs in the mammalian inner ear.

METHODS

Animals

All experiments and procedures were approved by the University of Virginia Animal Care and Use Committee (protocol #1835 07 18). Swiss Webster mice were obtained from Charles River Laboratories. Animals of either sex were used for all experiments. In some experiments, 5-ethynyl-2-deoxyuridine (EdU, Cayman Chemical) was injected at 50 µg/g subcutaneously to trace the incidence of S-phase entry. Doxycycline hyclate (Sigma) was supplied to the mice in drinking water at 2 mg/mL, and/or via intraperitoneal injection at 100 µg/g body weight dissolved in saline.

Sox10$^{rtTA/+}$ mice were generated by the laboratory of Michael Wegner (Ludwig et al., 2004) and contain a knock-in allele of the reverse tetracycline controlled transactivator (rtTA) in the *Sox10* locus. *Yap-S127A* mice harbor a doxycycline-dependent human *Yap* transgene with a serine to alanine mutation at Serine 127 in the *Col1a1* locus (Camargo et al., 2007). Mice were maintained on a mixed background. *Lats1*$^{flox/flox}$ (Stock #024941) and *Lats2*$^{flox/flox}$ (Stock #025428) mice were obtained from The Jackson Laboratory and originally developed by the lab of Randy L. Johnson (Heallen et al., 2013). *Plp-CreER* mice were obtained from The Jackson Laboratory (Stock #005975) and originally developed by the lab of Brian Popko (Doerflinger et al., 2003). *Yap*$^{flox/flox}$*;Taz*$^{flox/flox}$ mice were generated and kindly provided by the lab of Eric Olson (Xin et al., 2011, 2013).

Fertilized White Leghorn (W-36) eggs were obtained from Hy-Line and incubated at 37°C in a humidified chamber with rocking until E18, after which eggs were incubated without rocking. Utricles were harvested from chicks of either sex between post-hatch days zero through four.

Utricle dissection and culture

Labyrinths were dissected from temporal bones in ice-cold PBS with Ca^{2+}/Mg^{2+}(Gibco) and isolated utricles were transferred to HEPES-buffered DMEM/F-12 (Invitrogen) for fine dissection. The utricular roof, otoconia, and nerve were mechanically removed under aseptic conditions. The dissected organs contained the entire sensory epithelium, a small portion of the surrounding non-sensory epithelium, and the underlying connective tissue matrix. For organ culture, dissected utricles were adhered to glass-bottom dishes (Mat-Tek, Ashland, MA) coated with 0.5 µL of dried Cell-Tak (BD Biosciences, San Jose, CA). Utricles were incubated at 37°C with 5% CO_2 and cultured in HEPES-buffered DMEM/F12 supplemented with 1% FBS (Gibco) and 10 µg/mL Ciprofloxacin (Bayer, Berlin, Germany).

In some experiments, 5-bromo-2′-deoxyuridine (BrdU, Sigma) was supplemented at 5 µg/mL or 5-ethynyl-2-deoxyuridine (EdU, Cayman Chemical) was supplemented at 2.5 µg/mL to trace cells that entered S-phase. CA3 was obtained from Selleck Chemicals (#S8661) and reconstituted in DMSO. Leptomycin B was obtained from Calbiochem pre-dissolved in ethanol (#431050) and used at 40 ng/mL. XMU-MP-1 was obtained from Cayman Chemical, reconstituted in DMSO, and used at 3 µM.

Adenoviral transduction

Type 5 adenoviral constructs were generated by Vector Biolabs. Viruses for transduction of wild type mouse YAP (#ADV-276436), mCherry (#1767), and mCherry-T2A-Cre (#1773) were purchased from stock inventory, and other constructs were custom-made from the following plasmids that were obtained from Addgene: pCMV-Flag-YAP-5SA (#27371), and pCMV-Flag-YAP-5SA/S94A (#33103). Cultured utricles were rinsed three times with warm DMEM/F12 + HEPES without serum, and then incubated with adenovirus at a final concentration of $1x10^8$

PFU/mL for 6 h. Vector Biolabs titers its viruses using the plaque formation assay. The transduction rate was assessed by counting mCherry+ cells in high magnification confocal images.

Immunohistochemistry and imaging

Utricles were fixed in 4% paraformaldehyde (Electron Microscopy Sciences) in PBS for one hour at room temperature or in Glyofixx (Shandon) at 4°C overnight. Then utricles were rinsed three times in PBS with 0.1% Triton X-100 (PBST) and blocked with 10% Normal Goat Serum (Vector Laboratories) for 2 h at room temperature. Primary antibodies were incubated at 4°C overnight in PBST supplemented with 2% Normal Goat Serum. Utricles were then rinsed three times in PBST and incubated with Alexa Fluor-conjugated goat secondary antibodies for 2 h at room temperature in PBST with 2% Normal Goat Serum. Utricles were then rinsed three times in PBST, mounted in Prolong Diamond, and imaged on a Zeiss 880 Laser Scanning Confocal Microscope. For BrdU-labeled specimens, utricles were treated with DNase I from bovine pancreas (50 Kunitz/mL, Sigma) for one hour at 37°C following permeabilization and prior to blocking and incubation with primary antibodies.

Mouse anti-E-cadherin (1:200, Clone 36) and mouse anti-BrdU (1:20, B44) were obtained from BD Biosciences. Mouse anti-YAP (1:50, 101199) was obtained from Santa Cruz Biotechnology, and was validated in *Yap*$^{flox/flox}$*;Taz*$^{flox/flox}$*;PlpCreER* mice. Mouse anti-Spectrin (1:50, MAB1622) was obtained from Millipore. Rabbit anti-Sox2 (1:200, D9B8N), Rabbit anti-Phospho-YAP (Ser127) (1:100, 4911), and Rabbit anti-TEAD1 (1:200, D9X2L) were obtained from Cell Signaling Technology. Rabbit anti-Ki67 (1:200, RM9106S0) was obtained from Thermo Fisher Scientific. Rabbit anti-Tectb (1:1000) was a generous gift from Guy Richardson. Rabbit anti-Pv3 (1:400) was a generous gift from Stefan Heller. Rabbit anti-Myosin VI (1:200, 25-6791) and Rabbit anti-Myosin VIIa (1:200, 25-6790) were obtained from Proteus. Mouse anti-Myosin VIIa (1:100, 138-1) was obtained from the Developmental Studies Hybridoma Bank. Rabbit anti-ZO-1 (1:200, 61-7300) was obtained from Zymed. Alexa Fluor-conjugated secondary antibodies

(1:500) and Alexa Fluor-conjugated phalloidin (1:200) were obtained from Thermo Fisher Scientific. EdU was visualized with the Click-it Alexa Fluor Imaging Kit (Thermo Fisher Scientific) according to the manufacturer instructions.

Quantification of S-phase entry

In experiments with chicken utricles, S-phase entry was measured by tabulating the number of EdU+ cells in three 225x225 micron confocal images acquired at high-magnification from the medial extrastriolar region. The incidence of S-phase entry *in vivo* in *Yap-S127A;Sox10*$^{rtTA/+}$ mice was measured by counting the number of EdU+ cells within confocal z-stacks obtained with 20x magnification. The average number of EdU+ cells across five standardized 100x100 micron regions were combined into a single value that was considered an independent replicate for statistical purposes. Two 100x100 micron regions were located in the lateral aspect of the macula (corresponding to the lateral extrastriola), one region was located in the center of the macula (roughly corresponding to the striolar region), and two regions were located in the medical aspect of the macula (corresponding to the medial extrastriolar region). Only one utricle per mouse was analyzed to quantify S-phase entry across genotypes in those *in vivo* experiments. In other experiments, we counted all cells in the utricular macula that incorporated BrdU or EdU using confocal z-stacks obtained at 20x magnification.

Quantification of YAP nuclear:cytoplasmic intensity ratio

Images were analyzed with FIJI (Schindelin et al., 2012). YAP nuclear:cytoplasmic intensity ratios (N:C ratios) were calculated from high magnification confocal images of the SC nuclear layer using a custom FIJI script available at https://github.com/utricle/YAP-NC-Ratio. Utricles were immunostained for YAP, phalloidin, and Myo7a or Sox2. In samples stained for Myo7a, pixels which exceeded an Otsu threshold for Myo7a were considered HCs and excluded from the analysis. On each individual image, the cytoplasmic region was defined by pixels which exceeded an Otsu threshold on phalloidin. The nuclear region was defined by pixels which exceeded an Otsu threshold on Sox2, or alternatively by using the inverse of the cytoplasm region.

The average YAP intensity in the cytoplasmic region divided by the nuclear region was computed for each individual image. Three to five locations were imaged per utricle. In mouse utricles, at least one lateral, one central, and one medial image was acquired. The lateral region corresponds to the extrastriolar cells lateral to the line of polarity reversal, the central region corresponds to striolar cells just medial to the line of polarity reversal, and the medial region corresponds to extrastriolar cells adjacent to the medial boundary of the macula. In chicken utricles, all images were acquired within the large medial extrastriolar region. All YAP N:C ratios from a given utricle were averaged together to form a single ratio for each utricle, which was considered an independent replicate for statistical analysis.

In P30 mouse utricles that were transduced with adenovirus, the YAP N:C ratios were collected by hand. Cells that expressed the mCherry reporter were identified in high magnification confocal images of the SC nuclear layer, and regions of interest (ROIs) were drawn in the nucleus (excluding nuclei) and in the thin surrounding cytoplasmic space. The number of cells analyzed per utricle ranged from 15-96, with at least 128 total cells analyzed per utricle. Values from the same utricle were averaged and considered a single independent replicate for statistical analysis.

Micropunch lesions

Micropunches were fabricated as previously described (Meyers and Corwin, 2007). Blunt 29 gauge hypodermic needles with internal diameter of 180 µm (Catalog #91029, Hamilton) were electrolytically etched in a solution of 34% sulfuric acid and 42% phosphoric acid at 1.5 V, 500 mA, and rough edges were removed with polishing paper (Catalog #337308, Rio Grande), creating a sharp, circular edge. After utricles from P2 chickens or P1 mice were cultured for 24 h, the micropunch was pressed into the center of the macula. The epithelium within the lesion site was excised with a sharpened tungsten filament (Catalog #716200, A-M Systems, Inc.), leaving the underlying stroma intact. Utricles were cultured for an additional 48 h with or without 10 µM EdU prior to fixation.

Confocal image stacks were acquired within the lesion site and an undamaged region at the periphery of the macula. Because the diameter of the micropunch exceeds the mediolateral span of the striola (~100 µm), lesion sites included both striolar and extrastriolar regions. In each utricle, SC apical domains in the lesion site were visualized with phalloidin staining and measured using hand-drawn ROIs in FIJI. The corresponding nuclei were identified in the z-stack for measurement of the YAP N:C ratio. For each SC, one ROI was drawn in the nucleus, avoiding nucleoli, and one ROI was drawn in the perinuclear region to serve as the cytoplasm ROI. The average intensity of YAP immunostaining in the nuclear ROI was divided by that in the cytoplasm ROI to calculate the YAP N:C ratio. In this manner, the 30 SCs at the center of each lesion site were analyzed in each of four utricles (120 SCs total). The regression analysis of SC area and YAP N:C ratio was performed using GraphPad Prism 8 software. To compare the YAP N:C ratio in chicken and mouse SCs, SCs were separated based on area into four different groups (<50 μm^2, 50-75 μm^2, 75-100 μm^2 , and >100 μm^2), with 19-58 SCs of each species per group. A two-way ANOVA was used to compare the YAP N:C ratio across species and area.

In the undamaged region outside of the lesion site, the area of 30 SC apical domains per utricle were measured as described above. The YAP N:C ratio in the undamaged region was calculated from a confocal image slice of the SC nuclear layer using the custom FIJI script described above.

Quantification of macular area and cell density

Yap-S127A$^{+/-}$;Sox10$^{rtTA/+}$ mice and littermate controls (wild type, *Yap-S127A$^{+/-}$*, *and Sox10$^{rtTA/+}$*) received an intraperitoneal injection of doxycycline at P1. Utricles were harvested and fixed on P5 for immunostaining for Rabbit anti-ZO-1 and Mouse IgG1 anti-Myo7a. After mounting as whole mounts, utricles were imaged on a Zeiss LSM 880 confocal microscope. Macular areas were measured from maximum intensity projections of Myo7a imaged with a 20x objective. High magnification images were obtained from the lateral, central, and medial region of each utricle, and the total number of SCs (Myo7a- cell apices) and HCs (Myo7a+ cell apices) were counted.

The lateral image corresponded to the lateral extrastriola, the central image roughly corresponded to the striola, and the medial image corresponded to the medial extrastriola. The totals from each region were averaged to produce an overall SC density, HC density, and total cell density for each utricle (normalized to 10,000 μm^2), which was considered an independent statistical replicate. Only one utricle was analyzed per mouse.

Quantification of E-cadherin immunoreactivity

Yap-S127A$^{+/-}$;Sox10$^{rtTA/+}$ mice and littermate controls (wild type, *Yap-S127A$^{+/-}$*, *and Sox10$^{rtTA/+}$*) received an intraperitoneal injection of doxycycline at P1. Utricles were harvested and fixed on P5 for immunostaining for E-cadherin as described above. High magnification confocal z-stacks were acquired of the lateral region at the boundary of the sensory and non-sensory epithelium. The E-cadherin intensity at SC-SC junctions was obtained by drawing a line across at least 30 SC-SC junctions and averaging the peak intensities from the maximal intensity projection. That was divided by the average E-cadherin intensity of at least 30 cell junctions within the non-sensory epithelium within the same image to generate a single normalized E-cadherin intensity value for the utricle, which was considered an independent statistical replicate. Only one utricle was analyzed per mouse.

RNA extraction, reverse transcription, and quantitative PCR

Eight to 14 utricles were dissected in ice cold PBS until only the sensory epithelia, stroma, and small portion of surrounding non-sensory tissue remained, and combined to serve as one biological replicate. Tissue was transferred to TRIzol (Ambion), and frozen at -80°C until further processing. Upon thawing, tubes were vortexed and chloroform was added. Following centrifugation, the aqueous phase was extracted, mixed 1:1 with isopropanol, supplemented with 20 µg/mL Linear Acrylamide (Ambion), and incubated at -20°C overnight. The following day, RNA was pelleted via centrifugation, washed twice in 1 mL chilled 75% ethanol, and then resuspended in 20 µL H_2O. RNA concentration was assessed using a NanoDrop ND-1000 spectrophotometer, and equal amounts of RNA were used for reverse transcription reactions for each biological

replicate. cDNA was synthesized using the iScript cDNA synthesis kit (Biorad). RT-qPCR was performed on a Biorad CFX Connect using iTaq Universal SYBR Green Supermix (Biorad). Primer specificity was determined by melt curve analysis and verified by analyzing amplicon size via gel electrophoresis. Primers are listed in Table 1. The qPCR was performed with two or three technical replicates per sample and at least four biological replicates. Fold change was calculated by the delta-delta Ct method with *Gapdh* as the reference gene. For statistical hypothesis testing, the Mann-Whitney test was used with each biological replicate considered an independent observation.

RNAscope in situ hybridization

Utricles from P0, P6, P16, and adult (≥P30) mice were dissected on the same day in ice cold PBS and fixed for 1.5 h at room temperature in fresh 4% paraformaldehyde reconstituted in RNAse-free PBS. Utricles were transferred through a sucrose gradient of RNAse-free PBS supplemented with 5%, 10%, 15%, 20%, and 30% sucrose for 2 h each at 4°C. Then utricles were incubated with PBS with 30% sucrose containing two drops of OCT compound, followed by incubation in a 1:1 mixture of PBS with 30% sucrose and OCT for one hour. A single utricle from each age group was then transferred to a cryomold filled with chilled OCT, frozen on dry ice, and stored at -80°C until further processing. Utricles were cryosectioned as 10 µm thick slices, stored on Superfrost Plus slides (Fisher Scientific) then stored at -80°C until further processing. The RNAscope Fluorescent Multiplex Assay was performed according to manufacturer instructions for fixed frozen samples. The probes Mm-Cyp26b1-O1-C3 (#524001-C3), Mm-Tead1-C1 (#457371), Mm-Tead2-C1 (#420281), Mm-Tead3-C2 (custom), Mm-Tead4-C2 (custom) were ordered from Advanced Cell Diagnostics.

Experimental design and statistical analysis

All data are displayed as mean ± standard deviation unless otherwise noted in the figure legend. Statistical hypothesis testing was performed in GraphPad Prism 8. For comparisons of two experimental groups, two-tailed unpaired t-tests were used unless otherwise noted. Paired t-

tests were used to compare rates of viral transduction and proliferation in striolar and extrastriolar regions. RT-qPCR experiments were analyzed with the non-parametric Mann-Whitney test. Comparisons of three or more experimental groups were analyzed with ANOVA along with pairwise post-hoc tests, as indicated in the Results section and figure legends. P-values below 0.05 were considered statistically significant. For *in vitro* experiments, each utricle was considered an independent biological observation (biological replicate) unless otherwise stated in the figure legend, and no methods were used to allocate utricles into treatment groups unless otherwise noted in the Results section or figure legend. For *in vivo* experiments, mice of either sex were allocated to experimental groups based on genotype, and each mouse was considered an independent observation. No methods were used for sample size determination. At least three independent biological replicates were used for all statistical comparisons. There was no special determination or handling of outliers. No masking was used for data analysis.

RESULTS

HC loss leads to nuclear accumulation of YAP in chicken SCs, but not in those of mice

Since cells regulate the activity of YAP in part by controlling its nuclear access (Shreberk-Shaked and Oren, 2019), we tested whether HC loss would trigger nuclear accumulation of YAP in the SCs that are essential for HC regeneration in posthatch chickens. Utricles were cultured with 1 mM streptomycin for 24 h to kill HCs and fixed after two additional days in streptomycin-free medium. Then nuclear:cytoplasmic intensity ratios (N:C ratios) of YAP immunostaining were computed for confocal images of the SC nuclear layer. Streptomycin treatment reduced the density of HCs to 11% of the level in untreated control cultures ($p<0.0001$, $t(10)=16.77$, $n=6$ utricles per condition, Figure5-1A, C, I), resulting in a 22% increase in the N:C ratio of YAP ($p<0.0001$, $t(10)=8.248$, $n=6$ utricles per condition, Figure 5-1B, D, J).

We used the same protocol to determine whether HC loss would induce nuclear translocation of YAP in SCs of the postnatal day 1 (P1) mouse utricle. Here, the streptomycin

treatment reduced the HC density to 55% of the level in undamaged control cultures ($p=0.0004$, $t(14)=4.583$, n=8 utricles per condition, Figure 5-1E, G, I), but we observed no difference in the N:C ratio of YAP (0.89±0.10 vs. 0.89±0.11, $p=0.9818$, $t(14)=0.02327$, n=8 utricles, Figure 5-1F, H, J).

To test whether YAP and TEAD mediate regenerative proliferation in chicken utricles, we cultured utricles either with or without streptomycin for 24 h to kill HCs. Then the utricles were cultured an additional two days in varying concentrations of CA3, a small-molecule inhibitor of YAP-TEAD transcriptional activity (Song et al., 2018). EdU was added 24 h before fixation to label cells that entered S-phase. The streptomycin-treated utricles contained 15-fold more EdU+ cells than undamaged controls ($p<0.0001$, $t(20)=5.48$, n=6-16 utricles, Figure 5-1M), and the CA3 treatment caused a dose-dependent reduction in that regenerative proliferation ($p=0.0010$, $F(3, 34)=2.528$, n=7-16 utricles, ANOVA, Figure 5-1M). Other streptomycin-treated utricles that were cultured with CA3 for six days contained fewer EdU+ cells that expressed the HC marker Myo7a than matched controls ($p=0.0337$, $t(6)=2.741$, n=4 utricles, Figure 5-1K-M). In contrast, HC ablation failed to induce significant regenerative proliferation in P1 mouse utricles during a three-day recovery period ($p=0.73$, $t(16)=0.35$, n=9 utricles, Figure 5-1N). Taken together, the results suggest that HC loss in chicken utricles modulated signaling that led to nuclear accumulation of YAP and regenerative proliferation of SCs, but the less severe HC loss in mouse utricles did not.

Mechanical wounds trigger the nuclear accumulation of YAP more potently in chicken SCs than in those of mice

As streptomycin killed fewer HCs in mouse utricles than in chicken utricles, we could not directly compare the nuclear accumulation of YAP in their SCs after damage. To circumvent that issue and test whether damage more readily activates YAP in chicken SCs than murine SCs, we analyzed their responses to a standardized excision lesion. After 24 h in culture, utricles from posthatch chickens and P1 mice were lesioned with a micropunch 180 µm in diameter, and the epithelium within the lesion area was removed (Meyers and Corwin, 2007; Collado et al., 2011a).

After an additional 48 h of culture with EdU, SCs at the lesion site changed shape and proliferated (Figure 5-2A, C, E, G). YAP immunoreactivity was enriched in the nuclei of chicken SCs at the lesion site (Figure 5-2B, D). The translocation was less pronounced in mouse utricles, with YAP evenly distributed between the nuclear and cytoplasmic compartments of SCs at the lesion site (Figure 5-2F, H).

Cellular shape change (i.e. strain) triggers the nuclear translocation of YAP in other cell types (Codelia et al., 2014; Benham-Pyle et al., 2015; Fletcher et al., 2018). To more closely examine the relationship between shape change and nuclear accumulation of YAP in SCs, we measured the apical domain area and YAP N:C ratio for individual SCs at the center of each lesion site. Regression analysis showed that in SCs of chickens, the N:C ratio of YAP positively correlated with the area of the apical domain ($r=0.531$, $n=120$ cells, $p<0.0001$, Figure 5-2I). There was a significant, but weaker positive correlation between the YAP N:C ratio and apical domain area of murine SCs within the lesion site ($r=0.255$, $n=120$ cells, $p=0.005$, Figure 5-2J). Chicken SCs had significantly greater N:C ratios of YAP than murine SCs, even when controlling for cell area ($p<0.0001$, $F(1, 232)=147$, $n=240$ cells, two-way ANOVA, Figure 5-2K). Outside of the lesion site, there were no significant differences in apical area ($p=0.69$, $t(6)=0.42$, $n=4$ utricles, Figure 5-2L) or YAP N:C ratio ($p=0.89$, $t(8)=0.15$, $n=4$-6 utricles, Figure 5-2M) between chicken and murine SCs. The results indicate that the nuclear accumulation of YAP in response to damage, and specifically shape change, is restricted in murine SCs relative to those of chickens.

Acute inhibition of MST1/2 kinase activity alters YAP localization in chicken SCs, but not those of mice

In the canonical Hippo pathway, a cascade of MST1/2 and LATS1/2 kinases phosphorylates YAP leading to its cytoplasmic sequestration (Dong et al., 2007). We used XMU-MP-1, a small molecule inhibitor of MST1/2 kinase activity (Fan et al., 2016), to test whether that canonical pathway regulates the nuclear access of YAP in utricles of posthatch chickens and P1 mice. After a 24 hour acclimation period in standard medium, we treated cultures for 12 h with

either XMU-MP-1, vehicle, or the nuclear export blocker leptomycin B as a positive control (Dupont et al., 2011). Leptomycin B significantly increased the N:C ratio of YAP in both species, indicating that YAP shuttles dynamically into and out of SC nuclei in the undamaged utricles of chickens and mice (Chicken: $p<0.0001$, $F(5, 20)=37$, n=4-5, ANOVA; Mouse: $p<0.0001$, $F(2,14)=56$, ANOVA, n=5-6, Figure 5-3A-K). In the chicken utricles, MST1/2 inhibition led to a significant increase in the YAP N:C ratio compared to negative controls (0.83±0.07 vs 1.14±0.10, $p<0.0001$, ANOVA with Sidak's test, Figure 5-3A, B), which was reversible after a 24-hour washout ($p<0.0001$, ANOVA with Sidak's test, Figure 5-3E, J). We did not observe an increase in the YAP N:C ratio in mouse utricles after a 12 hour incubation with the MST1/2 inhibitor (0.90±0.11 vs 0.90±0.04, $p=0.9997$, n=6 utricles, ANOVA with Dunnett's test, Figure 5-3G, H), though a 72-hour incubation significantly increased the N:C ratios of YAP in both species compared to DMSO-treated controls (Chicken: 0.84±0.03 vs 1.04±0.13, $p=0.0008$, $t(14)=4.23$, n=8 utricles; Mouse: 0.88±0.07 vs 1.09±0.17, $p=0.0103$, $t(11)=3.09$, n=6-7 utricles, Figure 5-3L-P). The results suggest that canonical Hippo signaling is required for the cytoplasmic sequestration of YAP in chicken SCs. This inhibitory signaling was readily inactivated or bypassed upon damage, leading to the nuclear accumulation of YAP (Figure 5-1). In murine SCs, however, the cytoplasmic sequestration of YAP was less sensitive to damage or the acute inhibition of MST1/2.

YAP-S127A induces YAP-TEAD transcriptional activity and SC proliferation in neonatal mouse utricles

Our findings to this point suggested that YAP was restricted to the cytoplasm in murine SCs despite HC loss and acute inhibition of MST1/2. We hypothesized that overexpression of YAP-S127A, which contains an activating mutation at serine 127 that prevents binding to 14-3-3 proteins and retention in the cytoplasm (Basu et al., 2003), could bypass this regulation. For this, we crossed mice with an inducible *Yap-S127A* allele to *Sox10*$^{rtTA/+}$ mice to generate progeny in which the transgene would be expressed in SCs and other Sox10+ cells only upon administration of doxycycline (Ludwig et al., 2004; Camargo et al., 2007; Walters and Zuo, 2015). We injected

doxycycline intraperitoneally to P1 offspring and supplemented the dam's drinking water. EdU was injected subcutaneously on P2, P3, and P4, and utricles were harvested on P5. In the SCs of *Yap-S127A*$^{+/-}$*;Sox10*$^{rtTA/+}$ mice, YAP immunoreactivity was visibly increased compared to SCs in utricles from wild type, *Sox10*$^{rtTA/+}$, and *Yap-S127A*$^{+/-}$ littermates (Figure 5-4A-D). Moreover, the utricles of *Yap-S127A*$^{+/-}$*;Sox10*$^{rtTA/+}$ pups exhibited a 35-fold increase in EdU+ cells over the littermate controls (97±54 EdU+ cells/10,000 μm^2, $p<0.0001$, $F(3, 27)=20.8$, n=5-11 mice, ANOVA, Figure 5-4A-E). Those EdU+ cells expressed the SC marker Sox2 (Figure 5-4D'''). EdU+ SCs were located throughout the utricle but were slightly enriched in the lateral region ($p = 0.0011$, $F(2.9, 43.1) = 6.5$, n = 16 utricles, repeated measures ANOVA with Tukey's test, Figure 5-4F). It has been previously shown that cells along the lateral edge of the utricle are the last to exit the cell cycle in postnatal mice (Burns et al., 2012b).

To determine whether YAP-S127A would induce YAP-TEAD transcriptional activity, we gave doxycycline as described above and harvested utricles on P3 for RT-qPCR. Compared to littermate controls, the YAP-TEAD target genes *Ctgf*, *Cyr61*, and *Ankrd1* were upregulated in the utricles from the *Yap-S127A*$^{+/-}$*;Sox10*$^{rtTA/+}$ mice by 32-fold, 7-fold, and 181-fold, respectively ($p=0.0286$, Mann-Whitney test, Figure 5-4G). *Myc* expression was unchanged ($p=0.4571$, Mann-Whitney test), and the cell cycle regulator *Ccnd1* was upregulated 3-fold ($p=0.0286$, Mann-Whitney test, Figure 5-4H).

We next sought to determine whether the proliferating SCs in *Yap-S127A*$^{+/-}$*;Sox10*$^{rtTA/+}$ mice would be able to differentiate as HCs. Since *Yap-S127A*$^{+/-}$*;Sox10*$^{rtTA/+}$ pups that were administered doxycycline on P1 did not consistently tolerate the treatment beyond P5, we modified our protocol to ameliorate this toxicity and administered a reduced dose of doxycycline (10 mg/kg) to *Yap-S127A*$^{+/-}$*;Sox10*$^{rtTA/+}$ mice and littermate controls at P3. EdU was supplied on P4, P5, and P6, and utricles were harvested at P24. Utricles of *Yap-S127A*$^{+/-}$*;Sox10*$^{rtTA/+}$ mice contained 7±4 Myo7a+, EdU+ cells/10,000 μm^2, 49-fold more than littermate controls ($p=0.0006$, $t(9)=5.2$, n=3-8 mice, Figure 5-4I-L). Contralateral utricles which were immunostained for Myo6

contained 40-fold more Myo6+, EdU+ cells than littermate controls ($p<0.0001$, $t(8)=7.4$, n=3-7 mice, Figure 5-4K). Thus, reactivating YAP-TEAD signaling in SCs of the neonatal mouse utricle spurs them to generate progeny that express HC markers *in vivo*.

YAP-TEAD transcriptional activity can also induce negative feedback (Dai et al., 2015; Moroishi et al., 2015; Park et al., 2016). E-cadherin is reported to be a negative regulator of YAP in other epithelia (Kim et al., 2011; Benham-Pyle et al., 2015), and is hypothesized to restrict the activity of YAP in SCs of the mammalian utricle (Kozlowski et al., 2020). To test whether expression of YAP-S127A affects E-cadherin expression, we administered doxycycline to *Yap-S127A$^{+/-}$;Sox10$^{rtTA/+}$* mice and littermate controls at P1. At P5, the intensity of E-cadherin immunostaining at SC-SC junctions tripled in *Yap-S127A$^{+/-}$;Sox10$^{rtTA/+}$* utricles compared to littermate controls ($p=0.0002$, $t(22)=4.4$, n=12 mice, Figure 5-5A-C). In utricles that were harvested at P3 for RT-qPCR, transcript levels of E-cadherin were double those of controls ($p=0.0286$, Mann-Whitney test, n=4, Figure 5-5D).

High cell density has been proposed to inactivate YAP-TEAD signaling in the developing murine utricle (Gnedeva et al., 2017). To determine whether the induction of YAP-S127A at P1 overcame this regulation to increase cell density, we administered doxycycline to *Yap-S127A$^{+/-}$;Sox10$^{rtTA/+}$* mice and littermate controls at P1. Then we harvested utricles at P5 and immunostained for the HC marker Myo7a as well as ZO-1 to delineate apical junctions. The macular area did not significantly change as a result of YAP-S127A induction (Control: 0.15±0.02 mm^2 vs YAP-S127A: 0.11±0.05 mm^2, $p=0.208$, $t(7)=1.4$, n=4-5 mice, Figure 5-5E), but the spatial density of SCs increased 1.4-fold ($p=0.008$, $t(10)=3.3$, n=5-7 mice, Figure 5-5F-H). The total cell density increased 1.25-fold ($p=0.033$, $t(10)=2.5$), and the density of HCs was unchanged ($p=0.36$, $t(10)=0.96$). The results indicate that mutation of serine 127 to a non-phosphorylatable residue bypassed inhibition, enhancing YAP-TEAD transcriptional activity and driving SCs in the neonatal mouse utricle to proliferate.

The proliferative response to YAP-S127A declines during postnatal maturation

Expression of YAP-S127A stimulated TEAD-dependent transcription and SC proliferation in neonatal mouse utricles, but it was unclear whether SCs would remain responsive as they mature and enter a more persistent state of quiescence. To test that, we injected doxycycline intraperitoneally in one group of *Yap-S127A*$^{+/-}$*;Sox10*$^{rtTA/+}$ mice on P3, another group on P5, and a third on P9. EdU was injected subcutaneously once daily over the following three days, and the utricles were harvested four days post-doxycycline. Following induction on P3, utricles of *Yap-S127A*$^{+/-}$*;Sox10*$^{rtTA/+}$ mice contained 95-fold more EdU+ cells than littermate controls. The incidence of S-phase entry fell to less than half of that level following induction on P5, and declined to 5% of the P3 level when induced on P9 ($p<0.0001$, $F(2, 56)=61$, two-way ANOVA, n=5-16 mice, Figure 5-6A-G).

One potential confounding variable in this *in vivo* experiment was that the bioavailability of doxycycline in the ear is reported to decline during postnatal maturation (Walters and Zuo, 2015). We confirmed that the YAP-S127A transgene was expressed at all time points by comparing YAP immunoreactivity in the utricles of *Yap-S127A*$^{+/-}$*;Sox10*$^{rtTA/+}$ mice to those of age-matched littermate controls (Figure 5-6A-F). To circumvent any bioavailability issue, we cultured utricles from P1 and P9 *Yap-S127A*$^{+/-}$*;Sox10*$^{rtTA/+}$ mice in the presence of 10 µg/mL doxycycline and EdU for 72 h. Utricles from the P1 mice contained seven-fold more Sox2+ EdU+ cells than utricles from the P9 mice ($p=0.0277$, $t(13)=2.48$, n=6-9, Figure 5-6H-J), indicating that postnatal maturational changes in the utricle limit SC proliferation in response to YAP-S127A overexpression both *in vivo* and *in vitro*. However, it appeared that striolar SCs, which are located in the central region of the utricle, remained responsive to YAP-S127A even at P9 (Figure 5-6I).

To determine whether the age-dependent decrease in proliferation correlated with a decrease in YAP-TEAD transcriptional activity, we cultured utricles of P1 and P9 mice with doxycycline for 48 h and measured the expression of YAP-TEAD target genes using RT-qPCR. The expression of most target genes declined with age both in utricles from *Yap-S127A*$^{+/-}$

;Sox10$^{rtTA/+}$ mice and littermate controls (Figure 5-6K). However, YAP-S127A induction at P9 still resulted in a four-fold to five-fold increase in expression of the target genes compared to age-matched controls (each p=0.0286, n=4 biological replicates, Mann-Whitney test), indicating that a transcriptional response remained intact. Taken together, the data suggest that the responsiveness of SCs to YAP-TEAD signaling declines with age but is not eliminated by P9.

We examined expression patterns of the TEAD transcription factors to characterize their age-related changes in the utricle. RNAscope fluorescent *in situ* hybridization revealed that TEAD1 was broadly expressed at P0, P6, and P16 by RNAscope (Figure 5-7A-C). TEAD2 was expressed throughout the mouse utricle at P0, but expression was lower at P6 and nearly absent at P16 (Figure 5-7D-F). The age-related downregulation of TEAD2 correlated with declines in YAP-TEAD transcriptional activity and proliferation, and was consistent with published RNA-seq (Gnedeva and Hudspeth, 2015). TEAD3 and TEAD4 transcripts were not detected (data not shown). An antibody specific for TEAD1 labeled nuclei of SCs in newborn and adult mouse utricles (Figure 5-7G, H). Immunostaining of utricles from newborn and adult mice showed that YAP too remained expressed in adult SCs (Figure 5-7I, J), which we confirmed in a human specimen (Figure 5-7K). The continued expression of YAP and TEAD1 in adults raised the possibility that SCs in mature mammalian utricles may remain sensitive to YAP-TEAD signaling.

YAP-5SA triggers TEAD-dependent proliferation in utricles from adult mice

YAP-5SA contains five serine-to-alanine mutations which allow it to evade inhibitory phosphorylation that leads to cytoplasmic sequestration and degradation (Zhao et al., 2007, 2009, 2010). It also more potently stimulates YAP-TEAD signaling than YAP-S127A (Zhao et al., 2009). We explanted utricles from P30 mice and adenovirally transduced SCs with YAP-5SA. Matched utricles were transduced with mCherry as a negative control, or wild type YAP to evaluate the effect of inhibitory phosphorylation. The rate of SC transduction did not differ between the viruses (p=0.62, F(3,12)=0.61, ANOVA, n=4 utricles, Figure 5-8A), with approximately 30% of SCs and

less than 1% of HCs were transduced at the titer used (data not shown), consistent with previous reports (Burns et al., 2012c). After three days of culture in the presence of BrdU, utricles that were transduced with mCherry or wild type YAP averaged fewer than two Sox2+ BrdU+ cells (Figure 5-8B-F). In contrast, utricles transduced with YAP-5SA averaged 69±56 ($p<0.0001$, $F(3, 44)=15$, n=10-16, ANOVA, Figure 5-8D, F). The Sox2+ BrdU+ cells lacked apical F-actin bundles, suggesting that they were SCs and not Type II HCs (data not shown).

We measured N:C ratios of YAP in transduced cells, which expressed an mCherry reporter. SCs transduced with YAP-5SA exhibited significantly higher N:C ratios compared to SCs transduced with wild type YAP ($p=0.0446$, $F(2, 9)=10.5$, n=4, ANOVA with Tukey's test, Figure 5-8G-J). In addition, an antibody specific for phospho-YAP (S127) strongly labeled the cytoplasm of SCs transduced with wild type YAP, but not those transduced with YAP-5SA in which that epitope is mutated (Figure 5-8K, L). These results show that ectopic wild type YAP is phosphorylated and retained in the cytoplasm, while YAP-5SA, which lacks inhibitory phosphorylation sites, enters SC nuclei and promotes S-phase entry.

To test whether the TEAD transcription factors were required for the proliferation induced by YAP-5SA, we transduced P30 utricles with YAP-5SA/S94A, which contains the serine-to-alanine mutations of YAP-5SA plus a mutation at residue 94 that abolishes the YAP-TEAD interaction (Zhao et al., 2008). Immunolocalization showed that YAP-5SA/S94A was significantly enriched in SC nuclei relative to ectopic wild type YAP ($p=0.0036$, $F(2, 9)=10.5$, n=4, ANOVA with Tukey's test, Figure 5-8I, J), but no cell cycle re-entry occurred (Figure 5-8E, F). Taken together, the results suggested that liberating YAP from inhibitory phosphorylation would allow it to promote TEAD-dependent proliferation in mature striolar SCs.

Cell cycle re-entry in response to YAP-5SA preferentially occurred in the striolar region. In utricles transduced with YAP-5SA and immunostained for BrdU and the striolar SC marker β-tectorin (Tectb) after five days in culture, the density of BrdU+ cells was over three-fold greater in the Tectb+ region compared to the Tectb- region ($p=0.0001$, $t(4)=15.3$, n=5, paired t-test, Figure

5-9). There was no difference in the density of transduced SCs between the striolar and lateral extrastriolar region (Lateral: 83±22; Striolar: 83±20 SCs/10,000 μm^2, p=0.90, t(3)=0.14, n=4, paired t test). We attempted to determine whether the proliferating SCs would differentiate into HCs, however constitutive overexpression of YAP-5SA disrupted the morphology of the striola in cultures maintained five days or longer post-transduction (Figure 5-9A), precluding such analysis.

Conditional knockout of LATS1 and LATS2 stimulates proliferation in postnatal murine utricles

LATS1 and LATS2 are the major kinases that mediate inhibitory phosphorylation of YAP at HXRXXS motifs in order to regulate its localization and stability (Zhao et al., 2007, 2010). We detected phospho-YAP (S127) immunoreactivity, a measure of LATS kinase activity (Zhao et al., 2007), in SCs throughout the utricles of newborn and adult mice (Figure 5-10A, B), so we hypothesized that inactivation of LATS1/2 would lead to cell cycle re-entry in the postnatal murine utricle. We used an *in vitro* approach to test that, because the *Lats1*$^{flox/flox}$*;Lats2*$^{flox/flox}$*;Plp1-Cre*^{ERT2} mice we generated developed tumors even in the absence of tamoxifen administration. For this we explanted utricles of *Lats1*$^{flox/flox}$*;Lats2*$^{flox/flox}$ mice and adenovirally transduced their SCs with mCherry or mCherry-T2A-Cre (LATS1/2 cKO). Utricles were cultured for seven days, with EdU added for the final two days to label SCs that entered S-phase. In utricles from P30 mice, phospho-YAP (S127) immunoreactivity was reduced in SCs of *Lats1*$^{flox/flox}$*;Lats2*$^{flox/flox}$ utricles that were transduced with mCherry-T2A-Cre compared to neighboring non-transduced SCs and SCs transduced with mCherry alone (Figure 5-10C, D), indicating that LATS1/2 are expressed in mature SCs and mediate the continuous inhibitory phosphorylation of YAP.

Utricles from P1 *Lats1*$^{flox/flox}$*;Lats2*$^{flox/flox}$ mice that were transduced with mCherry-T2A-Cre averaged 38-fold more EdU+ SCs than controls (6±3 vs. 240±145, p=0.018, t(6)=3.2, n=4, Figure 5-10E-G), with some EdU+ nuclei visible as mitotic figures (Figure 5-10F'''). In P30 utricles, deletion of LATS1/2 significantly increased S-phase entry, albeit to a lesser extent than in P1. After seven days *in vitro*, LATS1/2 cKO utricles averaged 12±15 EdU+ cells, 4.4-fold more than

P30 controls (p=0.0342, t(28)=2.73, n=15). Extending the culture duration to eleven days resulted in 17±21 EdU+ cells in LATS1/2 cKO utricles, a 9-fold increase over controls (p=0.0393, t(18)=2.22, n=10, Figure 5-10H-J). The density of transduced SCs was not significantly different between P1 and P30 utricles (P1: 62 ± 15; P30: 53±27 SCs/10,000 μm^2; p = 0.60, t(5)=0.56, n = 3-4). In both P1 and P30 LATS1/2 cKO utricles, proliferating SCs were located in a striolar distribution (Figure 5-10E, F). Thus, LATS1/2 are required for maintaining quiescence in a major subset of mature mammalian SCs.

DISCUSSION

An emerging paradigm in epithelial repair specifies that upon damage, YAP accumulates in nuclei of stretched cells, where it promotes proliferation with TEAD transcription factors (Guillot and Lecuit, 2013; Benham-Pyle et al., 2015; Irvine and Shraiman, 2017). We found that YAP readily accumulated in SC nuclei of the chicken utricle in response to ototoxic and mechanical insult, but congruent with species differences in regenerative proliferation, YAP localization was less sensitive to shape change and acute inhibition of MST1/2 in murine SCs than in chicken SCs. Overexpressing a YAP-S127A variant which could enter nuclei elicited YAP-TEAD transcriptional activity and SC proliferation in the neonatal mouse utricle. This proliferative response declined with age, but persisted to an extent in mature SCs. Ectopic wild type YAP was phosphorylated and sequestered in the cytoplasm, but a YAP-5SA variant which lacks LATS1/2 phosphorylation sites entered nuclei of mature SCs and drove TEAD-dependent proliferation in the striola. Corroborating the importance of inhibitory phosphorylation, deletion of LATS1/2 reduced phospho-YAP and evoked proliferation of striolar SCs, even in adult mouse utricles. The results indicate that constitutive signaling by LATS1/2 kinases is required to phosphorylate YAP and hold SCs in mouse utricles in a persistent state of quiescence. The inhibitory Hippo pathway is active in SCs of the undamaged chicken utricle, but is inactivated or bypassed upon HC loss. Overall, these findings provide a novel mechanistic basis to explain why mammals and nonmammals differ

in their ability to replace sensory HCs, and demonstrate that reactivation of YAP-TEAD signaling is sufficient to induce SC proliferation in the mammalian balance epithelium.

The exact mechanism by which HC loss leads to the activation of YAP in chicken SCs remains to be elucidated. In chickens, HC loss results in rapid expansion of neighboring SC surfaces (Cotanche, 1987), and we found that shape changes correlated to the degree of YAP nuclear accumulation (Figure 5-2). These shape changes may disrupt the MST1/2-LATS1/2 kinase cascade, allowing YAP to accumulate in the nucleus. Shape changes appear to modulate MST1/2 in certain epithelia (Varelas et al., 2010; Fletcher et al., 2018) but not others (Kim et al., 2011; Codelia et al., 2014; Meng et al., 2015), and some forms of mechanical regulation of YAP require neither MST1/2 nor LATS1/2 (Dupont et al., 2011; Aragona et al., 2013). As cell junctions strongly regulate Hippo signaling (Karaman and Halder, 2018), HC loss may induce nuclear accumulation of YAP in the SCs of fish and amphibians, whose junctions are similar to avian SCs in that they contain little E-cadherin and have thin circumferential F-actin bands (Burns et al., 2008, 2013).

Streptomycin-induced HC loss did not affect YAP localization in murine SCs (Figure 5-1). Murine SCs must undergo larger shape changes than their avian counterparts in order to increase their likelihood of entering S-phase (Collado et al., 2011a). This corresponds to our observation that SC deformations induce nuclear accumulation of YAP in mammalian SCs, but to a lesser degree than in chicken SCs (Figure 5-2). Thus, the shape changes produced by HC loss in the murine utricle may be below the threshold to evoke the nuclear accumulation of YAP, and additional inhibitory signals may restrict nuclear access of YAP.

In contrast to chicken SCs, acute MST1/2 inhibition did not affect YAP localization in murine SCs (Figure 5-3). This suggests that MST1/2-independent mechanisms may activate LATS1/2 in murine SCs. E-cadherin is reported to activate LATS1/2 independently of MST1/2 in other epithelia (Kim et al., 2011) and is expressed at higher levels in mammalian SCs than those of birds, fish, and amphibians (Collado et al., 2011b; Burns et al., 2013). Pharmacologic

treatments that deplete E-cadherin from striolar SC junctions also affect YAP expression and induce SC proliferation (Kozlowski et al., 2020). Here, overexpression of YAP-S127A in mammalian SCs induced upregulation of E-cadherin in what may reflect negative feedback (Figure 5-5A-D). MAP4K kinases and metabolic changes can also activate LATS1/2 independent of MST1/2 (Meng et al., 2015; W. Wang et al., 2015; Nokin et al., 2016). Pinpointing which upstream signals activate LATS1/2 in mammalian SCs will aid efforts to overcome proliferative quiescence.

As the deletion of LATS1/2 reduced inhibitory phosphorylation of YAP and recapitulated the pattern of TEAD-dependent, striolar proliferation evoked by YAP-5SA overexpression, our data strongly suggest that LATS1/2 maintain proliferative quiescence by restricting YAP-TEAD signaling. Corroborating that notion, a recent report showed that pharmacologic inhibition of LATS1/2 kinase activity evokes YAP-dependent proliferation in mature mouse utricles (Kastan et al., 2020). However, these data do not exclude a contribution from YAP-independent mechanisms downstream of LATS1/2 inactivation, such as disassembly of the repressive DREAM complex (Tschöp et al., 2011).

LATS1 and LATS2 have overlapping functions and most prominently differ in their expression profiles (Furth and Aylon, 2017). These results do not distinguish whether one or both kinases is required to maintain SC quiescence. Likewise, YAP and its paralog TAZ have largely overlapping functions (Plouffe et al., 2018). Though we examined the localization and phosphorylation of YAP, damage and LATS1/2 deletion could similarly affect TAZ.

Overexpression of YAP-S127A is sufficient to stimulate widespread proliferation and increase cell density in the P1 mouse utricle (Figure 5-4, Figure 5-5), consistent with a model in which cell-density-dependent inactivation of YAP-TEAD signaling mediates cell cycle arrest in the developing utricle (Gnedeva et al., 2017). However, since cell density in the murine utricle plateaus around E17.5 (Gnedeva et al., 2017), the model does not account for postnatal declines in the capacity of SCs to overcome proliferative quiescence (Burns et al., 2012a). Since this age-

dependent decline occurs despite overexpression of YAP-S127A or deletion of LATS1/2, the data indicate that SC proliferation is further restricted by age-dependent changes that lie downstream of YAP inhibitory phosphorylation, such as the downregulation of TEAD2 or changes in parallel pathways such as canonical Wnt signaling, Notch signaling, Atoh1 expression, and SoxC expression (Gnedeva and Hudspeth, 2015; Maass et al., 2015; T. Wang et al., 2015; Samarajeewa et al., 2018; Sayyid et al., 2019).

It appears that multiple layers of regulation contribute to SC quiescence, albeit not equally across all HC epithelia. For example, chromatin is less accessible in cochlear SCs than utricular SCs (Jen et al., 2019), and f striolar SCs were more likely to proliferate than extrastriolar SCs when inhibitory phosphorylation of YAP was bypassed (Figure 5-6, Figures 8-10). The proliferation rates of striolar and extrastriolar SCs varied slightly between *in vivo* and *in vitro* experiments (Figure 5-4F, Figure 5-6), possibly due to doxycycline bioavailability or culture conditions. The progressive restriction of S-phase entry to the striolar region of the utricle after YAP-S127A overexpression *in vivo* and *in vitro* (Figure 5-6) suggests that striolar-extrastriolar differences widen throughout postnatal maturation. The low rate extrastriolar proliferation in P1 LATS1/2 cKO utricles may be due to aging of the explant during the processes of adenoviral transduction, Cre expression, recombination of LATS1/2 alleles, and degradation of pre-existing LATS1/2 mRNA and protein (Figure 5-10E-G). YAP was no more likely to accumulate in nuclei of striolar SCs than those in the extrastriola after streptomycin damage (Figure 5-1) or MST1/2 inhibition (Figure 5-3), suggesting that factors downstream of YAP nuclear accumulation or in parallel pathways account for the different responsiveness. Although expression of TEAD1 and TEAD2 did not appear to differ between striolar and extrastriolar SCs (Figure 5-7), their transcriptional activity may be uniquely restricted in extrastriolar SCs (Chang et al., 2018). Additionally, extrastriolar SCs may lack signals that promote proliferation downstream of YAP-TEAD signaling: Wnt is reported to control proliferation downstream of YAP in organoids derived cochlear progenitors that express Lgr5+ (Xia et al., 2020), and striolar SCs which express Lgr5+

are more responsive to Wnt than extrastriolar SCs (Lin et al., 2015; T. Wang et al., 2015; You et al., 2018). Retinoic acid receptor signaling is elevated in the developing extrastriola (Ono et al., 2020) and could limit proliferation there, consistent with its reported role in promoting cell cycle exit and differentiation in neural progenitors (Janesick et al., 2015).

Regenerative proliferation is essential to mitotically replace HCs and to replenish the pool of SCs after direct transdifferentiation. It has remained unclear why SCs in nonmammalian vertebrates readily proliferate following HC loss, and those in mammals do not (Forge et al., 1993; Warchol et al., 1993; Golub et al., 2012; Bucks et al., 2017; Senn et al., 2019). Our results uncover distinctions in the regulation of YAP which may contribute to that difference. While YAP is required for regenerative proliferation in the chicken utricle, mammalian SCs appear to regulate YAP with a different mechanism that is thus far insensitive to HC loss and may be related to the postnatal reinforcement of intercellular junctions that occurs uniquely in mammalian SCs (Burns et al., 2008; 2013; Collado et al., 2011b). We find that the quiescence of SCs in mature mammals is maintained in part by the constitutive activity of LATS1/2 kinases that phosphorylate YAP and restrict its ability to regulate gene expression with TEAD. Approaches to inhibit LATS1/2 kinase activity eventually may be used to promote replacement of lost HCs for the treatment of hearing loss and balance disorders.

FIGURES AND FIGURE LEGENDS

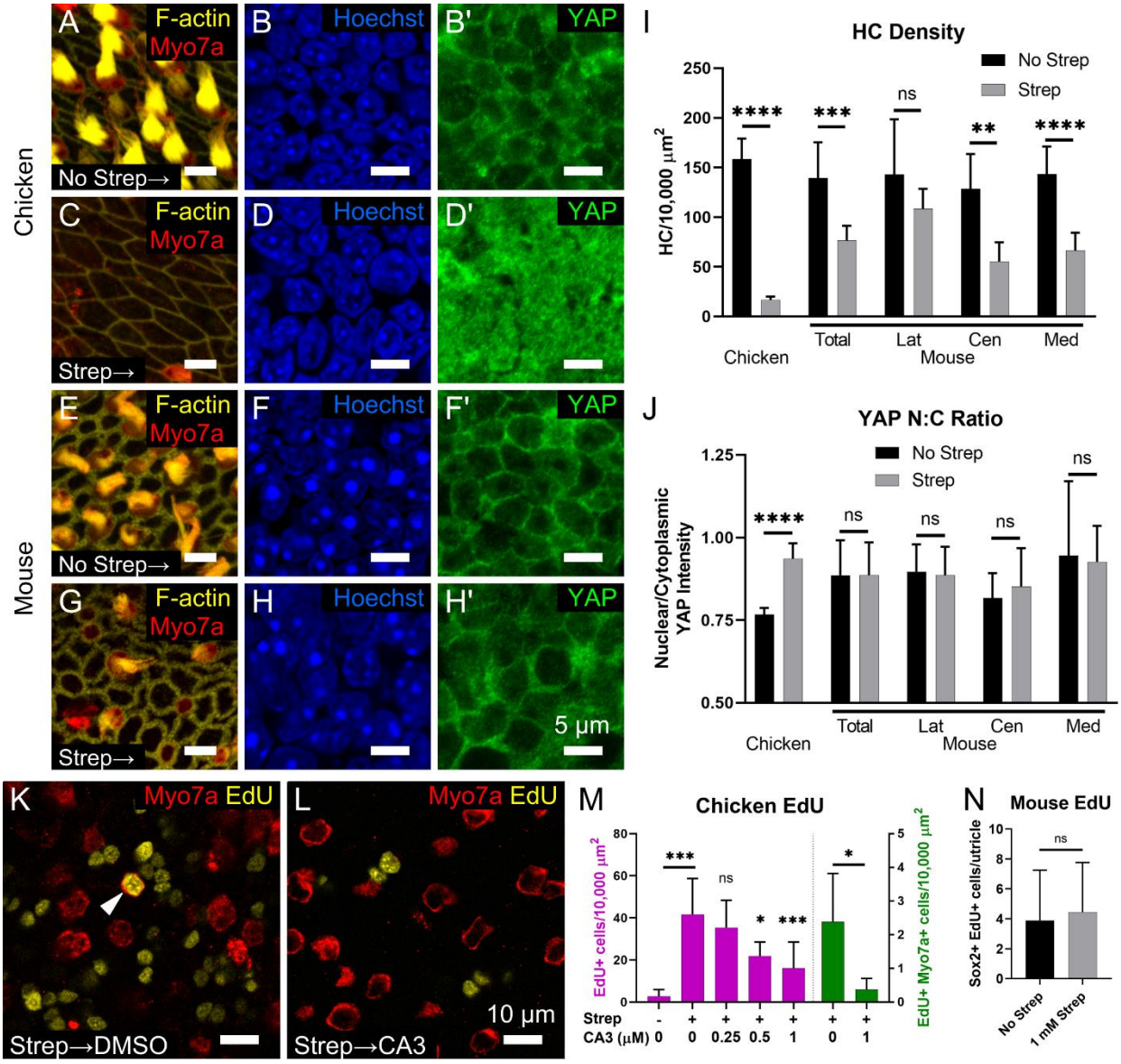

Figure 5-1: YAP accumulated in SC nuclei after HC loss and mediated regenerative proliferation in utricles of chickens, but not in those of mice. (A-H) Utricles from P2 chickens and P1 mice were cultured 24 h with or without streptomycin and fixed after 72 h to assess HC loss in confocal images of the apical surface and YAP N:C ratios in the SC nuclear layer. Streptomycin induced HC loss in both species, but YAP accumulated in SC nuclei only in damaged chicken utricles (D). Images E-H depict the central (putative striolar) region of the mouse utricle. **(I)** Quantification reveals significant HC loss in streptomycin-treated utricles of chickens ($p<0.0001$, n=6 utricles) and mice (total: $p=0.0004$, n=8). Regional comparisons for the mouse utricle were made with Sidak's test (Lat: $p=0.48$; Cen: $p=0.0065$, Med: $p<0.0001$, n=6-8). **(J)** Quantification of YAP N:C ratios reveals significant increases in streptomycin-treated chicken utricles ($p<0.0001$, n=6). Damage had no effect on mouse utricles (total: $p=0.98$, n=8). Regional comparisons for the mouse utricle were made with Sidak's test (Lat: $p=0.99$; Cen: $p=0.87$, Med: $p=0.996$, n=8). **(K, L)** Confocal image of streptomycin-treated P2 chicken utricles. Those cultured with DMSO (K) contained significantly more EdU+ cells and Myo7a+ EdU+ cells (arrowhead) than those cultured with 1 µM CA3 (L) through day seven. **(M)** Quantification of EdU+ cells after 3 d (magenta bars, left y-axis) and Myo7a+ EdU+ cells after 7 d (green bars, right y-axis) within P2 chicken utricles. Streptomycin-treated utricles contained significantly more EdU+

cells than undamaged utricles ($p<0.0001$, t-test). Streptomycin-treated utricles cultured with the YAP-TEAD inhibitor CA3 contained fewer EdU+ cells in a dose-dependent manner ($p=0.001$, ANOVA with Dunnett's multiple comparisons test; * indicates $p<0.05$, *** indicates $p<0.001$, n=6-16). CA3 treatment significantly reduced mitotic HC production ($p=0.034$, n=4). **(N)** P1 mouse utricles were cultured with or without 1 mM streptomycin for 24 h and then incubated 72 h in the presence of EdU. Damage did not significantly affect the density of Sox2+ EdU+ cells ($p=0.73$, n=9). All graphs depict mean±SD.

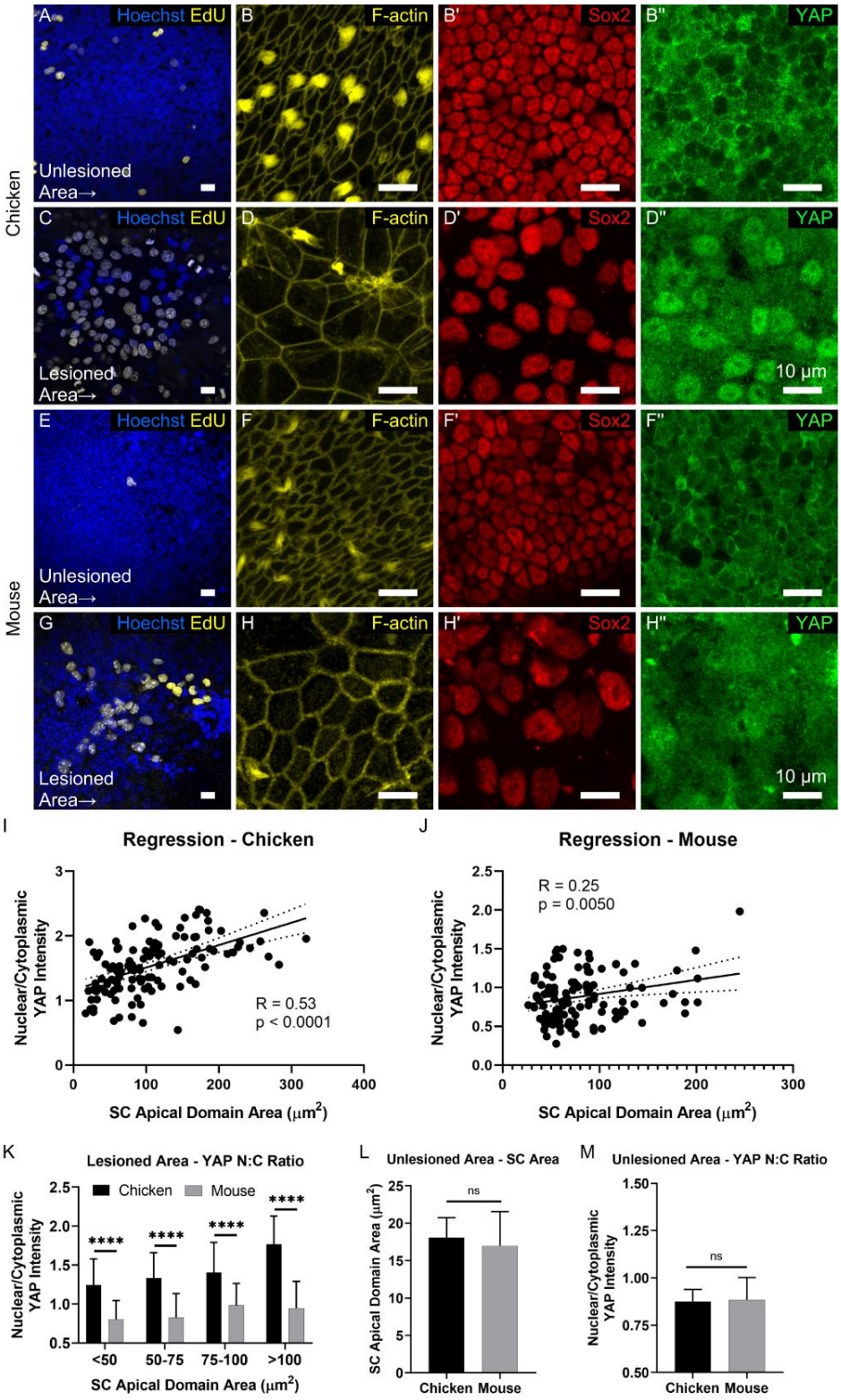

Figure 5-2: In SCs that changed shape to close excision lesions, nuclear accumulation of YAP was more prominent in chickens than mice. After 24 h in culture, standardized excision lesions were made in utricles from P2 chickens and P1 mice, which were cultured an additional 48 h before fixation. **(A-D)** Damage evoked a focal proliferative response in the chicken utricle (A, C). YAP markedly accumulated in the nuclei of SCs that expanded to

close the lesion (D) in comparison to the densely packed SCs outside of the lesioned area (B). **(E-H)** Damage also evoked a focal proliferative response in the mouse utricle (E, G). Modest nuclear accumulation of YAP was evident in SCs that expanded to close the lesion in the center of the macula (H) in comparison to those outside of the lesion area at the periphery of the macula (F). **(I)** Regression analysis revealed a significant association between YAP N:C ratio and SC apical domain size within the lesioned area of the chicken utricle (slope non-zero at $p<0.0001$, n=120 cells from 4 utricles). Dashed lines depict 95% confidence interval. **(J)** Regression analysis reveals a modest association between YAP N:C ratio and SC apical domain size within the lesioned area of the mouse utricle (slope non-zero at $p=0.0050$, n=120 cells from 4 utricles). **(K)** Quantification of the YAP N:C ratio in SCs within the lesioned area revealed that YAP was significantly enriched in nuclei of SCs of the chicken utricle compared to those of the mouse utricle, controlling for the apical domain area (each $p<0.0001$, two-way ANOVA with Sidak's test, n=19-58 cells per bin per species). **(L)** Quantification of SC apical domain size outside of the lesioned area revealed no significant difference between mouse and chicken utricles ($p=0.6870$, n=4 utricles). **(M)** Quantification of YAP N:C ratio from confocal images of the SC nuclear layer in the unlesioned area revealed no significant differences between mouse and chicken utricles ($p=0.8852$, n=4-6 utricles).

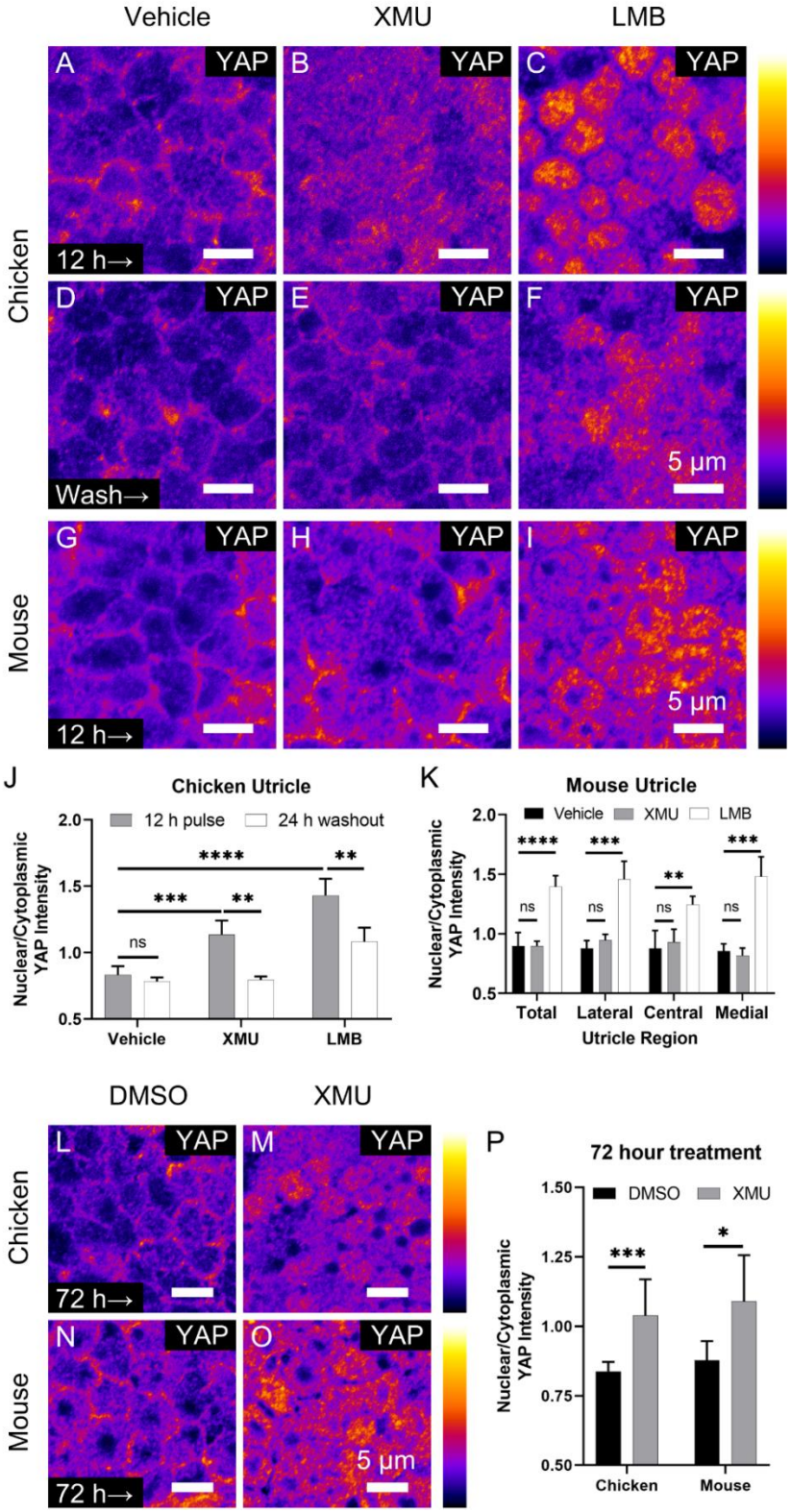

Figure 5-3: Acute inhibition of MST1/2 kinase activity induced nuclear accumulation of YAP in chicken SCs, but not in those of mice. (A-I) High magnification images of YAP immunoreactivity (pseudocolored) in the SC nuclear layer of explanted P2 chicken utricles (A-F) or P1 mouse utricles (G-I) cultured in either vehicle negative control, MST1/2 kinase inhibitor XMU-MP-1 (XMU) at 3 µM, or leptomycin B (LMB) at 40 ng/mL as a positive control.

After 12 h, YAP intensity is greater in the cytoplasm than in nuclei in vehicle controls (A, G), and enriched in nuclei in utricles treated with LMB (C, I). XMU treatment increases nuclear levels of YAP to an intermediate extent in the chicken utricle (B) and is reversible upon a 24 h washout (E). XMU did not affect YAP N:C ratios in the mouse utricle during a 12 h pulse (H). Images G-I depict the central (striolar) region of the mouse utricle. **(J)** Quantification shows that a 12 h pulse of XMU significantly increases the N:C ratio of YAP over vehicle controls in chicken utricles ($p<0.0001$, n=5 utricles, ANOVA with Sidak's test). Washout of XMU reverts the YAP N:C ratio to baseline levels ($p<0.0001$, n=4-5). LMB significantly increases YAP N:C ratio ($p<0.0001$, n=4-5). **(K)** Quantification reveals that a 12 h treatment with LMB significantly increased the YAP N:C ratio in mouse utricles compared to vehicle (ANOVA with Dunnett's test, $p<0.0001$, n=5-6), but XMU had no effect (ANOVA with Dunnett's test, $p=0.99$, n=6). Repeated measures ANOVA with Dunnett's test was used for region-specific comparisons (ns denotes $p>0.05$, **denotes $p<0.01$, ***denotes $p<0.001$). **(L-O)** Confocal images of YAP immunoreactivity from the SC nuclear layer in utricles from P2 chickens (L, M) and P1 mice (N, O) that were cultured in 3 μM XMU or DMSO for 72 h. **(P)** Quantification reveals that 72 h treatment with XMU significantly increased the YAP N:C ratio in chicken utricles ($p=0.0008$, n=8) and mouse utricles ($p=0.0103$, n=6-7) compared to DMSO-treated controls. Graphs depict mean±SD.

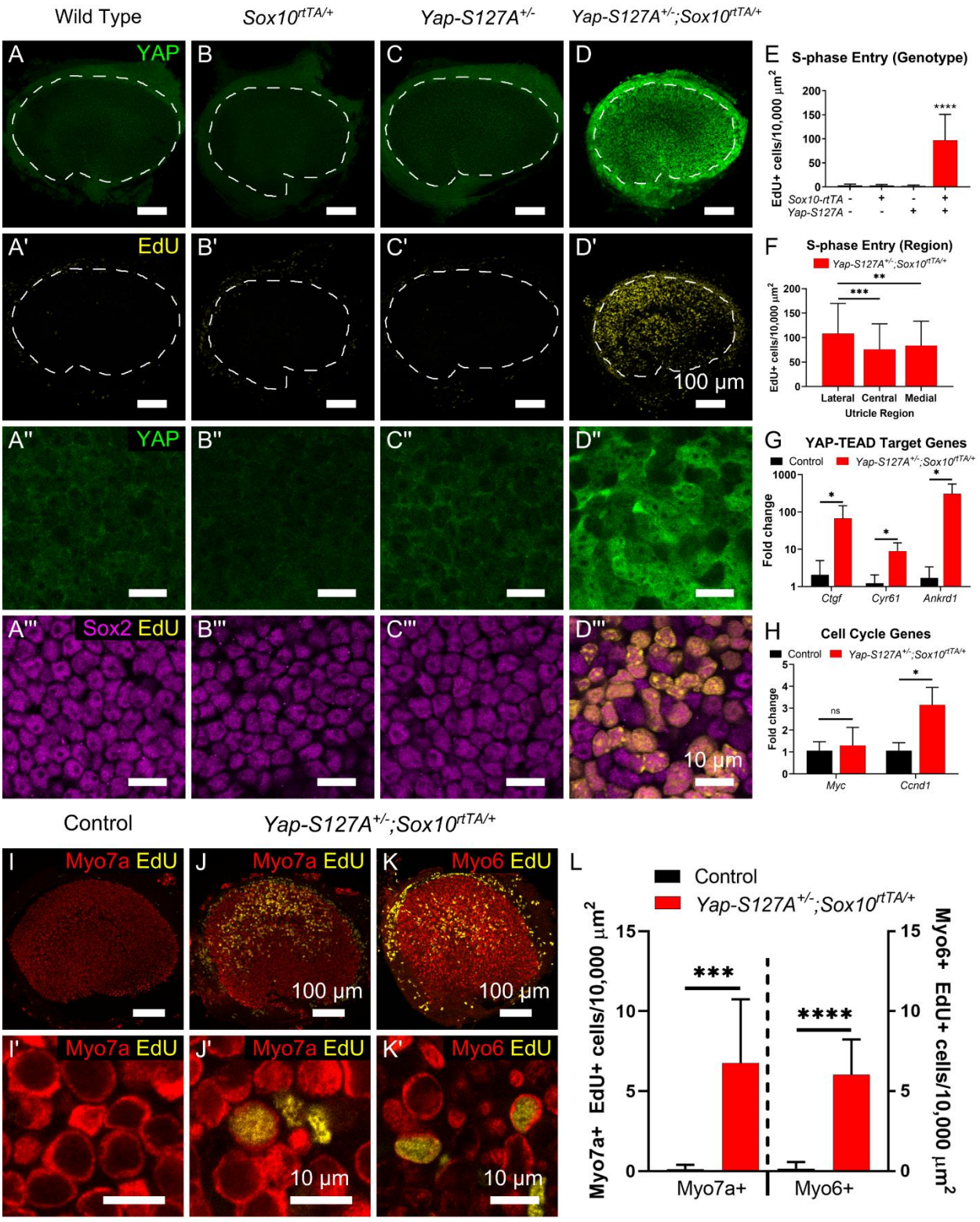

Figure 5-4: *In vivo* overexpression of YAP-S127A in the neonatal mouse utricle resulted in widespread S-phase entry, upregulation of YAP-TEAD target genes, and generation of progeny that expressed hair cell markers. (A-D) Doxycycline was administered on P1 and supplemented in the dam's drinking water. EdU was supplied on P2, P3, and P4, and utricles were harvested on P5. Low magnification images (A-D) show YAP immunoreactivity was more intense in *Yap-S127A*$^{+/-}$*;Sox10*$^{rtTA/+}$ mice (D) compared to littermate controls (A-C),

indicating induction of YAP-S127A expression. Dashed outlines indicate the boundary of the macula as evident by YAP-negative HC somas. EdU+ cells were abundant within the maculae of *Yap-S127A*$^{+/-}$*;Sox10*$^{rtTA/+}$ mice (D') but were rare in other genotypes (A'-C'). High magnification confocal images of the SC nuclear layer in the lateral extrastriolar region of the utricle depict immunoreactivity for YAP (A''-D'') and the SC marker Sox2 with EdU (A'''-D'''). **(E)** Quantification of EdU+ cells revealed utricles of *Yap-S127A*$^{+/-}$*;Sox10*$^{rtTA/+}$ mice had significantly greater S-phase entry (range 13-182 EdU+ cells/10,000 μm^2) than littermate controls ($p<0.0001$, ANOVA, n=5-11 mice per genotype). **(F)** Quantification of S-phase entry by utricular region (ANOVA with Tukey's test, n=16 utricles). **(G, H)** Pups were injected with doxycycline at P1 and utricles were harvested on P3 for RT-qPCR. Utricles from wild type, *Yap-S127A*$^{+/-}$, and *Sox10*$^{rtTA/+}$ pups were pooled as a negative control. Expression of YAP-TEAD target genes *Ctgf*, *Cyr61*, and *Ankrd1* (G) was significantly upregulated in *Yap-S127A*$^{+/-}$*;Sox10*$^{rtTA/+}$ mice compared to negative controls (each $p=0.0286$, Mann Whitney test, n=4 biological replicates). Expression of *Ccnd1*, but not *Myc*, significantly increased in the context of YAP-S127A overexpression (H) ($p=0.0286$, Mann Whitney test, n=4 biological replicates). **(I-L)** Doxycycline was administered to *Yap-S127A*$^{+/-}$*;Sox10*$^{rtTA/+}$ mice and littermate controls at P3 and EdU was supplied at P4, P5, and P6. Utricles were harvested at P24. Utricles from *Yap-S127A*$^{+/-}$*;Sox10*$^{rtTA/+}$ mice contained numerous Myo7a+ EdU+ cells (J, J') and Myo6+ EdU+ cells (K, K'), which were rare in controls (I, I'). **(L)** Quantification revealed that Myo7a+ EdU+ cells and Myo6+ EdU+ cells were significantly more abundant upon YAP-S127A overexpression at P3 (Myo7a: $p=0.0006$, n=3-8 mice; Myo6: $p<0.0001$, n=3-7 mice). Utricles from wild type, *Yap-S127A*$^{+/-}$, and *Sox10*$^{rtTA/+}$ pups were pooled to serve as a negative control. All graphs depict mean±SD.

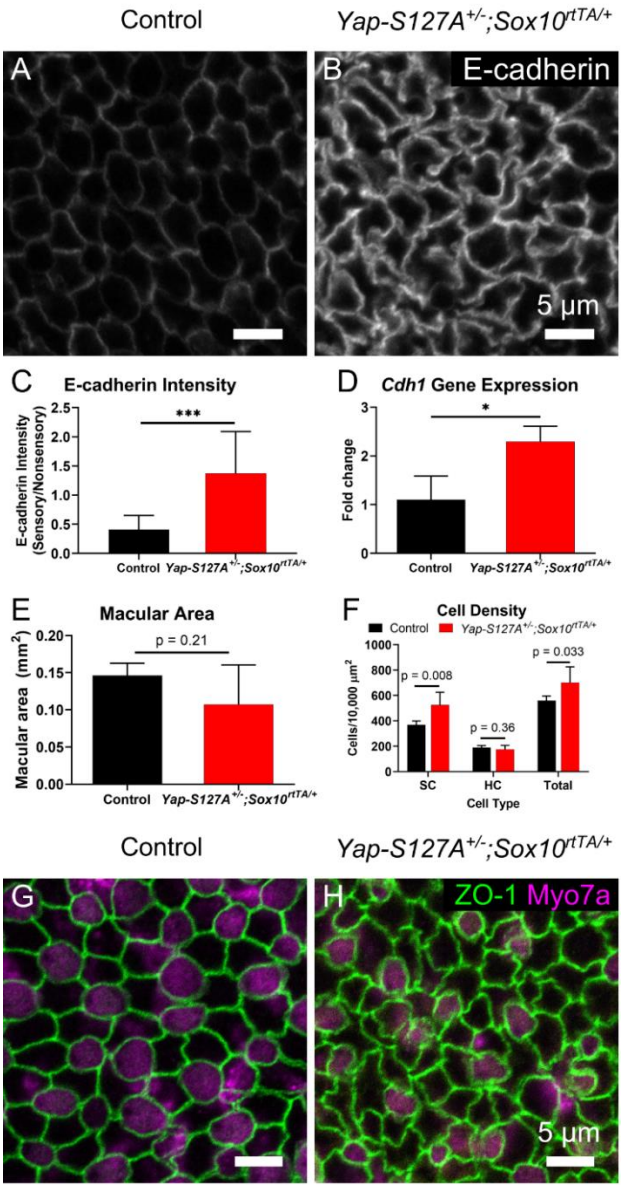

Figure 5-5: YAP-S127A overexpression at P1 led to upregulation of E-cadherin in SCs and drove an increase in cell density. Doxycycline was administered to *Yap-S127A*$^{+/-}$*;Sox10*$^{rtTA/+}$ mice and littermate negative controls at P1, and utricles were harvested either on P5 for immunohistochemistry or on P3 for RT-qPCR. **(A-B)** The intensity of E-cadherin immunolabeling in utricles of *Yap-S127A*$^{+/-}$*;Sox10*$^{rtTA/+}$ mice (B) was greater than that in negative control genotypes (A). **(C)** Quantification of E-cadherin staining intensity in SC-SC junctions normalized to E-cadherin levels in the non-sensory epithelium as an internal control (p=0.022, t-test, n = 12 utricles). **(D)** Quantification of *Cdh1* mRNA expression relative to *Gapdh* reveals that expression doubles in *Yap-S127A*$^{+/-}$*;Sox10*$^{rtTA/+}$ mice compared to negative control littermates (p=0.0238, Mann Whitney test, n=4 biological replicates). **(E)** Quantification of macular area as defined by Myo7a+ labeling reveals no significant differences between utricles from *Yap-S127A*$^{+/-}$*;Sox10*$^{rtTA/+}$ mice and controls (p=0.21, n=4-5 mice). **(F)** Quantification reveals that the total cell density (p=0.033) and SC density (p=0.008) were each significantly increased in utricles from *Yap-S127A*$^{+/-}$*;Sox10*$^{rtTA/+}$ mice compared to littermate controls (t-test, n=5-7 mice). HC density did not significantly vary between utricles of *Yap-S127A*$^{+/-}$*;Sox10*$^{rtTA/+}$ mice and controls (p=0.36, t-test, n=5-7 mice). **(G, H)** Immunostaining of apical junction marker ZO-1 and HC marker Myo7a in the lateral extrastriolar region of the utricle. Cells from the *Yap-S127A*$^{+/-}$*;Sox10*$^{rtTA/+}$ mouse utricle (H) are more densely packed and have irregular apical domain shapes in comparison to littermate controls (G). All graphs depict mean±SD.

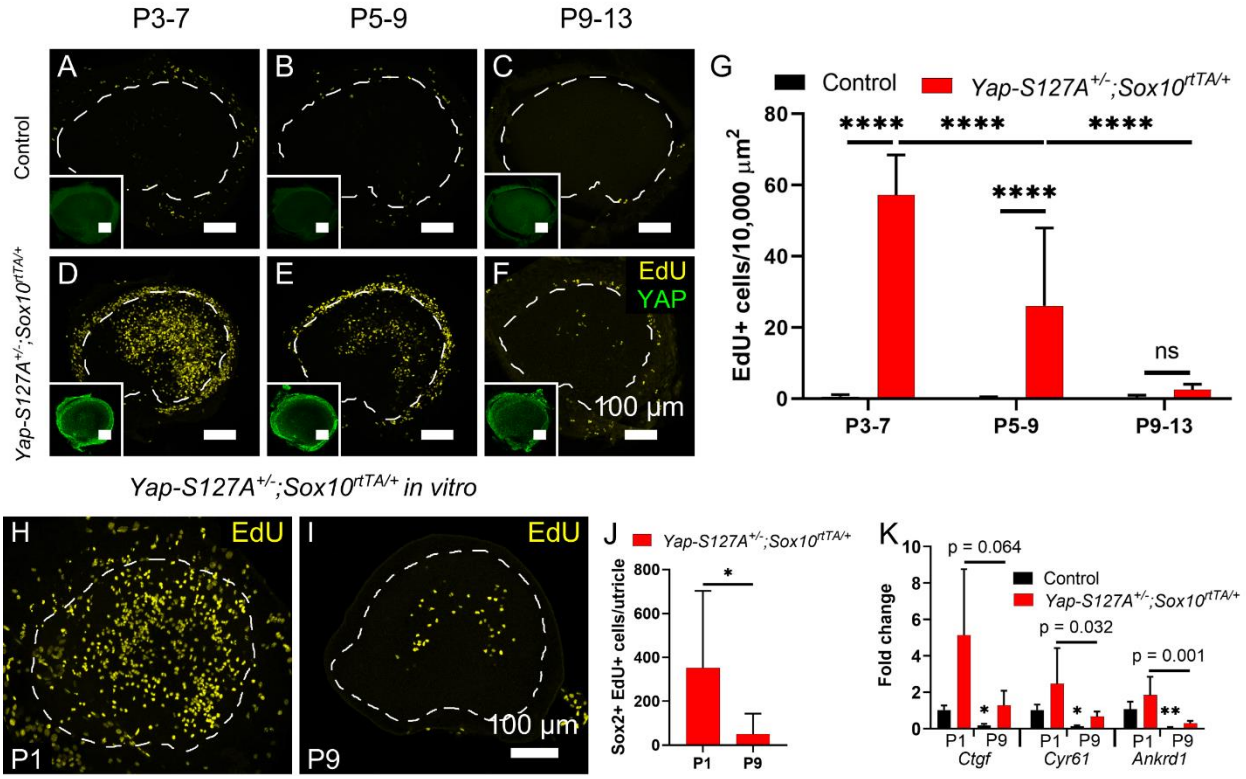

Figure 5-6: S-phase entry evoked by overexpression of YAP-S127A in the utricle declined during postnatal maturation. (A-F) Low magnification images of EdU showing that the S-phase entry in utricles of *Yap-S127A*$^{+/-}$*;Sox10*$^{rtTA/+}$ mice (D-F) declined in an age-dependent fashion. Utricles from wild type, *Sox10*$^{rtTA/+}$, and *Yap-S127A*$^{+/-}$ littermates were used as controls. Insets depict YAP immunoreactivity in age-matched utricles. **(G)** Quantification of EdU+ cell density revealed an age-dependent decrease in S-phase entry. A two-way ANOVA showed significant effects for genotype, age, and the age-genotype interaction (all $p<0.0001$, n=6-16 mice per condition). Sidak's multiple comparisons tests are depicted with **** indicating $p<0.0001$ and ns denoting $p>0.05$. **(H, I)** Low magnification images of explanted utricles from P1 and P9 *Yap-S127A*$^{+/-}$*;Sox10*$^{rtTA/+}$ mice that were cultured in the presence of 10 µg/mL doxycycline and EdU for 72 h. Dashed lines indicate the macular border as delineated by Sox2 immunostaining. **(J)** Quantification of Sox2+ EdU+ cells revealed that the incidence of S-phase entry was significantly lower in utricles from P9 *Yap-S127A*$^{+/-}$*;Sox10*$^{rtTA/+}$ mice compared to P1 mice of that genotype ($p=0.0277$, n=6-9 utricles). **(K)** RT-qPCR revealed that expression of YAP-TEAD target genes relative to *Gapdh* declined in an age-related manner regardless of YAP-S127A induction. Comparisons to P1 controls are indicated with * denoting $p=0.016$ and ** denoting $p=.0095$ (n=4-6 biological replicates, Mann-Whitney test). All graphs depict mean±SD.

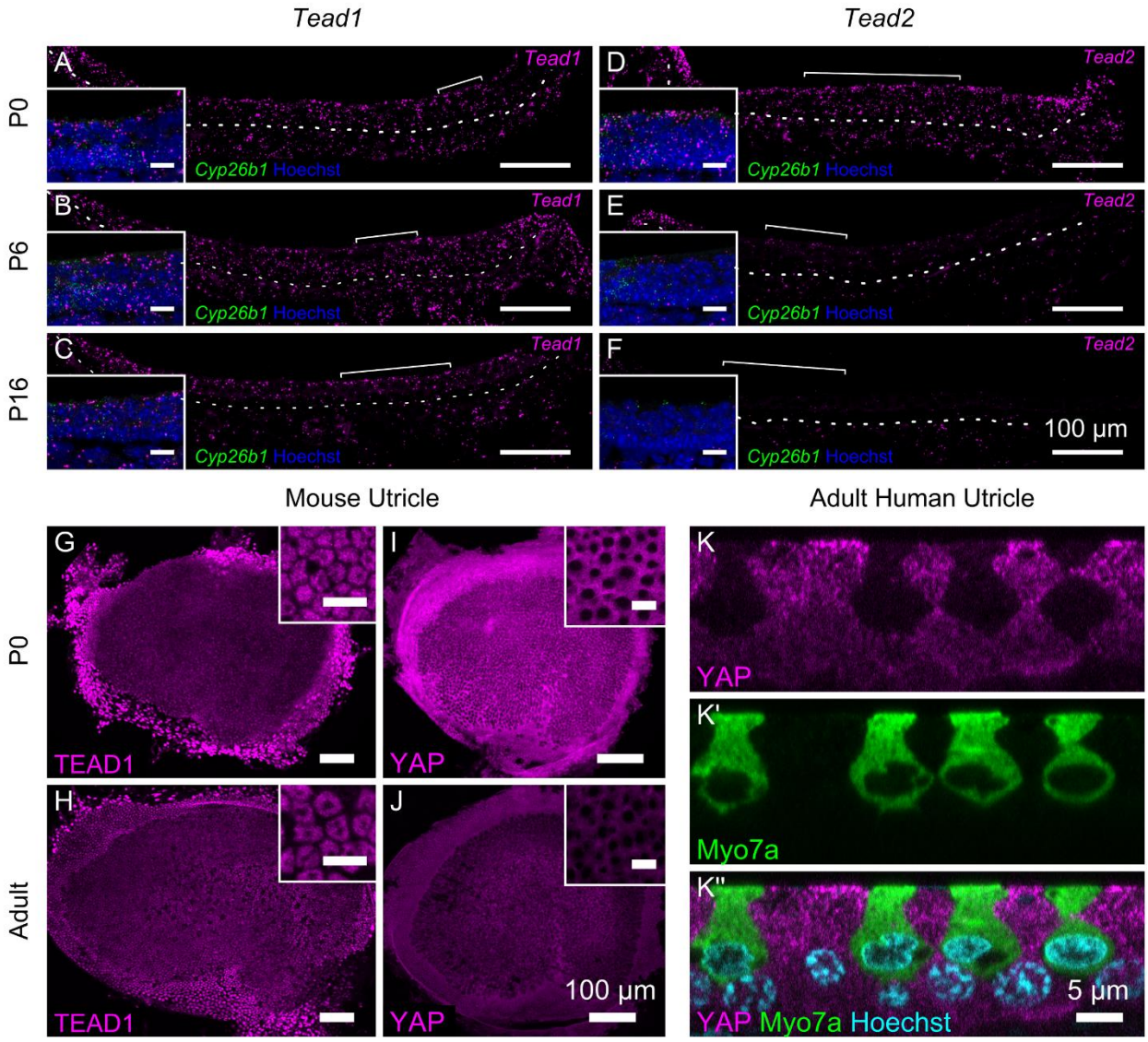

Figure 5-7: TEAD2 was downregulated as mice age, but expression of TEAD1 and YAP was maintained throughout the utricle. (A-F) Utricles of P0, P6, and P16 mice were fixed, frozen, sectioned, and probed for mRNA using RNAscope. TEAD1 message was detected throughout the utricle at all ages tested (A-C). TEAD2 message was detected throughout the utricle at P0, but declined in an age-dependent manner (D-F). Scale bars represent 100 µm. White brackets denote the Cyp26b1+ striolar domain, dashed lines indicate the border between the sensory epithelium and underlying stroma, and insets depict higher magnification with scale bars representing 10 µm. **(G-J)** TEAD1 and YAP antibody labeling in mouse utricles shows broad expression that persists from newborn (G, I) to adult (H, J) stages. Insets depict high magnification images of the SC nuclear layer (G, H) and apical surface (I, J) with scale bars representing 10 µm. **(K)** Orthogonal view of an adult human utricle immunostained for YAP and Myo7a with Hoechst labeling of cell nuclei.

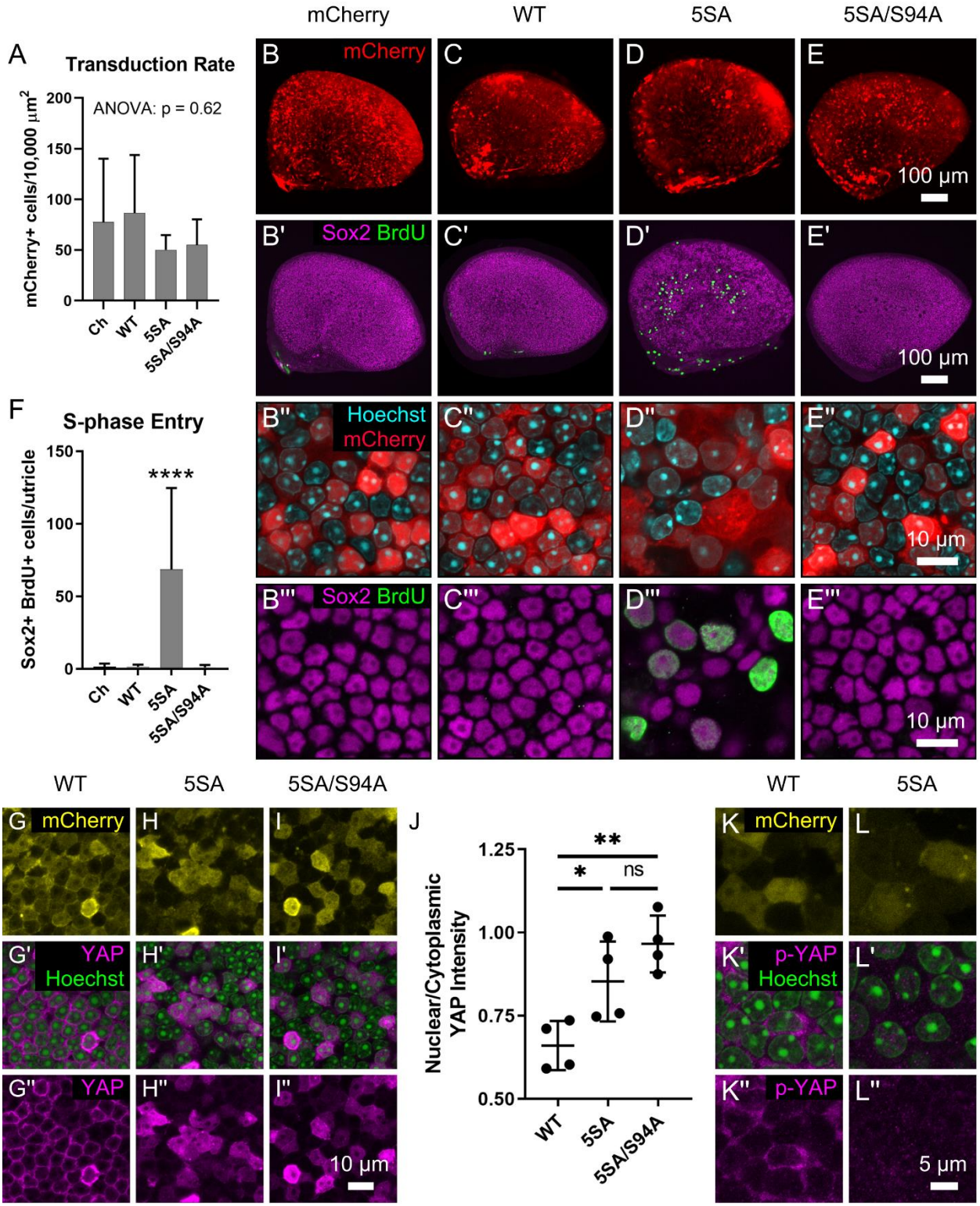

Figure 5-8: YAP-5SA entered SC nuclei and stimulated TEAD-dependent proliferation in P30 mouse utricles *in vitro*. Utricles of P30 mice were placed in culture and allowed to acclimate overnight. The following day, type 5 adenovirus was used to transduce SCs with either mCherry, wild-type YAP, YAP-5SA, or YAP-5SA/S94A. Utricles were maintained in the presence of BrdU for an additional three days before processing for immunohistochemistry. **(A)** Quantification reveals no significant differences in the transduction rates of the viruses (p=0.62, ANOVA, n=4

utricles). **(B-E)** Low magnification images show that transduction occurred in all conditions, but S-phase entry occurred exclusively in utricles that were transduced with YAP-5SA (B'-E'). High power images of the SC nuclear layer depicting expression of the mCherry reporter (B''-E'') as well as Sox2 and BrdU (B'''-E'''). The BrdU+ nuclei in utricles transduced with YAP-5SA co-labeled with the SC marker Sox2 (D''') and appeared at a lower density, possibly due to interkinetic nuclear migration or morphological disruption. **(F)** Quantification of Sox2+ BrdU+ cells per utricle after three days in culture. S-phase entry increased significantly in YAP-5SA treated utricles ($p<0.0001$, ANOVA, n = 10-16 utricles). **(G-H)** High magnification images of the SC nuclear layer of utricles transduced with wild type YAP, YAP-5SA, and YAP-5SA/S94A and analyzed 72 h post transduction. Wild type YAP was relatively enriched in cytoplasmic space surrounding SC nuclei (G''), whereas YAP-5SA and YAP-5SA/S94A were relatively enriched in the SC nuclei (H'', I''). **(J)** The average YAP N:C ratio in utricles transduced with wild-type YAP (0.66±0.07, mean±SD) was significantly lower than those transduced with YAP-5SA (0.85±0.12, $p=0.0446$) or YAP-5SA/S94A (0.97±0.09, $p=0.0036$, ANOVA with Tukey's multiple comparisons, * denotes $p<0.05$, ** denotes $p<0.01$, n = 4 utricles). **(K, L)** High magnification images of the SC nuclear layer of P30 mouse utricles transduced with wild type YAP and analyzed 72 h post transduction. Cells positive for the mCherry reporter also were labeled by an antibody specific for YAP that is phosphorylated at serine 127 (K). SCs transduced with YAP-5SA, which has a serine-to-alanine mutation at serine 127, served as a negative control for antibody specificity (L). Graphs depict mean±SD.

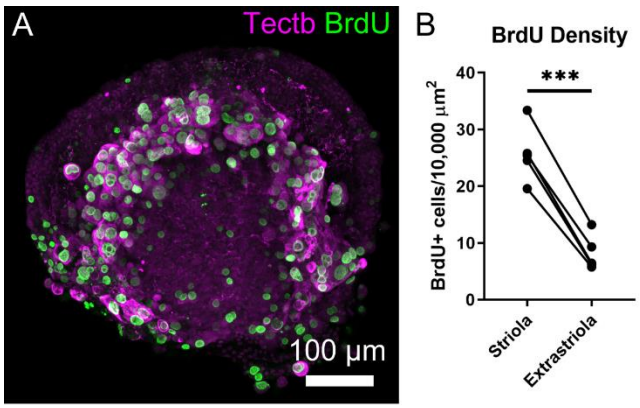

Figure 5-9: Cell cycle re-entry evoked by YAP-5SA occurred selectively in striolar SCs. Utricles from P30 mice were transduced with YAP-5SA after an overnight acclimation period and cultured for an additional five days with BrdU prior to processing for immunohistochemistry. **(A)** The majority of S-phase entry occurred in the Tectb+ striolar region. **(B)** Quantification of BrdU+ cell density shows that proliferating cells were significantly more numerous in the Tectb+ striolar region than in the extrastriola (p=0.0001, paired t-test, n=5 utricles). Graph depicts individual values from each utricle.

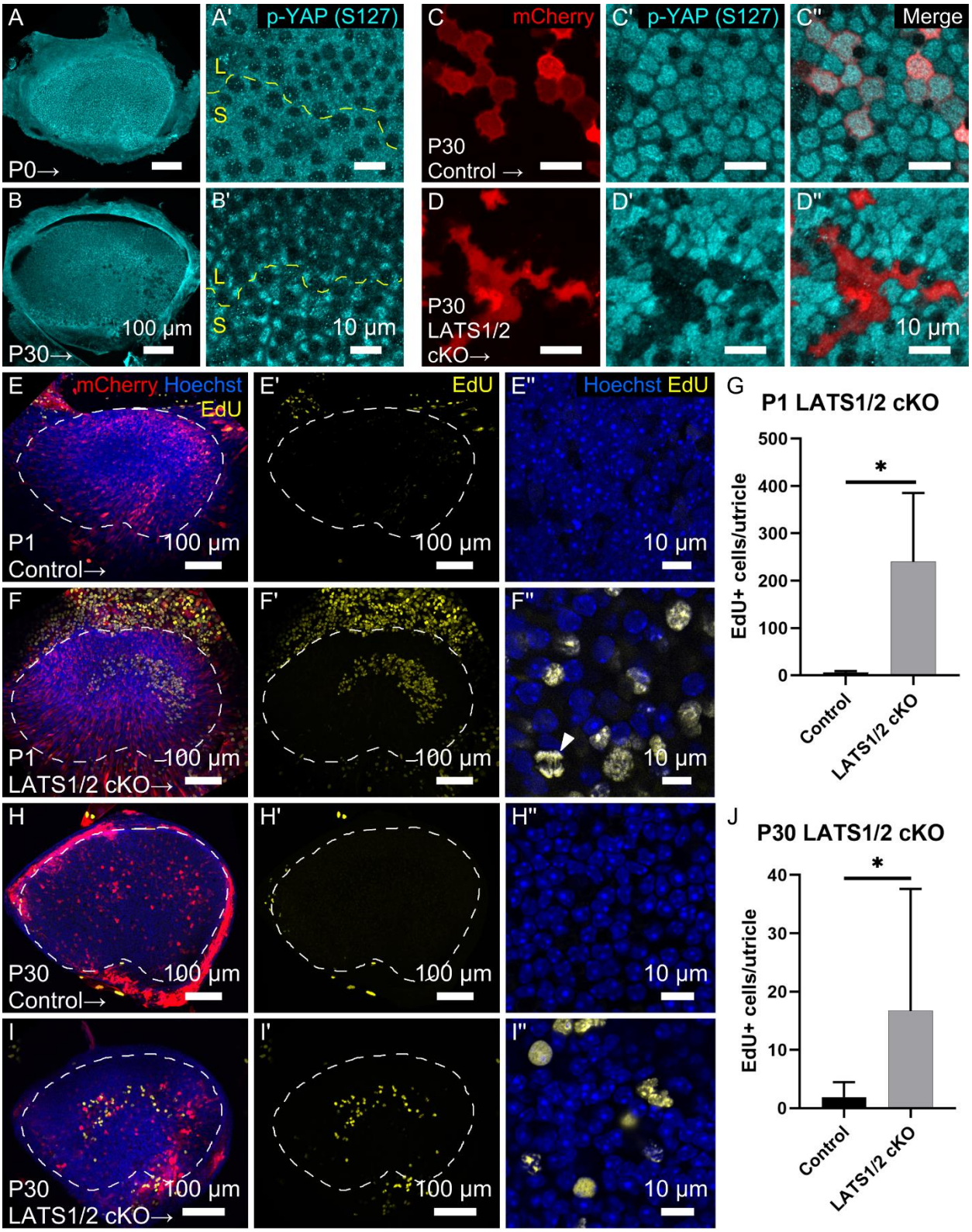

Figure 5-10: Deletion of LATS1 and LATS2 reduced the inhibitory phosphorylation of YAP and induced proliferation of SCs in utricles from neonatal and adult mice. (A, B) Utricles of P0 and P30 mice were immunolabeled for phospho-YAP (S127), a measure of LATS1/2 kinase activity. Phospho-YAP immunoreactivity was detectable in SCs within the striolar and lateral regions both at P0 and at P30. The dashed yellow line denotes the

line of polarity reversal, which separates the lateral extrastriolar and striolar regions. **(C, D)** High magnification image of the apical surface of utricles from P30 *Lats1*$^{flox/flox}$*;Lats2*$^{flox/flox}$ mice transduced with mCherry (Control) or mCherry-T2A-Cre (LATS1/2 cKO) and cultured for 11 d. SCs that expressed the mCherry reporter alone exhibited similar levels of phospho-YAP (S127) immunoreactivity compared to neighboring SCs that were not transduced (C). Levels of phospho-YAP (S127) were lower in SCs that expressed Cre, suggesting that deletion of LATS1 and LATS2 occurred (D). **(E, F)** Utricles were explanted from *Lats1*$^{flox/flox}$*;Lats2*$^{flox/flox}$ mice at P1 and transduced with mCherry (control) or mCherry-T2A-Cre (LATS1/2 cKO) and cultured for seven d. EdU was added for the final two days of culture to trace cells that entered S-phase. Few EdU+ cells were present in control utricles (E, E'), but substantial numbers were found in the central region of LATS1/2 cKO utricles (F, F'). High magnification images of the SC layer (E'', F'') show EdU+ nuclei and a mitotic figure in a LATS1/2 cKO utricle (F''). **(G)** Quantification of EdU+ cells in P1 control and LATS1/2 cKO utricles shows that LATS1/2 cKO significantly increased S-phase entry over controls ($p=0.018$, n=4 utricles). **(H, I)** Utricles were explanted from *Lats1*$^{flox/flox}$*;Lats2*$^{flox/flox}$ mice at P30 and transduced with mCherry (control) or mCherry-T2A-Cre (LATS1/2 cKO) and cultured for 11 d. EdU was added for the final two days of culture. Control utricles contained few EdU+ cells (H, H'), but significantly more EdU+ cells were observed in a striolar distribution of LATS1/2 cKO utricles (I, I'). **(J)** Quantification shows significantly increased EdU+ cell counts in P30 LATS1/2 cKO utricles compared to controls ($p=0.0393$, n=10 utricles). Dashed lines denote the boundary of the macula. Graphs depict mean±SD.

Gene	Species	Direction	Sequence	Amplicon Size (bp)
Ctgf	Mouse	Forward	ACTATGATGCGAGCCAACTG	117
		Reverse	CTCCAGTCTGCAGAAGGTATTG	
Cyr61	Mouse	Forward	CCAGTGTACAGCAGCCTAAA	92
		Reverse	CTGGAGCATCCTGCATAAGTAA	
Ankrd1	Mouse	Forward	CGACGTCTGCGATGAGTATAAA	92
		Reverse	CTCCAGCCTCCATTAACTTCTC	
Gapdh	Mouse	Forward	AGGTCGGTGTGAACGGATTTG	123
		Reverse	TGTAGACCATGTAGTTGAGGTCA	
Cdh1	Mouse	Forward	TGTGGGTCAGGAAATCACATCTT	79
		Reverse	CCAAATCCGATACGTGATCTTCT	
Ccnd1	Mouse	Forward	TCCCCTTGACTGCCGAGAAGT	103
		Reverse	TTCCACTTGAGCTTGTTCA	
Myc	Mouse	Forward	TGACCTAACTCGAGGAGGAGCTGGAATC	170
		Reverse	AAGTTTGAGGCAGTTAAAATTATGGCTGAAGC	
YAP1-S127A	Human transgene	Forward	CCCTCGTTTTGCCATGAACC	122
		Reverse	GTTGCTGCTGGTTGGAGTTG	

Table 5-1. Primers for RT-qPCR

CHAPTER 6
Conclusions and Future Directions

Summary of Thesis

The principal question driving my thesis research was the following: *Why are nonmammals able to efficiently replace HCs as well as recover hearing and balance function, but mammals are not?* At the outset of my research, evidence suggested a role for mechanics. In cultured utricular sheets, SCs of newborn mice readily spread and then proliferate, but these phenomena decline with age (Davies et al., 2007). In contrast, SCs in chicken utricles rapidly change shape and divide, regardless of age (Burns et al., 2008). Subsequent investigations revealed a structural correlate to this phenomenon. As their plasticity declines, mammalian SCs develop E-cadherin-rich junctions that are bracketed by exceptionally thick F-actin bands—unlike the SCs of birds, fish, and amphibians which express little E-cadherin and retain thin bands (Burns et al., 2008, 2013; Collado et al., 2011b). The reinforced junctions between mammalian SCs even appeared to impede cellular deformations after HC loss (Burns and Corwin, 2014).

Building on these initial studies, I specifically asked the following questions: Do the reinforced junctions impede mechanical signals arising from HC loss? Would dismantling the junctions, or bypassing their hypothesized inhibitory control, enable long-quiescent SCs to proliferate? What molecular mechanism controls proliferative responses to shape change and other mechanical signals, and is it restricted in the SCs of mammals? My research yielded the following conclusions:

- The apical surfaces of mouse utricles were significantly more resistant to deformation than those of chickens, due to the thick circumferential bands of F-actin that develop postnatally (Chapter 3). **I conclude that the thick F-actin bands impede the mechanical signals arising from HC loss that govern epithelial repair.**

- Treatment with EGF and a GSK3 inhibitor led to the dismantling of F-actin bands throughout the utricle and depletion of E-cadherin in striolar SCs before inducing the proliferation of striolar SCs (Chapter 4). These results demonstrated for the first time that the reversal of junctional reinforcement is sufficient to induce a resurgence of SC proliferation, even in adult mammals. **I conclude that the E-cadherin-rich junctions between mature, mammalian SCs inactivate intracellular signaling pathways essential for proliferation.**
- The mechanosensitive transcriptional co-activator YAP was required for regenerative proliferation in SCs of the chicken utricle and readily accumulated in nuclei after HC loss, shape change, and pharmacologic disruption of the inhibitory Hippo pathway. In SCs of the mouse utricle, YAP localization was less sensitive to these manipulations, but striolar proliferation could be induced by deleting LATS kinases in SCs or bypassing their inhibitory phosphorylation (Chapter 5). **Thus, I conclude that the persistent quiescence of mammalian SCs is maintained by constitutive LATS-mediated suppression of YAP, whereas damage readily overcomes this inhibitory signaling in SCs of birds.**

This body of work advances a model for understanding how the reinforced junctions that develop in mammalian SCs limit their regenerative responses. The thick F-actin bands impose a "biomechanical brake" that restricts shape changes and the generation of actomyosin tension in SCs after HC loss. The E-cadherin rich junctions impose a "biochemical brake" by inactivating intracellular mitogenic signaling. Each of these processes impinge upon the activation of YAP in mammalian SCs.

FUTURE DIRECTIONS AND KEY OPEN QUESTIONS

Does experimental depletion of E-cadherin promote proliferation in mammalian SCs?

The findings herein constitute the strongest evidence yet that E-cadherin adhesions limit the proliferation of mature mammalian SCs. Future work should follow up on this correlational

evidence and seek to test directly whether experimental depletion of E-cadherin releases mature vestibular SCs from proliferative quiescence. E-cadherin restricts activation of EGFR, YAP, and β-catenin, so its depletion is akin to the multifactorial stimulation of pathways known to stimulate proliferation of SCs.

Previous attempts to investigate the effect of conditional knockout of E-cadherin or αE-catenin from vestibular SCs were inconclusive; genetic recombination failed to efficiently deplete those proteins from SC junctions and eventually resulted in upregulation of N-cadherin and αN-catenin, respectively (M.S. Collado and J.T. Corwin, unpublished results). Use of dominant-negative E-cadherin constructs has the potential to circumvent the pitfalls of a conditional knockout strategy, as it is reported that ectopic expression of dominant negative variants leads to downregulation of endogenous E-cadherin (Troxell et al., 2000). In addition, various dominant-negative variants exist, enabling one to isolate the effects of extracellular adhesion, p120-catenin binding, beta-catenin binding, and connection to the F-actin cytoskeleton. These constructs could be introduced to SCs in utricles from mice P3 or older (after completion of cell cycle exit) via electroporation, adenoviral transduction, or via creation of a transgenic mouse model. I hypothesize that expression of the most potent of these dominant negative constructs, E-cadherin/Δβ-catenin, would induce SC proliferation by inactivating LATS1/2, and by liberating β-catenin from cell junctions so that it could function in a signaling role.

What activates LATS1/2 in mammalian SCs?

LATS1/2 kinases have a multitude of upstream regulators, so their regulation is likely to be cell-type specific and depend on the unique weights of each input in a given cell. Pinpointing which of these upstream inputs is most important in mammalian SCs could allow for the identification of additional druggable targets.

MST1/2 lie immediately upstream of LATS1/2 in the canonical Hippo pathway and would appear to be the most logical upstream regulator. However, experiments presented in Chapter 5 suggest that acute inhibition of those kinases does not affect YAP localization in SCs of the

murine utricle, despite having an effect in the chicken utricle. Similar results were obtained by another group (Kastan et al., 2020). Testing the effects of conditional deletion of MST1/2 in SCs would improve upon this evidence, and the role of MST1/2 in cochlear SCs has not been tested. Taking this evidence at face value, I will discuss MST1/2-independent regulators of LATS1/2.

E-cadherin was shown to regulate the LATS1/2-YAP-TEAD axis in cell lines independent of MST1/2 (Kim et al., 2011). This appears to be the likeliest candidate to activate LATS1/2 in SCs based on available evidence. I report that depletion of E-cadherin from cell junctions was accompanied by a depletion of YAP immunoreactivity (Chapter 4), and ectopic YAP-S127A induces upregulation of E-cadherin (Chapter 5), suggesting that the proteins mutually regulate one another. Also, E-cadherin is minimally expressed in chicken SCs, in which LATS1/2 appear to be regulated by MST1/2 (Chapter 5, Figure 6-1). It seems likely that E-cadherin would exert its effects through α-catenin, which has also been shown to restrict the activity of YAP in the epidermis (Schlegelmilch et al., 2011; Silvis et al., 2011), heart (Li Jifen et al., 2015; Vite et al., 2018), and tooth (Li et al., 2016), and likely neural progenitor cells (Lien et al., 2008), though this connection has not been explicitly shown.

Merlin, or NF2, appears to regulate YAP via a variety of mechanisms. Merlin acts downstream in the E-cadherin-dependent pathway (Kim et al., 2011) and facilitates nuclear export of YAP independent of inhibitory phosphorylation (Furukawa et al., 2017). It would be possible to perform conditional knockout of NF2 and investigate its effect on YAP regulation and SC proliferation, an assay similar to that used in Chapter 5.

MAP4K kinases were shown to phosphorylate LATS1/2 in parallel to MST1/2, including in the context of high cell density (Meng et al., 2015). High cell density is correlated to the inactivation of YAP-TEAD signaling in SCs (Gnedeva et al., 2017), making that kinase family a potential candidate.

LATS1/2 activity is controlled by **GPCR signaling**, including downstream of lysophosphatidic acid (LPA) receptors. Stimulation with LPA inactivates LATS1 in organoids

derived from Lgr5+ cochlear progenitors (Xia et al., 2020), and accelerates wound closure and stimulates proliferation in mechanically lesioned mouse utricles (Meyers and Corwin, 2007). Conversely, stimulation of Gs-coupled receptors has been shown to activate LATS1/2 (Yu et al., 2012).

Finally, **metabolic changes** have been shown to regulate LATS1/2 (Santinon et al., 2016), though little is known about the metabolism of SCs.

PHILOSOPHICAL PERSPECTIVES

The Bioenergetics Hypothesis

My research focused on the mechanisms underlying the different regenerative capacity in vertebrates. But I would also like to speculate about a larger-picture question: Why did mammals lose the capacity to regenerate? Does this ability not confer reproductive advantage? Is there some trade-off gained by the lack of regeneration?

Firstly, it is probably safe to assume based on previous findings that continuous growth and regeneration is the evolutionarily "default" condition (Hariharan et al., 2016). Therefore, we can rephrase the question as, "Why would this capacity have been lost in mammals?" and "Why would it have been retained in nonmammals?"

One of the assumptions of the "evolution question" is that HC losses harm the evolutionary fitness of an individual, thus imposing a selective pressure to maintain regenerative capacity. Is that true? HC losses are caused by aging, loud sound, congenital anomaly, exposure to ototoxic substances, infections, and trauma (with prevalence approximately in that order). Inspecting that list, it is questionable whether there would be evolutionary pressure to maintain the capacity to replace lost HCs. Many of these insults either manifest beyond reproductive years, would not be present before modern times, or would be associated with other conditions that are detrimental to reproductive fitness. It may be that HC losses do not significantly harm evolutionary fitness, and therefore regenerative capacity is not significantly selected for.

A common answer to the “evolution question” is that mammals experienced an evolutionary trade-off in which regenerative capacity was exchanged for the ability to detect a wider frequency range in the auditory system. While it is true that mammals can generally hear significantly higher frequencies than nonmammals (up to 20 kHz in humans and 100 kHz in some other mammalian species, compared to only about 9 kHz in barn owls), there are notable exceptions to this, such as frog species capable of ultrasonic communication (Feng et al., 2006). It is certainly plausible that the highly differentiated SCs within the organ of Corti are essential for its exquisite sensory performance and inherently less able to revert to a plastic state for the purposes of regeneration. However, this explanation fails to account for the low regenerative capacity in the mammalian vestibular system.

The development of specialized supporting cell subtypes and subcellular structures such as thickened F-actin bands suggests that SCs in mammals “evolved” to be more differentiated than SCs in other vertebrates. *I hypothesize that the differentiated state of mammalian vestibular SCs allows them to reduce the energetic cost of the balance organ while maintaining equivalent performance, at the expense of regeneration.*

The findings presented in Chapter 3 demonstrate that the unique F-actin bands of mammalian utricular SCs stabilize the reticular lamina. Because the mechanical stability appears not to rely on actomyosin contractility, SCs may expend less energy maintaining their shape than the vestibular SCs of chickens, which require continuous activity of nonmuscle myosin II (an ATP-hydrolyzing enzyme) to do so. An analogy may be a rubber band under constant tension vs. the vulcanized rubber of a car’s tire.

A preliminary test of the “bioenergetics tradeoff hypothesis” would be to determine whether there is a decrease in metabolic demand as mammalian SCs mature. I hypothesize that the less differentiated SCs of nonmammals would maintain higher energy demand throughout life. Metabolic shifts have been shown to occur in neuroepithelia: During retinal development in *Xenopus*, proliferating progenitor cells rely more on aerobic glycolysis (i.e. the conversion of

glucose to lactic acid in the presence of oxygen), whereas differentiated cells relied more upon oxidative phosphorylation (Agathocleous et al., 2012). Whether such metabolic changes occur during development of the inner ear remains unknown, but the relationship between metabolic signaling and chromatin remodeling is being increasingly recognized (Morrison, 2020).

Reflections on the experimental approach

The advances reported here are a credit to the comparative approach—contrasting mammals with nonmammals. The power of this approach is that it allows us to discount processes which occur in both mammals and nonmammals as potential causes for regenerative failure and focus instead on those which are unique to mammals. In this way, nonmammals serve as an important conceptual and experimental control.

It is also clear that the line of investigation was guided by the constraints of studying the inner ear, as well as the sophistication of our technology. The organs of the inner ear contain small numbers of intermingled cell types, making it difficult to study with traditional biochemistry. Therefore, much of what has been discovered arose from direct microscopic observation. Accordingly, the first differences between mammalian and nonmammalian SCs that garnered attention have been physical and structural characteristics, e.g. cell morphology, cytoskeletal components, and constituents of cell junctions. The findings reported here are a natural extension of those observations in that they relate to mechanical differences, and ultimately differences in intracellular signaling in a mechanosensitive pathway.

Applying emerging techniques (especially single-cell transcriptomics and proteomics) through this lens of interspecies comparison (as well as age-related comparison) will likely remain a fruitful approach to generate entirely new hypotheses as to why regenerative responses in mammalian SCs become restricted.

Besides interspecies comparisons, what other potential “lenses” may be fruitful? Some have found success comparing different inner ear organs within the same species (i.e. utricle vs cochlea) (Jen et al., 2019). It could also be informative to compare HC epithelia to other

neuroepithelia. For example, retinal Müller glia mechanically and metabolically support retinal ganglion cell neurons and serve as a source of replacement photoreceptors in amphibians and fish. YAP was shown to be required for proliferation of Müller glia in Xenopus, and LATS1/2 deletion or expression of LATS-insensitive variant YAP-5SA reprograms the typically quiescent Müller glia in the murine retina, inducing upregulation of EGFR signaling and cell cycle re-entry (Hamon et al., 2019).

Final Words and Practical Implications

In identifying two potentially related mechanisms (EGF stimulation combined with GSK inhibition, and LATS1/2 inhibition) that evoke proliferation of a major subset of mature, mammalian SCs, these findings advance the development of a therapy to promote regenerative replacement of HCs and functional recovery from otherwise permanent deficits in hearing and balance.

However, the challenge ahead should not be minimized. It remains unknown whether the progeny of mature SCs are capable of differentiating into HCs that promote functional recovery. The regenerated HCs must survive, develop apical bundles, and form synaptic connections to nerves. Furthermore, cochlear SCs appear less susceptible to YAP stimulation than those throughout the vestibular system (Figure 6-2), appearing to develop additional layers of regulation limiting their regenerative responses. Yet excitingly, the idea of an intra-otic pharmacologic therapy to promote the limited endogenous regenerative capacity of the mature mammalian vestibular system appears within reach.

To examine the efficacy of such an approach, a logical next step would be to conduct *in vivo* studies in the context of damage, and test whether intra-otic delivery of an EGFR agonist and GSK3β inhibitor would lead to SC proliferation, subsequent differentiation into HCs, and enhance functional recovery. Sayyid *et al.* 2019 provided a template of such work, using the toxin IDPN to ablate vestibular HCs in adult mice and using vestibular evoked potentials to monitor

function. Likewise, the novel pharmacologic inhibitor of LATS1/2 kinase activity developed by Kastan *et al.* could be tested in this manner.

As over 1/3 of adults suffer from vestibular dysfunction (Agrawal et al., 2009), the public health impact of such a therapy could be substantial.

Figures and Figure Legends

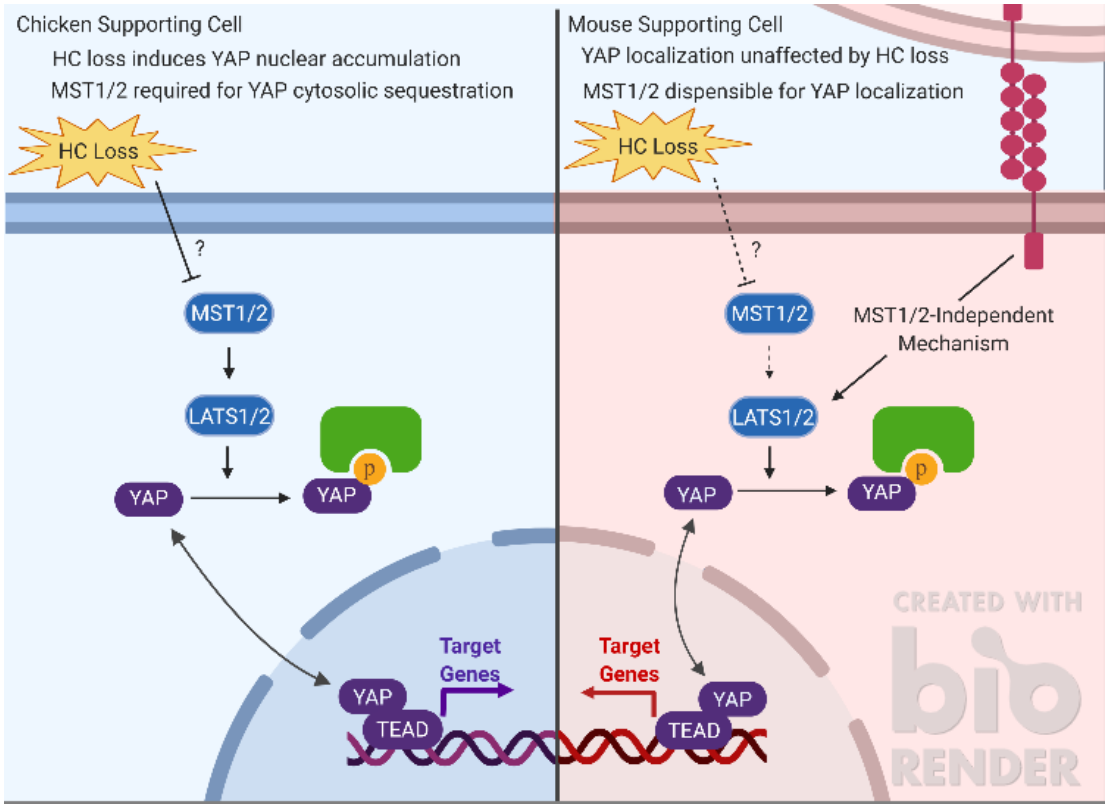

Figure 6-1 In SCs of the chicken utricle, YAP is regulated by the MST1/2-dependent pathway among other mechanisms. In SCs of the mouse utricle, LATS1/2 kinases appear to be activated by an MST1/2-independent mechanism. E-cadherin adhesions represents one such plausible mechanism.

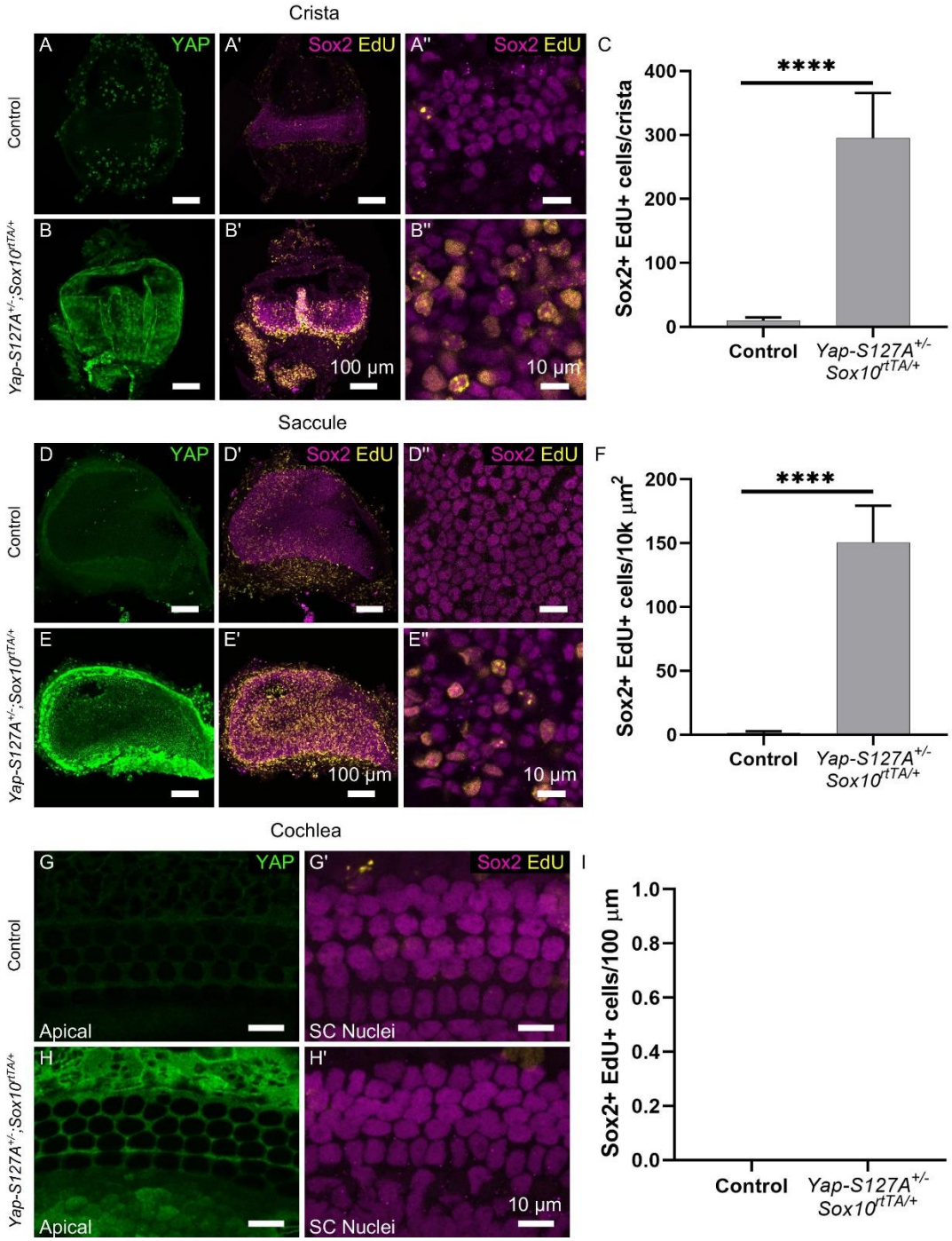

Figure 6-2 Overexpression of YAP-S127A in Sox10+ cells of the P1 mouse evoked robust proliferation in vestibular organs, but not in the cochlea. 100 mg/kg doxycycline was administered IP to P1 *Yap-S127A*$^{+/-}$*;Sox10*$^{rtTA/+}$ pups and littermate controls that had either wild type, *Yap-S127A*$^{+/-}$, or *Sox10*$^{rtTA/+}$ genotype. EdU was administered subcutaneously on P2, P3, and P4, and utricles were harvested on P5. **(A-C)** YAP-S127A overexpression resulted in an over 30-fold increase in the number of Sox2+ EdU+ cells in the cristae. **(D-F)** YAP-S127A overexpression resulted in a 108-fold increase in the number of Sox2+ EdU+ cells in the saccule. (G-I) No Sox2+ EdU+ cells were identified in the organ of Corti in mice of either genotype, though YAP immunoreactivity was enriched in *Yap-S127A*$^{+/-}$*;Sox10*$^{rtTA/+}$ mice (H). ****$p < 0.0001$, unpaired t-test, n = 3-5 mice per condition.

REFERENCES

Adler HJ, Raphael Y. 1996. New hair cells arise from supporting cell conversion in the acoustically damaged chick inner ear. *Neurosci Lett* **205**:17–20. doi:10.1016/0304-3940(96)12367-3

Agarwala S, Duquesne S, Liu K, Boehm A, Grimm L, Link S, König S, Eimer S, Ronneberger O, Lecaudey V. 2015. Amotl2a interacts with the Hippo effector Yap1 and the Wnt/β-catenin effector Lef1 to control tissue size in zebrafish. *eLife* **4**:e08201. doi:10.7554/eLife.08201

Agathocleous M, Love NK, Randlett O, Harris JJ, Liu J, Murray AJ, Harris WA. 2012. Metabolic differentiation in the embryonic retina. *Nat Cell Biol* **14**:859–864. doi:10.1038/ncb2531

Agrawal Y, Carey JP, Della Santina CC, Schubert MC, Minor LB. 2009. Disorders of Balance and Vestibular Function in US Adults: Data From the National Health and Nutrition Examination Survey, 2001-2004. *Arch Intern Med* **169**:938. doi:10.1001/archinternmed.2009.66

Andreeva A, Lee J, Lohia M, Wu X, Macara IG, Lu X. 2014. PTK7-Src signaling at epithelial cell contacts mediates spatial organization of actomyosin and planar cell polarity. *Dev Cell* **29**:20–33. doi:10.1016/j.devcel.2014.02.008

Anselmi F, Hernandez VH, Crispino G, Seydel A, Ortolano S, Roper SD, Kessaris N, Richardson W, Rickheit G, Filippov MA, Monyer H, Mammano F. 2008. ATP release through connexin hemichannels and gap junction transfer of second messengers propagate Ca2+ signals across the inner ear. *Proc Natl Acad Sci* **105**:18770–18775. doi:10.1073/pnas.0800793105

Anttonen T, Belevich I, Kirjavainen A, Laos M, Brakebusch C, Jokitalo E, Pirvola U. 2014. How to Bury the Dead: Elimination of Apoptotic Hair Cells from the Hearing Organ of the Mouse. *JARO J Assoc Res Otolaryngol* **15**:975–992. doi:10.1007/s10162-014-0480-x

Anttonen T, Belevich I, Laos M, Herranen A, Jokitalo E, Brakebusch C, Pirvola U. 2017. Cytoskeletal Stability in the Auditory Organ In Vivo: RhoA Is Dispensable for Wound Healing but Essential for Hair Cell Development. *eNeuro* **4**. doi:10.1523/ENEURO.0149-17.2017

Anttonen T, Kirjavainen A, Belevich I, Laos M, Richardson WD, Jokitalo E, Brakebusch C, Pirvola U. 2012. Cdc42-dependent structural development of auditory supporting cells is required for wound healing at adulthood. *Sci Rep* **2**. doi:10.1038/srep00978

Aragona M, Panciera T, Manfrin A, Giulitti S, Michielin F, Elvassore N, Dupont S, Piccolo S. 2013. A mechanical checkpoint controls multicellular growth through YAP/TAZ regulation by actin-processing factors. *Cell* **154**:1047–1059. doi:10.1016/j.cell.2013.07.042

Arnold TR, Stephenson RE, Miller AL. 2017. Rho GTPases and Actomyosin: partners in regulating epithelial cell-cell junction structure and function. *Exp Cell Res* **358**:20–30. doi:10.1016/j.yexcr.2017.03.053

Atkinson PJ, Dong Y, Gu S, Liu W, Najarro EH, Udagawa T, Cheng AG. 2018. Sox2 haploinsufficiency primes regeneration and Wnt responsiveness in the mouse cochlea. *J Clin Invest* **128**:1641–1656. doi:10.1172/JCI97248

Baird RA, Steyger PS, Schuff NR. 1996. Mitotic and Nonmitotic Hair Cell Regeneration in the Bullfrog Vestibular Otolith Organsa. *Ann N Y Acad Sci* **781**:59–70. doi:10.1111/j.1749-6632.1996.tb15693.x

Balak KJ, Corwin JT, Jones JE. 1990. Regenerated hair cells can originate from supporting cell progeny: evidence from phototoxicity and laser ablation experiments in the lateral line system. *J Neurosci Off J Soc Neurosci* **10**:2502–2512. doi:10.1523/JNEUROSCI.10-08-02502.1990

Bartsch TF, Hengel FE, Oswald A, Dionne G, Chipendo IV, Mangat SS, Shatanofy ME, Shapiro L, Müller U, Hudspeth AJ. 2019. Elasticity of individual protocadherin 15 molecules implicates tip links as the gating springs for hearing. *Proc Natl Acad Sci* **116**:11048–11056. doi:10.1073/pnas.1902163116

Basu S, Totty NF, Irwin MS, Sudol M, Downward J. 2003. Akt phosphorylates the Yes-associated protein, YAP, to induce interaction with 14-3-3 and attenuation of p73-mediated apoptosis. *Mol Cell* **11**:11–23. doi:10.1016/S1097-2765(02)00776-1

Behrndt M, Salbreux G, Campinho P, Hauschild R, Oswald F, Roensch J, Grill SW, Heisenberg C-P. 2012. Forces Driving Epithelial Spreading in Zebrafish Gastrulation. *Science* **338**:257–260. doi:10.1126/science.1224143

Benham-Pyle BW, Pruitt BL, Nelson WJ. 2015. Mechanical strain induces E-cadherin-dependent Yap1 and β-catenin activation to drive cell cycle entry. *Science* **348**:1024–1027. doi:10.1126/science.aaa4559

Bird JE, Daudet N, Warchol ME, Gale JE. 2010. Supporting cells eliminate dying sensory hair cells to maintain epithelial integrity in the avian inner ear. *J Neurosci Off J Soc Neurosci* **30**:12545–12556. doi:10.1523/JNEUROSCI.3042-10.2010

Borse V, Barton M, Arndt H, Kaur T, Warchol ME. 2020. Dynamic patterns of YAP1 expression and cellular localization in the developing and injured utricle. *bioRxiv* 2020.05.06.081323. doi:10.1101/2020.05.06.081323

Brand Y, Sung M, Chavez E, Wei E, Pak KK, Housley GD, Bodmer D, Ryan AF. 2013. Neural cell adhesion molecule L1 modulates type I but not type II inner ear spiral ganglion neurite outgrowth in an in vitro alternate choice assay. *J Mol Neurosci MN* **51**:663–670. doi:10.1007/s12031-013-0040-6

Bredberg G. 1968. Cellular pattern and nerve supply of the human organ of Corti. *Acta Otolaryngol (Stockh)* Suppl 236:1+.

Bucks SA, Cox BC, Vlosich BA, Manning JP, Nguyen TB, Stone JS. 2017. Supporting cells remove and replace sensory receptor hair cells in a balance organ of adult mice. *eLife* **6**. doi:10.7554/eLife.18128

Burns J, Christophel JJ, Collado MS, Magnus C, Carfrae M, Corwin JT. 2008. Reinforcement of cell junctions correlates with the absence of hair cell regeneration in mammals and its occurrence in birds. *J Comp Neurol* **511**:396–414. doi:10.1002/cne.21849

Burns JC, Collado MS, Oliver ER, Corwin JT. 2013. Specializations of intercellular junctions are associated with the presence and absence of hair cell regeneration in ears from six vertebrate classes. *J Comp Neurol* **521**:1430–1448. doi:10.1002/cne.23250

Burns JC, Corwin JT. 2014. Responses to Cell Loss Become Restricted as the Supporting Cells in Mammalian Vestibular Organs Grow Thick Junctional Actin Bands That Develop High Stability. *J Neurosci* **34**:1998–2011. doi:10.1523/JNEUROSCI.4355-13.2014

Burns JC, Corwin JT. 2013. A historical to present-day account of efforts to answer the question, “What puts the brakes on mammalian hair cell regeneration?” *Hear Res* **297**:52–67. doi:10.1016/j.heares.2013.01.005

Burns JC, Cox BC, Thiede BR, Zuo J, Corwin JT. 2012a. In vivo proliferative regeneration of balance hair cells in newborn mice. *J Neurosci* **32**:6570–6577. doi:10.1523/JNEUROSCI.6274-11.2012

Burns JC, Kelly MC, Hoa M, Morell RJ, Kelley MW. 2015. Single-cell RNA-Seq resolves cellular complexity in sensory organs from the neonatal inner ear. *Nat Commun* **6**:8557. doi:10.1038/ncomms9557

Burns JC, On D, Baker W, Collado MS, Corwin JT. 2012b. Over Half the Hair Cells in the Mouse Utricle First Appear After Birth, with Significant Numbers Originating from Early Postnatal Mitotic Production in Peripheral and Striolar Growth Zones. *JARO J Assoc Res Otolaryngol* **13**:609–627. doi:10.1007/s10162-012-0337-0

Burns JC, Yoo JJ, Atala A, Jackson JD. 2012c. MYC Gene Delivery to Adult Mouse Utricles Stimulates Proliferation of Postmitotic Supporting Cells In Vitro. *PLOS ONE* **7**:e48704. doi:10.1371/journal.pone.0048704

Camargo FD, Gokhale S, Johnnidis JB, Fu D, Bell GW, Jaenisch R, Brummelkamp TR. 2007. YAP1 Increases Organ Size and Expands Undifferentiated Progenitor Cells. *Curr Biol* **17**:2054–2060. doi:10.1016/j.cub.2007.10.039

Campinho P, Behrndt M, Ranft J, Risler T, Minc N, Heisenberg C-P. 2013. Tension-oriented cell divisions limit anisotropic tissue tension in epithelial spreading during zebrafish epiboly. *Nat Cell Biol* **15**:1405–1414. doi:10.1038/ncb2869

Carey J, Fuchs A, Rubel E. 1996. Hair Cell Regeneration and Recovery of the Vestibuloocular Reflex in the Avian Vestibular System. *J Neurophysiol* **76**:3301–3312. doi:10.1152/jn.1996.76.5.3301

Cartagena-Rivera AX, Le Gal S, Richards K, Verpy E, Chadwick RS. 2019. Cochlear outer hair cell horizontal top connectors mediate mature stereocilia bundle mechanics. *Sci Adv* **5**:eaat9934. doi:10.1126/sciadv.aat9934

Chacon-Heszele MF, Ren D, Reynolds AB, Chi F, Chen P. 2012. Regulation of cochlear convergent extension by the vertebrate planar cell polarity pathway is dependent on p120-catenin. *Dev Camb Engl* **139**:968–978. doi:10.1242/dev.065326

Chai R, Xia A, Wang T, Jan TA, Hayashi T, Bermingham-McDonogh O, Cheng AG-L. 2011. Dynamic Expression of Lgr5, a Wnt Target Gene, in the Developing and Mature Mouse Cochlea. *JARO J Assoc Res Otolaryngol* **12**:455–469. doi:10.1007/s10162-011-0267-2

Chang L, Azzolin L, Biagio DD, Zanconato F, Battilana G, Xiccato RL, Aragona M, Giulitti S, Panciera T, Gandin A, Sigismondo G, Krijgsveld J, Fassan M, Brusatin G, Cordenonsi M, Piccolo S. 2018. The SWI/SNF complex is a mechanoregulated inhibitor of YAP and TAZ. *Nature* **563**:265. doi:10.1038/s41586-018-0658-1

Chen S, Xie L, Xu K, Cao H-Y, Wu X, Xu X-X, Sun Y, Kong W-J. 2018. Developmental abnormalities in supporting cell phalangeal processes and cytoskeleton in the Gjb2 knockdown mouse model. *Dis Model Mech* **11**. doi:10.1242/dmm.033019

Codelia VA, Sun G, Irvine KD. 2014. Regulation of YAP by Mechanical Strain through Jnk and Hippo Signaling. *Curr Biol CB* **24**:2012–2017. doi:10.1016/j.cub.2014.07.034

Cohen R, Amir-Zilberstein L, Hersch M, Woland S, Taiber S, Matsuzaki F, Bergmann S, Avraham KB, Sprinzak D. 2019. Shear forces drive precise patterning of hair cells in the mammalian inner ear. *bioRxiv* 707422. doi:10.1101/707422

Colin-York H, Eggeling C, Fritzsche M. 2017. Dissection of mechanical force in living cells by super-resolved traction force microscopy. *Nat Protoc* **12**:783–796. doi:10.1038/nprot.2017.009

Collado MS, Burns JC, Meyers JR, Corwin JT. 2011a. Variations in Shape-Sensitive Restriction Points Mirror Differences in the Regeneration Capacities of Avian and Mammalian Ears. *PLoS ONE* **6**. doi:10.1371/journal.pone.0023861

Collado MS, Thiede BR, Baker W, Askew C, Igbani LM, Corwin JT. 2011b. The postnatal accumulation of junctional E-cadherin is inversely correlated with the capacity for supporting cells to convert directly into sensory hair cells in mammalian balance organs. *J Neurosci Off J Soc Neurosci* **31**:11855–11866. doi:10.1523/JNEUROSCI.2525-11.2011

Corwin JT. 1985. Perpetual production of hair cells and maturational changes in hair cell ultrastructure accompany postembryonic growth in an amphibian ear. *Proc Natl Acad Sci U S A* **82**:3911–3915.

Corwin JT. 1983. Postembryonic growth of the macula neglecta auditory detector in the ray, Raja clavata: continual increases in hair cell number, neural convergence, and physiological sensitivity. *J Comp Neurol* **217**:345–356. doi:10.1002/cne.902170309

Corwin JT. 1981. Postembryonic production and aging in inner ear hair cells in sharks. *J Comp Neurol* **201**:541–553. doi:10.1002/cne.902010406

Corwin JT, Cotanche DA. 1988. Regeneration of sensory hair cells after acoustic trauma. *Science* **240**:1772–1774.

Corwin JT, Jones JE, Katayama A, Kelley MW, Warchol ME. 1991. Hair cell regeneration: the identities of progenitor cells, potential triggers and instructive cues. *Ciba Found Symp* **160**:103-120-130.

Cost A-L, Khalaji S, Grashoff C. 2019. Genetically Encoded FRET-Based Tension Sensors. *Curr Protoc Cell Biol* **83**:e85. doi:10.1002/cpcb.85

Cotanche DA. 1987. Regeneration of hair cell stereociliary bundles in the chick cochlea following severe acoustic trauma. *Hear Res* **30**:181–195.

Cotanche DA, Corwin JT. 1991. Stereociliary bundles reorient during hair cell development and regeneration in the chick cochlea. *Hear Res* **52**:379–402.

Cox BC, Chai R, Lenoir A, Liu Z, Zhang L, Nguyen D-H, Chalasani K, Steigelman KA, Fang J, Cheng AG, Zuo J. 2014. Spontaneous hair cell regeneration in the neonatal mouse cochlea in vivo. *Development* **141**:816–829. doi:10.1242/dev.103036

Dai X, Liu H, Shen S, Guo X, Yan H, Ji X, Li L, Huang J, Feng X-H, Zhao B. 2015. YAP activates the Hippo pathway in a negative feedback loop. *Cell Res* **25**:1175–1178. doi:10.1038/cr.2015.101

Davies D, Magnus C, Corwin JT. 2007. Developmental changes in cell–extracellular matrix interactions limit proliferation in the mammalian inner ear. *Eur J Neurosci* **25**:985–998. doi:10.1111/j.1460-9568.2007.05355.x

Davis AC. 1989. The Prevalence of Hearing Impairment and Reported Hearing Disability among Adults in Great Britain. *Int J Epidemiol* **18**:911–917. doi:10.1093/ije/18.4.911

Díaz-Coránguez M, Liu X, Antonetti DA. 2019. Tight Junctions in Cell Proliferation. *Int J Mol Sci* **20**. doi:10.3390/ijms20235972

Doerflinger NH, Macklin WB, Popko B. 2003. Inducible site-specific recombination in myelinating cells. *Genes N Y N 2000* **35**:63–72. doi:10.1002/gene.10154

Dong J, Feldmann G, Huang J, Wu S, Zhang N, Comerford SA, Gayyed MF, Anders RA, Maitra A, Pan D. 2007. Elucidation of a Universal Size-Control Mechanism in Drosophila and Mammals. *Cell* **130**:1120. doi:10.1016/j.cell.2007.07.019

Dupont S. 2016. Role of YAP/TAZ in cell-matrix adhesion-mediated signalling and mechanotransduction. *Exp Cell Res* **343**:42–53. doi:10.1016/j.yexcr.2015.10.034

Dupont S, Morsut L, Aragona M, Enzo E, Giulitti S, Cordenonsi M, Zanconato F, Le Digabel J, Forcato M, Bicciato S, Elvassore N, Piccolo S. 2011. Role of YAP/TAZ in mechanotransduction. *Nature* **474**:179–183. doi:10.1038/nature10137

Ebrahim S, Fujita T, Millis BA, Kozin E, Ma X, Kawamoto S, Baird MA, Davidson M, Yonemura S, Hisa Y, Conti MA, Adelstein RS, Sakaguchi H, Kachar B. 2013. NMII forms a contractile transcellular sarcomeric network to regulate apical cell junctions and tissue geometry. *Curr Biol CB* **23**:731–736. doi:10.1016/j.cub.2013.03.039

Elbediwy A, Vincent-Mistiaen ZI, Spencer-Dene B, Stone RK, Boeing S, Wculek SK, Cordero J, Tan EH, Ridgway R, Brunton VG, Sahai E, Gerhardt H, Behrens A, Malanchi I, Sansom OJ, Thompson BJ. 2016. Integrin signalling regulates YAP and TAZ to control skin homeostasis. *Dev Camb Engl* **143**:1674–1687. doi:10.1242/dev.133728

Elosegui-Artola A, Andreu I, Beedle AEM, Lezamiz A, Uroz M, Kosmalska AJ, Oria R, Kechagia JZ, Rico-Lastres P, Le Roux A-L, Shanahan CM, Trepat X, Navajas D, Garcia-Manyes S, Roca-Cusachs P. 2017. Force Triggers YAP Nuclear Entry by Regulating Transport across Nuclear Pores. *Cell* **171**:1397–1410.e14. doi:10.1016/j.cell.2017.10.008

Ennomani H, Letort G, Guérin C, Martiel J-L, Cao W, Nédélec F, De La Cruz EM, Théry M, Blanchoin L. 2016. Architecture and Connectivity Govern Actin Network Contractility. *Curr Biol* **26**:616–626. doi:10.1016/j.cub.2015.12.069

Fan F, He Z, Kong L-L, Chen Q, Yuan Q, Zhang S, Ye J, Liu H, Sun X, Geng J, Yuan L, Hong L, Xiao C, Zhang W, Sun X, Li Y, Wang P, Huang L, Wu X, Ji Z, Wu Q, Xia N-S, Gray NS, Chen L, Yun C-H, Deng X, Zhou D. 2016. Pharmacological targeting of kinases MST1 and

MST2 augments tissue repair and regeneration. *Sci Transl Med* **8**:352ra108-352ra108. doi:10.1126/scitranslmed.aaf2304
Feng AS, Narins PM, Xu C-H, Lin W-Y, Yu Z-L, Qiu Q, Xu Z-M, Shen J-X. 2006. Ultrasonic communication in frogs. *Nature* **440**:333–336. doi:10.1038/nature04416
Fischer M, Kaech S, Knutti D, Matus A. 1998. Rapid actin-based plasticity in dendritic spines. *Neuron* **20**:847–854. doi:10.1016/s0896-6273(00)80467-5
Fletcher GC, Diaz-de-la-Loza M-C, Borreguero-Muñoz N, Holder M, Aguilar-Aragon M, Thompson BJ. 2018. Mechanical strain regulates the Hippo pathway in Drosophila. *Development* **145**. doi:10.1242/dev.159467
Forge A. 1985. Outer hair cell loss and supporting cell expansion following chronic gentamicin treatment. *Hear Res* **19**:171–182.
Forge A, Jagger DJ, Kelly JJ, Taylor RR. 2013. Connexin30-mediated intercellular communication plays an essential role in epithelial repair in the cochlea. *J Cell Sci* **126**:1703–1712. doi:10.1242/jcs.125476
Forge A, Li L, Corwin JT, Nevill G. 1993. Ultrastructural evidence for hair cell regeneration in the mammalian inner ear. *Science* **259**:1616–1619.
Francis SP, Cunningham LL. 2017. Non-autonomous Cellular Responses to Ototoxic Drug-Induced Stress and Death. *Front Cell Neurosci* **11**. doi:10.3389/fncel.2017.00252
Francou A, De Bono C, Kelly RG. 2017. Epithelial tension in the second heart field promotes mouse heart tube elongation. *Nat Commun* **8**. doi:10.1038/ncomms14770
Furth N, Aylon Y. 2017. The LATS1 and LATS2 tumor suppressors: beyond the Hippo pathway. *Cell Death Differ* **24**:1488–1501. doi:10.1038/cdd.2017.99
Furukawa KT, Yamashita K, Sakurai N, Ohno S. 2017. The Epithelial Circumferential Actin Belt Regulates YAP/TAZ through Nucleocytoplasmic Shuttling of Merlin. *Cell Rep* **20**:1435–1447. doi:10.1016/j.celrep.2017.07.032
Gale JE, Piazza V, Ciubotaru CD, Mammano F. 2004. A mechanism for sensing noise damage in the inner ear. *Curr Biol CB* **14**:526–529. doi:10.1016/j.cub.2004.03.002
Geng R, Noda T, Mulvaney JF, Lin VYW, Edge ASB, Dabdoub A. 2016. Comprehensive Expression of Wnt Signaling Pathway Genes during Development and Maturation of the Mouse Cochlea. *PloS One* **11**:e0148339. doi:10.1371/journal.pone.0148339
Getsios S, Simpson CL, Kojima S, Harmon R, Sheu LJ, Dusek RL, Cornwell M, Green KJ. 2009. Desmoglein 1-dependent suppression of EGFR signaling promotes epidermal differentiation and morphogenesis. *J Cell Biol* **185**:1243–1258. doi:10.1083/jcb.200809044
Gnedeva K, Hudspeth AJ. 2015. SoxC transcription factors are essential for the development of the inner ear. *Proc Natl Acad Sci U S A* **112**:14066–14071. doi:10.1073/pnas.1517371112
Gnedeva K, Hudspeth AJ, Segil N. 2018. Three-dimensional Organotypic Cultures of Vestibular and Auditory Sensory Organs. *JoVE J Vis Exp* e57527. doi:10.3791/57527
Gnedeva K, Jacobo A, Salvi JD, Petelski AA, Hudspeth AJ. 2017. Elastic force restricts growth of the murine utricle. *eLife* **6**:e25681. doi:10.7554/eLife.25681
Golub JS, Tong L, Ngyuen TB, Hume CR, Palmiter RD, Rubel EW, Stone JS. 2012. Hair Cell Replacement in Adult Mouse Utricles after Targeted Ablation of Hair Cells with Diphtheria Toxin. *J Neurosci Off J Soc Neurosci* **32**:15093–15105. doi:10.1523/JNEUROSCI.1709-12.2012
Goodyear RJ, Gates R, Lukashkin AN, Richardson GP. 1999. Hair-cell numbers continue to increase in the utricular macula of the early posthatch chick. *J Neurocytol* **28**:851–861.
Grimsley-Myers CM, Sipe CW, Wu DK, Lu X. 2012. Redundant functions of Rac GTPases in inner ear morphogenesis. *Dev Biol* **362**:172–186. doi:10.1016/j.ydbio.2011.12.008
Gu R, Montcouquiol M, Marchionni M, Corwin JT. 2007. Proliferative responses to growth factors decline rapidly during postnatal maturation of mammalian hair cell epithelia. *Eur J Neurosci* **25**:1363–1372. doi:10.1111/j.1460-9568.2007.05414.x

Gudipaty SA, Lindblom J, Loftus PD, Redd MJ, Edes K, Davey CF, Krishnegowda V, Rosenblatt J. 2017. Mechanical stretch triggers rapid epithelial cell division through Piezo1. *Nature* **543**:118–121. doi:10.1038/nature21407

Guillot C, Lecuit T. 2013. Mechanics of Epithelial Tissue Homeostasis and Morphogenesis. *Science* **340**:1185–1189. doi:10.1126/science.1235249

Gulley RL, Reese TS. 1976. Intercellular junctions in the reticular lamina of the organ of Corti. *J Neurocytol* **5**:479–507. doi:10.1007/bf01181652

Hackett L, Davies D, Helyer R, Kennedy H, Kros C, Lawlor P, Rivolta MN, Holley M. 2002. E-cadherin and the Differentiation of Mammalian Vestibular Hair Cells. *Exp Cell Res* **278**:19–30. doi:10.1006/excr.2002.5574

Hamburger V, Hamilton HL. 1951. A series of normal stages in the development of the chick embryo. *J Morphol* **88**:49–92.

Hamon A, García-García D, Ail D, Bitard J, Chesneau A, Dalkara D, Locker M, Roger JE, Perron M. 2019. Linking YAP to Müller Glia Quiescence Exit in the Degenerative Retina. *Cell Rep* **27**:1712–1725.e6. doi:10.1016/j.celrep.2019.04.045

Hariharan IK, Wake DB, Wake MH. 2016. Indeterminate Growth: Could It Represent the Ancestral Condition? *Cold Spring Harb Perspect Biol* **8**. doi:10.1101/cshperspect.a019174

Harris AR, Daeden A, Charras GT. 2014. Formation of adherens junctions leads to the emergence of a tissue-level tension in epithelial monolayers. *J Cell Sci* **127**:2507–2517. doi:10.1242/jcs.142349

Harris JA, Cheng AG, Cunningham LL, MacDonald G, Raible DW, Rubel EW. 2003. Neomycin-induced hair cell death and rapid regeneration in the lateral line of zebrafish (Danio rerio). *J Assoc Res Otolaryngol JARO* **4**:219–234. doi:10.1007/s10162-002-3022-x

Heallen T, Morikawa Y, Leach J, Tao G, Willerson JT, Johnson RL, Martin JF. 2013. Hippo signaling impedes adult heart regeneration. *Dev Camb Engl* **140**:4683–4690. doi:10.1242/dev.102798

Hertwig O. 1884. Das Problem der Befruchtung und der Isotropie des Eies, eine Theorie der Vererbung. *Jenaische Z Naturwissenschaft* **18**:276–318.

Hochmuth RM. 2000. Micropipette aspiration of living cells. *J Biomech* **33**:15–22. doi:10.1016/S0021-9290(99)00175-X

Hume CR, Kirkegaard M, Oesterle EC. 2003. ErbB Expression: The Mouse Inner Ear and Maturation of the Mitogenic Response to Heregulin. *J Assoc Res Otolaryngol* **4**:422–443. doi:10.1007/s10162-002-3008-8

Hunter MV, Lee DM, Harris TJC, Fernandez-Gonzalez R. 2015. Polarized E-cadherin endocytosis directs actomyosin remodeling during embryonic wound repair. *J Cell Biol* **210**:801–816. doi:10.1083/jcb.201501076

Irvine KD, Shraiman BI. 2017. Mechanical control of growth: ideas, facts and challenges. *Development* **144**:4238–4248. doi:10.1242/dev.151902

Ishiyama A, Mowry SE, Lopez IA, Ishiyama G. 2009. Immunohistochemical distribution of basement membrane proteins in the human inner ear from older subjects. *Hear Res* **254**:1–14. doi:10.1016/j.heares.2009.03.014

Jacques BE, Puligilla C, Weichert RM, Ferrer-Vaquer A, Hadjantonakis A-K, Kelley MW, Dabdoub A. 2012. A dual function for canonical Wnt/β-catenin signaling in the developing mammalian cochlea. *Development* **139**:4395–4404. doi:10.1242/dev.080358

Jagger DJ, Forge A. 2015. Connexins and gap junctions in the inner ear – it's not just about K+ recycling. *Cell Tissue Res* **360**:633–644. doi:10.1007/s00441-014-2029-z

Jagger DJ, Nickel R, Forge A. 2014. Gap Junctional Coupling is Essential for Epithelial Repair in the Avian Cochlea. *J Neurosci* **34**:15851–15860. doi:10.1523/JNEUROSCI.1932-14.2014

Janesick A, Wu SC, Blumberg B. 2015. Retinoic acid signaling and neuronal differentiation. *Cell Mol Life Sci* **72**:1559–1576. doi:10.1007/s00018-014-1815-9

Jansson L, Ebeid M, Shen JW, Mokhtari TE, Quiruz LA, Ornitz DM, Huh S-H, Cheng AG. 2019. β-Catenin is required for radial cell patterning and identity in the developing mouse cochlea. *Proc Natl Acad Sci* **116**:21054–21060. doi:10.1073/pnas.1910223116

Jen H-I, Hill MC, Tao L, Sheng K, Cao W, Zhang H, Yu HV, Llamas J, Zong C, Martin JF, Segil N, Groves AK. 2019. Transcriptomic and epigenetic regulation of hair cell regeneration in the mouse utricle and its potentiation by Atoh1. *eLife* **8**:e44328. doi:10.7554/eLife.44328

Johnson JL, Najor NA, Green KJ. 2014. Desmosomes: Regulators of Cellular Signaling and Adhesion in Epidermal Health and Disease. *Cold Spring Harb Perspect Med* **4**. doi:10.1101/cshperspect.a015297

Jones JE, Corwin JT. 1996. Regeneration of sensory cells after laser ablation in the lateral line system: hair cell lineage and macrophage behavior revealed by time- lapse video microscopy. *J Neurosci* **16**:649–662. doi:10.1523/JNEUROSCI.16-02-00649.1996

Karaman R, Halder G. 2018. Cell Junctions in Hippo Signaling. *Cold Spring Harb Perspect Biol* **10**. doi:10.1101/cshperspect.a028753

Karsch S, Kong D, Großhans J, Janshoff A. 2017. Single-Cell Defects Cause a Long-Range Mechanical Response in a Confluent Epithelial Cell Layer. *Biophys J* **113**:2601–2608. doi:10.1016/j.bpj.2017.10.025

Kastan N, Gnedeva K, Alisch T, Petelski AA, Huggins DJ, Chiaravalli J, Aharanov A, Shakked A, Tzahor E, Nagiel A, Segil N, Hudspeth AJ. 2020. Small-molecule inhibition of Lats kinases promotes Yap-dependent proliferation in postmitotic mammalian tissues. *bioRxiv* 2020.02.11.944157. doi:10.1101/2020.02.11.944157

Kasza KE, Zallen JA. 2011. Dynamics and regulation of contractile actin-myosin networks in morphogenesis. *Curr Opin Cell Biol* **23**:30–38. doi:10.1016/j.ceb.2010.10.014

Kaufman MH. 1992. The Atlas of Mouse Development.

Kaur T, Hirose K, Rubel EW, Warchol ME. 2015. Macrophage recruitment and epithelial repair following hair cell injury in the mouse utricle. *Front Cell Neurosci* **9**. doi:10.3389/fncel.2015.00150

Kil J, Warchol ME, Corwin JT. 1997. Cell death, cell proliferation, and estimates of hair cell life spans in the vestibular organs of chicks. *Hear Res* **114**:117–126.

Kim N-G, Gumbiner BM. 2015. Adhesion to fibronectin regulates Hippo signaling via the FAK–Src–PI3K pathway. *J Cell Biol* **210**:503–515. doi:10.1083/jcb.201501025

Kim N-G, Koh E, Chen X, Gumbiner BM. 2011. E-cadherin mediates contact inhibition of proliferation through Hippo signaling-pathway components. *Proc Natl Acad Sci U S A* **108**:11930–11935. doi:10.1073/pnas.1103345108

Kim T-S, Nakagawa T, Lee J-E, Fujino K, Iguchi F, Endo T, Naito Y, Omori K, Lefebvre PP, Ito J. 2004. Induction of cell proliferation and beta-catenin expression in rat utricles in vitro. *Acta Oto-Laryngol Suppl* 22–25. doi:10.1080/03655230310016672

Kitajiri S, Furuse M, Morita K, Saishin-Kiuchi Y, Kido H, Ito J, Tsukita S. 2004. Expression patterns of claudins, tight junction adhesion molecules, in the inner ear. *Hear Res* **187**:25–34. doi:10.1016/S0378-5955(03)00338-1

Kozlowski MM, Rudolf MA, Corwin JT. 2020. EGF and a GSK3 Inhibitor Deplete Junctional E-cadherin and Stimulate Proliferation in the Mature Mammalian Ear. *J Neurosci*. doi:10.1523/JNEUROSCI.2630-19.2020

Kuipers D, Mehonic A, Kajita M, Peter L, Fujita Y, Duke T, Charras G, Gale JE. 2014. Epithelial repair is a two-stage process driven first by dying cells and then by their neighbours. *J Cell Sci* **127**:1229–1241. doi:10.1242/jcs.138289

Lahne M, Gale JE. 2008. Damage-induced activation of ERK1/2 in cochlear supporting cells is a hair cell death-promoting signal that depends on extracellular ATP and calcium. *J Neurosci Off J Soc Neurosci* **28**:4918–4928. doi:10.1523/JNEUROSCI.4914-07.2008

Leonova EV, Raphael Y. 1997. Organization of cell junctions and cytoskeleton in the reticular lamina in normal and ototoxically damaged organ of Corti. *Hear Res* **113**:14–28. doi:10.1016/s0378-5955(97)00130-5

Li C-Y, Hu J, Lu H, Lan J, Du W, Galicia N, Klein OD. 2016. αE-catenin inhibits YAP/TAZ activity to regulate signalling centre formation during tooth development. *Nat Commun* **7**. doi:10.1038/ncomms12133

Li L, Nevill G, Forge A. 1995. Two modes of hair cell loss from the vestibular sensory epithelia of the guinea pig inner ear. *J Comp Neurol* **355**:405–417. doi:10.1002/cne.903550307

Li Jifen, Gao Erhe, Vite Alexia, Yi Roslyn, Gomez Ludovic, Goossens Steven, van Roy Frans, Radice Glenn L. 2015. Alpha-Catenins Control Cardiomyocyte Proliferation by Regulating Yap Activity. *Circ Res* **116**:70–79. doi:10.1161/CIRCRESAHA.116.304472

Lien W-H, Klezovitch O, Null M, Vasioukhin V. 2008. αE-catenin is not a significant regulator of β-catenin signaling in the developing mammalian brain. *J Cell Sci* **121**:1357–1362. doi:10.1242/jcs.020537

Lim R, Brichta AM. 2016. Anatomical and physiological development of the human inner ear. *Hear Res* **338**:9–21. doi:10.1016/j.heares.2016.02.004

Lin J, Zhang X, Wu F, Lin W. 2015. Hair cell damage recruited Lgr5-expressing cells are hair cell progenitors in neonatal mouse utricle. *Front Cell Neurosci* **9**. doi:10.3389/fncel.2015.00113

Lu Z, Corwin JT. 2008. The influence of glycogen synthase kinase 3 in limiting cell addition in the mammalian ear. *Dev Neurobiol* **68**:1059–1075. doi:10.1002/dneu.20635

Ludwig A, Schlierf B, Schardt A, Nave K-A, Wegner M. 2004. Sox10-rtTA mouse line for tetracycline-inducible expression of transgenes in neural crest cells and oligodendrocytes. *Genes N Y N 2000* **40**:171–175. doi:10.1002/gene.20083

Luo W, Wang X, Ma R, Chi F, Chen P, Cong N, Gu Y, Ren D, Yang J. 2018. Junctional E-cadherin/p120-catenin Is Correlated with the Absence of Supporting Cells to Hair Cells Conversion in Postnatal Mice Cochleae. *Front Mol Neurosci* **11**. doi:10.3389/fnmol.2018.00020

Lush ME, Piotrowski T. 2014. Sensory hair cell regeneration in the zebrafish lateral line. *Dev Dyn* **243**:1187–1202. doi:10.1002/dvdy.24167

Maass JC, Gu R, Basch ML, Waldhaus J, Lopez EM, Xia A, Oghalai JS, Heller S, Groves AK. 2015. Changes in the regulation of the Notch signaling pathway are temporally correlated with regenerative failure in the mouse cochlea. *Front Cell Neurosci* 110. doi:10.3389/fncel.2015.00110

Mangiardi DA, McLaughlin-Williamson K, May KE, Messana EP, Mountain DC, Cotanche DA. 2004. Progression of hair cell ejection and molecular markers of apoptosis in the avian cochlea following gentamicin treatment. *J Comp Neurol* **475**:1–18. doi:10.1002/cne.20129

Matamoro-Vidal A, Levayer R. 2019. Multiple Influences of Mechanical Forces on Cell Competition. *Curr Biol* **29**:R762–R774. doi:10.1016/j.cub.2019.06.030

Matsui JI, Ogilvie JM, Warchol ME. 2002. Inhibition of Caspases Prevents Ototoxic and Ongoing Hair Cell Death. *J Neurosci* **22**:1218–1227.

McLean WJ, Yin X, Lu L, Lenz DR, McLean D, Langer R, Karp JM, Edge ASB. 2017. Clonal Expansion of Lgr5-Positive Cells from Mammalian Cochlea and High-Purity Generation of Sensory Hair Cells. *Cell Rep* **18**:1917–1929. doi:10.1016/j.celrep.2017.01.066

Meiteles LZ, Raphael Y. 1994. Distribution of Cytokeratins in the Vestibular Epithelium of the Guinea Pig. *Ann Otol Rhinol Laryngol* **103**:149–155. doi:10.1177/000348949410300212

Méjat A, Misteli T. 2010. LINC complexes in health and disease. *Nucleus* **1**:40–52. doi:10.4161/nucl.1.1.10530

Mendonsa AM, Na T-Y, Gumbiner BM. 2018. E-cadherin in contact inhibition and cancer. *Oncogene* **37**:4769–4780. doi:10.1038/s41388-018-0304-2

Meng Z, Moroishi T, Mottier-Pavie V, Plouffe SW, Hansen CG, Hong AW, Park HW, Mo J-S, Lu W, Lu S, Flores F, Yu F-X, Halder G, Guan K-L. 2015. MAP4K family kinases act in parallel to MST1/2 to activate LATS1/2 in the Hippo pathway. *Nat Commun* **6**:1–13. doi:10.1038/ncomms9357

Mesa KR, Kawaguchi K, Cockburn K, Gonzalez D, Boucher J, Xin T, Klein AM, Greco V. 2018. Homeostatic epidermal stem cell self-renewal is driven by local differentiation. *Cell Stem Cell* **23**:677–686.e4. doi:10.1016/j.stem.2018.09.005

Meyers JR, Corwin JT. 2007. Shape change controls supporting cell proliferation in lesioned mammalian balance epithelium. *J Neurosci Off J Soc Neurosci* **27**:4313–4325. doi:10.1523/JNEUROSCI.5023-06.2007

Miroshnikova YA, Le HQ, Schneider D, Thalheim T, Rübsam M, Bremicker N, Polleux J, Kamprad N, Tarantola M, Wang I, Balland M, Niessen CM, Galle J, Wickström SA. 2018. Adhesion forces and cortical tension couple cell proliferation and differentiation to drive epidermal stratification. *Nat Cell Biol* **20**:69–80. doi:10.1038/s41556-017-0005-z

Mizutari K, Fujioka M, Hosoya M, Bramhall N, Okano HJ, Okano H, Edge ASB. 2013. Notch inhibition induces cochlear hair cell regeneration and recovery of hearing after acoustic trauma. *Neuron* **77**:58–69. doi:10.1016/j.neuron.2012.10.032

Monzack EL, May LA, Roy S, Gale JE, Cunningham LL. 2015. Live imaging the phagocytic activity of inner ear supporting cells in response to hair cell death. *Cell Death Differ* **22**:1995–2005. doi:10.1038/cdd.2015.48

Moroishi T, Park HW, Qin B, Chen Q, Meng Z, Plouffe SW, Taniguchi K, Yu F-X, Karin M, Pan D, Guan K-L. 2015. A YAP/TAZ-induced feedback mechanism regulates Hippo pathway homeostasis. *Genes Dev* **29**:1271–1284. doi:10.1101/gad.262816.115

Morrison AJ. 2020. Chromatin-remodeling links metabolic signaling to gene expression. *Mol Metab* 100973. doi:10.1016/j.molmet.2020.100973

Nadol JB. 1993. Hearing loss. *N Engl J Med* **329**:1092–1102. doi:10.1056/NEJM199310073291507

Nelson WJ, Nusse R. 2004. Convergence of Wnt, beta-catenin, and cadherin pathways. *Science* **303**:1483–1487. doi:10.1126/science.1094291

Nokin M-J, Durieux F, Peixoto P, Chiavarina B, Peulen O, Blomme A, Turtoi A, Costanza B, Smargiasso N, Baiwir D, Scheijen JL, Schalkwijk CG, Leenders J, De Tullio P, Bianchi E, Thiry M, Uchida K, Spiegel DA, Cochrane JR, Hutton CA, De Pauw E, Delvenne P, Belpomme D, Castronovo V, Bellahcène A. 2016. Methylglyoxal, a glycolysis side-product, induces Hsp90 glycation and YAP-mediated tumor growth and metastasis. *eLife* **5**:e19375. doi:10.7554/eLife.19375

Noll N, Mani M, Heemskerk I, Streichan SJ, Shraiman BI. 2017. Active tension network model suggests an exotic mechanical state realized in epithelial tissues. *Nat Phys* nphys4219. doi:10.1038/nphys4219

Ono K, Keller J, López Ramírez O, González Garrido A, Zobeiri OA, Chang HHV, Vijayakumar S, Ayiotis A, Duester G, Della Santina CC, Jones SM, Cullen KE, Eatock RA, Wu DK. 2020. Retinoic acid degradation shapes zonal development of vestibular organs and sensitivity to transient linear accelerations. *Nat Commun* **11**:1–15. doi:10.1038/s41467-019-13710-4

Oshima K, Grimm CM, Corrales CE, Senn P, Martinez Monedero R, Géléoc GSG, Edge A, Holt JR, Heller S. 2007. Differential Distribution of Stem Cells in the Auditory and Vestibular Organs of the Inner Ear. *J Assoc Res Otolaryngol* **8**:18–31. doi:10.1007/s10162-006-0058-3

Pan Y, Heemskerk I, Ibar C, Shraiman BI, Irvine KD. 2016. Differential growth triggers mechanical feedback that elevates Hippo signaling. *Proc Natl Acad Sci* **113**:E6974–E6983. doi:10.1073/pnas.1615012113

Park G-S, Oh H, Kim M, Kim T, Johnson RL, Irvine KD, Lim D-S. 2016. An evolutionarily conserved negative feedback mechanism in the Hippo pathway reflects functional difference between LATS1 and LATS2. *Oncotarget* **7**:24063–24075. doi:10.18632/oncotarget.8211

Pećina-Slaus N. 2003. Tumor suppressor gene E-cadherin and its role in normal and malignant cells. *Cancer Cell Int* **3**:17. doi:10.1186/1475-2867-3-17

Perez Gonzalez N, Tao J, Rochman ND, Vig D, Chiu E, Wirtz D, Sun SX, Edelstein-Keshet L. 2018. Cell tension and mechanical regulation of cell volume. *Mol Biol Cell* **29**:0–0. doi:10.1091/mbc.E18-04-0213

Perrais M, Chen X, Perez-Moreno M, Gumbiner BM. 2007. E-cadherin homophilic ligation inhibits cell growth and epidermal growth factor receptor signaling independently of other cell interactions. *Mol Biol Cell* **18**:2013–2025. doi:10.1091/mbc.e06-04-0348

Plouffe SW, Lin KC, Moore JL, Tan FE, Ma S, Ye Z, Qiu Y, Ren B, Guan K-L. 2018. The Hippo pathway effector proteins YAP and TAZ have both distinct and overlapping functions in the cell. *J Biol Chem* **293**:11230–11240. doi:10.1074/jbc.RA118.002715

Porazinski S, Wang H, Asaoka Y, Behrndt M, Miyamoto T, Morita H, Hata S, Sasaki T, Krens SFG, Osada Y, Asaka S, Momoi A, Linton S, Miesfeld JB, Link BA, Senga T, Castillo-Morales A, Urrutia AO, Shimizu N, Nagase H, Matsuura S, Bagby S, Kondoh H, Nishina H, Heisenberg C-P, Furutani-Seiki M. 2015. YAP is essential for tissue tension to ensure vertebrate 3D body shape. *Nature* **521**:217–221. doi:10.1038/nature14215

Prevedel R, Diz-Muñoz A, Ruocco G, Antonacci G. 2019. Brillouin microscopy: an emerging tool for mechanobiology. *Nat Methods* **16**:969–977. doi:10.1038/s41592-019-0543-3

Rauch SD, Velazquez-Villaseñor L, Dimitri PS, Merchant SN. 2001. Decreasing Hair Cell Counts in Aging Humans. *Ann N Y Acad Sci* **942**:220–227. doi:10.1111/j.1749-6632.2001.tb03748.x

Rauskolb C, Sun S, Sun G, Pan Y, Irvine KD. 2014. Cytoskeletal Tension inhibits Hippo signaling through an Ajuba-Warts complex. *Cell* **158**:143–156. doi:10.1016/j.cell.2014.05.035

Ravasio A, Cheddadi I, Chen T, Pereira T, Ong HT, Bertocchi C, Brugues A, Jacinto A, Kabla AJ, Toyama Y, Trepat X, Gov N, Neves de Almeida L, Ladoux B. 2015. Gap geometry dictates epithelial closure efficiency. *Nat Commun* **6**:1–13. doi:10.1038/ncomms8683

Romero-Carvajal A, Acedo JN, Jiang L, Kozlovskaja-Gumbrienė A, Alexander R, Li H, Piotrowski T. 2015. Regeneration of sensory hair cells requires localized interactions between the Notch and Wnt pathways. *Dev Cell* **34**:267–282. doi:10.1016/j.devcel.2015.05.025

Rudolf MA, Andreeva A, Kozlowski MM, Kim CE, Moskowitz BA, Anaya-Rocha A, Kelley MW, Corwin JT. 2020. YAP Mediates Hair Cell Regeneration in Balance Organs of Chickens, But LATS Kinases Suppress Its Activity in Mice. *J Neurosci* **40**:3915–3932. doi:10.1523/JNEUROSCI.0306-20.2020

Ryals BM, Rubel EW. 1988. Hair cell regeneration after acoustic trauma in adult Coturnix quail. *Science* **240**:1774–1776. doi:10.1126/science.3381101

Samarajeewa A, Lenz DR, Xie L, Chiang H, Kirchner R, Mulvaney JF, Edge ASB, Dabdoub A. 2018. Transcriptional response to Wnt activation regulates the regenerative capacity of the mammalian cochlea. *Development* **145**:dev166579. doi:10.1242/dev.166579

Santinon G, Pocaterra A, Dupont S. 2016. Control of YAP/TAZ Activity by Metabolic and Nutrient-Sensing Pathways. *Trends Cell Biol* **26**:289–299. doi:10.1016/j.tcb.2015.11.004

Sayyid ZN, Wang T, Chen L, Jones SM, Cheng AG. 2019. Atoh1 Directs Regeneration and Functional Recovery of the Mature Mouse Vestibular System. *Cell Rep* **28**:312–324.e4. doi:10.1016/j.celrep.2019.06.028

Scheibinger M, Ellwanger DC, Corrales CE, Stone JS, Heller S. 2018. Aminoglycoside Damage and Hair Cell Regeneration in the Chicken Utricle. *JARO J Assoc Res Otolaryngol* **19**:17–29. doi:10.1007/s10162-017-0646-4

Schindelin J, Arganda-Carreras I, Frise E, Kaynig V, Longair M, Pietzsch T, Preibisch S, Rueden C, Saalfeld S, Schmid B, Tinevez J-Y, White DJ, Hartenstein V, Eliceiri K, Tomancak P, Cardona A. 2012. Fiji: an open-source platform for biological-image analysis. *Nat Methods* **9**:676–682. doi:10.1038/nmeth.2019

Schlegelmilch K, Mohseni M, Kirak O, Pruszak J, Rodriguez JR, Zhou D, Kreger BT, Vasioukhin V, Avruch J, Brummelkamp TR, Camargo FD. 2011. Yap1 acts downstream of α-catenin to control epidermal proliferation. *Cell* **144**:782–795. doi:10.1016/j.cell.2011.02.031

Senn P, Mina A, Volkenstein S, Kranebitter V, Oshima K, Heller S. 2019. Progenitor Cells from the Adult Human Inner Ear. *Anat Rec* **0**. doi:10.1002/ar.24228

Shi F, Hu L, Jacques BE, Mulvaney JF, Dabdoub A, Edge ASB. 2014. β-Catenin Is Required for Hair-Cell Differentiation in the Cochlea. *J Neurosci* **34**:6470–6479. doi:10.1523/JNEUROSCI.4305-13.2014

Shreberk-Shaked M, Oren M. 2019. New insights into YAP/TAZ nucleo-cytoplasmic shuttling: new cancer therapeutic opportunities? *Mol Oncol* **13**:1335–1341. doi:10.1002/1878-0261.12498

Silvis MR, Kreger BT, Lien W-H, Klezovitch O, Rudakova GM, Camargo FD, Lantz DM, Seykora JT, Vasioukhin V. 2011. α-Catenin Is a Tumor Suppressor That Controls Cell Accumulation by Regulating the Localization and Activity of the Transcriptional Coactivator Yap1. *Sci Signal* **4**:ra33-ra33. doi:10.1126/scisignal.2001823

Smith ME, Coffin AB, Miller DL, Popper AN. 2006. Anatomical and functional recovery of the goldfish (Carassius auratus) ear following noise exposure. *J Exp Biol* **209**:4193–4202. doi:10.1242/jeb.02490

Smolders JW. 1999. Functional recovery in the avian ear after hair cell regeneration. *Audiol Neurootol* **4**:286–302. doi:10.1159/000013853

Song S, Xie M, Scott AW, Jin J, Ma L, Dong X, Skinner HD, Johnson RL, Ding S, Ajani JA. 2018. A Novel YAP1 Inhibitor Targets CSC-Enriched Radiation-Resistant Cells and Exerts Strong Antitumor Activity in Esophageal Adenocarcinoma. *Mol Cancer Ther* **17**:443–454. doi:10.1158/1535-7163.MCT-17-0560

Spector AA, Brownell WE, Popel AS. 1996. A model for cochlear outer hair cell deformations in micropipette aspiration experiments: An analytical solution. *Ann Biomed Eng* **24**:241–249. doi:10.1007/BF02667353

Szarama KB, Gavara N, Petralia RS, Kelley MW, Chadwick RS. 2012. Cytoskeletal changes in actin and microtubules underlie the developing surface mechanical properties of sensory and supporting cells in the mouse cochlea. *Dev Camb Engl* **139**:2187–2197. doi:10.1242/dev.073734

Takai Y, Miyoshi J, Ikeda W, Ogita H. 2008. Nectins and nectin-like molecules: roles in contact inhibition of cell movement and proliferation. *Nat Rev Mol Cell Biol* **9**:603–615. doi:10.1038/nrm2457

Togashi H, Kominami K, Waseda M, Komura H, Miyoshi J, Takeichi M, Takai Y. 2011. Nectins Establish a Checkerboard-Like Cellular Pattern in the Auditory Epithelium. *Science* **333**:1144–1147. doi:10.1126/science.1208467

Tomo I, Boutet de Monvel J, Fridberger A. 2007. Sound-Evoked Radial Strain in the Hearing Organ. *Biophys J* **93**:3279–3284. doi:10.1529/biophysj.107.105072

Totaro A, Panciera T, Piccolo S. 2018. YAP/TAZ upstream signals and downstream responses. *Nat Cell Biol* **20**:888–899. doi:10.1038/s41556-018-0142-z

Troxell ML, Gopalakrishnan S, McCormack J, Poteat BA, Pennington J, Garringer SM, Schneeberger EE, Nelson WJ, Marrs JA. 2000. Inhibiting cadherin function by dominant mutant E-cadherin expression increases the extent of tight junction assembly. *J Cell Sci* **113 (Pt 6)**:985–996.

Tschöp K, Conery AR, Litovchick L, DeCaprio JA, Settleman J, Harlow E, Dyson N. 2011. A kinase shRNA screen links LATS2 and the pRB tumor suppressor. *Genes Dev* **25**:814–830. doi:10.1101/gad.2000211

Uroz M, Wistorf S, Serra-Picamal X, Conte V, Sales-Pardo M, Roca-Cusachs P, Guimerà R, Trepat X. 2018. Regulation of cell cycle progression by cell–cell and cell–matrix forces. *Nat Cell Biol* **20**:646–654. doi:10.1038/s41556-018-0107-2

Uttagomol J, Ahmad US, Rehman A, Huang Y, Laly AC, Kang A, Soetaert J, Chance R, Teh M-T, Connelly JT, Wan H. 2019. Evidence for the Desmosomal Cadherin Desmoglein-3 in Regulating YAP and Phospho-YAP in Keratinocyte Responses to Mechanical Forces. *Int J Mol Sci* **20**. doi:10.3390/ijms20246221

Varelas X, Samavarchi-Tehrani P, Narimatsu M, Weiss A, Cockburn K, Larsen BG, Rossant J, Wrana JL. 2010. The Crumbs Complex Couples Cell Density Sensing to Hippo-Dependent Control of the TGF-β-SMAD Pathway. *Dev Cell* **19**:831–844. doi:10.1016/j.devcel.2010.11.012

Vassilev A, Kaneko KJ, Shu H, Zhao Y, DePamphilis ML. 2001. TEAD/TEF transcription factors utilize the activation domain of YAP65, a Src/Yes-associated protein localized in the cytoplasm. *Genes Dev* **15**:1229–1241. doi:10.1101/gad.888601

Vite A, Zhang C, Yi R, Emms S, Radice GL. 2018. Alpha-catenin-dependent cytoskeletal tension controls Yap activity in the heart. *Dev Camb Engl*. doi:10.1242/dev.149823

Walters BJ, Zuo J. 2015. A Sox10rtTA/+ Mouse Line Allows for Inducible Gene Expression in the Auditory and Balance Organs of the Inner Ear. *JARO J Assoc Res Otolaryngol* **16**:331–345. doi:10.1007/s10162-015-0517-9

Wang T, Chai R, Kim GS, Pham N, Jansson L, Nguyen D-H, Kuo B, May LA, Zuo J, Cunningham LL, Cheng AG. 2015. Lgr5+ cells regenerate hair cells via proliferation and direct transdifferentiation in damaged neonatal mouse utricle. *Nat Commun* **6**:6613. doi:10.1038/ncomms7613

Wang W, Xiao Z-D, Li X, Aziz KE, Gan B, Johnson RL, Chen J. 2015. AMPK modulates Hippo pathway activity to regulate energy homeostasis. *Nat Cell Biol* **17**:490–499. doi:10.1038/ncb3113

Wang X, Hou H, Song K, Zhang Z, Zhang S, Cao Y, Chen L, Sang Q, Lin F, Xu H. 2018. Lpar2b Controls Lateral Line Tissue Size by Regulating Yap1 Activity in Zebrafish. *Front Mol Neurosci* **11**. doi:10.3389/fnmol.2018.00034

Warchol ME. 2007. Characterization of supporting cell phenotype in the avian inner ear: implications for sensory regeneration. *Hear Res* **227**:11–18. doi:10.1016/j.heares.2006.08.014

Warchol ME. 2002. Cell Density and N-Cadherin Interactions Regulate Cell Proliferation in the Sensory Epithelia of the Inner Ear. *J Neurosci* **22**:2607–2616.

Warchol ME, Corwin JT. 1996. Regenerative Proliferation in Organ Cultures of the Avian Cochlea: Identification of the Initial Progenitors and Determination of the Latency of the Proliferative Response. *J Neurosci* **16**:5466–5477.

Warchol ME, Lambert PR, Goldstein BJ, Forge A, Corwin JT. 1993. Regenerative proliferation in inner ear sensory epithelia from adult guinea pigs and humans. *Science* **259**:1619–1622.

Whitlon DS, Rutishauser US. 1990. NCAM in the organ of Corti of the developing mouse. *J Neurocytol* **19**:970–977. doi:10.1007/bf01186824

Whitlon DS, Zhang X, Pecelunas K, Greiner MA. 1999. A temporospatial map of adhesive molecules in the organ of Corti of the mouse cochlea. *J Neurocytol* **28**:955–968. doi:10.1023/a:1007038609456

Woolley SMN, Wissman AM, Rubel EW. 2001. Hair cell regeneration and recovery of auditory thresholds following aminoglycoside ototoxicity in Bengalese finches. *Hear Res* **153**:181–195. doi:10.1016/S0378-5955(00)00217-3

World Health Organization. 2020. Deafness and hearing loss. https://www.who.int/news-room/fact-sheets/detail/deafness-and-hearing-loss

Wu Z, Grillet N, Zhao B, Cunningham C, Harkins-Perry S, Coste B, Ranade S, Zebarjadi N, Beurg M, Fettiplace R, Patapoutian A, Müller U. 2017. Mechanosensory hair cells express two molecularly distinct mechanotransduction channels. *Nat Neurosci* **20**:24–33. doi:10.1038/nn.4449

Wyatt TPJ, Harris AR, Lam M, Cheng Q, Bellis J, Dimitracopoulos A, Kabla AJ, Charras GT, Baum B. 2015. Emergence of homeostatic epithelial packing and stress dissipation through divisions oriented along the long cell axis. *Proc Natl Acad Sci U S A* **112**:5726–5731. doi:10.1073/pnas.1420585112

Xia M, Chen Y, He Y, Li H, Li W. 2020. Activation of the RhoA-YAP-β-catenin signaling axis promotes the expansion of inner ear progenitor cells in 3D culture. *STEM CELLS* 1–15. doi:10.1002/stem.3175

Xin M, Kim Y, Sutherland LB, Murakami M, Qi X, McAnally J, Porrello ER, Mahmoud AI, Tan W, Shelton JM, Richardson JA, Sadek HA, Bassel-Duby R, Olson EN. 2013. Hippo pathway effector Yap promotes cardiac regeneration. *Proc Natl Acad Sci U S A* **110**:13839–13844. doi:10.1073/pnas.1313192110

Xin M, Kim Y, Sutherland LB, Qi X, McAnally J, Schwartz RJ, Richardson JA, Bassel-Duby R, Olson EN. 2011. Regulation of insulin-like growth factor signaling by Yap governs cardiomyocyte proliferation and embryonic heart size. *Sci Signal* **4**:ra70. doi:10.1126/scisignal.2002278

You D, Guo L, Li W, Sun S, Chen Y, Chai R, Li H. 2018. Characterization of Wnt and Notch-Responsive Lgr5+ Hair Cell Progenitors in the Striolar Region of the Neonatal Mouse Utricle. *Front Mol Neurosci* **11**. doi:10.3389/fnmol.2018.00137

Yu F-X, Zhao B, Panupinthu N, Jewell JL, Lian I, Wang LH, Zhao J, Yuan H, Tumaneng K, Li H, Fu X-D, Mills GB, Guan K-L. 2012. Regulation of the Hippo-YAP pathway by G-protein coupled receptor signaling. *Cell* **150**:780–791. doi:10.1016/j.cell.2012.06.037

Zhao B, Kim J, Ye X, Lai Z-C, Guan K-L. 2009. Both TEAD-Binding and WW Domains Are Required for the Growth Stimulation and Oncogenic Transformation Activity of Yes-Associated Protein. *Cancer Res* **69**:1089–1098. doi:10.1158/0008-5472.CAN-08-2997

Zhao B, Li L, Tumaneng K, Wang C-Y, Guan K-L. 2010. A coordinated phosphorylation by Lats and CK1 regulates YAP stability through SCFβ-TRCP. *Genes Dev* **24**:72–85. doi:10.1101/gad.1843810

Zhao B, Wei X, Li W, Udan RS, Yang Q, Kim J, Xie J, Ikenoue T, Yu J, Li L, Zheng P, Ye K, Chinnaiyan A, Halder G, Lai Z-C, Guan K-L. 2007. Inactivation of YAP oncoprotein by the Hippo pathway is involved in cell contact inhibition and tissue growth control. *Genes Dev* **21**:2747–2761. doi:10.1101/gad.1602907

Zhao B, Ye X, Yu J, Li L, Li W, Li S, Yu J, Lin JD, Wang C-Y, Chinnaiyan AM, Lai Z-C, Guan K-L. 2008. TEAD mediates YAP-dependent gene induction and growth control. *Genes Dev* **22**:1962–1971. doi:10.1101/gad.1664408

Zhu Y, Scheibinger M, Ellwanger DC, Krey JF, Choi D, Kelly RT, Heller S, Barr-Gillespie PG. 2019. Single-cell proteomics reveals changes in expression during hair-cell development. *eLife* **8**:e50777. doi:10.7554/eLife.50777